# BLACK CARBON IN THE GULF OF MAINE: NEW INSIGHTS INTO INPUTS AND CYCLING OF COMBUSTION-DERIVED ORGANIC CARBON

by

Déborah Xanat Flores-Cervantes

M. Eng. Civil and Environmental Engineering (2003)

Massachusetts Institute of Technology

Submitted to the Department of Civil and Environmental Engineering in partial fulfillment of the requirements for the degree of

Doctor of Philosophy

at the

MASSACHUSETTS INSTITUTE OF TECHNOLOGY

June 2008



Signature of the Author _____
Department of Civil and Environmental Engineering
May 11, 2008

Certified by _____
Philip M. Gschwend
Professor of Civil and Environmental Engineering
Thesis Supervisor

Accepted by _____
Daniele Veneziano
Chairman, Departmental Committee for Graduate Students

# BLACK CARBON IN THE GULF OF MAINE: NEW INSIGHTS INTO INPUTS AND CYCLING OF COMBUSTION-DERIVED ORGANIC CARBON

by

Déborah Xanat Flores-Cervantes

Submitted to the Department of Civil and Environmental Engineering on May 11, 2008, in partial fulfillment of the requirements for the degree of Doctor of Philosophy in the field of Environmental Chemistry

## ABSTRACT

Emissions of black carbon (BC), the soot and char formed during incomplete combustion of fossil and biomass fuels, have increased over the last century and are estimated to be between 8 and 270 Tg BC/yr. BC may affect problems as diverse as global warming, human health, carbon cycling in ecosystems, and pollutant dynamics. However, currently there is substantial uncertainty with respect to the fate of BC released to the environment. To increase our understanding of BC's fate and effects, modifications to the Chemo-Thermal Oxidation method at 375 °C (CTO 375), a current method used to quantify BC in marine sediments, were made to measure BC concentrations in, and fluxes out of, the water column in the Gulf of Maine (GoM), a representative coastal area downwind of important BC sources of the Northeastern United States. In addition, an alternative method to infer BC concentrations in seawater by observing pyrene fluorescence losses (PFL) in spiked samples was developed. Average concentrations measured in the GoM were 5 and 4 μg/L using the modified CTO 375 and PFL methods, respectively. Although these two methodologies involve independent observations, correspondence between the modified CTO 375 and PFL methods suggested that the isolated material was both highly sorptive and refractory. These concentrations also suggested that (a) up to 50% of the "molecularly uncharacterized" particulate organic carbon (POC) in surface seawater is BC; (b) the presence of this recalcitrant organic carbon may explain why some POC is not recycled to $CO_2$ during its transport to depth and even within the sediment beds below; and (c) hydrophobic pollutants like polycyclic aromatic hydrocarbons (PAHs) and dioxins would have their "bioavailabilities" controlled by sorption to BC. The observed BC spatial distributions and average water-column export fluxes near 10 $gBC/m^2$ year imply that most of the BC is carried offshore by wind and is accumulated in the coastal zone. Finally, sediment records of CTO-375-derived BC inputs into the GoM for the past 100 years were consistent with historical changes in fossil and biomass fuel emissions to this area.

Thesis advisor: Philip M. Gschwend

Title: Professor of Civil and Environmental Engineering

To my grandma and my mom

## ACKNOWLEDGMENTS

There have been ups and downs along the way, but overall it has been a long, pleasant road, and there have been numerous people that have made this journey fun, exciting...and feasible. From random conversations and e-mail exchanges with people here and in Mexico, to long discussions and working hours in the lab with my labmates, they have all inspired me to be where I am today.

I am very thankful to Phil Gschwend for all the energy and enthusiasm that he has put in this project as a teacher, advisor, mentor, educator, and friend; and for sharing the love of doing things right, and making things better wherever we go and whatever we do.

In addition, I want to thank Chris Reddy for his active involvement as a second advisor through every step of this project. From the conception of the idea, through the realization of the project, Chris has always been there enthusiastically advising me and pointing out new possible pathways and directions to move forward in this work where it is today.

I am also very thankful to Harry Hemond, member of my thesis committee, for sharing his knowledge, thoughts, and ideas, and for the great discussions that helped shape and direct this work.

My work depended heavily on data collection, and it would have not been possible without all the people that were involved in making the two data-collection cruises possible. I am very thankful to the captains, crews, and CTD technicians from *Oceanus* and *Cape Hatteras*, and to all the people who participated in the data collection of water and sediment samples: R. K. Nelson, K. Pangallo, E. Peacock, E. Roosen, S. Silva, E. Tauten, and L. Xu; thank you all very much.

I owe many, many thanks to John MacFarlane and Desiree Plata. Everything, from the sample collection to the data analysis would have been twice as long and three times a difficult without their help. John, thank you very, very much for all your help from the moment I first stepped into Phil's lab, through the intensive work of preparing to go to sea, the long hours without any sleep while collecting water samples, and all the constant and continuous help in finding things or figuring things out in the lab. Desiree, I am deeply thankful to you, first for being such a caring and loving person to anyone or anything that surrounds you, but also for all of the time and energy that you have put into this work, without having any commitment to it. Thank you very much for your key participation in the logistics and sampling of both cruises, for your help in sample analysis, for your continuous cheering in the lab, and for all the great fruitful discussions.

Dave Kuo and Loretta Fernandez are also gratefully acknowledged for their help along the way. Dave, thank you very much for all the great discussions regarding black carbon and pyrene fluorescence and the difficulties of the measurements...and figuring out the literature. Loretta, thank you very much for all the sampling trips in the middle of the summer to the harbor or the beach, for always being ready to help, and for the positive energy that you share with everyone around you. I have really enjoyed getting to hang out with you and your family.

I am really glad I was part of the formation of the "Parsons Super Group". Thanks to Beca, Charu, Sarah Jane, Amy, and Matt for all your input into this work through discussions in our "Super Group Meetings". Special thanks go to Matt for helping make the transition from MEng to PhD candidate smoother, for the numerous discussions about whether or not to continue at MIT, and for your friendship through all the years I spent at MIT.

Thanks very much to everyone that makes Parsons a great place to work at, and special thanks to Jim Long, Sheila Frankel, Vicky Murphy. Also, thank you very much to all the great people over at Bldg. 1, Pat Dixon, Kris Kipp, Patty Glidden, Donna Hudson, and Jeannette Marchocki. Thank you all for your help during these past six years at MIT.

I am very thankful to all the many friends I have made at MIT, and whom I am going to miss a lot after I leave. Thanks to Marcus, Madhu, and Laurant, my orientation buddies; thanks to present and past members of the BAD Coop and to Sam Arey for introducing me to them; thanks to the TCC family, and in special to Elizabeth, Christine and Jeanne; many thanks to the many present and past members of Clubmex, in special to Ferran, Alexis, Carlos, Rogelio, Pepe, Federico, Ale, Paulina, and Alfonso. Also thanks a lot to Maureen and Jake; it has been great sharing with you the daily ups and downs of grad school...and finishing grad school.

Thanks to my family and my grandparents for all their love and constant cheering and support, and many especial thanks to my brother, Homero, who has always been there to support me and help me out in any way he can. Home, thank you very much for all your help in this long journey, from the moment I first arrived in Boston. Thank you also to Lore, Niche, Ruth, Deni, Maye, Eddy, and Ambru, and many other friends from Mexico who have helped me stay in contact with my home country.

Thanks to Gregory Tkac, for all his love, care, and support in the most difficult years of my PhD, and for keeping me grounded and connected to the world around me while working at MIT.

Finally, I would like to thank God for all his blessings, for the opportunity to be at MIT, and for bringing such beautiful and amazing people into my life.

This work was supported by NFS grants (OCE-0223441 and BES-0607136) and CONACYT and MSFS fellowships.

## TABLE OF CONTENTS

## LIST OF FIGURES

## LIST OF TABLES

# CHAPTER 1. GENERAL INTRODUCTION

While carbon dioxide ($CO_2$) gains the greatest attention as a product of combustion processes, other products such as black carbon (BC), the soot and char formed and emitted during the incomplete combustion of fossil and biomass fuels (Kuhlbusch, 1995), warrants awareness. BC, is widely distributed (e.g., Goldberg, 1985; Masiello and Druffel, 1998; Park et al., 2003; Schmidt and Noack, 2000; Suman et al., 1997), and recent studies show that BC in the atmosphere exerts an important influence on global warming and may be responsible for the floods and droughts in recent years in China and India (Menon and Hansen, 2002) by absorbing solar radiation, cooling the ground underneath (Jacobson, 2004; Kaufman and Fraser, 1997), and participating in cloud droplet nucleation (Kaufman and Fraser, 1997). In addition, it has been suggested that BC is carcinogenic and affects respiratory health due to dust retention in the lungs (Dockery, et al., 1993; Grigg, 2002; Künzli, 2000); BC formation sequesters carbon into a microbially and chemically inert material that would otherwise turn into $CO_2$ (Kuhlbusch, 1995); BC may represent an important fraction of the uncharacterized and old $^{14}C$ organic carbon buried in sediments; and BC can represent an important carrier-phase of organic pollutants such as polycyclic aromatic hydrocarbons (PAHs) and polychlorinated dibenzodioxins (PCDDs), affecting their transport and transformations in the environment by substantially controlling their speciation (Lohmann et al., 2005). In light of these diverse effects, it is paramount that we understand what controls the environmental distributions of BC itself, if we hope to predict and control future impacts of this important combustion product.

Despite the immediate need to better understand the lifetime of soot in the atmosphere and the fate of this material once it settles out, there is a low level of scientific understanding

regarding the sources, sinks, transport, and chemical transformations of soot in the environment (IPCC, 2001). Unlike $CO_2$ that is well defined and relatively easy to measure, BC represents a spectrum of materials that range from slightly charred biomass to soot, and no single definition or technique to measure it has been established. Additionally, unlike greenhouse gases, soot has a short residence time in the atmosphere (from days to weeks) and its concentrations and properties can vary significantly depending on the sources and locations (e.g. rural vs. urban-industrial areas). Finally, unlike $CO_2$ where the main contributors are developed regions like North America, Europe and Japan, BC emissions are largest in the developing world, where China and India are of great importance to the global total emissions (Bond et al., 2004).

Several measurements of BC have been made in soils, oceanic and lacustrine sediments, and the atmosphere (e.g., Bond et al., 2004; Goldberg et al., 1981; Schmidt and Noack, 2000; Suman et al., 1997) and the results have been used to infer BC transport and transformation processes (Figure 1). However, there are only few measurements of BC in river and estuary water (e.g., Mannino and Harvey; 2004; Masiello and Druffel, 1998; Mitra et al., 2002). Since BC is found in coastal and open ocean sediments, it is reasonable to assume that BC travels through the oceanic water column in particulate matter. After production, BC particles smaller than 100 μm can travel hundreds (within the planetary boundary layer) to thousands (within the free troposphere) of kilometers (Garstang et al., 1997; Seinfeld and Pandis, 1998) reaching even the most remote ocean sites (Currie, 2000; Goldberg, 1985). However, there are no measurements of BC in particulate organic matter in coastal or open oceans. As a result, currently we do not know: (1) the relative importance of BC transport to the sea via rivers versus through the atmosphere; (2) the percentage of particulate organic carbon (POC) in seawater that is BC; (3)

the fluxes of BC out of the water column; and (4) whether any BC transformation mechanisms might occur within the water column.

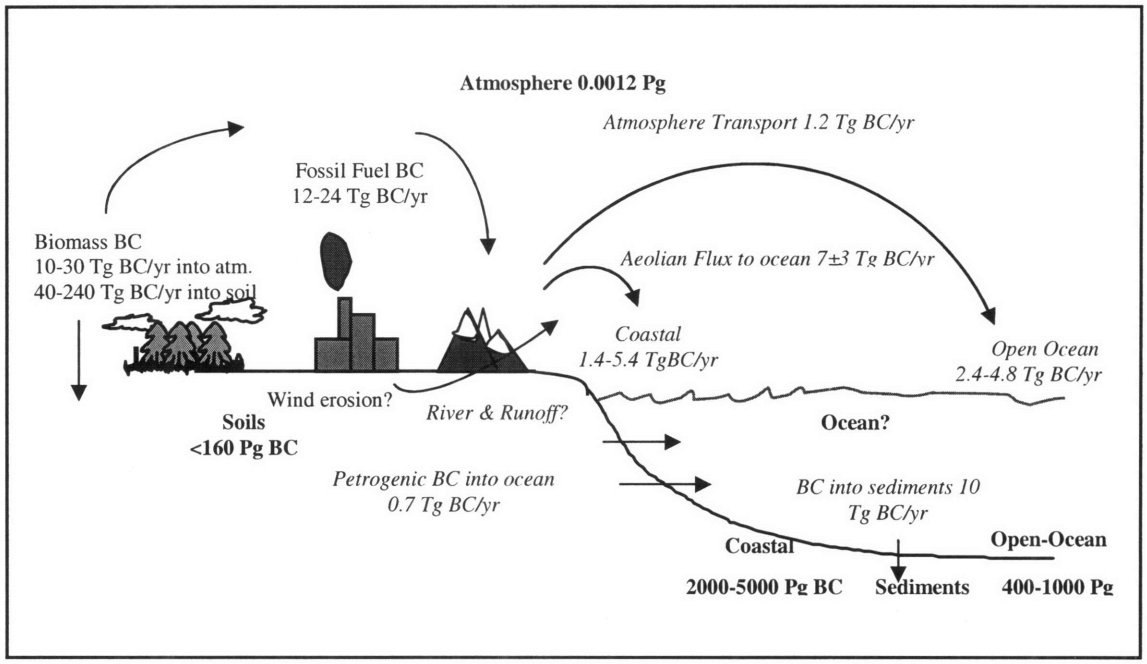


**Figure 1**. Black Carbon (BC) cycling in the environment: sources, fluxes and major reservoirs. Sources are in normal text, fluxes are in italics, and reservoirs are in bold (Figure adapted from Kuhlbusch, 1998; data from Czimczik et al., 2003; Dickens et al., 2004, 2004b; Hedges and Keil, 1995; Kuhlbusch and Crutzen, 1995; Masiello and Druffel, 1998; Masiello and Druffel, 2001; Mitra et al, 2002; Penner at al, 1993; Schmidt and Noak, 2000; Suman et al., 1997).

One of the main reasons for the lack of measurements in aquatic environments is the absence of a procedure to collect and quantify BC among potentially interfering matrices. BC quantification methodologies need to be able to differentiate between three different types of carbon: inorganic carbonates (IC), organic carbon that has not been thermally altered (OC), and BC. Present BC measurement techniques have been developed around the field of study of interest, and they are often designed to measure a particular characteristic of interest in a specific sample matrix. For example, atmospheric scientists are interested in a technique that relates to light absorption (hence blackness) of BC (e.g., Hansen et al., 1983; Liousse et al., 1996) in a matrix with relatively low concentrations of interfering particles. In contrast, geologists are mainly interested in the refractory properties of BC (e.g., Schmidt and Noack, 2001; Czimczik et al., 2003) in a more complex matrix with interfering particles at very high concentrations. A method that has been widely used and tested against potentially interfering materials in soils and sediments is the thermal oxidation method known as CTO 375 (Chemo-Thermal Oxidation at 375°C). However, recent studies have questioned the applicability of this method to quantify samples containing appreciable amounts of proteins, lipids, and carbohydrates, such as particulate organic matter (POM) in aqueous environments (Gustafsson et al., 1997; Gustafsson et al., 2001; Gelinas et al., 2001; Accardi-Day, 2003).

This thesis presents the first measurements of BC concentrations in POC samples collected from coastal seawaters and BC export fluxes from the water column. This study also presents the first comparison between BC fluxes out of the atmosphere into the water, out of the water column into the bed, and into the bed sediments in a coastal ocean. To this end, river water, coastal seawater, and sediment samples were collected from the Gulf of Maine (GoM), a representative coastal area downwind of important industrial and urban BC sources along the

Northeastern coast of the United States of America, in April and September of 2004. BC content in seawater was measured using the CTO 375 method (Gustafsson et al., 1997) with pre-combustion modifications to avoid charring. In addition, in order to examine the accuracy of the measurements, two secondary approaches to estimate BC were considered. First, since BC has a strong affinity for pyrene (Accardi-Dey and Gschwend, 2002), BC concentrations were inferred by observing diminished pyrene fluorescence when the samples were added to 1 ppb pyrene solutions. Second, geochemical consistency was verified within our samples, and between our measured water column export fluxes, atmospheric BC deposition estimates, and sediment burial in this region. Finally, to characterize the cycling of BC in the GoM, we calculated the various BC sources and sinks into and out of the GoM using box models that included estimates of atmospheric deposition and sedimentation rates.

**Organization and contributions of this thesis**

The contributions of this thesis are multidisciplinary. Measurements of BC in seawater provide useful information to account for BC losses and residence times in the water column; fluxes of BC out of the water column provide useful information to constrain atmospheric deposition and sedimentation rates allowing a better assessment of the influence of BC in different environments and the global carbon cycling; and finally, information about BC concentrations in seawater and sediments provide more accurate information to estimate sorption of hydrophobic organic compounds to the solid phase. The outline of this thesis is as follows:

Chapter 2 describes the CTO 375 methodology and the modifications made to this technique to prevent overestimation in matrices with high concentrations of interfering material. The modified CTO 375 was then tested with positive and negative controls, and applied to environmental samples of seawater POM. To have a better understanding of the physical,

chemical, and biological dynamics of the GoM, and to better assess the processes that might influence the fate and transformations of OC (and BC) in this coastal area, in Chapter 3 the cycling of OC in the GoM is assessed, and some of the main inputs, outputs, and particulate export fluxes of OC from the surface waters are identified. In Chapter 4, the modified CTO 375 methodology is applied to seawater POM samples collected during two cruises to the GoM in April and August, 2004. Using ancillary data, BC export fluxes from the water column are estimated; and geochemical consistency between atmospheric deposition and sedimentation rates is used to address the accuracy of the measurement. A mass balance is then used to estimate the main inputs, outputs, and possible transformations of BC in the water column. Chapter 5 describes the use of a novel methodology to measure BC by observing pyrene fluorescence losses (PFL) in a spiked sample, and compares the measured BC concentrations with the modified CTO 375 method in selected positive and negative standards, and our samples collected in the GoM. In Chapter 6 measurements of BC in sediment records provide information to assess the temporal and spatial variations in BC inputs into the GoM over the last 100 years. These observations indicate changes in the intensity and occurrence of BC sources and transport mechanisms in past decades. Chapter 7 is a concluding chapter to summarize the outcomes and implications of this study, and propose directions for future research in this area.

## References


Accardi-Dey, A., Gschwend, P.M., 2002. Assessing the combined roles of natural organic matter and black carbon as sorbants in sediments. Environ. Sci. Technol. 36, 21-29.

Accardi-Dey, A.M. 2003. Black carbon in marine sediments: quantification and implications for the sorption of polycyclic aromatic hydrocarbons. MIT-WHOI: Cambridge, MA.

Bond, T.I., Streets, D.G., Yarber, K.F., Nelson, S.M., Woo, J., Klimont, Z., 2004. A technology-based global inventory of black and organic carbon emissions from combustion. J. Geophys. Res. 109, D14203.

Currie, L.A., 2000. Evolution and multidisciplinary frontiers of $^{14}C$ aerosol science. Radiocarbon 42, 115-126.

Czimczik, C. I., Preston, C. M., Schmidt, W. I., Schulze, E., 2003. How surface fire in Siberia Scots pine forests affect soil organic carbon in the forest floor: Stocks, molecular structure, and conversion to black carbon (charcoal). Global Biogeochem. Cycles 17, 20.1-20.14.

Dickens, A. F., Gelinas, Y., Masiello, C. A., Wakeham, S., Hedges, J., 2004. Reburial of fossil organic carbon in marine sediments. Nature 427, 336-339.

Dickens, A. F., Gelinas, Y., Hedges, J., 2004b. Physical separation of combustion and rock sources of graphic BC in sediments. Mar. Chem. 92, 215-223.

Dockery, D.W., Pope, C.A., Xu, X.P., Spengler, J.D., Ware J.H., Fay, M.E., Ferris, B.G., Speize, F.E., 1993. An association between air pollution and mortality in six United States cities. N. Engl. J. Med. 329, 1753-1759.

Garstang, M., Tyson, P.D., Cachier, H., Radke, L., 1997. Atmospheric transports of particulate and gaseous products by fire. In Sediment Records of Biomass Burning and Global Change, Clark, J. S., Cachier, H., Goldammer, J. G., and Stocks Brian, Ed. Springer-Verlag, Berlin, Heildelberg.

Gelinas, Y., Prentice, K., Baldock, J. A., Hedges, J. I., 2001. An improved thermal oxidation method for the quantification of soot/graphitic BC in sediments and soils. Environ. Sci. Technol. 35, 3519-3525.

Goldberg, E. D., 1985. Black Carbon in the Environment. John Wiley & Sons, New York, NY, 198 pp.

Goldberg, E. D., Hodge, V. F., Griffin, J. J., Koide, M., 1981. Impact of fossil fuel combustion on the sediments of Lake Michigan. Environ. Sci. Technol. 15, 466-471.

Grigg, J., 2002. The effects of fossil fuel derived particles. Arch. Dis. Child 86, 79-83

Gustafsson, Ö., Haghseta, F., Chan, C., MacFarlane, J, Gschwend, P.M., 1997. Quantification of the dilute sedimentary soot phase: implications for PAH speciation and bioavailability. Environ. Sci. Technol. 31, 203-209.

Gustafsson, Ö., Bucheli, T. D., Kukulska, Z., Andersson, M., Largeau, C., Rouzad, J., Reddy, C. M., Eglinton, T. I., 2001. Evaluation of a protocol for the quantification of black carbon in sediments. Global Biogeochem. Cycles 15, 1-10.

Hansen, A. D. A., Rosen, H., Novakov, T., 1983. Aethalometer: An instrument for real-time measurement of optical absorption by aerosol particles. In Second Intern. Conf. on Carbonaceous Particles in the Atmosphere: Linz, Austria.

Hedges, J.I., Keil, R. G., 1995. Sedimentary organic matter preservation: an assessment and speculative synthesis. Mar. Chem., 49, 81-115.

IPCC (Intergovernmental Panel on Climate Change). Houghton, J. T., Ding, Y., Griggs, D. J., Noguer, M., Van der Linden, P. J., Dai, X., Maskell, K., Johnson, C. A., 2001. "Climate

Change 2001: The Scientific Basis. Contribution of Working Group 1 to the Third Assessment Report of the Intergovernmental Panel on Climate Change." Cambridge University Press, Cambridge, UK and New York, NY, USA.

Jacobson, M. Z., 2004. Climate response of fossil fuel and biofuel soot, accounting for soot's feedback to snow and sea ice albedo and emissivity. J. Geophys. Res. doi:10.1029/2004JD004945.

Kaufman, Y.J., Fraser, R. S., 1997. The effect of smoke particles on clouds and climate forcing. Science 277, 1636-1639.

Kuhlbusch, T. A., Crutzen, P. J., 1995. Toward a global estimate of black carbon in residues of vegetation fires representing a sink of atmospheric $CO_2$ and a source of $O_2$. Global Biogeochem. Cycles 9, 429-501.

Kuhlbusch, T. A., 1995. Method for determining black carbon in residues of vegetation fires. Environ. Sci. Technol. 29, 2695-2702.

Kuhlbusch, T.A., 1998. Black Carbon and the Carbon Cycle. Science, 280, 1903-1904.

Künzli, N., et al., 2000. Public-health impact of outdoor and traffic-related air pollution: a European assessment. Lancet 356, 795-801.

Lohmann, R., MacFarlane, J.K., Gschwend, P.M., 2005. Importance of black carbon to sorption of native PAHs, PCBs, and PCDDs in Boston and New York Harbor sediments. Environ. Sci. Technol. 39, 141-148.

Liousse, C., Penner, J.E., Chuang, C., Walton, J.J., Eddleman, H., 1996. A global three-dimensional study of carbonaceous aerosols. J. Geophys. Res. 101, D14, 19,411-19,423.

Mannino, A., Harvey, H.R., 2004. Black carbon in estuarine and coastal ocean dissolved organic matter. Limnol. Oceanogr. 49, 735 (2004).

Masiello, C.A., Druffel, E.R.M., 1998. Black carbon in deep-sea sediments. Science 280, 1911-1913.

Masiello, C.A., Druffel, E.R.M., 2001. Carbon isotope geochemistry of the Santa Clara River. Global Biogeochem. Cycles 15, 407-416.

Menon, S., Hansen, J., Nazarenko, L., Luo, Y., 2002. Climate effects of black carbon aerosols in China and India. Science 297, 2250-2253

Mitra, S., Bianchi, T.S., Mckee, B.A., Sutula, M., 2002. Black carbon from the Mississippi Rive: quantities, sources, and potential implications for the global carbon cycle. Environ. Sci. Technol. 36, 2296.

Park, R. J., Jacob, D. J., Chin, M., Martin, R. V., 2003. Sources of carbonaceous aerosols over the United States and implications for natural visibility. J. Geophys. Res. 108, 4355, doi:10.1029/2002JD003190.

Penner, J.E., Eddleman, H., Novakov, T., 1993. Towards the development of a global inventory for black carbon emissions. Atmos. Environ., 27A, 1277-1295.

Schmidt, M.W., Noack, A.G., 2000. Black carbon in soils and sediments: analysis, distribution, implications, and current challenges. Global Biogeochem. Cycles 14, 777-793.

Suman, D.O., Kuhlbusch, T.A.J., Lim, B., 1997. Marine sediments: a reservoir for black carbon and their use as spatial and temporal records of combustion. In Sediment Records of Biomass Burning and Global Change H. C. J. S. Clark, J. G. Goldammer, B. J. Stocks, Ed. (Springer-Verlag, Berlin) pp. 489.

# CHAPTER 2: EXAMINATION OF THE USE OF A THERMAL OXIDATION METHOD TO QUANTIFY BLACK CARBON IN SEAWATER PARTICULATE ORGANIC CARBON


## Abstract

Black carbon (BC), the name given to the material produced during incomplete combustion of biomass and fossil fuels, has potential implications for carbon sequestration. Nevertheless, due to scarce measurements of BC in the aqueous environments, we cannot currently assess the importance of BC cycling in the global carbon cycle. A method that has been widely used and tested against potentially interfering materials in soils and sediments is the thermal oxidation method known as CTO 375 (Chemo-Thermal Oxidation at 375°C). However, recent studies have questioned the applicability of this method to quantify BC in samples containing appreciable amounts of proteins, lipids, and carbohydrates, such as particulate organic matter (POM) in aqueous environments. In this chapter, the potential of the CTO 375 method is examined for quantifying BC in seawater POM after a series of sample manipulations to increase oxygen penetration into the sample matrix. To this end, we tested the modified CTO 375 method in positive and negative BC controls, as well as seawater phytoplankton as a proxy for seawater POM; then we applied the method to natural seawater POM. Our results suggest that such manipulations reduced charring of the non-BC, while underestimation of BC, if any, was minimal. BC concentration measured in natural seawater POM using this modified CTO 375 method of 3.41 ± 0.74 μg/L was consistent with previous measurements of BC in sediments. These results promote the application of this method to measure BC in seawater POM, while pointing out the importance of $O_2$ diffusion relative to heat diffusion in potentially interfering

matrices. Further testing of this method in natural seawater POM will provide valuable information to estimate BC budgets in the ocean, and to assess the impact of this material on the global carbon cycle.

## 1. Introduction

Black carbon (BC) is the name given to the soot and char produced during incomplete combustion of biomass and fossil fuels. Emissions of these materials have increased over the last century and are estimated to be between 6 to 24 Tg BC/yr for fossil fuels (Hendricks, 2004; Penner, 1993; Reddy, 2004) and 50 to 270 Tg BC/yr for biomass fuels (Kuhlbusch, 1995). Black carbon formation places carbon that would otherwise turn into $CO_2$ into a material relatively resistant to degradation in natural environments (Mader et al., 1997; Masiello and Druffel, 2003; Middleburg et al., 1999; Kuhlbusch and Crutzen, 1995). As a result, BC affects the dynamics and storage characteristics of organic matter by removing carbon from a fast cycling biosphere into a long-term geological carbon cycle. Thus, BC might account for 2-16% of the 1800 to 2400 Tg C/yr of the "missing C" of the dynamic carbon cycle.

Although measurements of BC have increased in the past 30 years (Masiello, 2004), little is known about the fate of BC transported along rivers and the size of the ocean BC reservoir. Measurements of BC in the atmosphere (e.g., Bond et al., 2004; Cooke and Wilson, 1993; Park et al, 2003), soil (e.g., Accardi-Dey and Gschwend, 2003; Czimczik et al., 2003; Schmidt and Noack, 2000; Schmidt et al., 2001), and sediments (e.g., Gustafsson and Gschwend, 1998; Masiello and Druffel, 1998; Middleburg et al., 1999; Suman et al., 1997) are extensive. In contrast, there are only few measurements of BC in rivers and coastal waters (Mannino and Harvey, 2004; Masiello and Druffel, 2001; Mitra et al., 2002; Kim et al., 2004; Simpson and Hatcher, 2004). Since BC has been found to be ubiquitous in marine sediments (Goldberg, 1985; Suman et al., 1996), it is reasonable to assume that BC is present in the ocean's water column. However, no generally accepted methodology to measure BC in particulate organic matter

(POM) has been developed. As a result, currently we cannot assess with confidence the importance of BC in the oceans in the global carbon cycle.

BC quantification methodologies need to be able to differentiate between three different types of carbon: inorganic carbonate (IC), organic carbon that has not been thermally altered (OC), and BC. Present BC measurement techniques, developed around the fields of study dedicated to BC, are often designed to measure a particular characteristic of interest in a specific sample matrix. For example, atmospheric scientists interested in the effect of BC in the radiative heat balance measure the blackness of the carbonaceous material present in airborne aerosols (e.g., Hansen et al., 1983; Liousse et al., 1996). In contrast, oceanographers interested in the refractory properties of carbon in the ocean sediments measure the recalcitrance of the organic carbon accumulated at the bottom of the ocean (e.g., Dickens et al., 2004; Gustafsson et al., 1997; Middleburg et al., 1999). It is clear that the matrices of these two environments are very different. BC-containing aerosol particles in the atmosphere are more dispersed and found at lower concentrations than in soils and sediments. In addition, the presence of interfering particles is lower in atmospheric sample matrices than in sediments. Therefore, the selection of a methodology to quantify BC should be based on the characteristic of interest (e.g., darkness or resistance), but also the presence of potential interfering materials.

One of the most widely used and evaluated methodologies to quantify BC in soils and sediments is a thermal oxidation technique known as CTO 375 (Gustafsson et al., 1997). CTO 375 stands for Chemo-Thermal Oxidation at 375 °C, and this method is designed to oxidize the labile OC present in a sample during a 24 h oxidation at 375 °C under excess air, followed by an acidification to remove any IC present in the sample, and carbon quantification of the remaining material (e.g., using an elemental analyzer). The results of recent intercomparison studies

showed a wide range of concentrations in individual samples when measured using different methods (Currie et al., 2001; Hammes et al., 2007; Schmidt and Noack, 2000). It was concluded that one of the most consistent methodologies for measuring BC in the presence of interfering materials was CTO 375. However, the applicability of this methodology to measure BC in sample matrices other than soil and sediments has been questioned. Common critiques of the CTO 375 technique are (1) underdetection of charcoal, a more labile form of BC (Elmquist et al., 2006; Hammes et al., 2007; Nguyen et al., 2004), and other less robust BC particles (Jonker and Koelmans, 2002; Nguyen, 2004); and (2) overdetection due to charring of the non-BC fraction in samples where particle agglomerates (Accardi-Dey, 2003) or appreciable amounts of proteins, lipids and carbohydrates are present (Accardi-Day, 2003; Gelinas et al., 2001; Gustafsson et al., 2001; Gustafsson et al., 1997).

While underdetection of more labile forms of BC using CTO 375 is generally accepted (Hammes et al., 2007), the main factors leading to overdetection of BC due to deficient oxygen penetration into the sample matrix are still under debate. Gelinas et al. (2001) pointed out that positive biases of the CTO 375 method could be caused by the incomplete removal of non-BC, or the formation of condensation products (during "browning" reactions) produced when macromolecular biopolymers (e.g., lipids, proteins and carbohydrates) are present, leading to the creation of enclosed spaces that reduce oxygen penetration to the sample matrix. As a result, Gelinas et al. (2001) suggested an acid treatment step prior to application of the CTO 375 method to expose any biochemical entrapped in a mineral matrix to complete oxidation. Accardi-Dey (2003) also observed that samples containing macromolecular bipolymers led to overestimation of the BC, but she also pointed out the importance of small particle sizes and the lack of agglomerates to guarantee complete oxidation of non-BC organic carbon. However, in

an attempt to further evaluate the use of CTO 375 for potentially interfering materials, Gustafsson et al. (2001) analyzed different sample matrices, and found that in most cases, with the exception of phytoplankton, charring due to interferences was low and didn't affect BC concentration estimates. Overall, these previous studies have shown the importance of $O_2$ diffusion and heat transfer throughout the sample matrix to overestimate or underestimate BC using CTO 375.

The main purpose of this study was to assess the potential of a modified CTO 375 to quantify BC in seawater particulate organic matter (POM), a complex matrix prone to charring. The modified CTO 375 includes a number of pre-combustion manipulation techniques to ensure oxygen access to internal locations of the sample: (1) we only used small sample sizes; (2) if solid, the samples were ground to less than 100 μm particle size to minimize diffusive distances; or if wet, the samples were passed through a 53 μm Nitex screen and frozen to promote cell lysing; (4) the combustion temperature was slowly increased to ensure heat penetration into the sample did not substantially precede oxygen penetration from the air. We tested the modified method in standard samples, where BC had been previously measured, and algae cultures as proxy for seawater POM. Finally, we applied the method to natural seawater POM and compared our values with BC concentrations previously reported for sediments in areas nearby.

## 2. Methods and Materials

### *2.1. Samples used for CTO 375 method testing*

To test whether BC underestimation or overestimation was present after manipulation of our samples and to ensure complete combustion of the non-BC fraction, we used (a) positive controls where BC has been previously measured, and where charring has not been reported to

be a concern, (b) negative controls that contain no pyrogenic BC, but where charring has been previously reported, and (c) algae culture samples as a proxy for seawater particulate organic carbon.

*Positive controls.*

*NIST 1649a and 1650 SRM*. The National Institute of Standards & Technology (NIST) Standard Reference Materials 1649a, urban dust, and 1650, diesel particulate matter (NIST, Gaithersburg, MD), have been thoroughly characterized and used as a positive standard for the development and testing of CTO 375 (Currie et al., 2001; Gelinas et al., 2001; Gustafsson et al., 2001; Gustafsson et al., 1997; Hammes et al., 2007).

*Negative controls.*

*Melanoidin*. This synthetic material was prepared through a hot acid treatment of glucose and urea (by K. Hammes, University of Zürich, Switzerland) and, although it has been suggested to have structural similarity to organic matter, it contains no material produced by combustion. Still, nonzero BC values have been previously reported for this material using CTO 375 (Elmiquist et al., 2006; Gustafsson et al., 2001; Hammes et al., 2007).

*Bovine Serum Albumin*. Bovine serum albumin (BSA; Fluka BioChemika; MW = 67,000 g/mol) is a globular protein high in nitrogen, an element which have been suggested to be responsible for charring (Accardi Dey, 2003; Gelinas et al., 2001; Gustafsson et al., 2001).

*Algae samples.*

Eight algae samples were used to test CTO 375. The first algae sample consisted of a mixture of seawater cultures (Table 1) obtained from Carolina Biological Supply Company (Burlington, NC). This algae mixture included diatoms and coccolithophores, phytoplankton typically observed in coastal areas, such as the Gulf of Maine (Menden-Deuer and Lessard,

2000; Townsend and Keller, 1996). The other seven samples were individual algae cultures (Table 1) kindly provided by Dr. Zachary Johnson (at the time in the Chisholm Lab, MIT, USA) and included cells from different taxonomic classes grown in different excess or limiting nitrogen conditions (Table 2).

*Natural sample: Fluen Point, Marblehead, Massachusetts seawater POM*

Fluen Point is a small private beach in Marblehead, MA, a small suburban area (20,200 people) about 25 km from Boston. Surface seawater was collected in two 40 L glass containers that had been thoroughly washed with methylene dichloride, methanol, and low-carbon water (produced using an Aries Vaponic system, Rockland, MA). After collection, the samples were taken immediately to the lab and stored at 4 °C in dark for 1 day to allow larger particles to settle.

*2.2. Total organic carbon (TOC) and BC quantification*

*Quantification of TOC in solid samples*

Solid samples were homogenized by shaking and stirring in the containers in which the samples were stored. Triplicates of each sample (between 1 and 10 mg) were transferred into precombusted and tared crucible-shaped Ag capsules (D2008, 8 x 5 mm; Elemental Microanalysis Ltd, EMAL Tech, OH). The Ag capsules were placed into precombusted 10-mm glass petri dishes in arrays of six capsules per petri dish and dried at 60 °C overnight (~15 hr). After cooling to room temperature, the samples were weighed using a microbalance (Cahn 25 Automatic Electrobalance; Ventron Corp., Cerritos, CA), acidified with about 100 μL of 6% by volume sulfurous acid ($H_2SO_3$; Fisher Chemicals, Fairlawn, NJ), and re-dried at 60 °C overnight. The carbon weight percent of the samples was determined using a carbon-hydrogen-nitrogen

(CHN) analyzer (Vario EL, Elementar America, Inc., NJ) operated with a copper oxide catalyst at 950 °C, a thermal conductivity detector (TCD), and helium (He) as the flushing and carrier gas. The detection limit of the analyzer was < 1 μg of carbon.

*Quantification of BC in solid samples*

For solid samples, about 25 mg of each sample were ground to <100-μm sized particles with an agate mortar and pestle (Figure 1). Samples between 2 and 7 mg of the ground material were placed into precombusted and tared crucible-shaped Ag capsules (D2008, 8x5 mm; Elemental Microanalysis Limited, EMAL Tech, OH) and carefully spread over the entire surface of the capsules with the purpose of avoiding sample agglomeration. The Ag capsules were then placed into precombusted 10 mm glass petri dishes in arrays of six capsules per petri dish and dried at 60 °C overnight (~ 15 hr). After cooling to room temperature, the samples were weighed using a microbalance (Cahn 25 Automatic Electrobalance; Ventron Corp., Cerritos, CA) and combusted in a F47915 Thermolyne muffle furnace (Barnstead Thermolyne International, Dubuque, IA) at 375 °C for 24 hr under excess air. The single set controller of the muffle furnace was initially set at 60 °C, ramped from 60 °C to 150 °C at a rate of 1 °C/s where it was held for 25 min, again ramped from 150 °C to 250 °C at a rate of 1 °C/s and held there for 25 min, and finally ramped from 250 °C to 360°C at a rate of 1 °C/s, from 360 °C to 370 °C at a rate of 0.2 °C/s, and from 370 to 375 °C at a rate of 0.05 °C/s. Following, the temperature remained at 375 ± 1 °C for 24 hr. The temperature was measured using a chromel/alumel thermocouple.

After cooling, 25 μl of low-carbon water (Aries Vaporics, Rockland, MA) were added to each Ag capsule, followed by about 100 μl of 0.73 M $H_2SO_3$ (Fisher Chemicals, Fairlawn, NJ) to decompose any carbonates. The samples were allowed to sit at room temperature for 1 hr, and this procedure was repeated until no effervescence was observed in the sample after the addition

of acid. Then, the sample was dried overnight at 60 °C (~15 hr), and the composition of the oxidized and acidified samples was determined using a CHN analyzer (Vario EL, Elementar America, Inc., NJ) operated under the same conditions as the ones described above.

For every three samples of TOC or BC, a pair of sample blanks, which consisted of an empty silver capsule processed in the same manner as all the samples, was included in the batch.

*Quantification of TOC in aqueous-suspension samples*

To collect the samples in aqueous suspensions, a 53-μm mesh-opening pre-cleaned Nitex screen (TETKO, Depew, NY) was used as a prefilter, followed by a 0.7-μm pre-combusted fiber glass (GFF) filter (Pall Gelman Sciences, Ann Harbor, MI; Figure 2) . The sample was placed on a pre-combusted 300 mL glass funnel locked to a 45-mm pre-combusted glass filter holder with a fitted glass screen (Millipore, Billerca, MA) containing the prefilter and filter, and vacuum was applied to filter the sample. However, if the sample was highly concentrated, only a small volume of the suspension was dripped directly onto the prefilter and filter. After filtration, all samples were rinsed immediately with about 20 mL of 10 mM $H_2SO_3$ (Fisher Chemicals, Fairlawn, NJ) to remove carbonates and then about 30 mL of low-carbon water (Aries Vaporic, Rockland, MA) to remove salts. Sample blanks consisted of filtering a similar volume of low-carbon water (Aries Vaporic, Rockland, MA) and processing the blank-sample in the same manner as all the samples. One fourth of the sample was used for OC measurements, and the rest was stored frozen in pre-combusted 10-mm glass petri dishes. Carbon content of the samples was determined using a CHN analyzer (Vario EL, Elementar America, Inc., NJ) operated under the same conditions as described above.

*Quantification of BC in aqueous-suspension samples*

Half of the frozen filtered samples were dried at 60 °C overnight (~15 hr) and combusted in a F47915 Thermolyne muffle furnace (Barnstead Thermolyne International, Dubuque, IA) at 375 °C for 24 hr under excess air (Figure 2). The temperature program of the muffle furnace was the same as used for the solid samples. The composition of the samples was determined using a CHN analyzer (Vario EL, Elementar America, Inc., NJ) operated under the same conditions described above.

Special precautions to consider when quantifying BC in aqueous-suspension samples include: (a) Remove as much water as possible from the filter before taking it off from the filtration device; water stagnation in the filter promotes particle aggregation (that might lead to charring) and heterogeneity of the sample; (b) avoid compaction of the filter, since this mechanism reduces the porous space of the filter, limiting oxygen to the filtered sample; (c) cut off the edges of the filter with an acetone cleaned razor blade (or other sharp stainless steal object), as this part of the filter is subject to sample manipulation and might be prone to charring; and (d) use variability of BC measurements between replicates of the same sample as a tool to address whether or not charring might be present; substantial differences between replicates might be indicative of charring.

## 3. Results and Discussion

### *3.1. Positive controls.*

Our measured concentration of BC in NIST 1649a SRM urban dust ($1.51 \pm 0.19\%_{dw}$) was statistically indistinguishable from what Gustafsson et al. (2001) reported (Table 2). Similar to this study, Gustafsson et al. (2001) paid close attention to minimizing charring in samples. In order to ensure enough oxygen throughout the sample matrix, in addition to using a muffle

furnace with a controlled temperature for the 375 °C combustion, Gustafsson et al. (2001) also used a tube furnace system with a constant air flow rate of 200 mL/min. However, their BC concentrations reported using the muffle furnace or the tube furnace were not statistically different from each other (1.36 ± 0.07 and 1.40 ± 0.14%$_{dw}$) or from our observed values. In contrast, the BC concentration we had previously reported (2.52 ± 0.06; team no.5 in Hammes et al., 2007), where no temperature program was used, was significantly higher than what we report here. The difference between these BC values suggested that a rapid increase in temperature (and heat diffusion) may not allow enough time for oxygen to penetrate deeper into the sample matrix as the non-BC material starts to oxidize, leading to charring of the non-BC material and an overestimation of BC content. Furthermore, the higher carbon-to-nitrogen (C/N) ratio observed in this study (35.7 ± 4.8) than in previous studies (team no. 5 in Hammes et al., 2007; 13.3 ± 7.2) suggested less charring of proteinaceous molecules in the sample.

BC concentration in NIST 1650 SRM diesel soot of 38.4 ± 4.6%$_{dw}$ (Table 2) and our observed C/N ratio of > 1030 suggested that the remaining material was highly carbonaceous (Fernandes et al., 2003), and for this sample charring was not an issue. This value is lower than the value previously reported by Gustafsson et al. (2001) (48.1 ± 0.5%$_{dw}$), but is equivalent to the value reported by Gelinas et al. (2001) after removing hydrolysable OC (38.4 ± 0.6%$_{dw}$). Gustafsson et al. (2001) also paid close attention to thinly spreading the samples before combusting them, and they showed high resolution TEM (Transmission Electron Microscope) images to further corroborate the absence of charring in their measurements. Therefore, our lower value may be an indication of BC underestimation.

*3.2. Negative controls*

BC concentrations in the synthetic melanoidin using the described sample manipulations were $0.04 \pm 0.06\%_{dw}$. This value is lower than what others have reported. Gustafsson et al. (2001) reported a value of $0.18 \pm 0.14\%_{dw}$, and Elmiquist et al. (2006) reported a value of $2.5 \pm 0.2\%_{dw}$ (Table 1). However, in contrast with our observation for NIST 1649a, the value that we report here is not different from the one we had previously estimated (Hammes et al., 2007; team no. 5). This observation may indicate that, while for NIST 1649a a slow temperature increase may be more important to reduce charring, in melanoidin-like samples, sample manipulation (i.e., using small sample sizes and thinly spreading the sample) might be more important. Although our calculated BC concentrations were not significantly different from zero, our very low C/N ratios (about 1:1) may indicate the survival of N-containing macromolecules.

Although no pyrogenic material should be present, we observed BC concentrations different from zero ($0.50 \pm 0.04\%_{dw}$) in our BSA samples. This BC concentration is close to the value reported by Accardi-Dey (2003), but is significantly lower than BC values previously measured by Gustafsson et al. (2001) for the same material. TOC of the BSA used by Accardi-Dey (2003) was significantly lower, indicating that the percentage of non-BC charred in TOC was higher than in our samples. However, C/N ratios reported by Accardi-Dey (2003) were similar to ours (between 2 and 3 to 1) , suggesting that N-containing macromolecules survived oxidation in both cases.

To further evaluate the potential of BSA-like materials to interfere with BC measurement, we used a standard addition approach that consisted of adding increasing amounts of NIST 1650 to an initial mass of BSA (Figure 5). Instead of seeing an increase in the BC measured (indicative of charring) when NIST 1650 was added to BSA, we measured lower BC values than when only NIST 1650 was present. Elmiquist et al. (2004) reported a similar

observation when adding a standard (NIST 2975 SRM) to sediments, and suggested that the underestimation was due to the presence of a mineral matrix acting as an oxidation catalyst. Melanoidin does not have a mineral matrix. However, melanoidin and NIST 1650 may interact in a way that promotes a more complete combustion.

*3.3. Algae samples.*

Similar to the process of grinding and thinly spreading solid samples to ensure complete combustions of the non-BC material, freezing has the potential to enhance $O_2$ penetration in a sample matrix that contains small amounts of water. Cellular level studies have shown that freezing, widely used for RNA extraction, causes the cells to lyse (Kahan et al., 1997; Klebe et al., 1996; Tran-Son-Tay et al., 1990). The theory behind this lysing process is that, as water freezes, ice crystals grow, disrupting cellular organelles and cell walls as well as other molecular aggregates present in the sample. To further understand the influence of freezing as a tool to expose any entrapped material present in potentially interfering matrices, we compared BC values of frozen and unfrozen samples (Table 2).

Both carbon and nitrogen concentrations observed in the frozen subsamples of the algae mixture were below detection limits. However, C levels in the non-frozen samples were also very close to zero, and no N was detected after combustion. Gustafsson et al. (2001) previously reported charring in freeze-dried coccolithophore exudates but not in other (whole) phytoplankton cultures using the CTO 375 method. Yet, they also pointed out that a modified procedure to enhance oxygen diffusion into the exudates or temperature ramping to slow the increase of temperature in the samples could lead to less charring. Consistent with this discussion, the slow increase of the combustion temperature in our modified procedure might

have lead to the complete combustion of the coccolithophores in our samples. To further corroborate this hypothesis, we measured the remaining C after the combustion at 375 °C for 24 hours without a temperature ramp. The resulting concentration of 0.016 ± 0.001 μg/mL and C/N ratio of 0.08 ± 0.01 supported our hypothesis.

Comparison of BC values between frozen and unfrozen subsamples of the individual algae cultures were not significantly different from one another, and, in both cases concentrations were close to zero. However, in most of the frozen samples no N remained after the 375 °C combustion, whereas in the non-frozen samples low C/N ratios indicate that appreciable amounts of N remained in the sample. This observation suggests that freezing successfully exposed N-containing macromolecules, and that the remaining carbon material may be due to the presence of small aggregates or impurities (BC or BC-like materials) present in the samples. Two exceptions where N remained in the frozen samples after the 375 °C combustion were *Nannochloropsis gaditana* and *Pelagomonas calceolata*. Differences in the structure and composition of the sampled algae cultures might explain the observed differences. Popp et al. (1998) observed that phytoplankton cell geometry (volume-to-surface-area ratio; V/S) had an effect on carbon isotopic fractionation due to differences in $CO_2$ diffusive fluxes; i.e., $CO_2$ diffusion would be lower for higher V/S. Since V/S is largest for sphere-shaped phytoplankton (Lewis, 1976) lower $O_2$ diffusion into *N. gaditana* (Figure 4) might explain the higher C and N values observed for this algae species. In contrast, the shapes of phytoplankton species from the Chlorophyceae and Bacillariophyceae classes (Figure 4) have lower V/S (Lewis, 1976). Furthermore, previous studies (Canavate and Lubin, 1995; 1995b) have reported that *N. gaditana* belongs to a small group of algae (Estigmatophyceae) that has a cryopreservative mechanism (i.e., these algae are freezing resistant and able to recover after thawing) and contain non-

hydrolysable macromolecular constituents (algaenans; Gelin et al., 1997; Grossi et al., 2001) that might reduce $O_2$ diffusion throughout the phytoplankton cell. Similarly, although the shape of *P. calceolate* has a higher V/S than *N. gaditana*, this algae species is known to have an organic shell, or theca, composed of polysaccharides (Andersen et al., 1993). Some dinoflagellates present in the algae mixture (*Prorocentrum micans* and *Amphidiniumcarterae*; Figure 3) also have a theca, but have a cell geometry with a much higher V/S than *N. gaditana* and *P. calceolate* (Lewis, 1976). These results suggested that both geometry and exterior constituents of phytoplankton cells were responsible for the observed C and N values.

*3.4. Natural seawater POM*

TOC and BC concentrations in seawater POM collected in Fluen Point were 83.0 ± 6.33 and 3.41 ± 0.74 μg/L ($n$=2), respectively. Seawater C/N ratios before CTO 375 of 16.53 ± 0.27 indicated terrestrial inputs to this area. Nitrogen concentrations after combustion were below detection limits (C/N > 3.4 μg /N detection limit in μg), suggesting that no N-containing macromolecules survived the modified CTO 375. Ratios of BC to TOC previously reported in near-urban sediments in New England were between 0.03 and 0.13 (Gustafsson et al., 1998), which is consistent with our BC to TOC ratio of 0.04 ± 0.01 measured in seawater POM.

To further test the modified CTO method's ability to quantify BC in seawater POM, we added increasing amounts of NIST 1650 to about 500 mL of Fluen Point seawater. Due to its high hydrophobicity, to be able to add this material to the aqueous sample, we made a suspension of NIST 1650 SRM in ethyl acetate. However, our observed BC concentrations were below the predicted concentrations and presented high variability between samples (Figure 6). While it is possible that some of the NIST 1650 was lost to the glass walls of the micropipette and sample

vessels, this result also suggests that in suspension NIST 1650 particles became more dispersed and labile to combustion, leading to underestimation of BC. The development of a thermogram for the NIST 1650 ethyl acetate suspension supported our hypothesis (Figure 7a). The percentage of BC in TOC measured in the NIST 1650 suspension at 375 °C was 9.26% (as opposed to the previous value of 52.15% BC/TOC). In addition, the concentration of carbon remaining after combustion remained relatively constant (84.27 ± 7.93%), indicating that other elements, besides carbon, also became more labile in the ethyl acetate suspension (Figure 7b).

## 4. Conclusions

We assessed the use of CTO 375 to quantify BC in seawater POC. To this end, we used positive and negative controls to quantify over- or under-estimations of BC due to various sample manipulations. BC values for positive standards were very close to values in literature, and C/N ratios of the remaining material indicated the presence of soot-like materials (Fernandes et al., 2003). These results indicated that underestimation due to the modification of CTO 375, if present, was minimal. BC concentrations in TOC of the negative controls were different from zero, but smaller than what has been previously reported, and represented a percentage of less or equal to 1% of the TOC. Although this is a good indicator that the modified CTO 375 possibly reduced charring, the very low C/N ratios observed for both, melanoidin and BSA, may have resulted either from the encapsulation of N-containing macromolecules that limited oxygen accessibility to the sample matrix, or the presence of an organic nitrogen recalcitrant enough to survive CTO 375. However, a standard additions approach, where BC concentrations in NIST 1650 did not increase as BSA was added to it, suggested that the potential of BSA-like materials to interfere with our measurements in BC-containing matrices was small. The application of this

modified CTO 375 to phytoplankton indicated that BC measurements using this method are reliable for the most part, but precaution should be taken if certain phytoplankton species (e.g., those with high V/S, cryopreservants, algaenans, and/or theca) are present at high concentrations in the collected seawater POC. For example, during spring or fall blooms, when diatoms are the most common species, BC measurements might be more reliable than during the summer, when theca-containing dinoflagellate blooms may be more abundant. Finally, our measured fraction of BC in natural seawater POM was consistent with proportions of this material in near-urban sediments. The application of this modified method to a wide range of sample matrices and its evaluation for geochemical consistency in environmental samples provided further information to assess the broader applicability of these results, as well as a good understanding of the advantages and limitations of the modified CTO 375.

Further testing in diverse environmental aqueous matrices and the application of this method to POM in aqueous environments will provide valuable information to assess the role of aqueous bodies in the global carbon cycle.

## 5. Acknowledgments

Zachary Johnson is gratefully acknowledged for providing algae cultures. We are grateful for support from NFS grants (OCE-0223441 and BES-0607136) and CONACYT and MSFS fellowships to D. F.

## References

Accardi-Dey, A .M. 2003. Black carbon in marine sediments: quantification and implications for the sorption of polycyclic aromatic hydrocarbons. MIT-WHOI: Cambridge, MA.

Accardi-Dey, A., Gschwend, P.M., 2002. Assessing the combined roles of natural organic matter and black carbon as sorbants in sediments. Environ. Sci. Technol. 36, 21-29.

Allar, B., Templier, J., and Largeau, C. Artifactual origin of mycobacterial bacteran. Formation of melanoidin like artifact macromolecular material during the usual isolation process. *Org. Geochem.* 1997, 26: 691-703

Andersen, R. A., Saunders, G. W., Paskind, M. P., Sexton, J. P., 1993. Ultrastructure and 18S rRNA gene sequence for Pelagomonas calceolate gen. et. sp. nov. and the description of a new algae class, the pelagophyceae classis nov. J. Phycol. 29, 701-715.

Bond, T.I., Streets, D. G., Yarber, K. F., Nelson, S. M., Woo, J., Klimont, Z., 2004. A technology-based global inventory of black and organic carbon emissions from combustion. J. Geophys. Res. 109, D14203.

Canavate, J. P., Lubian, L. M., 1995. Some aspects on the cryopreservation of microalgae used as food for marine species. Aquaculture 136, 277-290.

Canavate, J. P., .Lubian, L. M., 1995b. Relationship between cooling rates, cryoprotectant concentrations and salinities in the cryopreservation of marine microalgae. Marine Biol. 124, 325-334.

Cooke, W. F., Wilson, J. J. N., 1993. A global carbon aerosol model. J. Geophys. Res. 101, 19.292-19.409.

Currie, L. A., Benner, B. A., Kessler, J. D., Klinedinst, D. B., Klouda, G. A., Marolf, J. V., Slater, J. F., Wise, S. A., Cachier, H., Cary, R., Chow, J. C., Watson, J., Druffel, E. R. M., Masiello, C. A., Eglinton, T. I., Pearson, A., Reddy, C. M., Gustafsson, Ö., Quinn, J. G., Hartmann, P. C., Hedges, J. I., Prentice, K. M., Kirchstetter, T. W., Novakow, T., Puxbaum, H., and Schmid, H. A Critical Evaluation of Interlaboratory Data on Total, Elemetnal, and Isotopic Carbon in the Carbonaceous Particle Reference Material, NIST SRM 1649a. *J. Res. Natl. Inst. Stand. Technol.* 2002, 107: 279-298

Czimczik, C. I., Preston, C. M., Schmidt, W. I., Schulze, E., 2003. How surface fire in Siberia Scots pine forests affect soil organic carbon in the forest floor: Stocks, molecular structure, and conversion to black carbon (charcoal). Global Biogeochem. Cycles 17, 20.1-20.14.

Dickens, A. F., Gelinas, Y., Masiello, C. A., Wakeham, S., Hedges, J., 2004. Reburial of fossil organic carbon in marine sediments. Nature 427, 336-339.

Elmquist, M., Cornelissen, G., Kukulska, Z., Gustafsson, Ö.., 2006. Distinct oxidative stabilities of char versus soot black carbon: Implications for quantification and environmental recalcitrance. Global Biogeochem. Cycles 20, doi:10.1029/2005GB002629

Fernandes, M. B., Skjemstad, J. O., Johnson, B. B., Wells, J. D., Brooks, P., 2003. Characterization of carbonaceous combustion residues. I. Morphological, elemental and spectroscopic features. Chemosphere 51, 785-795.

FIRM (Finnish Institute of Marine Research), 2008. The Baltic Sea Portal. www.balticseaportal.fi (accessed March 05, 2008).

Gelin, F., Boogers, I., Noordeloos, A. A. M., Sinninghe Damste, J. S., Riegman, R., De Leeuw, J. W., 1997. Resistant biomacromolecules in marine microalgae of the classes Eustigmatophyceae and Chlorophyceae: Geochemical implications. Org. Geochem. 26, 659-675.

Gelinas, Y., Prentice, K., Baldock, J. A., Hedges, J. I., 2001. An improved thermal oxidation method for the quantification of soot/graphitic BC in sediments and soils. Environ. Sci. Technol. 35, 3519-3525.

Grossi, V., Blokker, P., Sinninghe Damsté, J. S., 2001. Anaerobic biodegradation of lipids of the marine microalga Nannochloropsis salina. Org. Geochem. 32, 795-808.

Gustafsson, Ö., Bucheli, T. D., Kukulska, Z., Andersson, M., Largeau, C., Rouzad, J., Reddy, C. M., Eglinton, T. I., 2001. Evaluation of a protocol for the quantification of black carbon in sediments. Global Biogeochem. Cycles 15, 1-10.

Gustafsson, Ö., Haghsete, F., Chan, C., MacFarlane, J., and Gschwend, P. M.. Quantification of the Dilute Sedimentary Soot Phase: Implications for PAH Speciation and Bioavailability. *Environ. Sci. Technol.*1997, 31: 203-209.

Gustafsson, Ö., Gschwend, P. M., 1998. The flux of black carbon to surface sediments on the New England continental shelf. Geochim. Cosmochim. Acta, 62, 465-472.

Hammes, K., Schmidt, M. W., Curri, L. A., Ball, W. P., Nguyen, T. H., Louchouarn,, P., Houel, S., Gustafsson, O., Elmquist, M., Cornelissen, G., Smernik, R. J., Skjemstad, J. O., Masiello, C. A., et al., 2007. Comparison of black carbon quantification methods using reference materials form soil, water, sediment and the atmosphere, and implications for the global carbon cycle. Global Biogeochem. Cycles 21, doi: 10.1029/2006GB002914.

Hansen, A. D. A., Rosen, H., Novakov, T., 1983. Aethalometer: An instrument for real-time measurement of optical absorption by aerosol particles. In Second Intern. Conf. on Carbonaceous Particles in the Atmosphere: Linz, Austria.

Hendricks, J., Kächer, B., Döpelheuer, A., Feichter, J., Lohmann, U., 2004. Simulating the global atmospheric black carbon cycle: a revisit to the contribution of aircraft emissions. Atmos. Chem. And Phys. Discuss., 4, 3485-3533.

Jonker, M. T., Koelmans, A. A., 2002. Sorption of PAHs and PCBs to soot and soot-like materials in the aqueous environment: mechanistic consideration. Environ. Sci. Technol. 36, 3725-3734.

Kahan, A. A., Cerniglia, C. E., 1997. Rapid and sensitive method for the detection of Aeromonas caviae and Aeromonas trota by polymerase chain reaction. Letters Appl. Microbiol. 24, 233-239.

Kim, S., Kaplan, L. A., Benner, R., Hatcher, P. G., 2004. Hydrogen deficient molecules in natural riverine water samples – evidence for the existence of BC in dissolved organic matter. Mar. Chem. 92, 225-234.

Klebe, R. J., Grant, G. M., Grant, A. M., Garcia, M. A.,Giambernardi, T. A., Taylor, G. P., 1996. RT-PCR without RNA isolation. Biotechniques 21, 1094-1100.

Kuhlbusch, T. A., 1995. Method for determining black carbon in residues of vegetation fires. Environ. Sci. Technol. 29, 2695-2702.

Kuhlbusch, T. A. J., Crutzen, P. J., 1995b. Toward a global estimate of black carbon in residues of vegetation fires representing a sink of atmospheric CO2 and a source of O2. Global Biogeochem. Cycles 9, 491-501.

Lewis, W. M., 1976. Surface/volume ratio: Implications for phytoplankton morphology. Science 192, 885-887.

Liousse, C., Penner, J. E., Chuang, C., Walton, J. J., Eddleman, H., 1996. A global three-dimensional study of carbonaceous aerosols. J. Geophys. Res. 101, D14, 19,411-19,423.

Mader, B. T., Uwe-Goss, K., Eisenreich, S. J., 1997. Sorption of nonionic, hydrophobic organic chemicals to mineral surfaces. Environ. Sci. Technol. 31, 1079-1086.

Mannino, A., Harvey, H. R., 2004. Black carbon in estuarine and coastal ocean dissolved organic matter. Limnol. Oceanogr. 49, 735 (2004).

Masiello, C. A., 2004. New directions in black carbon organic geochemistry. Marine Chemistry 92, 201-213.

Masiello, C. A., Druffel, E. R. M., 2001. Carbon isotope geochemistry of the Santa Clara River. Global Biogeochem. Cycles 15, 407-416.
Masiello, C. A., Druffel, E. R. M., 2003. Organic and black carbon C-13 and C-14 through the Santa Monica Basin sediment oxic-anoxic transition. Geophys. Res. Lett. 20, 1185.
Menden-Deuer, S., Lessard, E. J., 2000. Carbon to volume relationships for dinoflagellates, diatoms, and other protist plankton. Limnol. Oceanogr. 45, 569-579.
Middleburg, J. J., Nieuwenhuize, J., Can Breuge, P., 1999. Black carbon in marine sediments. Mar. Chem. 65, 245-252.
Mitra, S., Bianchi, T. S., Mckee, B. A., Sutula, M., 2002. Black carbon from the Mississippi Rive: quantities, sources, and potential implications for the global carbon cycle. Environ. Sci. Technol. 36, 2296.
NIST Certificate of Analysis, Standard Reference Material (SRM) 1941b, Marine Sediments, National Institute of Standards and Technology, Gaithersburg, MD, 2002.
NIST Certificate of Analysis, Standard Reference Material (SRM) 1649a, Urban Dust/Organics, National Institute of Standards and Technology, Gaithersburg, MD, 2001.
Nguyen, T., Brown, R. A., Ball, W. P., 2004. An evaluation of the thermal resistance as a measure of black carbon content in diesel soot, wood char, and sediment. Org. Chem. 35, 217-234.
Park, R. J., Jacob, D. J., Chin, M., Martin, R. V., 2003. Sources of carbonaceous aerosols over the United States and implications for natural visibility. J. Geophys. Res. 108, doi:10.1029/2002JD003190.
Penner, J. E., Eddleman, H., Novakov, T., 1993. Towards the development of a global inventory for black carbon emissions. Atmos. Environ., 27A, 1277-1295.
Planktonnet@AWI, 2008. http://planktonnet.awi.de (accessed March 05, 2008)
Planktonnet@Roscoff, 2008. http://planktonnet.sb-roscoff.fr (accessed March 05, 2008)
Popp, B. N., Laws, E. A., Bidigare, R. R., Dore, J. E., Hanson, K. L., Wakeham, S. G., 1998. Effect of phytoplankton cell geometry on carbon isotopic fractionation. Geochim. Cosmochim. Acta 62, 69-77.
Reddy, M. S., Boucher, O., 2004. A study of global cycle of carbonaceous aerosols in the LMDZT general circulation model. J. Geophys. Res., 109, D14203.
Schmidt, M. W., Noack, A. G., 2000. Black carbon in soils and sediments: analysis, distribution, implications, and current challenges. Global Biogeochem. Cycles 14, 777-793.
SCCOOS (Southern California Coastal Ocean Observing System), 2008. Chlorophyll and harmful algal blooms. http://www.sccoos.org/data/chlorophyll (accessed March 05, 2008)
Simpson, M., Hatcher, P., 2004. Determination of black carbon in natural organic matter by chemical oxidation and solid-state 13C nuclear magnetic resonance spectroscopy. Org. Chem. 35, 923-935.
Suman, D. O., Kuhlbusch, T. A. J., Lim, B., 1997. Marine sediments: a reservoir for black carbon and their use as spatial and temporal records of combustion. In Sediment Records of Biomass Burning and Global Change H. C. J. S. Clark, J. G. Goldammer, B. J. Stocks, Ed. (Springer-Verlag, Berlin) pp. 489.
Townsend, D. W., Keller, M. D., 1996. Dimethylsulfide (DMS) and dimethylsulfoniopropionate (DMSP) in relation to phytoplankton in the Gulf of Maine. Mar. Ecol. Progress 137, 229-241.

Tran-Son-Tay, R., Beaty, B. B., Coffey, B. E., 1990. Effects of cell lysing on the rheological behavior of red blood cell suspensions. J. Biomech. Eng., 112, 257-262.

## Figure Captions

**Figure 1.** Detailed procedure of BC quantification in solid samples.

**Figure 2.** Detailed procedure of BC quantification in aqueous-suspension samples.

**Figure 3.** Algae mixture. a) *Prorocentrum micans* (av. length ~ 50 μm); b) *Amphidiniucarterae* (av. length ~ 40 μm); c) *Gymnodium sp.* (av. length ~ 20 μm); d) *Glenodinium sp.* (av. length ~ 15 μm); e) *Coccolithophora* (av. length ~ 5 μm). Sources: Planktonnet@AWI (2008); SCCOOS (2008); FIMR (2008)

**Figure 4.** Individual algae cultures. a) *Dunaliella tertiolecta*; b) *Nannochloris sp.*; c) *Nitzchia frustulum*; d) *Phaedactylum sp.*; e) *Skeletonema costatum*; f) *Nannochloropsis gaditana*; g) *Pelagomonas calceolata.* Source: Planktonnet@Roscoff (2008).

**Figure 5.** Standard addition approach to evaluate the potential of BSA to overestimate BC. Dashed line shows predicted amounts of BC based on amount of NIST 1650 added, open diamonds represent observations of BC when increasing amounts of NIST 1650 are added to BSA, and open triangles represent BC values when only NIST 1650 is added.

**Figure 6.** Standard addition approach to evaluate the potential of Fluen Point seawater POM to overestimate BC. Dashed line shows predicted amounts of BC based on amount of NIST 1650 added. Open triangles represent observations.

**Figure 7.** Thermograms of NIST 1650 SRM in ethyl acetate suspension showing (a) the percentage of TOC remaining after 24 hr exposure at different temperatures, and (b) the percentage of carbon present in the remaining material.

## Table Captions

**Table 1**. Algae species subject to the modified CTO 375 method in this study.

**Table 2.** TOC and BC concentrations (reported as weight percentage ± σ ($n$=3) for positive and negative controls; and ± propagated error for algae suspensions).

**Table 1**. Algae species subjected to the modified CTO 375 method in this study.

| Class | Species |
|---|---|
| Algae mixture | |
| Dinophyceae | *Prorocentrum micans* |
| Dinophyceae | *Amphidiniumcarterae* |
| Dinophyceae | *Gymnodium sp* |
| Dinophyceae | *Glenodinium sp* |
| Prymnesiophyceae | *Coccolithophora* |
| Individual algae cultures | |
| Chlorophyceae | *Dunaliella tertiolecta* |
| Chlorophyceae | *Nannochloris sp.* |
| Bacillariophyceae | *Nitzschia frustulum* |
| Bacillariophyceae | *Phaeodactylum sp.* |
| Bacillariophyceae | *Skeletonema costatum* |
| Eustigmatophyceae | *Nannochloropsis gaditana* |
| Pelagophyceae | *Pelagomonas calceolata* |

**Table 2.** TOC and BC concentrations (reported as weight percentage ± σ ($n$=3) for positive and negative controls; and ± propagated error for algae suspensions).

| Name | $TOC\%_{dw}$ | Initial C/N | $BC\%_{dw}$ | | Final C/N | |
|---|---|---|---|---|---|---|
| | | *Positive controls* | | | | |
| NIST 1649a urban dust | 17.2 ± 2.1[a], 17. 6 ± 1.9[b], 17.7 ± 0.1[c] | 7.5 ± 2.0[a] | 1.51 ± 0.19[a], 1.36 ± 0.07[b], 2.52 ± 0.06[d] | | 35.7 ± 4.8[a], 13.3 ± 7.2[d] | |
| NIST 1650 diesel soot | 73.7± 1.6[a], 77.0 ± 1.8[b], 78.2[d] | 109 ± 27[a] | 38.4 ± 4.6[a], 48.1 ± 0.5[b], 38.4 ± 0.6[e] | | > 1030[a] | |
| | | *Negative controls* | | | | |
| Melanoidin | 54.4 ± 0.2[a], 57.9[f], 6.4[g] | 6.94 ± 0.07[a] | 0.04 ± 0.06[a], 0.18 ± 0.14[b], 0.07 ± 0.04[d] | | 1.05 ± 0.63[a], 1.01 ± 0.53[d] | |
| Bovine Serum Albumin | 42.7 ± 0.9[a], 56[b] | 3.84 ± 0.01[a] | 0.50 ± 0.04[a], 1.72 ± 0.29[b], 0.37 ± 0.02[g] | | 2.11 ± 0.17[a], 2.87 ± 0.26[g] | |
| | | *Algae suspensions*[h] | | | | |
| Algae mixture[i] | 0.468 ± 0.005 | 7.34 ± 0.10 | <0.001[l], 0.007 ± 0.001[j] | | --[l], N b.d.l[j] | |
| Individual algae colonies[k] | | | | | | |
| *Dunaliella tertiolecta* | 24.0 ± 0.1 | 11.6 ± 0.1 | 0.059 ± 0.018[l] | 0.095 ± 0.018[m] | N b.d.l.[l] | 0.12 ± 0.02[m] |
| *Nannochloris sp.* | 14.4 ± 0.1 | 4.40 ± 0.02 | 0.152 ± 0.015[l] | 0.758 ± 0.016[m] | N b.d.l.[l] | N b.d.l.[m] |
| *Nitzschia frustulum* | 10.0 ± 0.1 | 4.44 ± 0.03 | 0.058 ± 0.051[l] | 0.054 ± 0.051[m] | N b.d.l.[l] | 0.06 ± 0.06[m] |
| *Phaeodactylum sp.* | 56.9 ± 0.1 | 19.6 ± 0.1 | 0.160 ± 0.019[l] | 0.143 ± 0.019[m] | N b.d.l.[l] | 0.16 ± 0.02[m] |
| *Skeletonema costatum* | 19.8 ± 0.1 | 6.57 ± 0.03 | 0.176 ± 0.026[l] | 0.147 ± 0.025[m] | N b.d.l.[l] | 0.11 ± 0.02[m] |
| *Nannochloropsis gaditana* | 60.7 ± 0.1 | 11.9 ± 0.1 | 0.250 ± 0.026[l] | 0.280 ± 0.026[m] | 3.05 ± 0.63[l] | 0.28 ± 0.03[m] |
| *Pelagomonas calceolata* | 14.3 ± 0.1 | 5.37 ± 0.03 | 0.063 ± 0.043[l] | 0.099 ± 0.045[m] | 0.21 ± 0.14[l] | 0.18 ± 0.08[m] |

[a]This study; [b]Gustafsson et al., 2001; [c]Curie et al., 2001; [d]Hammes et al., 2007; team no.5; [e]Gelinas et al., 2001; [f]Allar et al., 1997; initial material used by Gustafsson et al., 2001; [g]Accardi-Dey, 2003; [h]TOC in (μg/mL); [i]Total volume filtered: 200 mL; [j]without temperature ramp; [k]volume filtered for each sample: 30 mL; [l]frozen; [m]not frozen; N b.d.l.: Nitrogen Below Detection Limits.

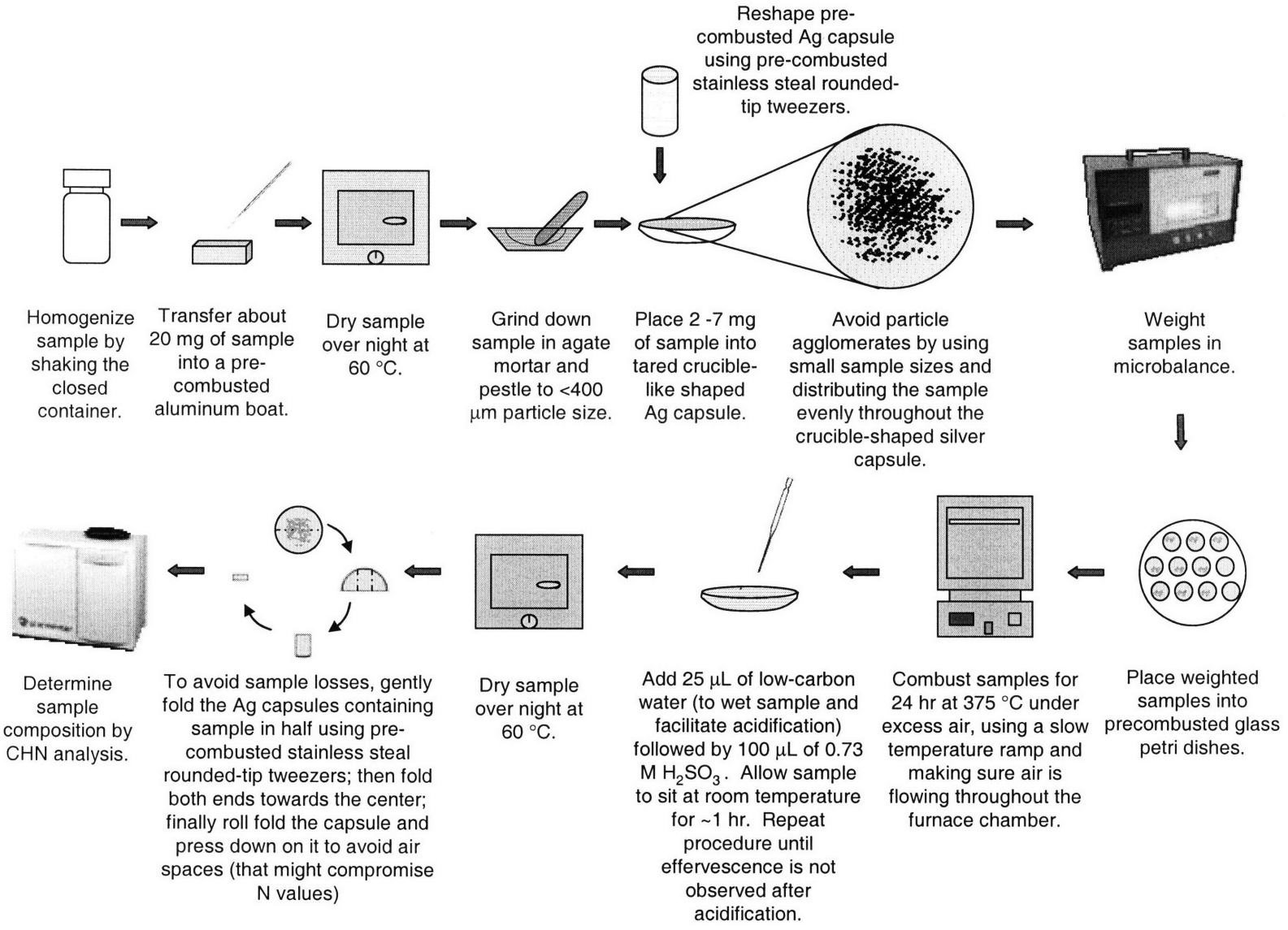


**Figure 1.** Detailed procedure of BC quantification in solid samples.

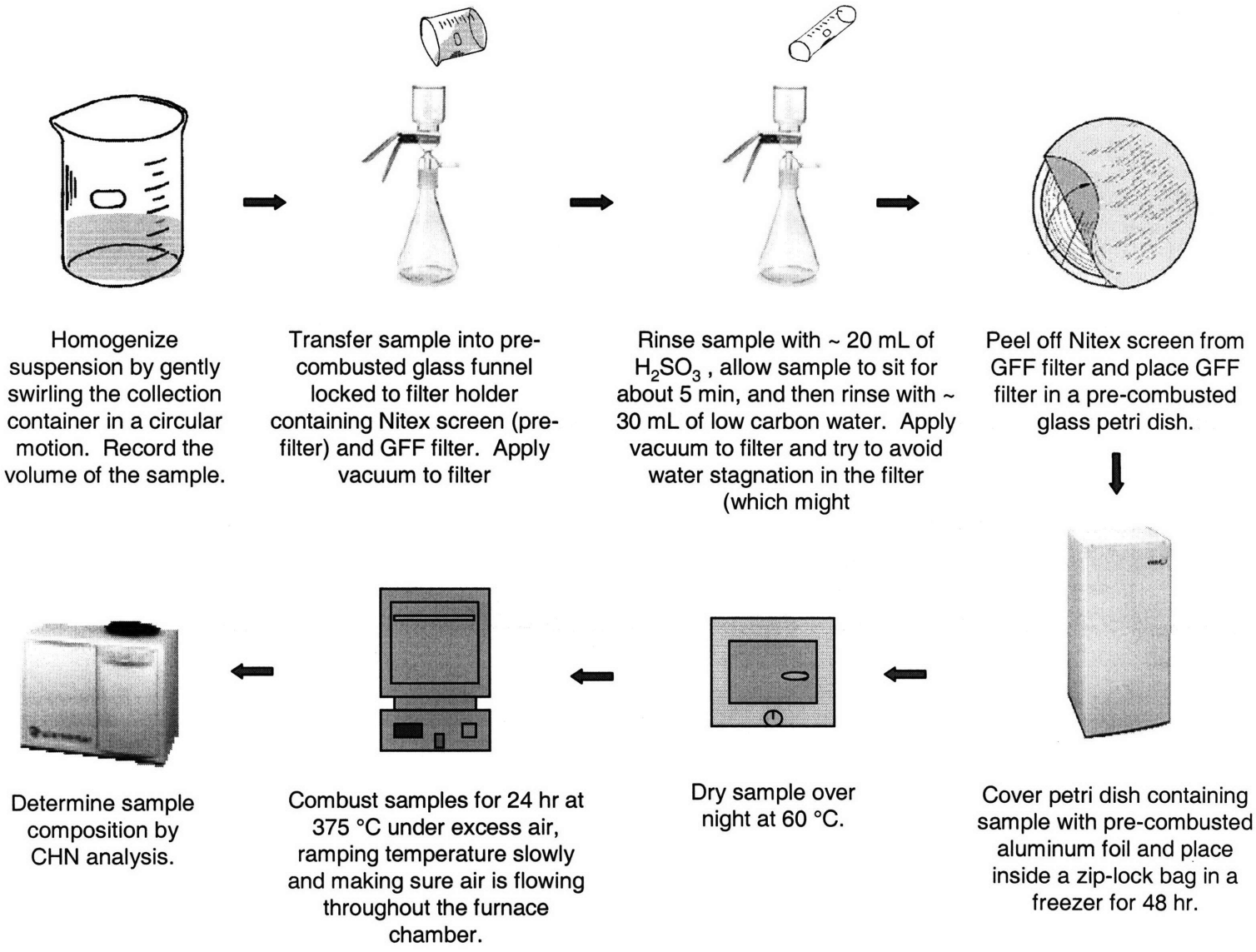


**Figure 2.** Detailed procedure of BC quantification in aqueous-suspension samples.

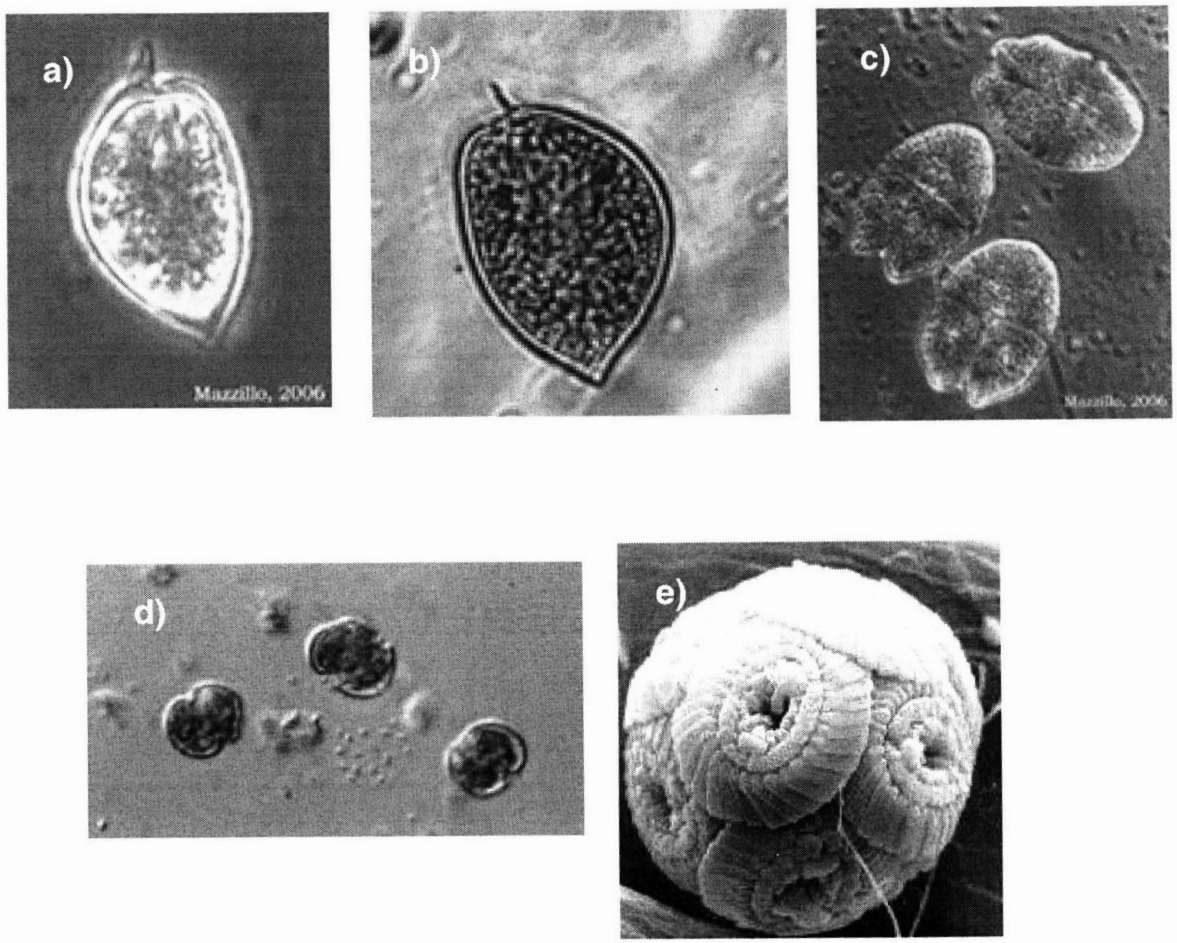


**Figure 3.** Algae mixture. a) *Prorocentrum micans* (av. length ~ 50 μm); b) *Amphidiniucarterae* (av. length ~ 40 μm); c) *Gymnodium sp.* (av. length ~ 20 μm); d) *Glenodinium sp.* (av. length ~ 15 μm); e) *Coccolithophora* (av. length ~ 5 μm). Sources: Planktonnet@AWI (2008); SCCOOS (2008); FIMR (2008)

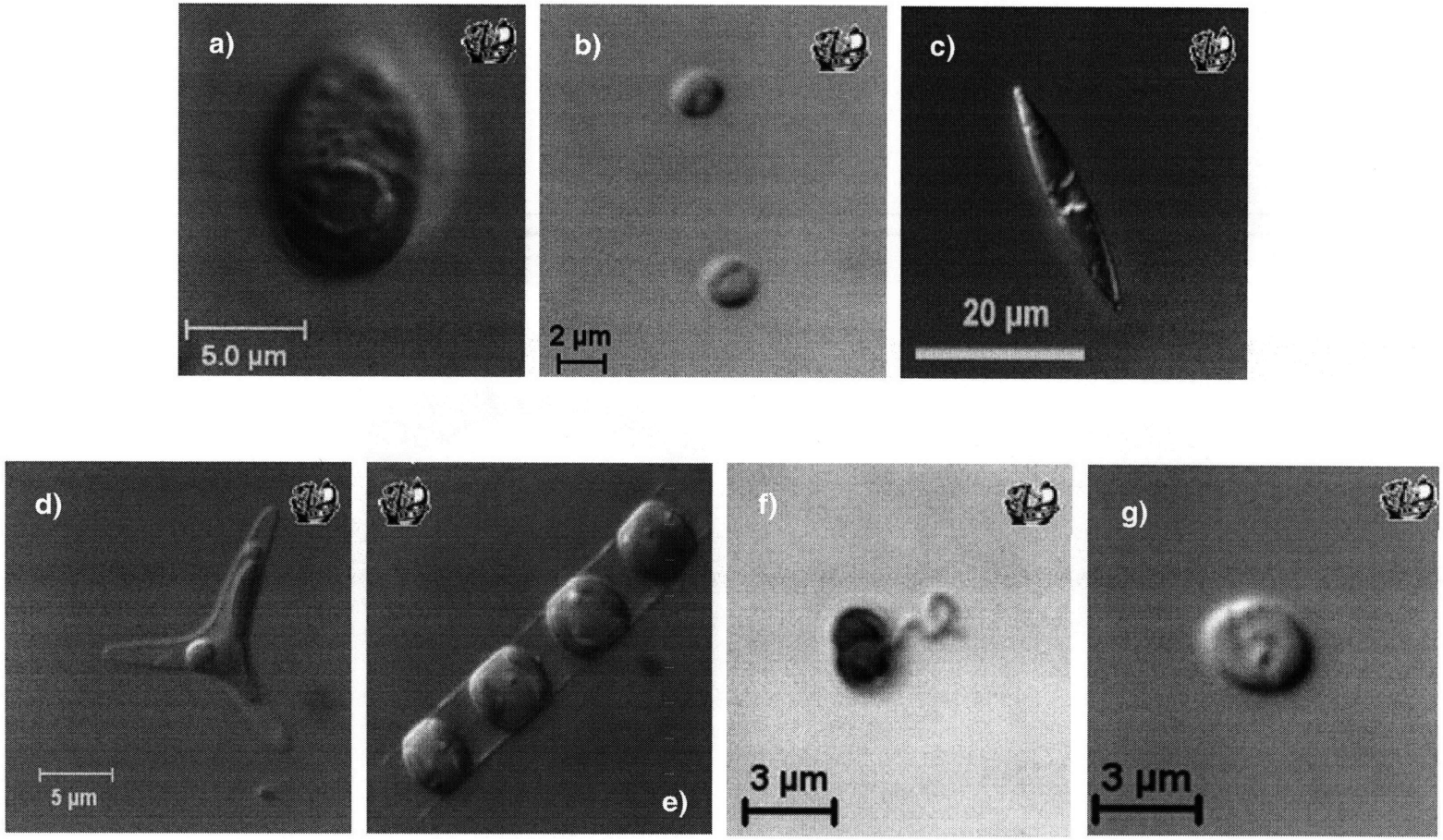


**Figure 4.** Individual algae cultures. a) *Dunaliella tertiolecta*; b) *Nannochloris sp.*; c) *Nitzchia frustulum*; d) *Phaedactylum sp.*; e) *Skeletonema costatum*; f) *Nannochloropsis gaditana*; g) *Pelagomonas calceolata*. Source: Planktonnet@Roscoff (2008).

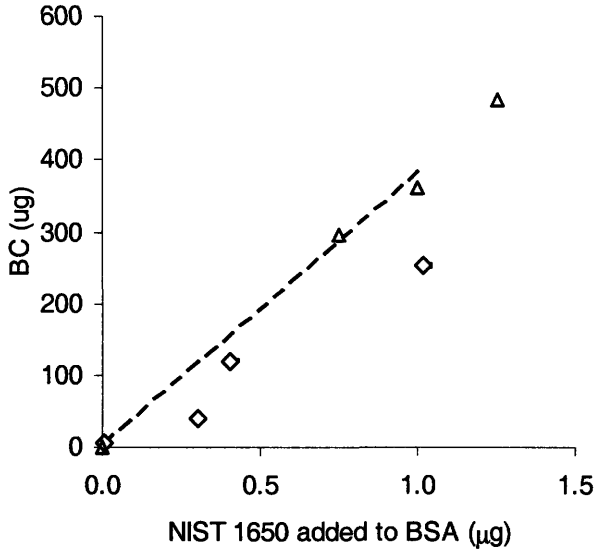


**Figure 5.** Standard addition approach to evaluate the potential of BSA to overestimate BC. Dashed line indicates predicted amounts of BC based on amount of NIST 1650 added, open diamonds represent observations of BC when increasing amounts of NIST 1650 are added to BSA, and open triangles represent BC values when only NIST 1650 is added.

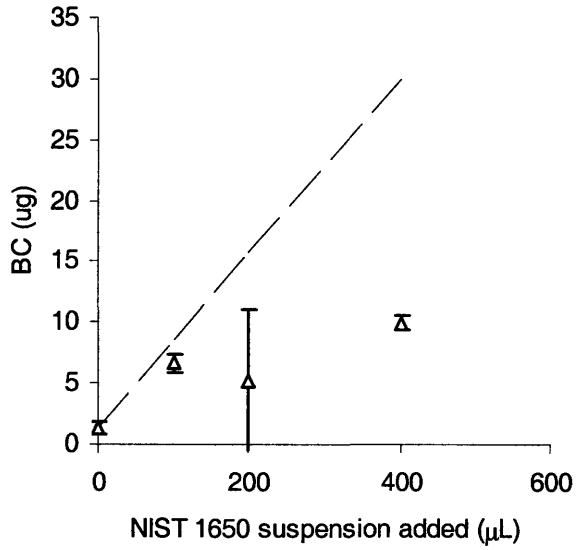


**Figure 6.** Standard addition approach to evaluate the potential of Fluen Point seawater POM to overestimate BC. Dashed line indicates predicted amounts of BC based on amount of NIST 1650 added. Open diamonds represent observations.

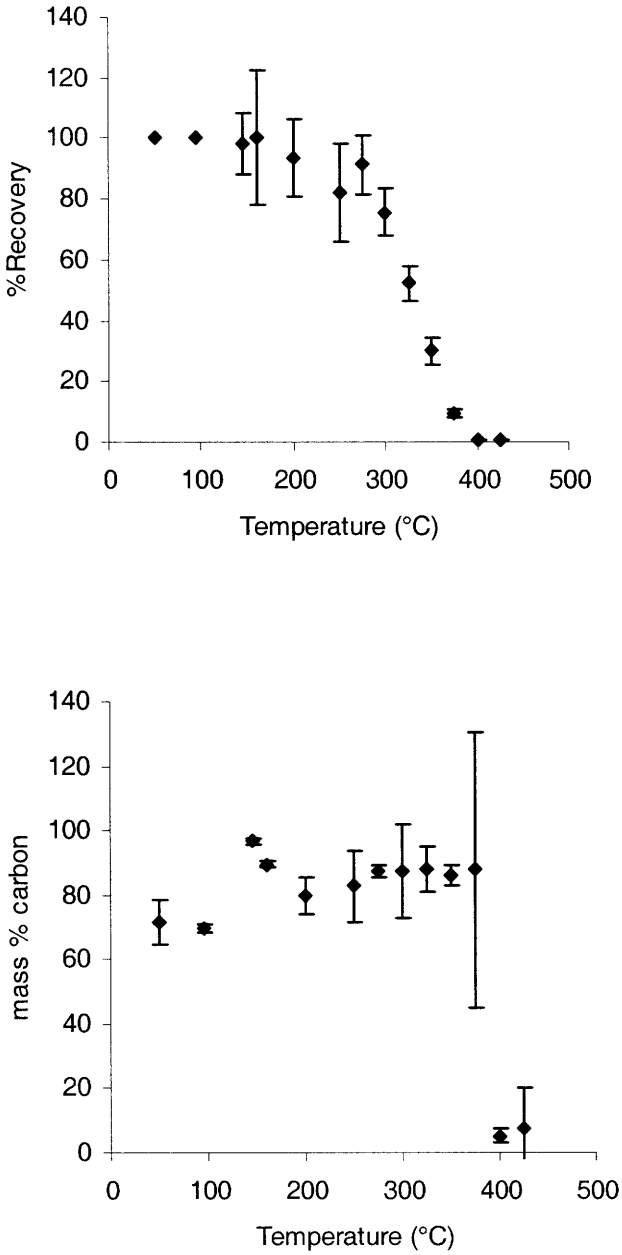


**Figure 7.** Thermograms of NIST 1650 SRM in ethyl acetate suspension showing (a) the percentage of TOC remaining after 24 hr exposure at different temperatures, and (b) the mass percentage of carbon in the remaining material.

# Organic carbon cycling and water column characterization in the Gulf of Maine

D. Xanat Flores-Cervantes[1], Desiree L. Plata[1,2], John K. MacFarlane[1], Christopher M. Reddy[2], and Philip M. Gschwend[1].

[1]R.M. Parsons Laboratory, MIT 48-413, Department of Civil and Environmental Engineering, Massachusetts Institute of Technology, Cambridge, Massachusetts 02139, USA

[2]Department of Marine Chemistry and Geochemistry, Woods Hole Oceanographic Institution, Woods Hole, Massachusetts, 02543

xanatf@mit.edu, dplata@whoi.edu. jmac@mit.edu, creddy@whoi.edu, pmgschwe@mit.edu.

**Journal format**

**Abstract**

An organic carbon (OC) mass balance of the Gulf of Maine (GoM), a continental shelf area in the northeastern USA, was used to assess the local cycling of organic carbon. To this end, different size fractions of organic matter, naturally occurring $^{234}Th$, and hydrographic data (temperature, salinity, and chlorophyll *a* and $O_2$ concentrations) were collected during April and August/September 2004 to address the effects of the physical, chemical, and biological characteristics on the cycling of OC in the GoM. Results from our OC mass balance indicate that: (a) primary production was the main source of OC to the GoM, about 70% of this material was respired or exported from the surface ocean to the deeper ocean, and that less than 6% of the OC produced in the surface ocean is buried in the sediments; (b) the GoM is a net source of carbon to the northeastern North America coastal ocean circulation system; and (c) rivers and atmospheric deposition are negligible inputs of organic carbon to the GoM. In addition, carbon-to-nitrogen (C/N) ratios measured in the seawater particulate organic matter (POM) and sediment samples provided insights to address carbon production and remineralization within the water column and the sediment bed. During April 2004, decreasing C/N ratios with increasing depth are indicative of deep nutrient-rich water inputs, while during August/September, increasing C/N ratios with increasing depth indicate nitrogen-preferential remineralization. In all of our sampled sites, a relatively constant C/N ratio in organic matter after deposition indicated the lack of preferential mineralization, or minimal remineralization of organic matter after deposition in this coastal area. Identifying August/September as an important off-bloom export season indicated that previous estimates of POC export in this area might have been underestimated. These findings have important implications for the identification of sources and burial of OC in this

coastal area, and provide a better understanding of the processes that other particle-reactive materials may undergo.

## 1. Introduction

The study of organic carbon (OC) and, in particular, how and to what extent does OC survive mineralization in the water column or the sediments, is crucial to understanding the role of oceanic sequestration of anthropogenic $CO_2$ in the global carbon cycle; yet, this study remains one of the main challenges for marine organic geochemists. Although there have been great advances in the past 30 years, the source of the "old" dissolved organic carbon in the water column and of the organic material preserved in the sediments remains unclear (Eglinton and Repeta, 2004). While terrestrial fluxes to the oceans alone account for more than twice the organic carbon (OC) burial rate in marine sediments (Hedges and Keil, 1995), molecular and isotopic studies of organic matter in both the water column and marine sediments indicate dominant autochthonous inputs (Gough et al., 1993; Aluwihare et al., 1997). This indicates that either terrestrial OC is lost before it gets out to sea, or is rapidly and extensively remineralized within the water column or surface marine sediments. However, previous studies (Hedges and Keil, 1995) suggest that the sources, composition, and preservation mechanisms of OC in marine sediments are site specific and need to be studied and addressed on an individual basis.

Although coastal areas represent less than 10% of the world oceans (Sverdrup et al., 1946), these are highly productive areas that contribute up to 40% of the global marine primary productivity (Eppley and Peterson, 1979) and account for an important fraction of the OC burial in surface sediments (Hedges, 1992). In addition, it has been known that these coastal zones may also supply much of the OC beyond the continental shelf (Hedges and Keil, 1995). River runoff, continuous mixing, and coastal upwelling are responsible for increased loads of suspended particulate organic matter (SPOM) and higher burial estimates closer to the shore (Berner, 1989). Aeolian fluxes of OC to the oceans are considered to be small and much less

constrained than riverine inputs (Romankevich, 1984), but may be of significant importance for more distant marine locations downwind form major OC sources (e.g. Gagosian and Peltzer, 1986).

The Gulf of Maine (GoM; Figure 1) is a semi-enclosed coastal area located along the northeastern coast of the United States of America, and southwest of Nova Scotia, Canada. The GoM is the largest semi-enclosed coastal sea in the continental United States with an aerial extent of $2 \times 10^5$ km$^2$ (GoMOOS, 2007). It is isolated from the North Atlantic Ocean by the Georges and Browns Banks, and has three major basins, Georges, Jordan, and Wilkinson Basins. These physical characteristics are believed to be important for organic carbon production as well as for burial of organic matter (Townsend, 1996). River systems throughout the coast also flow into the GoM providing terrestrial inputs of OC and other nutrients to this coastal system (Townsend, 1996). In addition, this GoM is heavily populated and downwind of important urban and industrial areas that contribute with significant atmospheric contaminant fallout. The Gulf of Maine is, therefore, a good representative of coastal oceans where riverine and eolian inputs, as well as primary production, may be important components of the carbon cycling.

There have been intensive studies in the GoM in the last three decades that have provided a better understanding of the carbon cycling, hydrography and water flow dynamics in this important coastal area (Beardsley et al., 1996; Benitez-Nelson et al., 2000; Charette et al., 2001; Dai and Benitez-Nelson., 2001; Mown and Yoder, 2005; Thomas et al., 2003; Townsend, 1996). These studies have pointed out significant temporal (inter- and intra-annual) and spatial variations in the circulation and water properties in the GoM. However, further understanding of internal recycling processes within the GoM is still needed, as it remains unclear why the

average export ratio (POM export versus total primary production) in the GoM is low compared to other similar coastal environments (Townsend et al., 1996).

This study intends to be complementary and provide additional information that has not been previously obtained to have a better understanding of the sources and fate of OC in the GoM. Here we present an organic carbon mass balance that includes riverine and aeolian transport of OC into the GoM; and, based on concurrent measurements of water column and sediment records, we address cycling and preservation mechanisms of OC in this coastal area. Seawater OC and sediment samples were collected during two cruises to the GoM in April (*R/V Oceanus*) and August (*R/V Cape Hatteras*) of 2004. We measured concentrations of the different size fractions of OC: total organic carbon (TOC), settling particulate organic carbon (53 μm < POC), and suspended particulate organic carbon (0.7 μm < POC < 53 μm); we coupled this information with $^{234}Th/^{238}U$ radionuclide disequilibrium to estimate the fluxes of OC out of the surface ocean; we estimated the TOC sedimentation rates for the past 100 years at different locations of the GoM; and we estimated atmospheric deposition fluxes from reported OC concentrations in the New England area. Finally, we used this information and previous estimates of primary productivity to develop an organic carbon mass balance to better understand the main inputs and outputs of OC into the GoM.

## 2. Methods and Materials

### *2.1. Characterization of the water column*

At each station during both cruises, April and August 2004, vertical profiles of pressure (dbar), salinity (PSU), temperature (°C), chlorophyll fluorescence (roughly corresponding to

chlorophyll *a* (μg/L) without correction for phaeophytin fluorescence) and oxygen ($O_2$) concentrations (μg/L) were made at sea using CTD (Conductivity-Temperature-Depth) profilers. Density anomaly (sigma-t) was calculated from the equation of state of water with CTD values of pressure, temperature and salinity.

### *2.2. Water column sampling*

Different portions of the particulate organic carbon (POC), separated by size cut-off, were collected during two cruises to the GoM in 2004, one in April (*R/V Oceanus*) and a second one in August/September (*R/V Cape Hatteras*). At each sampling station, water was pumped from above and below the surface layer (based on hydrographic data) using a positive-displacement stainless-steel gear pump (Fultz Pump Inc, Lewis Town, NJ) from either a shallow (~ 6 m) or deeper depth (~ 60 m). Seawater was pumped from depth through stainless steel tubing that had been thoroughly washed with methylene chloride, methanol, low-carbon water (18 mΩ, produced using an Aries Vaponic system, Rockland, MA), and stored closed until use. The seawater came on-board without ever being exposed to the atmosphere, and it successively passed through a 142-mm diameter, stainless steel, filter holder containing a 53-μm mesh-opening pre-cleaned Nitex screen (TETKO, Depew, NY), followed by a 293-mm, stainless steel, filter holder with a 0.7-μm pre-combusted fiber glass (GFF) or quartz filter (Pall Gelman Sciences, Ann Arbor, MI). This particle fractionation was based on previous models and measurements (e.g., Buesseler, 1998; Charette et al., 2001; Gustafsson et al., 1998) made following the OC sampling procedure developed by Bishop and Edmond (1976), where the OC isolated in the > 53 μm from the Nitex screen was assumed to approximate the sinking/settling

POC ($POC_{SE}$), and the < 53 μm and > 0.7 μm from the glass fiber or quartz filter the non-sinking/suspended POC ($POC_{SU}$). All filter samples were rinsed immediately after collecting with a 100 mL of 10 mM sulfurous acid ($H_2SO_3$) to remove carbonates and a 100 mL low-carbon water (Aries Vaporic, Rockland, MA) rinse to remove salts, and kept frozen in aluminum foil envelops until further analysis. Sample blanks were collected throughout the sampling procedure and consisted of "wetting" the filtration devices by pumping only 1 L of seawater from the sampling station before processing in the same manner as all the samples.

During August/September 2004, after collecting the different fractions of POC, seawater was collected directly from the stainless steel tubing into 300 mL pre-combusted biological oxygen demand (BOD) glass bottles for TOC quantification, and kept at 4 °C in dark until analysis in less than a week after collection..

*Quantification of organic carbon in the GoM*

*Total organic carbon (TOC).* Back in the laboratory, phosphoric acid ($H_3PO_4$) was added to samples collected in the BOD bottles to lower the pH to < 2. Within a week, TOC in the samples was determined using high temperature catalytic combustion (680 °C) by injecting 27 μL subsamples into a Shidmadzu TOC-5000 analyzer. A 17 point standard calibration curve was generated from 0.0 to 2.0 mg/L, by diluting a potassium acid phthalate standard (1 mg/mL C; VWR Scientific, West Chester, PA) with low-carbon water (Aries Vaporic, Rockland, MA) in 25-mL pre-combusted volumetric flasks.

*Organic carbon in the POC > 53 μm ($POC_{SE}$)* The Nitex screen was sonicated for 20 min with 100 mL of GFF filtered (Whatman, Florham Park, NJ) seawater for 5 to 10 min to detach the $POC_{SE}$ from the Nitex screen. Following sonication, 50 mL of the collected sample were

kept in the plastic container for further $^{234}Th$ measurements, and another 50 mL were transferred to a 60 mL pre-combusted glass vial. Triplicates of 200 μL samples of the sonicated $POC_{SE}$ were placed in crucible shaped Ag capsules, acidified with ~ 20 μL of 1 mM $H_2SO_3$; (Fisher Chemicals, Fairlawn, NJ) and dried at 60 °C overnight. The carbon concentration was determined using a CHN analyzer (Vario EL, Elementar America, Inc., NJ) at a combustion temperature of 950 °C. Daily response factors were determined using acetanilide standards (Elemental Microanalysis, Manchester, MA), and the detection limit of the analyzer was 1 μg of C. Response factors for all elements remained stable throughout the experiment (± 0.5% for nitrogen, ± 0.07% for carbon, and ± 0.6% for hydrogen). A procedural-blank (empty Ag capsule that went through the same procedure as sample Ag capsules) and a sample blank (no sample introduced in the CHN analyzer) were added after every sample to account for any contamination and to verify that combustion was complete in the CHN. The signal-to-noise-ratio was always larger than 3:1, and blanks were subtracted from the raw sample data. Variation between replicates was < 10%.

*Organic carbon in the 53 μm > POC > 0.7 μm ($POC_{SU}$).* One sixteenth of the glass fiber filter or quartz filter was dried overnight at 60 °C, followed by elemental analysis in a Vario EL CHN analyzer (Elementar Americas, Inc., NJ; see above). Every run included two sample blanks to flush the CHN analyzer and verify that combustion was complete, and blanks (signal-to-noise ratio larger than 4:1) were subtracted from raw sample data.

*OC vertical fluxes thru the water column*

Half of the sonicated $POC_{SE}$ from the Nitex screen (see above) was collected in a pre-cleaned plastic container and spiked with $^{230}Th$ to serve as a recovery standard. The $^{234}Th$ activity was then measured using low-background beta detectors following the procedure of Buesseler et al.

(1992). The measurements were repeated 4-5 times within a week to check for background interferences, to improve precision and accuracy, and to correct for the date of sample collection. $^{238}U$ activities were estimated from salinity measurements (Chen et al., 1986) made on board during the cruise with a calibrated 8410A Portasal™ salinometer (Guildline, Smiths Falls, Ontario, Canada). Export fluxes from the water column were calculated using information from the measured $^{234}Th/^{238}U$ disequilibria and $OC/^{234}Th$ ratio in the settling fraction (> 53 μm) of the organic matter (OM) from the April and August/September cruises (Buesseler et al., 1992).

### *2.3. Sediment sampling.*

Sediment cores were collected using an MC-800 multicorer sediment sampler (Ocean Instruments, San Diego, CA) deployed off the stern of the research vessels (with help from crew staff) from five different stations in the Gulf of Maine (GoM) in April (*R/V Oceanus*) and August/September (*R/V Cape Hatteras*) 2004. The multicorer sampler was able to recover up to eight replicate samples of undisturbed surface sediments with an effective penetration of more than 45 cm. Upon retrieval, the cores were extruded after siphoning off water and sliced in sections by pushing out the cores from below. The outer sediment that had been in contact with the barrel was discarded, and the remainder was placed in pre-combusted glass jars with aluminum foil-lined screw caps, and stored in chest freezers (-18 °C). With the exemption of MWRA, the cores were sliced on board into 0.5 cm sections from 0 to 2 cm, 1 cm sections from 2 to 6 cm, 2 cm sections from 6 to 10 cm; 4 cm sections from 10 to 22 cm, and 8 cm sections for the remainder of the cores. MWRA was sliced into 0.5 cm sections from 0 to 2 cm, and 1 cm sections for the remainder of the core. Before analysis, the sediments were freeze dried and

homogenized with mortar and pestle. Due to demands on sample size and to avoid contamination, different parallel cores were used for gamma counting dating analysis.

*Sediment Dating*

Radionuclide depth profiles were determined for $^{137}Cs$ and unsupported $^{210}Pb$ ($^{210}Pb_{xs} = {}^{210}Pb_{total} - {}^{214}Pb$). Dry sediments (5 – 20 g) were analyzed by gamma spectrometry for $^{210}Pb$ (46.5 keV), $^{214}Pb$ (295.2 and 351.9 keV), and $^{137}Cs$ (661 keV) using a high-purity germanium detector (Canberra model GL2020). Counting efficiencies were between of 0.36% and 0.49% for $^{210}Pb$, and 1.34% and 1.60% for $^{214}Pb$ (calculated using Environmental Protection Agency (EPA) standard Pitch Blend Ore) depending on the amount of sample analyzed (geometry of the sample). The $^{210}Pb$ and $^{137}Cs$ activities for every sediment sample were calculated in disintegrations per minute and counts per minute per gram of salt-free sediment, respectively. Activities were decay-corrected to the sample collection date.

With the exemption of Inner Penobscott Bay (IPB) core, where disagreement between the calculated $^{210}Pb$ chronology and the appearance of $^{137}Cs$ was observed, sedimentation rates were determined using the constant rate of supply model (CRS; Appleby and Oldfield, 1978) with salinity-corrected density and porosity. To derive a more consistent chronology between sedimentation rates and $^{137}Cs$ appearance in the IPB the core (using CRS the appearance of $^{137}Cs$ was observed in 1920), IPB sedimentation rates were calculated using the constant initial concentration model (CIC), where the sedimentation rate was calculated from the slope of a straight line in a plot of ln $^{210}Pb$ vs depth of the sediment sample.

*Total organic carbon (TOC) analysis*

Triplicates of about 5 mg of the dry sediments were ground and weighed into manually shaped Ag capsules placed in pre-combusted Petri dishes, acidified with 100 µl of 6% volume $H_2SO_3$ (Fisher Chemicals, Fairlawn, NJ), and dried at 60 °C overnight. The carbon content of the remaining material was determined using a CHN analyzer (Vario EL, Elementar America, Inc., NJ; see above). A procedural blank (empty Ag capsule that went through the same procedure as sample Ag capsules) and a sample blank (no sample introduced in the CHN analyzer) were added for every sample to account for any contamination and to verify that combustion was complete in the CHN. All samples were blank corrected and variations between replicates were always < 5%.

## 3. Results and Discussion.

### *3.1. Characterization of the water column in the GoM*

Similar to what has been previously reported (Townsend et al., 1992), our hydrographic data showed that the properties of the water column in the GoM (Figure S1 and S2 in supplementary material) result from influences largely affected by bathymetry and seasonality in this coastal area (Beardsley et al., 1996, and references therein). During April our data showed two main water sources: (a) freshwater inputs from local runoff (e.g., low surface salinities at Inner Penobscot Bay (IPB), Merrimack River (MER), Casco Bay (CB), Massachusetts Water Resources Authority (MWRA), Cape Cod Bay I (CCB1), and Cape Cod Bay II (CCB2); Figure S1) and relatively fresh Scotian Shelf Water (identified as a low salinity, surface, cold water mass that enters the GoM around southwestern Nova Scotia; Smith, 1983) along the western coast and the northeastern part of the GoM (relatively low surface salinities at Jordan Basin (JB), but mainly at East Platts Bank (EPB), and Wilkinson Basin I (WB1); Figure S1); and (b) inputs

from deep, saltier Slope Water entering through the Northeast Channel (Brooks, 1985; low temperature and high salinity bottom water at JB, EPB, WB1, Wilkinson Basin II (WB2), and Great South Channel (GSC); Figure S1), producing water of intermediate salinity in the central gulf and flowing south-eastward into the Great South Channel (intermediate salinity and temperature at the middle of the water column depth at EPB, WB1, and GSC; Figure S1), and producing relatively salty waters throughout the water column at Georges Bank (GB; Figure S1) as a result of intense vertical exchange (Yoshida and Oakey, 1996). Although temperature gradients were small during April, lower temperatures in the northern part of the Gulf confirmed the presence of the colder Scotian Shelf Water. High chlorophyll *a* concentrations in the southwestern part of the Gulf and closer to shore indicated the presence of nutrient inputs from runoff or upwelling of deep-nutrient-rich waters, while relatively constant $O_2$ concentrations are consistent with the relatively low sigma-t vertical gradients observed during this time of the year (Figure S1).

A different scenario was observed during August/September. Slightly lower salinities closer to shore and in the northern part of the Gulf than in the central Gulf still reflected smaller runoff and Scotian Shelf freshwater inputs, but, overall, vertical and horizontal salinity gradients were less sharp during this time of the year. Conversely, vertical temperature, $O_2$ concentration, and sigma-t gradients were much sharper in August/September than in April, and were consistent with summer warming and thermal stratification. It was not surprising then to see lower chlorophyll *a* concentrations during August/September resulting from nutrient depletion (Durbin, 1996).

$O_2$ concentrations during both April and August/September cruises were close to $O_2$ solubility at the observed temperatures and salinities (Weiss, 1970) with $O_2$ saturations between

99.4 and 105% for both seasons at all depths (Table 1). Water bodies where biological processes affect $O_2$ saturation show values >120% at the surface (due to photosynthesis), and <<100% under the compensation depth (due to respiration; Von Arx, 1962; Riley and Chester, 1971). However, our observed $O_2$ saturation values indicated that $O_2$ saturation was determined to a greater extent by the mixing within the basin, as opposed to biological processes. The Slope Water entering the GoM through the Northeast Channel, which corresponds to recently formed deep water, is not only rich in nutrients, but also has close-to-saturation dissolved oxygen concentrations (Von Arx, 1962). Entrainment and upwelling of the Slope Water will then provide oxygen to deep waters of the GoM, while surface mixing might be responsible for $O_2$ concentrations close to the surface of the ocean.

*3.2. Spatial variations in seawater TOC*

TOC concentrations (Table 1) between 1.10 ± 0.07 and 1.64 ± 0.09 mg/L were consistent with previous observations (Dai and Benitez-Nelson, 2001). Concentrations were higher closer to shore, and the highest concentrations were measured at IPB, the station closest to shore. Although not as high as at IPB, moderately high TOC concentrations were also observed at the CB, MER, MWRA, and CCB1 sampling stations. Also, decreasing concentrations with increasing depth suggested that either terrestrial inputs or primary production were the main OC sources in surface waters.

We do not have data from April 2004 to examine the temporal variations of TOC in the GoM, but the close resemblance between our values and the ones reported by Dai and Benitez-Nelson (2001) measured during the summers of 1996 and 1997 (Table 1), indicate relatively small interannual variations of TOC in the GoM.

*3.3. Spatial and temporal variations in POC*

Consistent with the scenario described above for April (terrestrial runoff inputs, nutrient-rich deep Slope Water, and a spring phytoplankton bloom; Figure S1), higher concentrations of $POC_{SU}$ were found closer to the coast in the deep and shallow samples in the southwestern central GoM (WB1, WB2, GSC) and at GB. A slightly different scenario was observed for $POC_{SE}$. In this size fraction, the highest concentrations were observed at MWRA, WB2 and GB, and the lowest one at IPB. Since the phytoplankton population during the spring is mainly dominated by diatoms (Townsend, 1996b), and a large percentage of these organisms are larger then 53 μm (Kalff, 2002), these observations suggest that phytoplankton blooms were responsible for both $POC_{SU}$ and $POC_{SE}$ in WB1, WB2 and GB; while IPB was mainly influenced by terrestrial material of particulate size smaller than 53 μm. Low chlorophyll *a* concentrations measured at IPB further support this hypothesis. Autochthonous sources at GB are not surprising, since upwelling of deep, nutrient rich water and intense mixing in this area promote primary production (Durbin, 1996; Thomas et al., 2003).

Lower $POC_{SU}$ and $POC_{SE}$ observed at most stations during August/September were consistent with lower terrestrial runoff inputs and the remnants of a summer thermocline that reduced nutrient-rich deep water inputs (Figure S2) and thereby lead to lower primary production rates. One exception was IPB, where concentrations of $POC_{SU}$ were not very different from the ones observed in April, and $POC_{SE}$ concentrations were even higher than in the previous sampling season. Although runoff fluxes may not have been as large as in April (river discharge was much less), relatively high TOC concentrations were observed in this station during August/September as well, indicating a continuous input of nutrient-rich terrestrial sources. The

relatively low chlorophyll *a* concentrations observed at this station during April (Figure S1) indicated that conditions were not favorable for phytoplankton growth. The high concentrations of settling POC observed at IPB may then be a mixture of allochthonous and autochthonous sources.

Carbon-to-nitrogen (C/N) ratios can also serve as indicators of organic matter sources (e.g., Bergamaschi et al., 1997). Elevated C/N ratios compared to the Redfield C/N ratio of 6.6 (Redfield et al., 1963) in particles in the ocean suggest allochthonous sources or decreased net community production (Körztinger et al., 2001). Very distinct differences were observed in the C/N ratios of the material collected during April and August/September 2004 (Table 2). While average C/N ratios observed in the $POC_{SU}$ in the shallow samples of 6.2 ± 1.0 and 6.7 ± 0.7 for April and August/September, respectively, were not statistically different from the Redfield ratio, C/N ratios in the $POC_{SE}$ were much higher and variable (32 ± 29 and 64 ± 59 for April and August/September, respectively; Table 3). These high C/N ratios may indicate that the material collected in the $POC_{SU}$ was predominantly autochthonous. Relatively high C/N ratios close to shore suggests inputs of terrestrial cellulose-containing debris (MWRA, IPB, CB). Further from shore, the high C/N ratios observed in the shallow samples (WB1, JB, GB, GSC) may have been due to the presence of exopolymetric matter (formed by coagulation of dissolved organic matter; Mari et al., 2001) or zooplankton mucus webs (Beaulieu and Smith, 1997; Alldredge, 1976). These have C/N ratios larger than 14. The observed large variations could indicate mats or patches of a mixture of materials from different sources in the ocean.

Differences between shallow and deeper water C/N ratios also provide useful information about POC preservation and remineralization mechanisms throughout the water column. During April, the C/N ratio of the $POC_{SU}$ generally decreased with increasing depth (Table 2). This

possibly indicated diminishing nutrient inputs from deeper waters into the surface ocean caused the formation of POC with an evolving C/N ratio. In August/September, a higher C/N ratio in some of the stations indicated post-bloom particulate export of the nutrient-deficient mixed layer and preferential remineralization of nitrogen. Overall, our values of $POC_{SU}$ and $POC_{SE}$, as well as C/N ratios, were within the values previously reported by Charette et al. (2001) for this area (Table 2 and 3).

### *3.4. POC export fluxes into the GoM*

To estimate POC export fluxes we used our $POC_{SE}$ concentrations and contemporaneous measures of radioactive disequilibrium between the particle-reactive $^{234}Th$ and its water-soluble source, $^{238}U$, in the same seawaters. We followed the approach proposed by Buesseler et al. (1992) where the $POC_{SE}$ to $^{234}Th$ ratio and the estimated $^{234}Th$ flux ($F_{Th}$) were used to estimate POC fluxes in the water column at a given depth:

$$F_{POC} = \frac{POC_{SE}}{^{234}Th_p} \int_{z_1}^{z_2} F_{Th} \cdot dz, \qquad (1)$$

where $z_1$ and $z_2$ are the depth intervals over which $F_{Th}$ is estimated. $F_{Th}$ can be estimated from the total $^{234}Th$ activity ($A_{Th}$) balance (particulate and dissolved):

$$\frac{\partial A_{Th}}{\partial t} = A_U \lambda_{Th} - A_{Th} \lambda_{Th} - F_{Th} + K\nabla^2 A_{Th} + U\nabla A_{Th}, \qquad (2)$$

where $A_U$ is the $^{238}U$ activity and $\lambda_{Th}$ is the $^{234}Th$ decay constant (0.0288 1/d). The first term represents the radiogenic production of $^{234}Th$, the second term is the loss of total $^{234}Th$ by radioactive decay; and the last two terms represent the contribution of $^{234}Th$ from mixing (where

$K$ is the eddy diffusion coefficient vector) and advection (where $U$ is the velocity vector). Previous studies have reported that in pelagic, continental shelf, and many coastal regimes, there are modest variations between fluxes calculated using a one dimensional (1-D) or a three dimensional (3-D) model (usually <factor of 2 except during storm-driven resuspensions, Charette et al., 2001; Gustafsson et al., 1998). During both April and August/September 2004 cruises, the weather was relatively calm during our sampling close to the shore. Therefore, for this study, we assumed a steady state model with negligible advective and eddy diffusive transport (i.e., a 1-D, vertical model), but caution the reader about this assumption. Equation (2) can then be rewritten as:

$$F_{Th} = A_U \lambda_{Th} - A_{Th} \lambda_{Th} . \qquad (3)$$

Another assumption made to estimate export fluxes using this model is that $POC_{SE}$ is the primary component of the sinking particles; i.e., $^{234}Th$ deficiencies are associated with the same aggregates responsible for sinking $POC_{SE}$. Cochran et al. (1995) advised caution in the use of this method to estimate export fluxes in coastal areas where $^{234}Th$ removal may be subject to removal due to mineral-rich particles. Therefore, in particular when interpreting data from April (due to large runoff flows), we should be aware of the potential overestimation of $POC_{SE}$ export fluxes in the areas close to river mouths (i.e., IPB, CB, MER). It is also important to point out that POC fluxes estimated using the approach described above depend on the integration depth used (based on hydrographic data) and $POC/^{234}Th$ data available. For our analysis we chose the integration depth based on observations of density anomalies on our contemporaneous CTD profiles, and we used weighted average $POC/^{234}Th$ export ratios from our shallow and deep samples for our calculations.

$POC_{SE}$ export fluxes between 0.34 and 7.1 $g/m^2 \cdot d$ for April and 0.63 and 9.5 $g/m^2 \cdot d$ for August/September were similar to values previously reported by Charette et al. (2001) for this area at a similar depth (Table 4). In general, higher export fluxes were observed during August/September than April. Contrary to these observations Charette et al. (2001) observed the highest export fluxes during March, and the lowest ones during September. Our hydrographic data suggested that, although higher concentrations of $POC_{SE}$ were observed during April, surface mixing may have promoted particle resuspension (Brown and Irish, 1993; Gustafsson et al., 1998) and prevented settling of phytoplankton (Kalff, 2002). In contrast, during August/September the observed warmer, less dense surface seawater, may have reflected increased zooplankton feeding and fecal pellet sinking, thereby enhancing $POC_{SE}$ export fluxes. Destratification of the water column and phytoplankton blooms in this area are common during October-November and have been observed as early as September in the Jordan Basin (Thomas, 2003). However, the sharp temperature gradients, our low chlorophyll *a* concentrations, and our large $POC_{SE}$ fluxes indicate that our sampling was before the autumn destratification of the water column. Variations between our estimated POC export fluxes and those previously reported by Charette et al. (2001), point out to the sensitivity of these measurements due to seasonal and annual differences. For example, during certain years, phytoplankton peak blooms might occur earlier or be less intense than in other years (Thomas et al., 2003); similarly, variations in the intensity and the volume of runoff flows observed between years (Brown and Irish, 1987) might contribute to increased or decreased $POC_{SE}$ export fluxes.

### *3.5. Organic carbon (OC) sedimentation fluxes*

Unlike values previously reported for sediment traps (18 $g_{OC}/m^2 \cdot yr$ and 15 $g_{OC}/m^2 \cdot yr$ for WB and JB at 150 m deep during October 1995; Pilskaln, 1997) and average sedimentation burials (5 $g_{OC}/m^2 \cdot yr$; Christensen, 1989) in this area, our estimated sedimentation rates in surface sediments in the GoM were somewhat higher at between 21 (WB1) and 64 (CCB) $g_{OC}/m^2 \cdot yr$ (Figure 3). CCB and IPB, close to shore stations, presented the highest sedimentation rates, followed by MWRA (a close to shore site) and JB (an offshore site). However, the sediment-integrated $^{210}Pb$ inventory at JB of 94 $dpm/cm^2$ was more than twice the atmospheric input 39 $dpm/cm^2$ reported by Grausteing and Turekian (1986), indicating focusing of sedimentation material at this basin. Integrated $^{210}Pb$ inventories of 45, 33, 26, and 26 $dpm/cm^2$ were seen for MWRA, WB, CCB, and IPB, respectively, indicated that neither focusing nor horizontal transfers were main transport processes in these areas (Heit and Miller, 1987). Charette et al. (2001) reported organic carbon burials of 28 and 7.2 $mg/m^2 \cdot d$ for WB and JB, respectively, which correspond to 10 and 2.6 $g/m^2$ on an annual basis. These values are much lower than what we observed. For their calculations they considered a constant sediment accumulation rate for the whole region of 1 mm/yr previously reported by Hulbert and Given (1975), while Gustafsson et al. (1998b) reported 2.4 mm/yr for this area, and we measured sediment accumulation rates of 3.4 mm/yr for WB and 6.5 mm/yr for Jordan Basin (without focusing correction). However, due to our limited spatial data, we are unable to say whether or not this estimate may be more representative of the whole GoM area than the value reported by Charette et al. (2001).

Burial rates generally decreased with increasing depth into the sediment bed at MWRA, JB, and CCB; remained relatively constant at WB; and had an initial increase followed by an eventual decrease at IPB (Figure 3). Variations in the observed fluxes could be attributed to (a) variations in the amount of material and the sources of the material deposited; (b) differences in

the characteristics of the depositional basin (e.g. oxic vs anoxic); and, (c) changes in the concentrations of detrital mineral phases in the settling material (Hedges and Keil, 1995). To have a better understanding of the main factors involved in sedimentation rates in the GoM, here again we looked at C/N ratios. Consistent with our previous observations of increasing C/N ratios with increasing depths of the water column, C/N ratios at the surficial sediments in all of our samples were higher than in the water column. IPB and MWRA were the two stations with the highest C/N ratios, indicating the presence of terrestrial sources, while JB, WB and CCB were lower and presented similar values, possibly indicating similar sources. However, for the most part, C/N values remained unchanged with increasing depth or went back to the surficial value after an initial increase (Figure 4). Waskman et al. (1933) and Wang et al. (1998) reported similar C/N ratios for the same area of study (WB and JB) and the northeastern Pacific Ocean, respectively. From these observations, Wang et al. (1998) concluded that carbon and nitrogen degradation rate constants were about the same. However, since nitrogen-preferential remineralization was observed in the water column, we believe that a more likely explanation is that degradation at these sites is minimal (due to anoxic sediments or mineral entrapment; Hedges and Keil, 1995) and that changes in fluxes with decreasing depth indicate variations in the intensity and source of the buried material.

### *3.6. Mass balance of the GoM*

Our main goals in developing a carbon mass balance were (a) to estimate the main carbon inputs and outputs of organic matter into the GoM and (b) to identify internal or external sources or sinks, towards increasing our understanding of the carbon cycling in this region. For this purpose, we used our TOC concentrations to estimate total carbon inputs from rivers, the Scotian

Shelf Water, and the Slope Water; and outputs from the Maine Surface Water, and the Maine Intermediate Water (Figure 5; Table S3 and S4). To estimate export from the surface ocean into the deeper ocean, we used our April POC export fluxes (Table S3). To estimate export to the benthos, we used our measured sedimentation rates (Figure 3). To estimate wet and dry deposition of organic carbon from the atmosphere, we followed the model described in Seinfeld and Pandis (1998) using the scavenging coefficients reported by Daggupaty et al. (2003). We used average data from atmospheric TOC concentrations reported above the GoM during 2004 (Heald, et al., 2006). Finally, since we were not able to collect contemporary information of primary productivity during our sampling campaigns, to estimate the export/production ratio in this area (Buesseler, 1998), we used an average gross annual primary productivity of 420 $g/m^2 \cdot yr$ (Buesseler, 1998; Charette et al., 2001; O'Reilley and Bush, 1984). For this exercise, we considered the total area of the GoM to be 200,000 $km^2$, and detailed bathymetric data (surface area every 10m) that divided the GoM in 10 regions (Scotian Shelf and Eastern Coastal Shelf, Bay of Fundy, Northern Coastal Shelf, Southern Coastal Shelf, Great South Channel, Georges Bank, Georges Basin, Jordan Basin, Wilkinson Basin, and Central Gulf of Maine; USGS, 2004). Where data was not available, concentrations were extrapolated from our values and previous TOC measurements (Dai and Benitez-Nelson, 2001; Whitehouse et al., 1990).

Due to differences in the time scales of the processes under consideration (e.g., for practicality, sedimentation rates are measured on an annual basis while surface water export fluxes are calculated on a monthly basis) and seasonal and annual variations, here we present a mass balance on an annual basis. As mentioned before, comparing our August TOC concentrations with the values reported by Dai and Benitez-Nelson (2001) indicated that TOC remains relatively constant throughout the year, and, therefore, we consider our values to be

good approximation of average annual TOC concentrations. However, based on previous observations from primary production variability (O'Reilly and Dow, 2006) and to avoid overestimations due to above-average POC export fluxes observed in August/September, April values were considered to be good estimates for average annual export fluxes.

Our mass balance indicated that primary productivity was the main source of organic carbon to this area (Figure 5). The major external inputs of organic carbon into the GoM were the Scotian Shelf Water and the Slope Water, and the major outputs were the Maine Surface Water and the Maine Intermediate Water, while river and atmospheric inputs were relatively minor. Similar to what has been previously reported, our mass balance indicates that less than 7% of the primary production reached the sediments, while the other 93% was either recycled within the mixed layer or exported in the southern GoM water currents (Maine Surface and Intermediate Waters). Also, similar to previous studies in this area (Benitez-Nelson et al., 2000; Buesseler, 1998; O'Reilly and Busch, 1984), we found that our estimated POC export fluxes from the surface seawater layer corresponded to about 50% of the gross primary productivity. Considering all the inputs and outputs of our system, this finding indicates that about 80% of the gross primary productivity was respired, while only about 20% corresponded to net primary productivity. The GoM is known to be a very productive area, and previous estimates of net primary productivity in the euphotic zone have been estimated to be between 65 and 80% of the gross primary productivity (Duarte and Cebrian, 1996; O'Reilly and Dow, 2006; Ji et al., 2007). Although it is possible that our mass balance might be overlooking an important source term, our results suggest that carbon remineralization continued to be extensive below the euphotic zone. Finally, our estimated mass balance indicates that the GoM has a net export of OC into the

northeastern North America circulation system on its way towards Cape Hatteras (Beardsley et al., 1996).

## 4. Conclusions

Although uncertainties in the mass balance presented here arise from the lack of additional information regarding the inter- and intra-annual variations, this study allowed us to have a better understanding of some of the main process that organic carbon undergoes before and after burial in the GoM. Our measured TOC and POC concentrations and our estimated POC fluxes were consistent with the contemporaneous measurements of salinity, temperature, chlorophyll *a*, and dissolved $O_2$ concentrations, and the annual cycle in the GoM. Consistent with phytoplankton blooms, OC concentrations (TOC, $POC_{SE}$ and $POC_{SU}$) were generally higher in April than in August/September and closer to the shore. Contrary to previous investigators (Buesseler, 1998; Charette et al., 2001) where it has been reported that phytoplankton blooms are responsible for most of the export fluxes of POC, we saw large fluxes when blooms were not apparent. In addition, the higher POC export observed during August/September than April may reflect changes in the food web structure during the summer, resulting in increased grazing and fecal pellet production (Meise and O'Reilly, 1996). Since most particulate export studies have been made during (or around) phytoplankton blooms, larger POC export fluxes measured during August/September instead of April (phytoplankton bloom), suggest that global estimates of OC export fluxes, and therefore the biological pump, may be underestimated. Finally, our mass balance indicated that a large part of the settling material was recycled within the water column and although preferential remineralization was observed within the water column (increased C/N

ratio), once the settling material reached the sediments, variations in C/N ratios were small, indicating minimal remineralization of organic material in these coastal sediments

Some of the caveats of the presented mass balance include the lack of colloidal and dissolved phase export fluxes; and the lack of contemporaneous primary productivity measurements. Dai and Benitez-Nelson (2001) reported that colloidal OC represented an important fraction of OC. However, they also reported that the estimated export fluxes of colloidal OC and dissolved OC were small compared to POC. This study and comparison with previous studies point out to the importance of including contemporary data to the fate and transformation processes of carbon due to inter- and intra-annual variations in the GoM. However, additional field studies are needed to address seasonal and intra-annual variations, to corroborate previous findings, and to monitor changes and variations that affect our understanding of this coastal system.

## 5. Acknowledgments

We thank the captains, crews, and CTD technicians of *R/V Oceanus* and *R/V Cape Hatteras*, and R. K. Nelson, S. Silva, Ellen Roosen, Kristin Pangallo, Emily Peaock, and Emma Feuten for their help in water and sediment sample collection. We are also grateful for support from NFS grants (OCE-0223441 and BES-0607136) and CONACYT and MSFS fellowships to D. F.

## References

Appleby, P. G., Oldfield, F., 1978. The calculation of lead-210 dates assuming a constant rate of supply of unsupported 210Pb to the sediment. Catena 5, 1-8.

Appleby, P. G., 2001. Chronostratigraphic techniques in recent sediments. In Tracking environmental change using lake sediments; Last, W., Smol. J., Ed.; Kluwer Academic Publishers: Dordrecht, The Netherlands; Vol 1, pp. 171-203. .

Alldredge, A. L., 1976. Discarded appendicularian houses as sources of food, surface habitats, and particulate organic matter in planktonic environments. Limnol. Oceanogr. 21, 14-23.

Aluwihare, L. I., Repeta, D. J., Chen, R. F., 1997. A major biopolymeric component to dissolved organic carbon in seawater. Nature 387, 166-169.

Beardsley, R. C., Butman, B., Geyer, W. R., Smith, P. 1996. Physical oceanography of the Gulf of Maine: an update. In Proceedings of the Gulf of Maine Ecosystem Dynamics; Wallace, G. T. and E. F. Braasch, Ed. Regional Association for Research on the Gulf of Maine: St. Andrews, New Brunswick, pp. 39-52.

Beaulieu, S. E., Smith, K. L., 1998. Phytodetritus entering the benthic boundary layer and aggregated on the sea floor in the abyssal NE Pacific: Macro- and microscopic composition. Deep-Sea Res. 45, 781-815.

Berner, R. A., 1989. Biogeochemical cycles of carbon and sulfur and their effect on atmospheric oxygen over Phanerozoic time. Global Planetary Change 1, 97-122, doi:10.1016/0921-8181(89)90018-0.

Benitez-Nelson, C. R., Buesseler, K. O., Crossin, G., 2000. Upper ocean carbon export, horizontal transport, and vertical eddy diffusivity in the southwestern Gulf of Maine.

Bishop, J. K. B., Edmond, J. M., 1976. A new large volume filtration system for the sampling of oceanic particulate matter. J. Mar. Res. 34, 181-198.

Brooks, D. A., 1985. Vernal circulation in the Gulf of Maine. J. Geophys. Res. 90, 4687-4705.

Brown, W.S., Irish, J.D., 1993. The annual variation of water mass structure in the Gulf of Maine: 1986-1987. J. Mar. Res. 51, 53-107.

Buesseler, K.O., Cochran, J.K., Bacon, M.P., Livingstone, H.D., Casso, A., Hirschberg, D., Hartman, M.C., Fleer, A.P., 1992. Determination of thorium isotopes in seawater by non-destructive and radiochemical procedures. Deep-Sea Res., 39, 1102-1114.

Buesseler, K. O., 1998. The decoupling of production and particulate export in the surface ocean. Global Biogeochem. Cycles. 12, 297-310.

Charette, M. A., Moran, S. B., Pike, S. M., 2001. Investigating the carbon cycle in the Gulf of Maine using the natural thorium tracer. J. Geophys. Res. 106, 553-579.

Chen, J.H., Edwards, R.L., Wasserburg, G.J., 1986. 238U, 234U and 232Th in seawater. Earth Planet Sci. Lett., 80: 241-251.

Cochran,J.K., Bames, C., Achman, D., Hirschberg, D. J., 1995. Thorium-234/Uranium-238 disequilibrium as an indicator of scavenging rates and particulate organic carbon fluxes in the Northeast Water Polynya, Greenland. J. Geophys. Res. 100, C3, 4399-4410.

Christensen, J. P., 1989. Sulfate reduction and carbon oxidation rates in continental shelf sediments, an examination of offshelf carbon transport. Cont. Shelf Res. 9, 223-246.

Dai, M.H., Benitez-Nelson, C.R., 2001. Colloidal organic carbon and 234Th in the Gulf of Maine. Mar. Chem. 2001, 74, 181-196.

Daggupaty, S.M., Banic, C.M., Cheung, P., Ma, J., 2006. Numerical simulation of air concentration and deposition of particulate metals around a copper smelter in northern Québec, Canada. Geochemistry: Exploration, Environment, Analysis, 6, 139–146.

Duarte, C. M. and J. Cebrian. 1996. The fate of autotrophic production in the sea. Limnol. Oceanogr. 41, 1758-1766.

Durbin, E., 1996. Zooplankton dynamics of the Gulf of Maine and Georges Bank region. In Proceedings of the Gulf of Maine Ecosystem Dynamics; Wallace, G. T. and E. F. Braasch, Ed. Regional Association for Research on the Gulf of Maine: St. Andrews, New Brunswick, pp. 53-67.

Eglinton, T.I., Repeta, D.J., 2004. Organic matter in the contemporary ocean. Treatise Geochem. 6, 145.

Eppley, R.W., Peterson, B. J., 1979. Particulate organic matter flux and phytoplankton new production in the deep ocean. Nature, 282: 677-680.

Gagosian, R. B., Peltzer, E. T., 1986. The importance of atmospheric input of terrestrial organic material to deep sea sediments. Org. Geochem. 10, 661-669.

GoMOOS (Gold of Maine Ocean Observing System), http://www.gomoos.org (accessed multiple times during 2007).

Graustein, W.C., Turekian, K. K., 1986. 210Pb and 137Cs in air and soils measure the rate and vertical distribution of aerosol scavenging. J. Geophys. Res. 91, 14,355-14,366.

Graziano, L. M., Balch, W. M., Drapeau, D., Bowler, B. C., Vaillancourt, R., Dunford, S., 2000. Organic and inorganic carbon production in the Gulf of Maine. Cont. Shelf. Res. 20, 685-705.

Gustafsson, Ö., Buesseker, K.O., Geyer, W.R., Moran, S.B., Gschwend, P.M., 1998. An assessment of the relative importance of horizontal and vertical transport of particle-reactive chemicals in the coastal ocean. Cont. Shelf Res. 18, 805-829.

Gustafsson, Ö., Gschwend, P.M., 1998. The flux of black carbon to surface sediments on the New England continental shelf. Geochim. Cosmochim. Acta, 62, 465-472.

Gough, M. A., Mantoura, R. F. C., Preston, M., 1993. Terrestrial plant biopolymers in marine sediments. Geochim. Cosmochim. Acta 57, 945-964.

Heald, C. L., Jacob, D. J., Turquety, s., Hudman, R. C., Weber, R. J., Sullivan, A. P., Peltier, R. E., Atlas, E. L., de Gouw, J. A., Warneke, C., Holloway, J. S., Neuman, A., Flocke, F. M., Seinfeld, J. H., 2006. Concentrations and sources of organic carbon aerosols in the free atmosphere over North America. J. Geophys. Res. 111, doi:10.1029/2006JD007705.

Hedges, J. I., 1992. Global biogeochemical cycles: progress and problems. Mar. Chem. 39, 67-93.

Hedges, J. I., Keil, R. G., 1995. Sedimentary organic matter preservation: an assessment and speculative synthesis. Mar. Chem., 49, 81-115.

Heit, M., Miller, K. V., 1987. Cesium-137 sediment profiles and inventories in Adirondack Lake sediments. Biogeochemistry, 3, 243-265.

Hulbert, M. A., Given, D.N., 1987. Geotechnical and chemical property relationships for Wilkinson Basin, Gulf of Maine, sediments. J. Sediment. Petrol., 45, 504-512.

Incze, L., Jakobbson, M., 2008. Hypsometric characterization of the Gulf of Maine, Georges Bank, Scotian Shelf and neighboring continental slope. http://www.usm.maine.edu/gulfofmaine-census/ (accessed October, 2004).

Kalff, J., 2002. Limnology; Prentice-Hall Inc.: Englewood, NJ, USA, pp. 608.

Körztinger, A., Hedges, J. I., Quay, P. D., 2001. Redfield ratios revisited: removing the biasing effect of anthropogenic CO2. Limnol. Oceanogr. 46, 964-970.

Mari, X., Beauvais, S., Lemee, R., Pedrotti, M. L., 2001. Non-Redfield C:N ratio of transparent exopolymeric particles in the northwestern Mediterranean Sea. Limnol. Oceanogr. 46, 1831-1836.

Meise, C.J., O'Reilley, J. E., 1996. Spatial and seasonal patterns in abundance and age-composition of *Calanus finmarchicus* in the Gulf of Maine and Georges Bank: 1977-1987. Deep-Sea Research II 43, 1473-1501.

Mown, C. B., Yoder, J. A., 2005. Primary production calculations in the Mid-Atlantic Bight, including effects of phytoplankton community size structure. Limnol. Oceanogr. 50, 1232-1243.

O'Reilly, J. E., Bush, D. A., 1984. Phytoplankton primary production on the northwestern Atlantic shelf. Rapp. P. V. Reun. Cons. Int. Explor. Mer. 183, 255-268.

O'Reilly, J. E., Dow, D. D., 2006. Phytoplankton and Primary Production. In Link JS, Griswold CA, Methratta ET, Gunnard J, Editors. 2006. Documentation for the Energy Modeling and Analysis eXercise (EMAX). US Dep. Commer., Northeast Fish. Sci. Cent. Ref. Doc. 06-15; 166 pp.

Pilskaln, C. H., 1997. Seasonal biogeochemical particle fluxes and sediment resuspension in the Gulf of Maine: preliminary results from an ongoing study. Fifth Meeting of The Oceanography Society, Program of abstracts: 67.

Redfield, A. C., Ketchum, B. H., Richards, F. A., 1963. The influence of organisms on the composition of seawater. In The sea. Hill, M. N., Ed.. Vol. 2; Wiley Interscience, New York, NY, pp. 26-77.

Riley, J. P., Chester, R., 1971. Introduction to Marine Chemistry. Academic Press, New York, NY, 465 pp.

Romankevich, E. A., 1984. Geochemistry of organic matter in the ocean. Springer, Berlin, 334 pp.

Seinfeld, J.H., Pandis, S.N., 1998. Atmospheric Chemistry and Physics: From Air Pollution to Climate Change. Wiley-Interscience: USA.

Smith, P.C., 1983. The mean and seasonal circulation off southwest Nova Scotia. J. Phys. Oceanogr., 13: 1034-1054.

Smith, P. C., 1996. Vertical exchange processes in the Gulf of Maine. In Proceedings of the Gulf of Maine Ecosystem Dynamics; Wallace, G. T. and E. F. Braasch, Ed. Regional Association for Research on the Gulf of Maine: St. Andrews, New Brunswick, pp. 117-134.

Sverdrup, H.U., Johnson, M.W., Fleming, R.H., 1946. The oceans: Their physics, chemistry, and general biology. Prentice Hall, Englewood Cliffs, NJ.

Thomas, A. T., Townsend, D. W., Weatherbee, R., 2003. Satellite-measured phytoplankton variability in the Gulf of Maine. Cont. Shelf Res. 23, 971-989.

Townsend, D.W., 1996. Cycling of carbon and nitrogen in the Gulf of Maine. In Proceedings of the Gulf of Maine Ecosystem Dynamics; Wallace, G. T. and E. F. Braasch, Ed. Regional Association for Research on the Gulf of Maine: St. Andrews, New Brunswick, pp. 117-134.

Townsend, D. W., Keller, M. D., 1996b. Dimethylsulfide (DMS) and dimethylsulfoniopropionate (DMSP) in relation to phytoplankton in the Gulf of Maine. Mar. Ecol. Prog. 137, 229-241.

USGS (United States Geological Survey). Publications warehouse. http://pubs.usgs.gov/. (accessed in 2004).

Von Arx, W. S., 1962. An introduction to physical oceanography. Addison-Wesley, Reading, MA. 422 pp.

Waksman, S. A., Reuszer, H. W., Carey, C. L., Hotchkiss, M., Renn, C.E., 1933. Studies on the biology and chemistry of the Gulf of Maine. III. Bacteriological investigations of the sea watter and marine bottoms. Biol. Bull. 64, 183-206.

Wang, X-C., Druffel, E. R. M., Griffin S., Lee, C., Kashgarian, M., 1998. Radiocarbon studies of organic compound classes in plankton and sediments of the northeastern Pacific Ocean. Geochim. Cosmochim. Acta 62, 1365-1378.

Weiss, R., 1970. The solubility of nitrogen, oxygen, and argon in water and seawater. Deep-Sea Res. 17, 721-735.

Whitehouse, B.G., Yeats, P.A., Strain, P.M., 1990. Cross-flow filtration of colloids from aquatic environments. Limnol. Oceanogr., 35(6): 1368-1375.

Yoshida, J., Oakey, N. S., 1996. Characterization of vertical mixing at a tidal front on Georges Bank. Deep Sea Res. 43, 1713-1744.

**Figure captions.**

**Figure 1**. Hydrography of the GoM and surface and deep layer circulation during the stratified season (Beardsley et al., 1996 after Brooks, 1985).

**Figure 2.** Seawater POC and sediment sampling locations.

**Figure 3.** TOC sedimentation rates ($g_{TOC}/m^2 \cdot yr$) in the GoM.

**Figure 4.** Carbon-to-nitrogen ratio in sediment profiles in the GoM. Filled diamonds and squares represent MRWA and JB, respectively; open triangles, circles, and squares represent IPB, WB, and CCB, respectively.

**Figure 5**. Organic carbon mass balance in the GoM. $Tg = 10^{15}$ g. Detailed bathymetric data from Incze and Jakobsson (2008); atmospheric BC concentrations from Heald et al. (2006); water volumetric flows from Townsend (1996), and TOC water content and sedimentation rates from this study (Table S3 and S4).

**Table captions**

**Table 1.** Gulf of Maine (GoM) sampling stations site identification, total organic carbon (TOC; mg/L), and oxygen saturation (%) observed during August 2004 (*R/V Cape Hatteras*).

**Table 2.** Suspended particulate organic carbon ($POC_{SU}$; μg/L) concentrations and C/N ratios in the GoM.

**Table 3.** Settling particulate organic carbon ($POC_{SE}$ μg/L) concentrations and C/N ratios in the GoM.

**Table 4.** $POC_{SE}$ export fluxes in the GoM ($g/m^2 \cdot d$).

**Table 1.** Gulf of Maine (GoM) sampling stations site identification, total organic carbon (TOC; mg/L), and oxygen saturation (%) observed during August 2004 (*R/V Cape Hatteras*).

| Location | Sample Name-depth (m) | Lat +N/-S | Long +E/-W | TOC[a] mg/L | | $O_2$ saturation (%) April | Aug/Sep |
|---|---|---|---|---|---|---|---|
| Mass. Water Resources Authority. (6 m) | MWRA-6 | 42.37 | -70.81 | 1.44 ± 0.03 | 1.76[b] | 99.6 | 99.8 |
| Mass. Water Resources Authority. (20 m) | MWRA-20 | 42.37 | -70.81 | 1.25 ± 0.04 | | 99.7 | 99.7 |
| North Mass. Bay (6 m) | NMB-6 | 42.52 | -70.45 | n.m. | | 100.3 | - |
| North Mass. Bay (50 m) | NMB-50 | 42.52 | -70.45 | n.m. | | 100.4 | - |
| Merrimack River (6 m) | MER-6 | 42.81 | -70.73 | 1.56 ± 0.04 | | 100.8 | 100.0 |
| Merrimack River (20 m) | MER-20 | 42.81 | -70.73 | 1.25 ± 0.03 | | 99.7 | 99.1 |
| Casco Bay (6 m) | CB-6 | 43.56 | -70.05 | 1.51 ± 0.04 | 1.54[b] | 100.4 | 99.5 |
| Casco Bay (15 m) | CB-15 | 43.56 | -70.05 | 1.40 ± 0.06 | | 99.9 | 100.0 |
| Wilkinson Basin I (6 m) | WB1-6 | 42.99 | -69.90 | 1.30 ± 0.02 | 1.19[b] | 99.2 | 102.5 |
| Wilkinson Basin I (80 m) | WB1-80 | 42.99 | -69.90 | 1.16 ± 0.07 | 0.85[b] | 100.1 | 99.5 |
| Wilkinson Basin II (8 m) | WB2-8 | 43.37 | -69.89 | n.m. | | 100.3 | - |
| Wilkinson Basin II (30 m) | WB2-30 | 43.37 | -69.89 | n.m. | | 99.8 | - |
| East Platts Bank (6 m) | EPB-6 | 43.11 | -69.18 | n.m. | | 99.8 | 105.2 |
| East Platts Bank (35 m) | EPB-35 | 43.11 | -69.18 | n.m. | | 100.0 | |
| East Platts Bank (80 m) | EPB-80 | 43.11 | -69.18 | 1.40 ± 0.09 | | - | 100.6 |
| Inner Penobscott Bay (3 m) | IPB-3 | 44.42 | -68.83 | 2.20 ± 0.04 | | 99.4 | 99.3 |
| Inner Penobscott Bay (6 m) | IPB-6 | 44.42 | -68.83 | 1.60 ± 0.04 | | 99.9 | 100.6 |
| Jordan Basin (8 m) | JB-8 | 43.41 | 67.41 | 1.40 ± 0.06 | | 99.9 | 101.6 |
| Jordan Basin (60 m) | JB-60 | 43.41 | 67.41 | n.m. | | 100.0 | - |
| Jordan Basin (80 m) | JB-80 | 43.41 | 67.41 | 1.11 ± 0.05 | | - | 99.6 |
| Georges Bank (8 m) | GB-8 | 41.75 | -68.00 | 1.22 ± 0.04 | | 100.1 | 97.9 |
| Georges Bank (60 m) | GB-60 | 41.75 | -68.00 | 1.10 ± 0.07 | | 100.3 | 100.2 |
| Great South Channel (8 m) | GSC-8 | 41.83 | -69.67 | 1.34 ± 0.06 | 1.42[b] | 100.5 | 99.7 |
| Great South Channel (60 m) | GSC-60 | 41.83 | -69.67 | 1.09 ± 0.04 | | 99.7 | 100.6 |
| Cape Cod Bay I (6 m) | CCB1-6 | 41.80 | -70.05 | n.m. | | 100.1 | |
| Cape Cod Bay II (6 m) | CCB2-6 | 41.92 | -70.17 | 1.64 ± 0.09 | 1.41[b] | 100.4 | 101.0 |
| Cape Cod Bay II (20 m) | CCB2-20 | 41.92 | -70.17 | 1.21 ± 0.04 | 1.35[b] | 100.2 | 101.5 |

[a]Collected during August 2004; [b]Dai and Benitez (2001); n.m. not measured

**Table 2.** Suspended particulate organic carbon ($POC_{SU}$; μg/L) concentrations and C/N ratios in the GoM.

| | April 2004 | | | August 2004 | | |
|---|---|---|---|---|---|---|
| **Sample** | **C (μg/L)** | | **C/N** | **C (μg/L)** | | **C/N** |
| MWRA-6 | 233 ± 1 | | 7.2 | 131 ± 1 | | 5.2 |
| MWRA-20 | 214 ± 1 | | 6.5 | 82.2 ± 1 | | 5.4 |
| NMB-6 | 220 ± 1 | | 5.9 | | | |
| NMB-50 | 29.8 ± 0.8 | | 4.5 | | | |
| MER-6 | 241 ± 1 | | N b.d.l. | 119 ± 1 | | 7.3 |
| MER-20 | 234 ± 2 | | 5.6 | 93.8 ± 0.1 | | 5.7 |
| CB-6 | 289 ± 1 | | 6.8 | 135 ± 1 | | 7.6 |
| CB-15 | 40.5 ± 0.5 | | 4.7 | 171 ± 1 | | 8.9 |
| WB1-6 | 112 ± 1 | 164[b] | 5.4 | 61.4 ± 0.1 | 38.9[c] | 6.2 |
| WB1-80 | 19.7[a] | 25.9[b] | | 14.3 ± 0.1 | | 24.6 |
| WB2-8 | 80.4 ± 0.5 | | 5.5 | | | |
| WB2-30 | 49.9 ± 1.4 | | 4.4 | | | |
| EPB-6 | 69.5 ± 0.4 | | 5.3 | 49.6 ± 0.1 | 216[d] | 7 |
| EPB-35 | 73.2 ± 0.5 | | 5.2 | | | |
| EPB-80 | | | | 27.4 ± 0.1 | 114[d] | 8.4 |
| IPB-3 | 280 ± 1 | | 8.8 | 270 ± 1 | | 6.4 |
| IPB-6 | 196 ± 1 | | 7.1 | 185 ± 1 | | 5.8 |
| JB-8 | 117[a] 87.5 ± 0.5 | 46.2[b] | 5.9 | 67.0 ± 0.1 | 29.2[c] | 7.4 |
| JB-60 | 23.7[a] 26.3 ± 0.6 | 72.2[b] | 5.3 | | | |
| JB-80 | | | | 19.9 ± 0.1 | | 8 |
| GB-8 | 132 ± 1 | | 6.2 | 49.4 ± 0.1 | ~29[d] | 7.1 |
| GB-60 | <1[e] | | - | 51.8 ± 0.1 | ~72[d] | 5.3 |
| GSC-8 | 120 ± 1 | | 5.7 | 167 ± 1 | 114[d] | 7 |
| GSC-60 | | | | 23.4 ± 0.1 | 60[d] | 5.1 |
| CCB1-6 | 230 ± 2 | | 5.9 | | | |
| CCB2-6 | 155 ± 1 | | 6.7 | 94.8 ± 0.1 | | 6.3 |
| CCB2-20 | | | | 85.2 ± 0.1 | | 8.9 |

[a]Charette et al. (2001) March, 1995; [b]Charette et al. (2001) June, 1995; [c]Charette et al. (2001) September, 1995; [d]Charette et al. (2001) August-September, 1997; [e]< x if signal to noise raitio is less than 3:1; Uncertainty for GFF/Quartz calculated error propagation (including sampling and analytical error); uncertainty for Nitex screen is ± 1σ (n=3).

**Table 3.** Settling particulate organic carbon concentrations ($POC_{SE}$; μg/L) and C/N ratios in the GoM.

| Sample | April 2004 | | | | | | August 2004 | | | |
|---|---|---|---|---|---|---|---|---|---|---|
| | C (mg/L) | | | C/N | | | C (mg/L) | | C/N | |
| MWRA-6 | | 89.2 ± 6.93 | | | 101.1 | | 13.0 ± 4.7 | | 24.5 | |
| MWRA-20 | | 33.7 ± 15.46 | | | N b.d.l. | | 21.2 ± 12.1 | | 48.9 | |
| NMB-6 | | 75.5 ± 2.84 | | | 8 | | | | | |
| NMB-50 | | 5.79 ± 0.66 | | | N b.d.l. | | | | | |
| MER-6 | | 47.1 ± 1.32 | | | 13.4 | | 9.87 ± 1.91 | | 16.3 | |
| MER-20 | | 23.9 ± 1.47 | | | N b.d.l. | | <1[e] | | N b.d.l. | |
| CB-6 | | 34.8 ± 1.91 | | | 9.7 | | 10.1 ± 3.1 | | 130.9 | |
| CB-15 | | 23.8 ± 0.76 | | | N b.d.l. | | 19.6 ± 0.7 | | 19.8 | |
| WB1-6 | 4.44[a] | 35.8 ± 1.86 | 14.8[b] | 9.3[a] | 48.9 | 18[b] | 1.80 ± 0.54 | 5.28[c] | 61.6 | 20[c] |
| WB1-80 | 2.04[a] | | 17.9[b] | | | | 2.47 ± 2.33 | | 49.4 | |
| WB2-8 | | 199 ± 4.59 | | | 20.1 | | | | | |
| WB2-30 | | 21.2 ± 1.95 | | | N b.d.l. | | | | | |
| EPB-6 | | 19.0 ± 0.14 | | | N b.d.l. | | 6.06 ± 2.20 | 2.4[d] | 168.6 | |
| EPB-35 | | 8.25 ± 0.59 | | | N b.d.l. | | | | | |
| EPB-80 | | | | | | | 1.45 ± 1.13 | 2.3[d] | N b.d.l. | |
| IPB-3 | | 6.08 ± 3.03 | | | N b.d.l. | | 20.7 ± 2.6 | | 12.3 | |
| IPB-6 | | 8.42 ± 12.39 | | | 49 | | 24.4 ± 0.9 | | 30.5 | |
| JB-8 | 16.9[a] | 39.2 ± 0.26 | 10.5[b] | 7.8[a] | 23.7 | 6.3[b] | 5.10 ± 0.17 | 6.72[c] | 45.9 | 21[c] |
| JB-60 | 2.28[a] | 10.7 ± 0.38 | 9.84[b] | | N b.d.l. | | | | | |
| JB-80 | | | | | | | <1[e] | | N b.d.l. | |
| GB-8 | | 23.8 ± 0.99 | | | 39.7 | | 3.47 ± 2.58 | ~6.6[d] | 23 | |
| GB-60 | | 45.2 ± 12.4 | | | | | <1[e], ~4.0[d] | | N b.d.l. | |
| GSC-8 | | 29.2 ± 1.40 | | | 24.2 | | 20.4 ± 1.6 | 5.2[d] | 139.3 | |
| GSC-60 | | | | | | | <1[e] | 4.8[d] | N b.d.l. | |
| CCB1-6 | | 10.2 ± 4.88 | | | N b.d.l. | | | | | |
| CCB2-6 | | 14.3 ± 4.81 | | | N b.d.l. | | 18.7 ± 4.9 | | 16.9 | |
| CCB2-20 | | | | | | | 29.0 ± 1.1 | | 35 | |

[a]Charette et al. (2001) March, 1995; [b]Charette et al. (2001) June, 1995; [c]Charette et al. (2001) September, 1995; [d]Charette et al. (2001) August-September, 1997; [e]< x if signal to noise raitio is less than 3:1; Uncertainty for GFF/Quartz calculated error propagation (including sampling and analytical error); uncertainty for Nitex screen is ± 1s (n=3).

**Table 4.** $POC_{SE}$ export fluxes in the GoM ($g/m^2 \cdot d$).

| Station | April 2004 C ($g/m^2 \cdot d$) | | | August 2004 C ($g/m^2 \cdot d$) | |
|---|---|---|---|---|---|
| MWRA | | 3.4 ± 0.3 | | 9.5 ± 1.6 | |
| NMB | | 1.2 ± 0.1 | | | |
| MER | | 0.34 ± 0.03 | | 3.2 ± 0.5 | |
| CB | | 2.3 ± 0.1 | | 3.6 ± 0.5 | |
| WB1 | 0.17 ± 0.04[a] | 0.90 ± 0.08 | 0.08 ± 0.05[b] | 2.6 ± 1.4 | 2.7 ± 0.1[c] |
| WB2 | | 2.6 ± 0.2 | | | |
| EPB | | 0.66 ± 0.08 | | 4.0 ± 1.4 | |
| IPB | | 0.51 ± 0.10 | | 4.7 ± 0.4 | |
| JB | 0.32 ± 0.17[a] | 0.30 ± 0.3 | 0.47 ± 0.13[b] | 2.6 ± 0.2 | 0.13 ± 0.02[c] |
| GB | | 4.1 ± 0.4 | | 0.63 ± 0.47 | |
| GSC | | 0.52 ± 0.04 | | 5.9 ± 0.6 | |
| CCB1 | | 2.4 ± 1.1 | | | |
| CCB2 | | 2.9 ± 1.0 | | 5.3 ± 0.4 | |

Charette et al. (2001) during: [a]March 1995, [b]June, 1995; and [c]September, 1995. Integration depth used to estimate POC fluxes was chosen based on observations on CTD profiles. Weighted average POC/$^{234}$Th export ratios were used for calculations (except when data was not available; see Table S1 and S2).

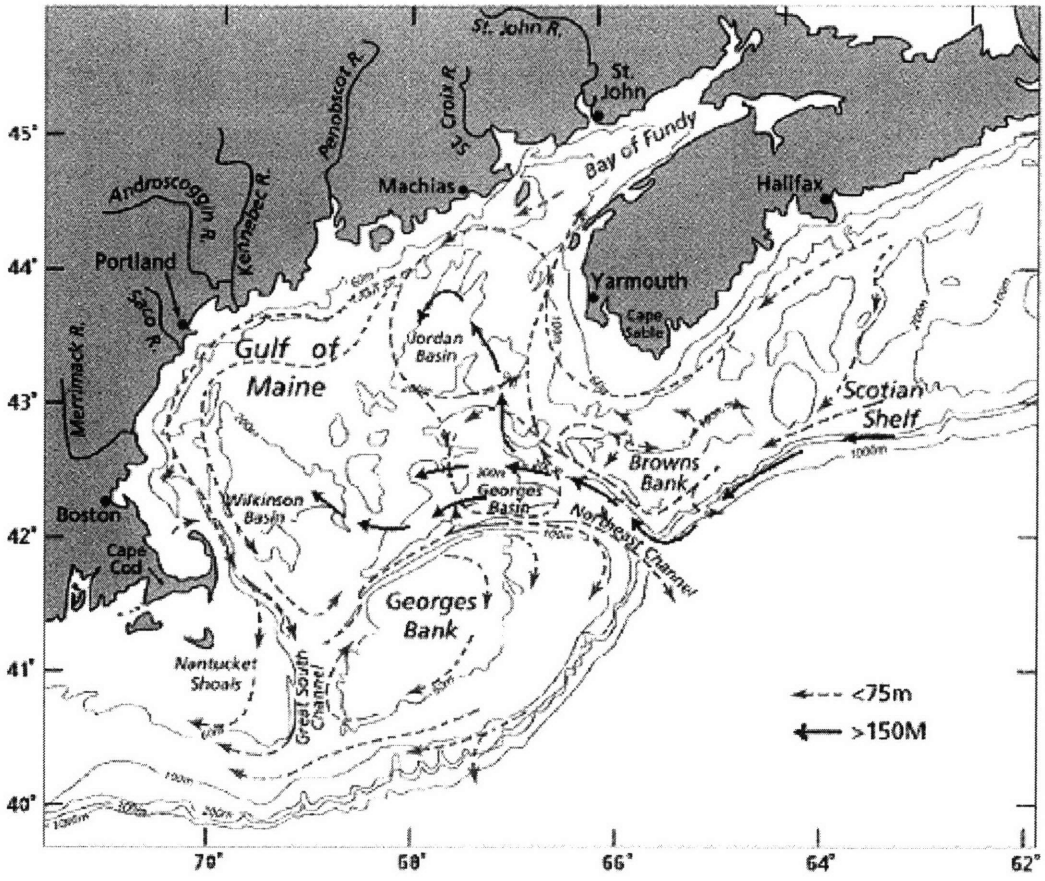


**Figure 1**. Hydrography of the GoM and surface and deep layer circulation during the stratified season (Beardsley et al., 1996 after Brooks, 1985).

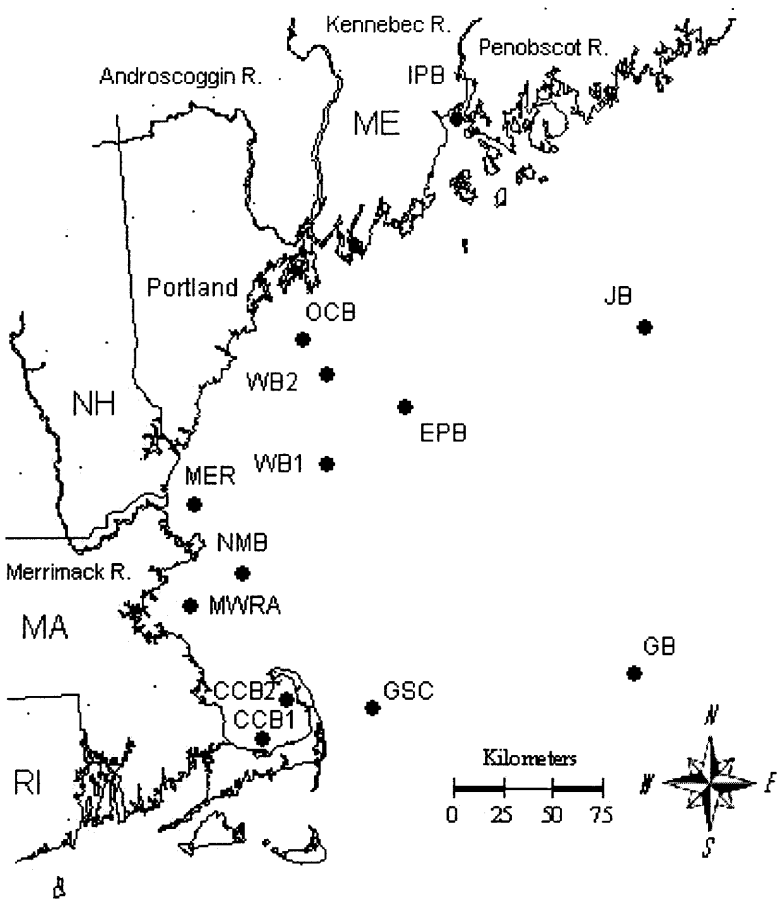


**Figure 2.** Seawater POC and sediment sampling locations

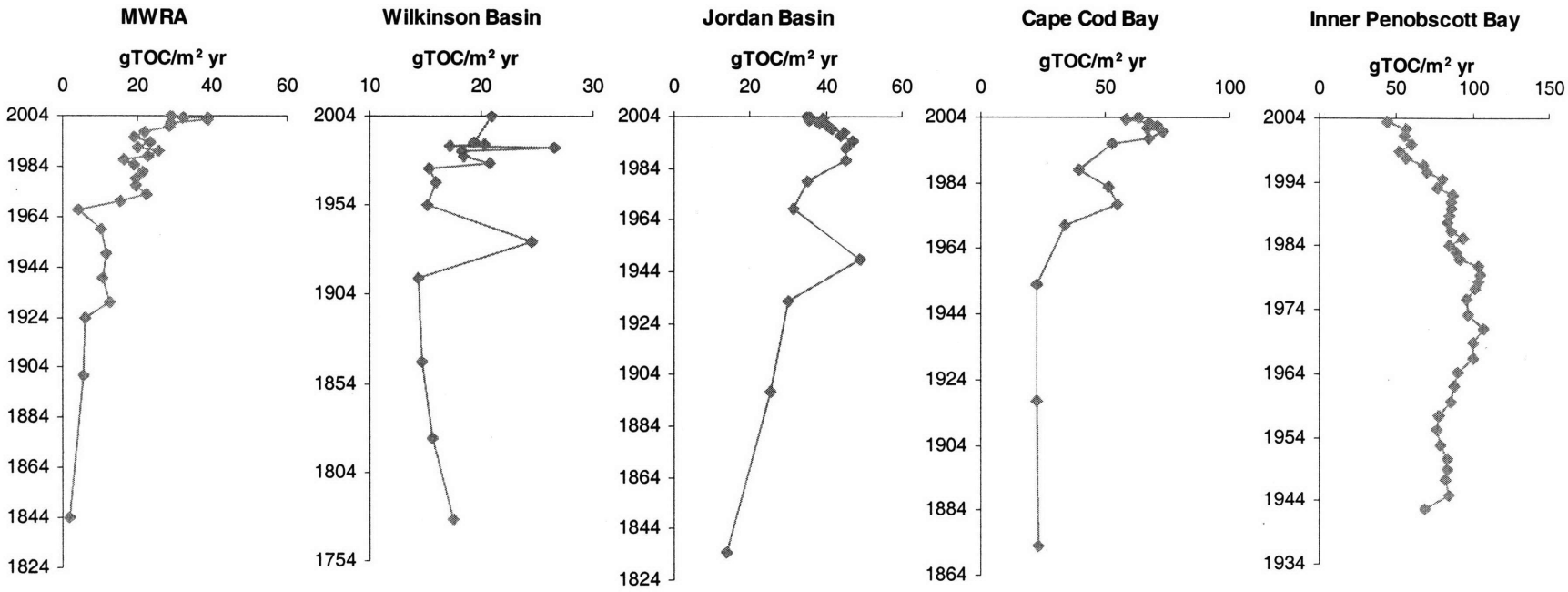


**Figure 3.** TOC fluxes ($g_{TOC}/m^2 \cdot yr$) in sediments in the GoM

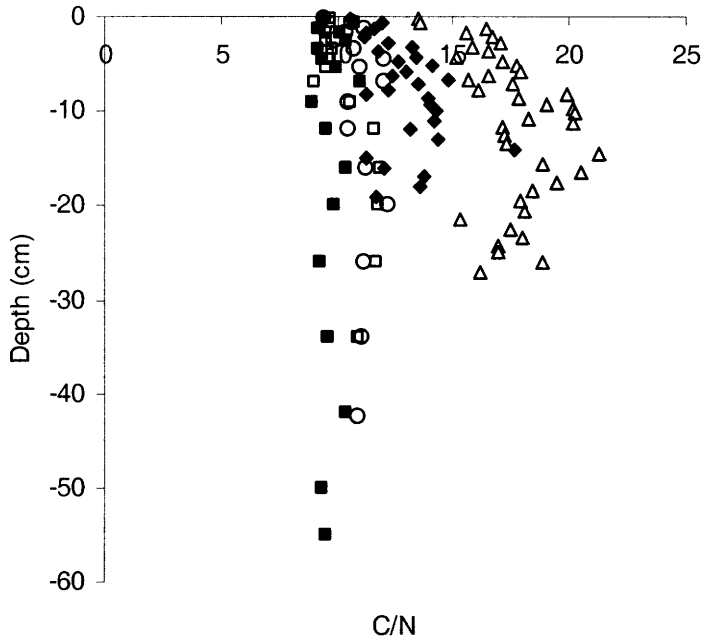


**Figure 4.** Carbon-to-nitrogen ratio in sediment profiles in the GoM. Filled diamonds and squares represent MRWA and JB, respectively; open triangles, circles, and squares represent IPB, WB, and CCB, respectively.

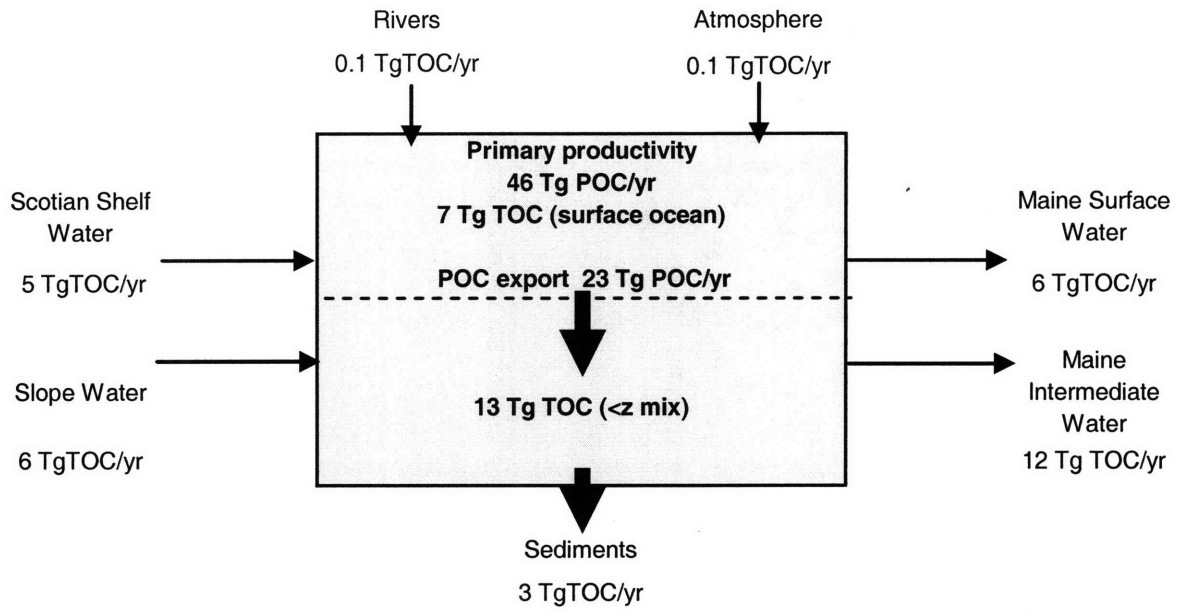


**Figure 5**. Organic carbon mass balance in the GoM. Tg = $10^{12}$ g. Detailed bathymetric data from Incze and Jakobsson (2008); atmospheric BC concentrations from Heald et al. (2006); water volumetric flows from Townsend (1996), and TOC water content and sedimentation rates from this study (Table S3 and S4).

**Supplementary Information for:**

**"Organic carbon cycling and water column characterization in the Gulf of Maine"**

D. Xanat Flores-Cervantes[1], Desiree L. Plata[1, 2], John K. MacFarlane[1], Christopher M. Reddy[2], and Philip M. Gschwend[1].

[1]R.M. Parsons Laboratory, MIT 48-413, Department of Civil and Environmental Engineering, Massachusetts Institute of Technology, Cambridge, Massachusetts 02139, USA

[2]Department of Marine Chemistry and Geochemistry, Woods Hole Oceanographic Institution, Woods Hole, Massachusetts, 02543

xanatf@mit.edu, dplata@whoi.edu, jmac@mit.edu, creddy@whoi.edu, pmgschwe@mit.edu.

This document includes:

Figures S1, S2

Tables S1, S2, S3, S4

## Figure Captions

**Figure S1.** Vertical profiles of temperature (°C, pink), salinity (PSU, orange), chlorophyll *a* (μg/L, green), $O_2$ (μg/L, blue), and density anomaly (sigma-t, black) for each station sampled during April (*R/V Oceanus*; OC-name of station) 2004.

**Figure S2.** Vertical profiles of temperature (°C, pink), salinity (PSU, orange), chlorophyll *a* (μg/L, green), $O_2$ (μg/L, blue), and density anomaly (sigma-t, black) for each station sampled during August (*R/V Cape Hatteras*, CH-name of station) 2004.

## Table Captions

**Table S1.** Nitex screen POC/$^{234}$Th ratios.

**Table S2.** $^{234}$Th and $POC_{SE}$ estimated fluxes.

**Table S3.** Mass balance Gulf of Maine.

**Table S4.** Gulf of Maine water inputs and outputs.

**Table S1.** Nitex screen POC/$^{234}$Th ratios.

| Station name (depth, m) | Nitex POC/$^{234}$Th April 2004 | | August 2004 | |
|---|---|---|---|---|
| Mass. Water Resources Authority (6 m) | 568 | 27 | 623 | 109 |
| Mass. Water Resources Authority (20 m) | 296 | 36 | 4450 | 764 |
| North Mass. Bay (6 m) | 193 | 11 | | |
| North Mass. Bay (50 m) | 109 | 16 | | |
| Merrimack River (6 m) | 111 | 6 | 489 | 73 |
| Merrimack River (20 m) | 181 | 13 | | |
| Casco Bay (6 m) | 1117 | 71 | 643 | 117 |
| Casco Bay (15 m) | 55.7 | 3.5 | 1070 | 70 |
| Wilkinson Basin I (6 m) | 141 | 9 | 210 | 86 |
| Wilkinson Basin I (80 m) | | | 195 | 121 |
| Wilkinson Basin II (8 m) | 82.6 | 4.2 | | |
| Wilkinson Basin II (30 m) | 477 | 40 | | |
| East Platts Bank (6 m) | 86 | 5 | 566 | 141 |
| East Platts Bank (35 m) | 107 | 11 | | |
| East Platts Bank (80 m) | | | 87.6 | 64.2 |
| Inner Penobscott Bay (3 m) | 68.1 | 19.8 | 1711 | 158 |
| Inner Penobscott Bay (6 m) | 64.6 | 12.2 | 1671 | 105 |
| Jordan Basin (8 m) | 70.2 | 3.6 | 277 | 26 |
| Jordan Basin (60 m) | 1655 | 127 | | |
| Jordan Basin (80 m) | | | | |
| Georges Bank (8 m) | 159 | 10 | 82.7 | 38.5 |
| Georges Bank (60 m) | 245 | 21 | | |
| Great South Channel (8 m) | 57.4 | 3.7 | 593 | 48 |
| Great South Channel (60 m) | | | | |
| Cape Cod Bay I (6 m) | 351 | 78 | | |
| Cape Cod Bay II (6 m) | 324 | 52 | 263 | 34 |
| Cape Cod Bay II (20 m) | | | 2171 | 133 |

**Table S2.** $^{234}Th$ and $POC_{SE}$ estimated fluxes.

**April**

| Station | Integration depth (m) | Integrated Flux dpm/m$^2$ d | ± | POC/$^{234}$Th µmol/dpm | ± | Flux POC mmol/m$^2$·d | ± | Flux POC g/m$^2$·d | ± |
|---|---|---|---|---|---|---|---|---|---|
| MWRA | 10 | 582 | 3 | 491 | 30 | 286 | 17 | 3.43 | 0.21 |
| NMB | 21 | 631 | 9 | 164 | 13 | 104 | 8 | 1.25 | 0.10 |
| MER | 10.5 | 210 | 13 | 133 | 8 | 28 | 2 | 0.34 | 0.03 |
| OCB | 12 | 467 | 10 | 410 | 26 | 191 | 13 | 2.30 | 0.15 |
| WB1 | 50 | 530 | 30 | 141 | 9 | 75 | 6 | 0.90 | 0.08 |
| WB2 | 50 | 451 | 20 | 477 | 40 | 215 | 20 | 2.58 | 0.24 |
| EPB | 63 | 518 | 22 | 107 | 11 | 55 | 6 | 0.66 | 0.08 |
| IPB | 6 | 661 | 3 | 64.6 | 12.2 | 43 | 8 | 0.51 | 0.10 |
| JB | 50 | 358 | 33 | 70.2[1] | 3.6 | 25 | 3 | 0.30 | 0.03 |
| GB | 50 | 1508 | 36 | 228 | 19 | 344 | 30 | 4.13 | 0.36 |
| GSC | 50 | 757 | 20 | 57.4 | 3.7 | 43 | 3 | 0.52 | 0.04 |
| CCB1 | 13 | 561 | 6 | 351 | 78 | 197 | 44 | 2.37 | 0.53 |
| CCB2 | 13 | 754 | 6 | 324 | 52 | 244 | 39 | 2.93 | 0.47 |

**August/September**

| Station | Integration depth (m) | Integrated Flux dpm/m$^2$ d | ± | POC/$^{234}$Th µmol/dpm | ± | Flux POC mmol/m$^2$·d | ± | Flux POC g/m$^2$·d | ± |
|---|---|---|---|---|---|---|---|---|---|
| MWRA | 12 | 353 | 2 | 2263 | 390 | 799 | 138 | 9.58 | 1.65 |
| MER | 12 | 542 | 2 | 489 | 73 | 265 | 39 | 3.18 | 0.47 |
| CB | 8 | 407 | 1 | 738 | 106 | 301 | 43 | 3.61 | 0.52 |
| WB | 50 | 1065 | 4 | 201 | 107 | 214 | 114 | 2.57 | 1.37 |
| EPB | 50 | 1199 | 8 | 281 | 96 | 337 | 115 | 4.05 | 1.37 |
| IPB | 3 | 229 | 0 | 1711 | 158 | 392 | 36 | 4.70 | 0.43 |
| JB | 50 | 777 | 6 | 277 | 26 | 215 | 20 | 2.58 | 0.25 |
| GB | 50 | 635 | 20 | 82.7 | 38.5 | 53 | 25 | 0.63 | 0.29 |
| GSC | 32 | 831 | 6 | 593 | 48 | 493 | 40 | 5.92 | 0.48 |
| CCB2 | 12 | 409 | 3 | 1081 | 76 | 442 | 31 | 5.30 | 0.38 |

[1]POC/$^{234}$Th ratio from deep sample was unusually high and decided to use ratio from shallow sample instead

**Table S3.** Mass balance Gulf of Maine (Tg = $10^{12}$g).

| Region[1] | Name | Surface Area ($km^2$) | Total Vol ($km^3$) | $z_{mix}$ | Surface Vol ($km^3$) | Deep Vol ($km^3$) | Surface [TOC] (μg/L) | deep [TOC] (μg/L) | Total TOC (Tg) | Surface TOC (Tg) | Deep TOC (Tg) | Export[1] area ($km^2$) | Export[2] ($g/m^2 \cdot yr$) | Total Export (Tg/yr) |
|---|---|---|---|---|---|---|---|---|---|---|---|---|---|---|
| 2 | Browns Bank | 1,780 | 160 | 50 | 106 | 54 | 1137 | 855 | 0.17 | 0.12 | 0.05 | 1,743 | 110 | 0.19 |
| 3 | Eastern Coastal Shelf | 13,794 | 1,165 | 50 | 712 | 453 | 1137 | 855 | 1.2 | 0.8 | 0.4 | 10,628 | 110 | 1.2 |
| 5 | Northern Coastal Shelf | 19,311 | 1,435 | 20 | 517 | 918 | 1676 | 1402 | 2.2 | 0.9 | 1.3 | 16,541 | 382 | 6.3 |
| 6 | Southern Costal Shelf | 8,239 | 466 | 20 | 221 | 246 | 1400 | 1210 | 0.61 | 0.31 | 0.30 | 7,133 | 296 | 2.11 |
| 7 | Great South Channel | 5,202 | 511 | 40 | 260 | 251 | 1340 | 1089 | 0.62 | 0.35 | 0.27 | 5,200 | 190 | 0.99 |
| 9 | Georges Basin | 4,104 | 1,224 | 50 | 246 | 978 | 1222 | 1103 | 1.4 | 0.3 | 1.1 | 4,104 | 110 | 0.5 |
| 10 | Jordan Basin | 6,696 | 1,494 | 50 | 402 | 1,092 | 1398 | 1111 | 1.8 | 0.6 | 1.2 | 6,696 | 110 | 0.7 |
| 11 | Wilkinson Basin | 7,076 | 1,623 | 60 | 495 | 1,128 | 1300 | 1160 | 2.0 | 0.6 | 1.3 | 7,076 | 328 | 2.3 |
| 12 | Central Gulf of Maine | 44,799 | 8,127 | 40 | 2,236 | 5,891 | 1399 | 1194 | 10 | 3 | 7 | 44660 | 205 | 9 |
| | **Total** | **111,001** | **16,206** | | **5,194** | **11,012** | | | **20** | **7** | **13** | | | **23** |

[1]See Appendix IV for description of region and detailed bathymetric data; [2]Based on previous observations from primary production variability (O'Reilly and Dow, 2006) April values were considered to be good estimates for average annual export fluxes.

**Table S4.** Gulf of Maine water inputs and outputs.

| Inflows | Vol[1] ($10^{12}$ $m^3$/yr) | TOC[2] (μg/L) | TOC ($g/m^3$) | TOC Tg/yr |
|---|---|---|---|---|
| Rivers | 0.08 | 1733 | 1.73 | 0.1 |
| Scotian Shelf Water | 6.3 | 723 | 0.72 | 5 |
| Slope Water | 8.7 | 723 | 0.72 | 6 |
| Maine Surface Water | 5.0 | 1217 | 1.22 | 6 |
| Maine Intermediate Water | 10 | 1180 | 1.18 | 12 |

[1]Townsend (1996); [2]This study and Whitehouse et al. (1990) for estimates of Scotian Shelf Water and Slope Water

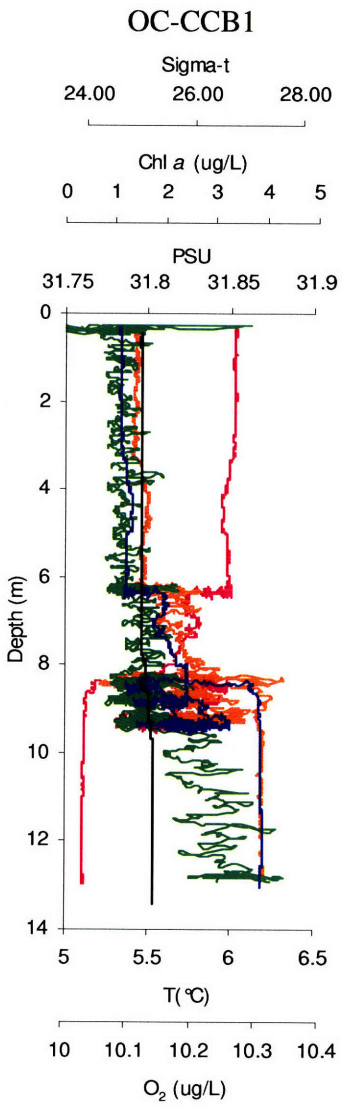
OC-CCB1
Sigma-t
24.00 26.00 28.00
Chl a (ug/L)
0 1 2 3 4 5
PSU
31.75 31.8 31.85 31.9
Depth (m)
0 2 4 6 8 10 12 14
5 5.5 6 6.5
T(℃)
10 10.1 10.2 10.3 10.4
O2 (ug/L)

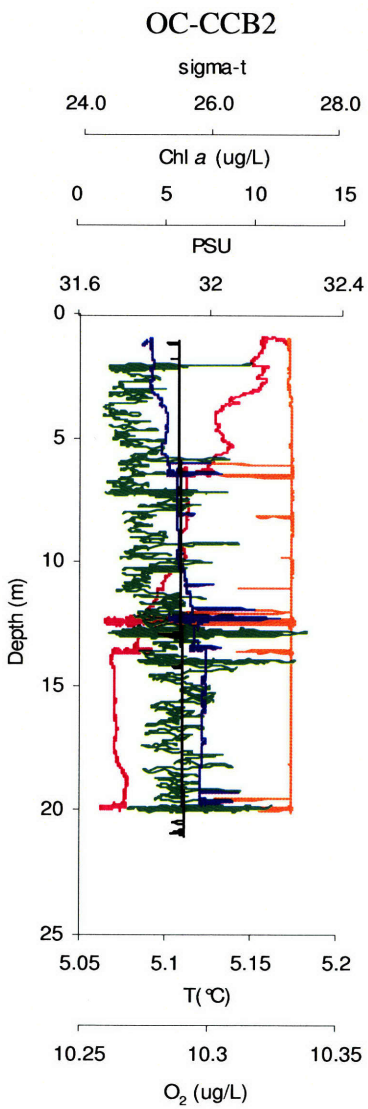
OC-CCB2
sigma-t
24.0 26.0 28.0
Chl a (ug/L)
0 5 10 15
PSU
31.6 32 32.4
Depth (m)
0 5 10 15 20 25
5.05 5.1 5.15 5.2
T(℃)
10.25 10.3 10.35
O2 (ug/L)

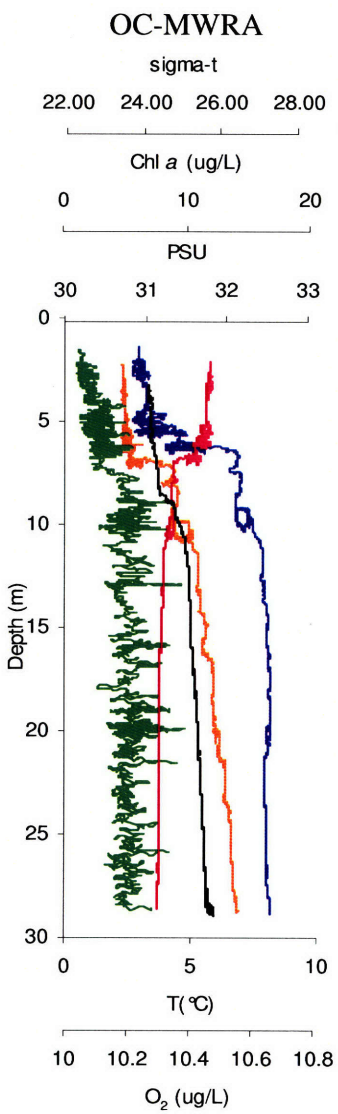
OC-MWRA
sigma-t
22.00 24.00 26.00 28.00
Chl a (ug/L)
0 10 20
PSU
30 31 32 33
Depth (m)
0 5 10 15 20 25 30
0 5 10
T(℃)
10 10.2 10.4 10.6 10.8
O2 (ug/L)

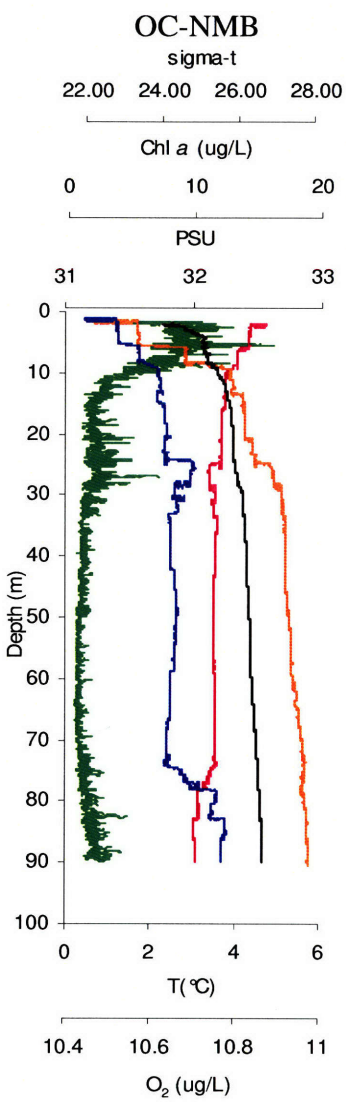
OC-NMB
sigma-t
22.00 24.00 26.00 28.00
Chl a (ug/L)
0 10 20
PSU
31 32 33
Depth (m)
0 10 20 30 40 50 60 70 80 90 100
0 2 4 6
T(℃)
10.4 10.6 10.8 11
O2 (ug/L)

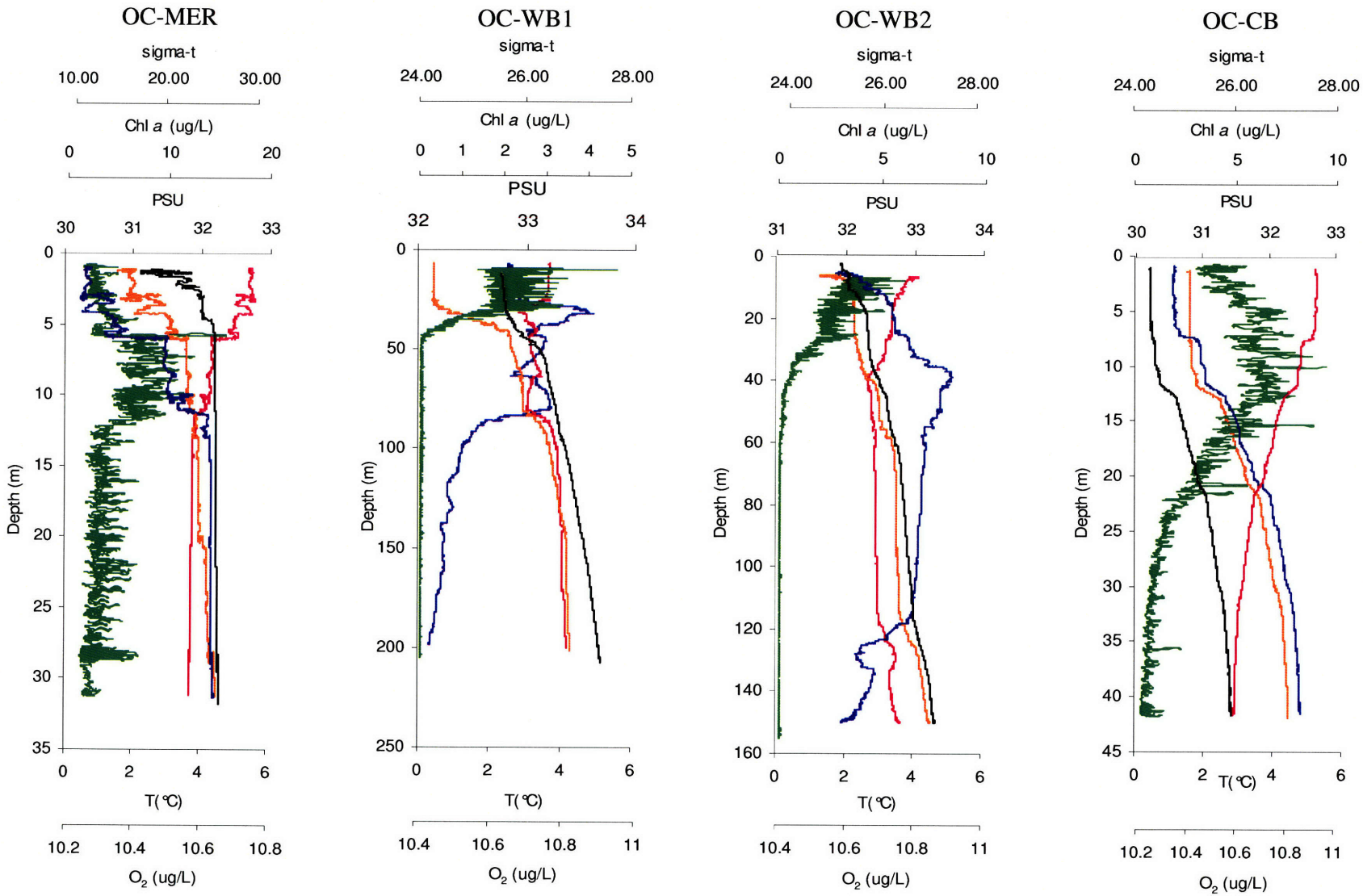
OC-MER
sigma-t
10.00 20.00 30.00
Chl a (ug/L)
0 10 20
PSU
30 31 32 33
Depth (m)
0 5 10 15 20 25 30 35
0 2 4 6
T(°C)
10.2 10.4 10.6 10.8
O2 (ug/L)
OC-WB1
sigma-t
24.00 26.00 28.00
Chl a (ug/L)
0 1 2 3 4 5
PSU
32 33 34
Depth (m)
0 50 100 150 200 250
0 2 4 6
T(°C)
10.4 10.6 10.8 11
O2 (ug/L)
OC-WB2
sigma-t
24.00 26.00 28.00
Chl a (ug/L)
0 5 10
PSU
31 32 33 34
Depth (m)
0 20 40 60 80 100 120 140 160
0 2 4 6
T(°C)
10.4 10.6 10.8 11
O2 (ug/L)
OC-CB
sigma-t
24.00 26.00 28.00
Chl a (ug/L)
0 5 10
PSU
30 31 32 33
Depth (m)
0 5 10 15 20 25 30 35 40 45
0 2 4 6
T(°C)
10.2 10.4 10.6 10.8 11
O2 (ug/L)

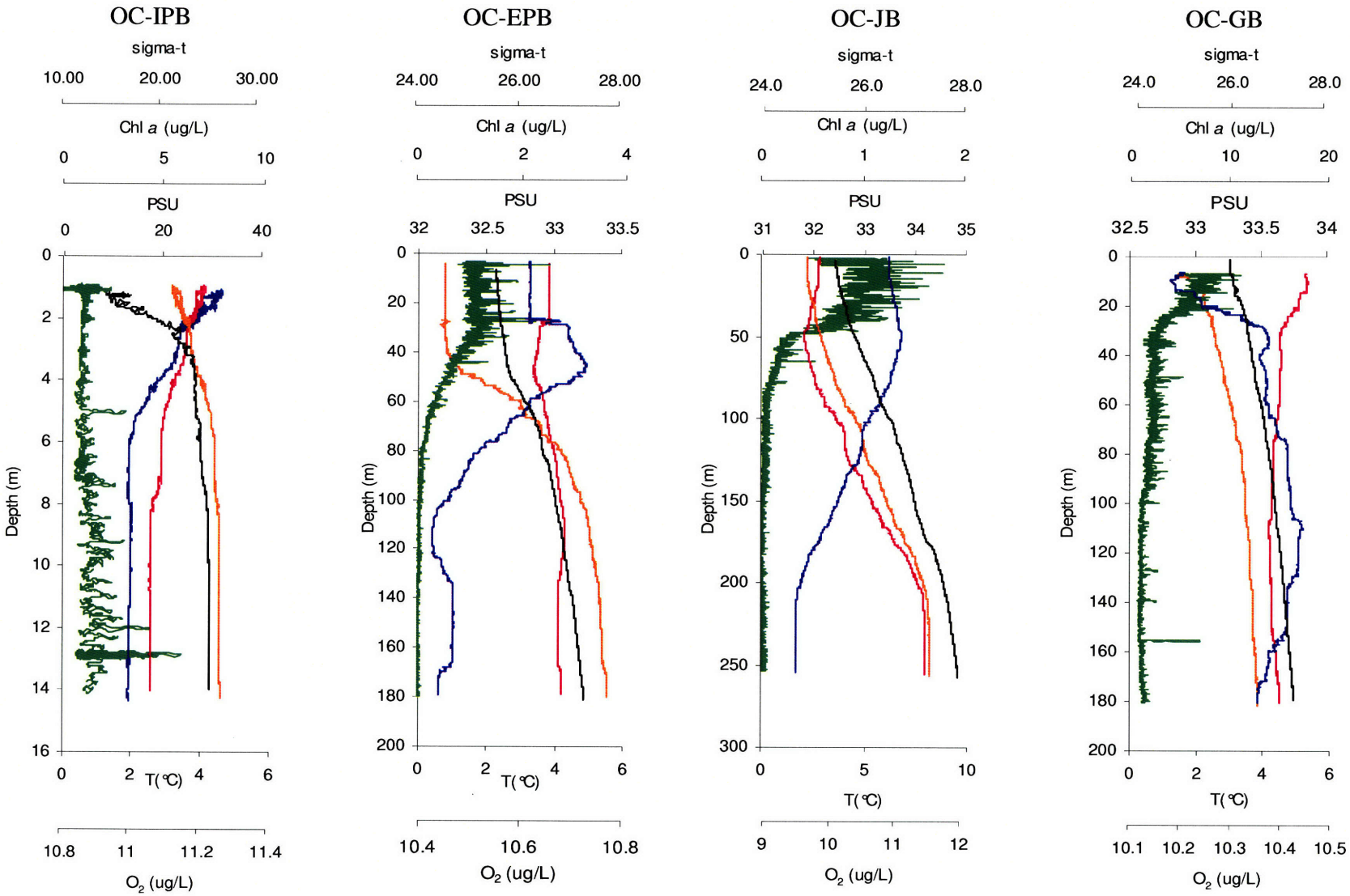


**Figure S1 (continuation).** Vertical profiles of temperature (°C, pink), salinity (PSU, orange), chlorophyll *a* (µg/L, green), $O_2$ (µg/L, blue), and density anomaly (sigma-t, black)for each station sampled during April (*R/V Oceanus*; OC-name of station) 2004.

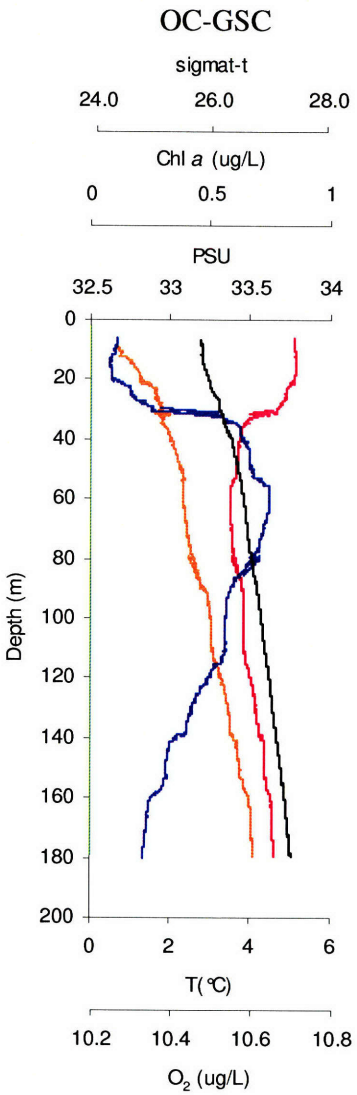


**Figure S1 (continuation).** Vertical profiles of temperature (°C, pink), salinity (PSU, orange), chlorophyll *a* (µg/L, green), $O_2$ (µg/L, blue), and density anomaly (sigma-t, black) for each station sampled during April (*R/V Oceanus*; OC-name of station) 2004.

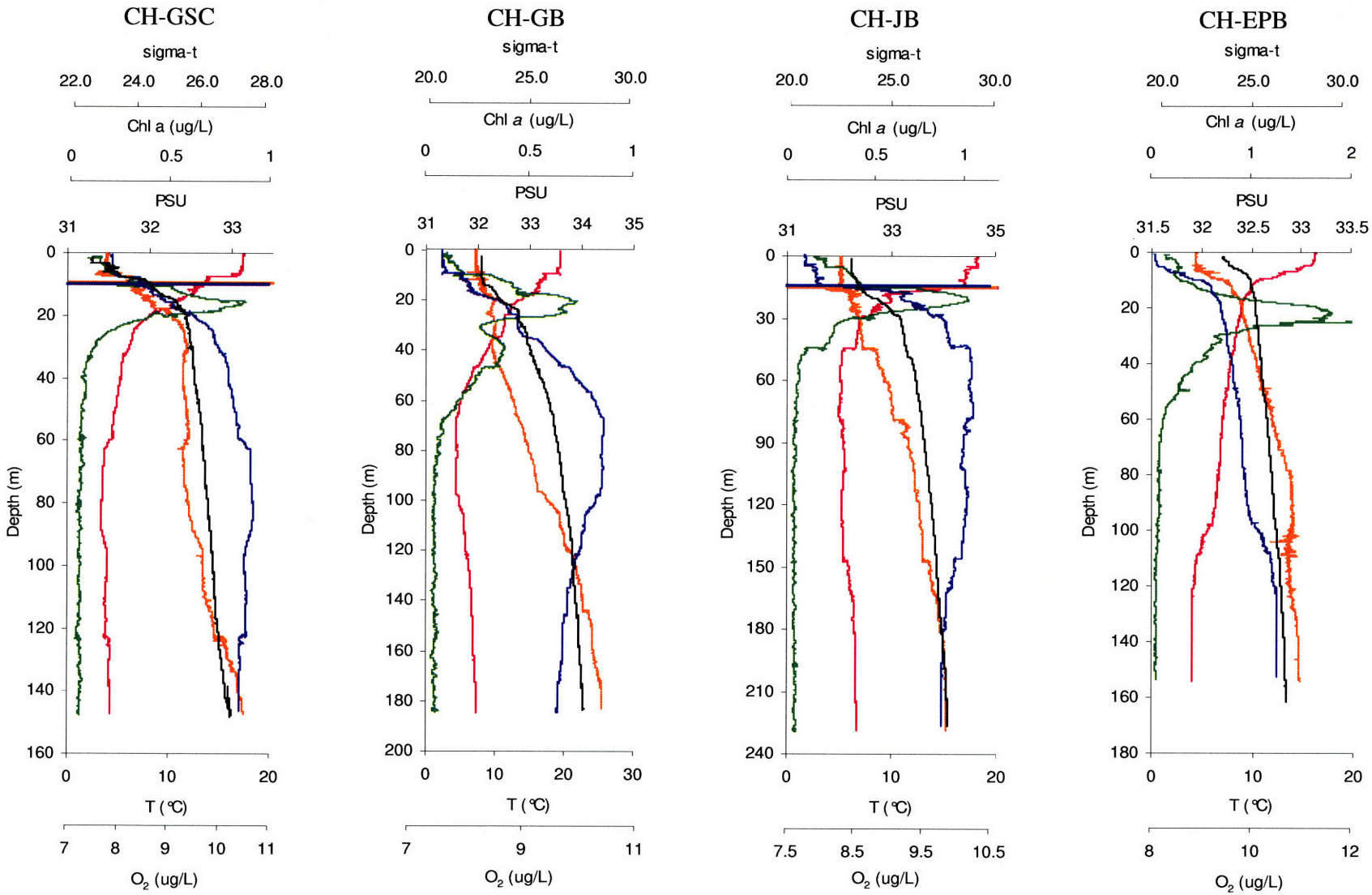


**Figure S2.** Vertical profiles of temperature (°C, pink), salinity (PSU, orange), chlorophyll *a* (µg/L, green), $O_2$ (µg/L, blue), and density anomaly (sigma-t, black) for each station sampled during August (*R/V Cape Hatteras*; CH-name of station) 2004.

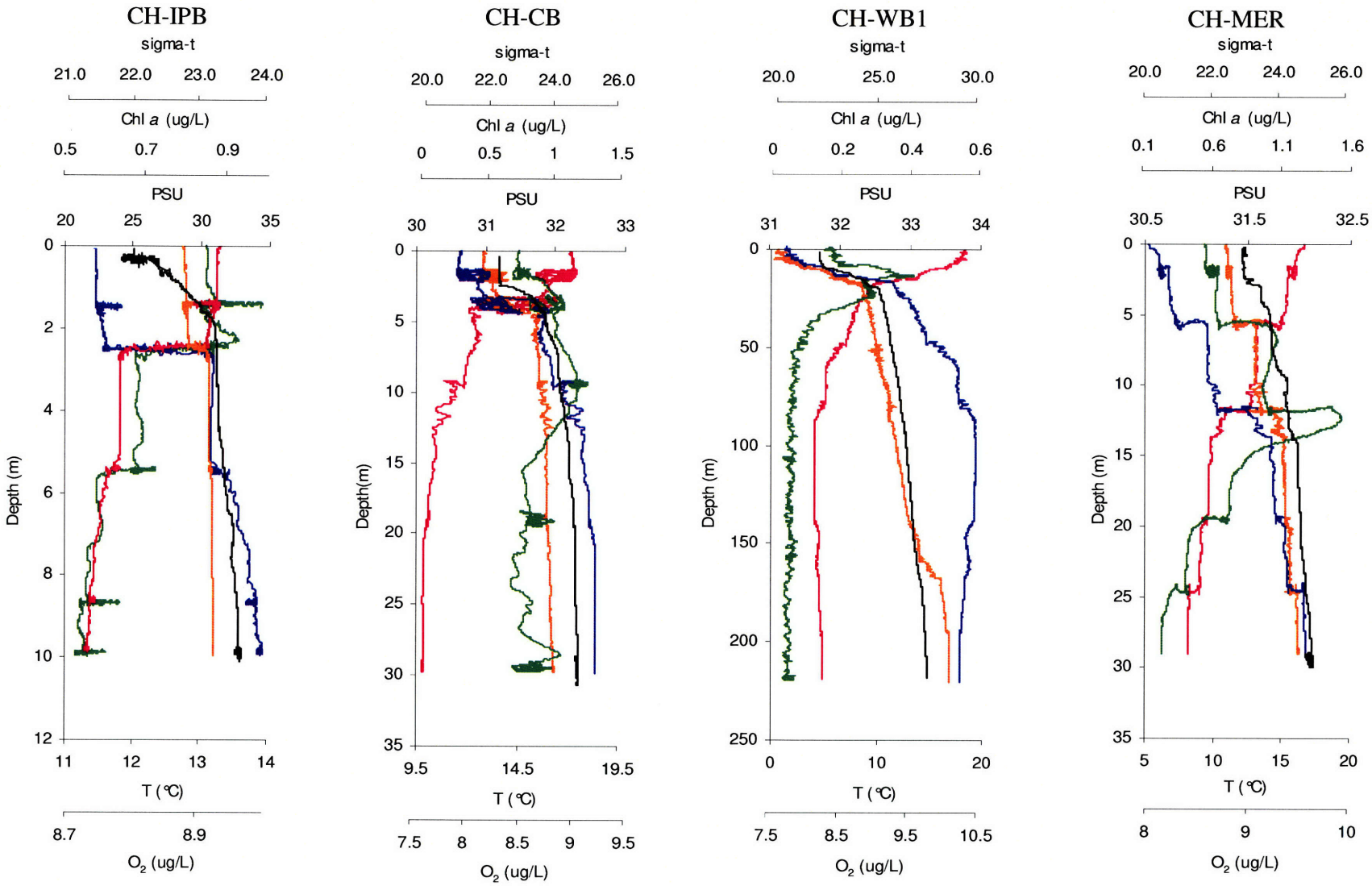


**Figure S2 (continuation).** Vertical profiles of temperature (°C, pink), salinity (PSU, orange), chlorophyll *a* (µg/L, green), $O_2$ (µg/L, blue), and density anomaly (sigma-t, black) for each station sampled during August (*R/V Cape Hatteras*; CH-name of

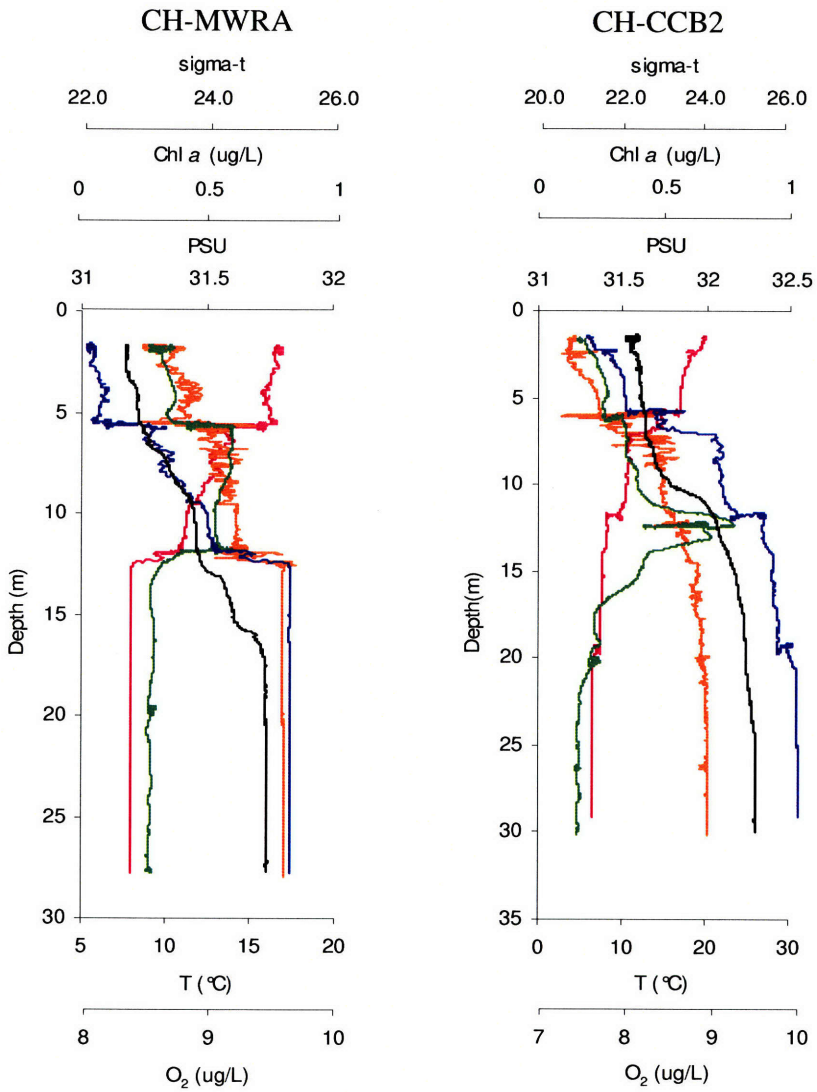


**Figure S2 (continuation).** Vertical profiles of temperature (°C, pink), salinity (PSU, orange), chlorophyll *a* (µg/L, green), $O_2$ (µg/L, blue), and density anomaly (sigma-t, black) for each station sampled during August (*R/V Cape Hatteras*; CH-name of

# Black carbon in the ocean: New insights into inputs and cycling of highly recalcitrant organic carbon

**One sentence description:** Black carbon (BC), a highly recalcitrant material, contributes 1 to 20% of the particulate organic carbon (POC) in coastal seawater, explaining why (1) some POC is not recycled to $CO_2$ and (2) the bioavailability of many organic substances in seawater is less than expected.

D. Xanat Flores-Cervantes[1], Desiree L. Plata[1,2], John K. MacFarlane[1], Christopher M. Reddy[2], and Philip M. Gschwend[1*].

[1]R.M. Parsons Laboratory, MIT 48-413, Department of Civil and Environmental Engineering, Massachusetts Institute of Technology, Cambridge, Massachusetts 02139, USA.

[2]Department of Marine Chemistry and Geochemistry, Woods Hole Oceanographic Institution, Woods Hole, Massachusetts, 02543, USA.

xanatf@mit.edu, dplata@whoi.edu. jmac@mit.edu, creddy@whoi.edu, pmgschwe@mit.edu.

**Journal format**

*Author to whom correspondence should be addressed (617) 253 1638; pmgschwe@mit.edu.

**Abstract**

To increase our understanding of the role of black carbon (BC), a highly sorptive and recalcitrant material, in the cycling of organic carbon, and its effects on other biogeochemical processes, we measured BC concentrations and fluxes out of the water column in the Gulf of Maine (GoM), a representative coastal area downwind of important BC sources of the Northeastern United States. Concentrations were between <0.1 and 16 μg/L in the spring and late summer, typically contributing between 1 and 20% of the particulate organic carbon (POC). These observations suggested that (a) up to 50% of the "molecularly uncharacterized" POC in surface seawater is combustion-derived BC, and (b) hydrophobic pollutants like polycyclic aromatic hydrocarbons (PAHs) and dioxins would have their "bioavailabilities" substantially influenced by sorption to BC. The observed BC spatial distributions and average water-column export fluxes near 10 $gBC/m^2 \cdot yr$ for this area imply that a large part of the BC is carried offshore by wind and that most of it is accumulated in the coastal zone. On a global scale, these results suggest the GoM and other coastal areas with similar BC export patterns contribute with significant amounts of highly recalcitrant organic carbon to the slowly cycling organic carbon pool in the world's oceans.

Keywords: Black carbon; seawater; Gulf of Maine; carbon cycle.

## 1. Introduction

Black carbon (BC), the soot and char formed during incomplete combustion of fossil and biomass fuels, is ubiquitous (e.g., Goldberg, 1985; Massielo and Druffel, 2001; Park et al., 2003; Schmidt and Noack; 2000; Suman et al., 1997) and may have significant implications for a wide range of biogeochemical processes. For example, upon its emission to the atmosphere, BC influences cloud droplet nucleation (Kaufman and Frase, 1997) and absorbs solar radiation, thereby affecting the temperature and water content of both the atmosphere and the ground underneath (Kaufman and Frase, 1997, Jacobson, 2004). It has even been suggested that these BC effects have caused floods and droughts in recent years in China and India (Menon et al., 2002). In addition, BC has been characterized as carcinogenic and a cause of respiratory problems such as asthma (Dockery et al., 1993; Künzli et al., 2000). Perhaps such impacts are not surprising since we know that BC is an important carrier of organic pollutants like polycyclic aromatic hydrocarbons (PAHs) and polychlorinated dibenzodioxins (PCDDs) (Lohmann et al., 2005).

Seiler and Crutzen (1980) first noted the potential implications of combustion processes to the global carbon cycle. BC formed during biomass and fossil fuel burning is relatively inert to biological and chemical processes and thus may be resistant to decomposition over geological time scales (Middleburg et al., 1999). As a result, BC formed during vegetation fires and wood burning transfers materials from a fast cycling biosphere (a more labile organic carbon) into a long-term geological carbon cycle (a more refractory organic carbon). A fraction of the BC emitted into the atmosphere is initially incorporated into soils (Eglinton et al., 2002; Schmidt and Noack, 2000). However, recent studies suggest that BC may constitute an important fraction of organic carbon in contemporary marine sediments (Gustafsson and Gschwend, 1998), where it

can be preserved for thousand of years (Masiello and Druffel, 1998; Middleburg et al., 1999). BC emissions have increased over the last century and are estimated to be between 6 to 24 Tg BC/yr for fossil fuels (Hendricks et al., 2004; Penner et al., 1993, Reddy and Boucher, 2004) and 50 to 270 Tg BC/yr for biomass fuels (Kuhlbusch and Crutzen, 1995). These estimates are of the same order of magnitude as those of riverine transport of particulate organic carbon (POC) into the oceans (Hedges and Keil, 1995), and, if correct, may account for 2-16 % (of the 1800 to 2400 Tg C/yr) of the "missing C" in the global carbon cycle (Kuhlbusch, 1998b).

Presently, there is substantial uncertainty with respect to the fate of BC released to the environment. After its production, BC particles can be deposited near their source or travel in the atmosphere hundreds to thousands of kilometers reaching even the most remote ocean sites (Goldberg, 1985; Garnstang et al., 1997). Observations of BC in rivers and estuaries (Mannino and Harvey, 2004; Masiello and Druffel, 2001; Mitra et al., 2002) suggest that these combustion-derived particles can be eroded from land and carried to sea. Since BC is found in coastal and open ocean sediments, it is reasonable to assume that BC is present within, and travels through, the oceanic water column. However, there are no measurements of BC in the seawater column. As a result, we do not know: (1) the relative importance of BC transport to the sea via rivers versus through the atmosphere; (2) the concentrations and residence times of BC in the oceanic water column; (3) the contribution of BC to the POC in seawater; and (4) whether any BC transformation mechanisms might occur within the water column.

Here we present the first measurements of BC concentrations in coastal seawater POC and BC export fluxes from the coastal water column. BC content in seawater was measured using the chemo-thermal oxidation method (CTO 375; Gustafsson et al., 1997) with pre-combustion modifications to avoid charring. However, to support these measurements, we also report the

use of a novel sorption-based procedure for quantifying BC suspended in water. And to place our observations into context, we compare estimates of BC fluxes (1) out of the atmosphere into the seawater, (2) out of the water column, and (3) into the coastal bed sediments.

## 2. Materials and Methods

### *2.1. Site description*

We filtered suspended solids from large-volume river and coastal seawater samples acquired in the Gulf of Maine (GoM) region in both April and August-September of 2004. The GoM is a semi-enclosed coastal sea located off the northeast coast of the United States and southwest of Nova Scotia, Canada (Fig. 1A). It is a good representative of coastal areas located downwind of important industrial and urban BC sources, as well as forested areas that regularly experience natural and human-directed burns. Other important examples of such waters include the Mediterranean Sea down wind of Western Europe, the coastal Pacific down wind of China, and the east coast down wind of Mexico City. The residence time of water in the GoM is about a year and the major inflows to this area are from the Scotian Shelf and the Northeast Channel (Townsend, 1996). Additionally, there have been intensive studies in this area in the last three decades that have provided a better understanding of the hydrography and water flow dynamics of the GoM, as well as of other carbon cycling studies (e.g. Charette et al., 2001; Dai and Benitez, 2001; Gustafsson and Gschwend, 1998, Chapter 3 of this thesis).

### *2.2. Sample collection*

Different portions of the POC, defined by separated by size cut-offs, were collected during two cruises to the GoM in 2004, one in April (*R/V Oceanus*) and another one in

August/September (*R/V Cape Hatteras*). At each sampling station, water was collected from two depths using a positive-displacement, stainless-steel, gear pump (Fultz Pump Inc, Lewis Town, NJ) from either a shallow (~ 6 m) or deeper depth (~ 60 m). Seawater was pumped from depth through stainless steel tubing that had been thoroughly washed with methylene dichloride, methanol, and low-carbon water (18 mΩ, produced using an Aries Vaponic system, Rockland, MA). The seawater was pumped on-board without ever being exposed to the atmosphere and successively passed through a 142-mm diameter, stainless steel, filter holder containing a 53-μm mesh-opening pre-cleaned Nitex screen (TETKO, Depew, NY) and then through a 293-mm, stainless steel, filter holder with a 0.7-μm pre-combusted glass fiber filter (GFF) or quartz filter (Pall Gelman Sciences, Ann Arbor, MI). All filter samples were rinsed immediately after collecting with sulfurous acid ($H_2SO_3$) to remove carbonates and then low-carbon water to remove salts. Finally, filters were stored frozen in aluminum foil envelops. Sample blanks were carried out throughout the sampling procedure and consisted of "wetting" the filters with 1 L of seawater, before processing in the same manner as all the samples.

*2.3. Organic carbon (OC) and black carbon (BC) measurements*

We measured the BC collected on the filters and Nitex screens from seawater using the chemo-thermal oxidation (CTO-375) method (Gustafsson et al., 1997) after slowly freezing the samples to lyse cells and therefore minimize charring artifacts. The CTO-375 method is thought to be particularly suited to analysis of the soot, as opposed to the biomass char, portion of the BC spectrum (Gustafsson et al., 1997); and it has been extensively evaluated against potential interferences from biogenic/diagenetic organic matter (Gustafsson et al., 1997; Reddy et al.,

2002; Hammes et al., 2007). The methodologies to characterize the two different size cutoff fractions of particulate organic carbon are described below.

### *2.3.1. OC and BC in the >53 μm POC*

The Nitex screen was sonicated with 100 mL of GFF-filtered seawater (Whatman, Florham Park, NJ) for 5 to 10 min to collect the >53 μm POC in a 150 mL pre-cleaned plastic container. Following sonication, 50 mL of the collected sample were kept in the plastic container for further $^{234}Th/^{238}U$ disequilibria measurements, and the other 50 mL were transferred to a 60 mL pre-combusted glass vial. Triplicates of 600 μL samples of the sonicated POC were placed in crucible-shaped Ag capsules and acidified with about 200 μL of 6% volume $H_2SO_3$ (Fisher Chemicals, Fairlawn, NJ). Half of the samples were kept frozen overnight and combusted at 375°C under air for 24 hr in a F47915 Thermolyne muffle furnace. Finally, the set of the non-combusted samples was dried at 60 °C overnight, and the carbon weight percentage of both sets of samples was determined using a CHN analyzer (Vario EL, Elementar America, Inc., NJ) at a combustion temperature of 950 °C. Daily response factors were determined using acetanilide standards, and the detection limit of the analyzer was 0.6 μg of C. Response factors for all elements remained stable throughout the experiment (± 0.5 % for nitrogen, ± 0.07 % for carbon, and ± 0.6 % for hydrogen). Every run included two sample blanks (no sample introduced in CHN analyzer) to verify that previous combustion was complete, and blanks were subtracted from raw sample data.

### *2.3.2. OC and BC in the 53 μm > POC > 0.7 μm.*

For OC measurements, 1/16 of the glass fiber filter or quartz filter was dried overnight at 60 °C, followed by elemental analysis in a Vario EL CHN analyzer (Elementar Americas, Inc., NJ; see above). For BC measurements, 1/8 of the fiber glass filter or quartz filter was combusted at 375 °C under air for 24 hr in a F47915 Thermolyne muffle furnace, followed by CHN analysis. Procedural blanks were carried throughout all OC and BC quantification procedures.

*2.4. Losses of pyrene fluorescence*

A complete description of this method is described elsewhere (Chapter 4 of this thesis and Flores-Cervantes et al., manuscript in preparation, 2008). In brief, pyrene fluorescence-loss experiments consisted of observing the decrease of pyrene fluorescence after additions of different filter sub-samples with known OC concentrations. A small piece of the GFF/Quartz filter (about 1/300) was added to precombusted 25 mL volumetric flasks containing pyrene at about 1 $\mu g_{pyrene}$/L. 10 mM $NaN_3$ was used to inhibit bacterial growth. The samples were equilibrated for 30 d under constant shaking using a wrist shaker. Control flasks and blank flasks were used to correct for losses and matrix interference.

Pyrene fluorescence was measured using a Perkin Elmer LS50B Luminescence Spectrofluorometer (Buckinghamshire, England). Fluorescence signals were quantified by synchronous $\Delta E$ scans, which were performed with $\Delta$Energy of -3000 $cm^{-1}$, an entrance slit of 5 nm, an exit slit of 5 nm, and a scan speed of 100 nm/min. Under those parameters, the detection limit of the spectrofluorometer was 0.2 μg pyrene/L. For this method, pyrene losses in control flasks for the duration of the experiment were <10%.

*2.5. BC vertical fluxes using $^{234}Th/^{238}U$ disequilibria*

Two different fractions of $^{234}Th$ were collected and analyzed. For analysis of dissolved/non-settling $^{234}Th$, water was collected at different depths in pre-cleaned Niskin bottles; once on board, the seawater was passed through $MnO_2$-impregnated adsorbers (Buesseler et al., 1992). Dissolved $^{238}U$ was calculated from salinity measurements (Chen et al., 1986) made on-board during the cruise with a calibrated 8410A Portasal™ salinometer (Guildline, Smiths Falls, Ontario, Canada). For analysis of particulate/settling $^{234}Th$, half of the sonicated > 53 μm POC from the Nitex screen (see above) was collected in a pre-cleaned plastic container, spiked with $^{230}Th$ to serve as a recovery standard, and filtered through a precombusted 25-mm quartz QM-A filter (pore size 2.2 μm; Whatman, Florham Park, NJ). The impregnated cartridges were spiked with $^{230}Th$, and both fractions were dissolved in acid solution, purified in ion-exchange columns, and electroplated onto stainless steal planchets following the procedure of Buesseler et al (1992). The $^{234}Th$ activity was then measured using low-background beta detectors. The measurements were repeated 4-5 times within a week to check for background interferences, to improve precision and accuracy, and to correct for the date of sample collection. The overall efficiencies for the $MnO_2$ cartridges (recovery, counting and beta detection) and the QM-A filter (counting and beta detection) were estimated to be 29 and 32%, respectively. Charette et al. (2001) reported detection efficiencies between 35 and 64% for the $MnO_2$ cartridges, and 35 ± 1.2% for the for QM-A filter geometry.

*2.6. Radiocarbon analysis*

Radiocarbon analyses of OC and the CTO 375-isolated BC were done following the procedure previously reported by Reddy et al. (2002) with some slight modifications. In brief, between 24 and 240 μg of BC present in one eighth of the quartz filters, and 320 to 1,600 μg of

OC present in one sixteenth of the filters were HCl-fumed, dried in a desiccator, rolled up and packed into a 12 mm x 20 cm precombusted quartz tube containing copper oxide (100 mg) and elemental silver wires. The tubes were then evacuated on a vacuum line, flame sealed, and combusted at 850 °C for 5 h. The carbon dioxide produced was then isolated and purified using a series of cold traps and quantified by manometry. About 10% of the isolated carbon dioxide was analyzed for $\delta^{13}C$, and the remainder was reduced to graphitic carbon, pressed and mounted on target wheels for $^{14}C$ analysis by accelerator mass spectrometry at the National Ocean Sciences Accelerator Mass Spectrometry (NOSAMS) facility at Woods Hole, MA, USA (McNichol et al., 1994). Radiocarbon results were normalized to $\delta^{13}C_{VPDB}$= -19 per mil and reported relative to NBS Oxalic Acid I as fraction modern ($f_m$) and $\Delta^{14}C$ (Stuiver and Polach, 1977).

## 3. Results and Discussion

### *3.1. Seasonal patterns observed in the Gulf of Maine (GoM).*

Our CTD measurements of salinity, temperature, chlorophyll *a* and $O_2$ concentration (Table 1) were able to identify two distinct seasonal patterns. During the spring (April) of 2004, we observed relatively low salinities in the shallow samples at the stations close to shore, high chlorophyll *a* concentrations in the surface waters at all of our stations, and small vertical and horizontal variations of temperature and $O_2$ throughout the GoM. In contrast, during August/September of 2004, we saw large temperature and $O_2$ concentration vertical gradients, but small variations in salinities between the shallow and the deep samples, and low chlorophyll *a* concentrations at all of our sampled stations. These observations are consistent with the GoM's annual cycle of: (a) winter cooling with deep surface mixing; (b) intense spring

phytoplankton blooms and large inputs of local river runoff and Scotian Shelf freshwater; (c) warming with summer stratification and nutrient depletion in the surface waters; and (d) time varying autumn phytoplankton blooms and vertical mixing (Townsend, 1996, Brown and Irish, 1993, Durbin, 1996, DFO, 2004).

The seasonal patterns observed in the GoM have important implications for BC cycling in the GoM. Phytoplankton blooms are thought to be responsible for a large fraction of the POC exported out of the surface waters. For example, Smetacek et al., (1978) reported that the spring bloom in the northern Baltic Sea contributes with as much as half of the total annual flux of organic matter to the benthos in shelf waters. In addition, river run off has also been recognized as an important source of terrestrial POC, especially to the coastal oceans (Hedges and Keil, 1995). Samples taken during high river flow during the month of April and low river flow during August/September 2004 allowed us to capture representative samples to assess the importance of river transport of BC to the ocean, while enhanced POC export fluxes resulting from spring (and possibly late summer) blooms, allowed to us to assess the importance of POC BC water column export.

*3.2. BC concentrations and percentages of OC in the GoM*

BC concentrations measured with the CTO-375 method in GoM seawater ranged from undetectable (<0.1 μg/L) to 15 μg/L (Fig. 1B and Table 2). Signal-to-noise ratios for were larger than 4:1 for April and 3:1 for August. Variations between replicate subsamples of the same filter were less than 20% ($n$ = 11), and we found excellent correspondence ($R^2$ = 0.99, $n$ = 6) between samples measured by our elemental analysis and the carbon yields from closed-tube combustion used for isotopic analysis. These BC values represent 1 to 20% of the POC in these seawaters.

We also observed 59 ± 7 μg/L ($n$ = 3) in the Charles River and 51 ± 6 μg/L ($n$ = 2) for Boston Harbor. These concentrations represented about 4% of the POC measured in these urban waters (data not in table).

To affirm the accuracy of these results, we used pyrene fluorescence losses (Chapter 4 of this thesis and Flores-Cervantes et al., manuscript in preparation, 2008) as a second approach to measure BC in Jordan Basin seawater. Since BC has a strong affinity for pyrene (Accardi-Dey and Gschwend, 2002), we inferred BC concentrations by observing diminished pyrene fluorescence when filter subsamples were added to pyrene solutions. Using the Jordan Basin surface samples and a range of initial pyrene concentrations (from 0.3 to 4 ppb), we observed a nonlinear sorption isotherm (Fig. 2). Previous researchers have recognized that PAHs exhibit high distribution coefficients and nonlinear isotherms for sorption onto BC (Bucheli and Gustafsson, 2000; Accardi-Dey and Gschwend, 2002; Lohmann et al., 2005). Hence, the isotherm was consistent with the presence of a BC adsorbent in the filtered solids (i.e., $K_d=f_{oc}K_{oc}+f_{bc}K_{bc}C_w^{n-1}$) (Gustafsson et al., 1997; Accardi-Dey and Gschwend, 2002). Moreover, the absolute value of the observed $K_d$ was much greater than expected using the traditional $f_{oc}K_{oc}$ model (Karickhoff et al., 1979; Chiou et al, 1979.) Using the isotherm and assuming a log $K_{bc}$ of 6.25 (Accardi-Dey and Gschwend, 2002), BC collected on the filter at this particular site was estimated to be present at 4.2 ± 1.4 μg BC/L, as compared to the 4.5± 1.8 μg BC/L seen by the CTO-375 procedure (Table 2). The strong correspondence of these diverse BC analytical approaches indicates that the CTO-375 method gave an accurate measure of soot-derived BC for our samples.

*3.3. Spatial and temporal variation of BC concentrations.*

BC concentrations generally decreased with distance from shore, but no general concentration trends were observed between April and August/September or as a function of water depth (Table 2). In contrast, OC concentrations for the GoM generally decrease with depth and are higher during the months of March and April than September and August (Charette et al., 2001; Table 1). These observations are not surprising since (1) BC is likely more recalcitrant than OC, therefore, surviving remineralization in the water column, and (2) atmospheric BC concentrations in this area, although generally higher during the winter (due to increased fuel used for heating) and summer (due to AC use and forest fires prevalent at this time of the year) months, show high variability throughout the year (Gryparis et al., 2006; http://airmap.unh.edu/).

The spatial distribution of BC concentrations compared well with previous studies of closely related compounds, PAHs, in the same coastal ocean (Windsor and Hites, 1979). Similar to the observations of Windsor and Hites (1979), during April our data showed a best-fit-exponential decay of the observed surface concentrations at $0.030 \pm 0.004$ per km in a straight line within a distance of 70 km from the Boston urban area, and of $0.022 \pm 0.006$ per km in the entire GoM within a distance of 70 km from shore (Fig. 3). Further away from the sources, the observed concentration decay was $0.004 \pm 0.003$ per km (data not shown). During August no statistical difference was observed between the exponential decays of the samples closer or further away from shore, and the overall exponential decay was much lower than in April ($0.002 \pm 0.001$ per km; data not shown). Consistent with these observations, Van Dingenen et al. (1995) observed an exponential concentration decay of BC in the atmosphere of 0.001 per km for distances between 600 and 2000 km from shore in the North Atlantic. The observed spatial distribution of BC concentrations suggests two important findings: (1) most of the BC produced on land and

exported offshore accumulates within 100 km of shore (here, on the continental shelf); and (2) BC will act as an important transport medium for combustion-derived contaminants like PAHs in the Gulf of Maine.

### *3.4. $^{234}Th/^{238}U$ disequilibria and BC water column export fluxes*

Using the BC concentrations and our contemporaneous measures of radioactive disequilibrium between the particle-reactive $^{234}$Th and its highly water-soluble radiogenic source, $^{238}$U, in the same seawaters (Table 3), we solved for the fluxes of BC out of the water column at some of our sampling stations. Buesseler et al. (1992) proposed that POC fluxes could be estimated empirically by measuring the ratio of POC-to-$^{234}$Th on settling particles (> 53 μm). By means of this same approach, we estimated BC export fluxes ($F_{BC}$) out of the mixed surface layer ($z_{mix}$) by measuring the BC-to-$^{234}$Th ratio on POC > 53 μm in the water column at a given depth:

$$F_{POC} = \frac{POC_{SE}}{^{234}Th_p} \int_{z_1}^{z_2} F_{Th} \cdot dz, \qquad (1)$$

where $z_1$ and $z_2$ are the depth intervals over which $F_{Th}$ is estimated. $F_{Th}$ is the $^{234}$Th particulate export flux and can be derived from the total $^{234}$Th activity balance (particulate and dissolved):

$$\frac{\partial A_{Th}}{\partial t} = A_U \lambda_{Th} - A_{Th} \lambda_{Th} - F_{Th} + K\nabla^2 A_{Th} + U\nabla A_{Th} \qquad (2)$$

where the first term represents the radiogenic production of $^{234}$Th with $A_U$ the $^{238}$U activity and $\lambda_{Th}$ is the $^{234}$Th decay constant (0.0288 1/d); the second term is the loss of total $^{234}$Th by radioactive decay and $A_{Th}$ is the total $^{234}$Th activity; and the last two terms represent the contribution of $^{234}$Th from mixing (where $K$ is the eddy diffusion coefficient vector) and advection (where $U$ is the velocity vector). Previous studies in this area have reported that in

pelagic, continental shelf, and many coastal regimes, there are modest (usually <<factor of 2 except during storm-driven resuspensions, Gustafsson et al., 1998) variations between fluxes calculated using a one dimensional (1-D) or a three dimensional (3-D) model (Gustafsson et al., 1998; Charette et al., 2001). The weather was relatively calm during our sampling close to the shore in April 2004, and much calmer throughout or August/September sampling campaign. Therefore, for this study, it was assumed that a steady state model with negligible advective and eddy diffusive transport could be used (i.e., a 1-D, vertical model), but we caution the reader about this assumption. Equation (2) can then be used and rewritten as:

$$F_{Th} = A_U \lambda_{Th} - A_{Th} \lambda_{Th} \qquad (3)$$

Substituting eq. (3) in eq. (1) and using our contemporaneous $^{238}$Th and $^{238}$U data (Table 3), the calculated BC export fluxes fell within a range of <0.3 and 36 $g_{BC}/m^2 \cdot yr$ with larger fluxes closer to shore and during the August/September sampling campaign (Table 4). Concentrations of particulate $^{234}$Th were highest during April, and, similar to what others have reported for this area (Charette et al., 2001; Gustafsson et al., 1997b) $^{234}$Th-to-$^{238}$U ratios increased with increasing distance from particle rich coastal areas. Smaller $^{234}$Th-to-$^{238}$U ratios closer to shore and in August/September suggested larger exports of particulate matter out of the surface ocean, while higher concentrations of particulate $^{234}$Th in April indicate the larger amounts of suspended particulates in the water column. These observations agree well with the larger BC export fluxes observed close to shore (urban, semi-urban, and close to shore areas) and during the month of August/September (Table 4), the higher concentrations of BC collected on the Nitex screens during the month of April (Table 2), and the GoM's annual cycle described above (section *3.1.*). During the spring, rivers discharge large amounts of terrestrial suspended particles that will settle as they enter slower flowing coastal waters. During the late summer,

reduced nutrient availability (consequence of the stratification of the water column) and warmer, calmer, and less dense surface water decreases primary productivity and causes phytoplankton to drift to the bottom of the ocean. Zooplankton grazing and fecal pellet production might have further contributed to the high POC fluxes observed in August/September (Durbin, 1996). In both of these cases, the falling particles will carry down with them highly "sorbing" chemicals/materials (such as $^{234}$Th and BC). The exceptionally low $^{234}$Th-to-$^{238}$U ratio observed at Inner Penobscot Bay (IPB) indicated the importance of particle export to the sediments in this area. However, IPB was a very shallow and close to shore sampling station where horizontal transport could be significant. Therefore, our BC fluxes might include both horizontal and vertical transport.

To check our estimated water-column export fluxes for geochemical consistency, we contrasted them with atmospheric BC deposition estimates and sediment BC burial rates for this region and similar regions (Table 4). Although there are difficulties in comparing BC data measured via different methods (see Hammes et al., 2007), our calculated water column BC export fluxes were of the same order of magnitude ($g_{BC}/m^2 \cdot yr$) as the estimated atmospheric BC deposition and reported BC sedimentation. Some of the observed variability could be due to the use of very different BC quantification methods. The concentration of aerosol BC used to check for geochemical consistency was measured using a combination of thermal and optical techniques (e.g., Hansen et al., 1983; Birch et al., 1996), while sedimentary and water column BC results were measured using chemical or chemo-thermal oxidation methods (e.g., Wolbach and Anders, 1989; Gustafsson et al., 1997). Recent method intercomparison studies (Currie et al., 2001; Hammes et al., 2007) show that thermal-optical techniques and chemo-thermal oxidation methods yield BC data that differ by more than a factor of 10. Further more, Liousse

et al. (1993) pointed out that variations in the specific attenuation cross-section ($\sigma$) used for measurements of BC in optical analyzers in remote areas can lead to the underestimation of about four times the measured BC concentration. Differences in our GoM observations could also be due to the substantially different time-scales integrated in each environmental compartment. Atmospheric concentrations and fluxes may vary on timescales of days as phenomena like wind direction and precipitation vary; in contrast, the water column export results reflect processes occurring over many months and burial observations reflect fluxes averaged over many-year time periods. For the purpose of data comparison, we extrapolated our seasonal results to an annual basis. However, our data indicate that large seasonal surface-water export fluxes were present during our sampling events, indicating that our values, calculated on an annual basis, may be somewhat uncertain. Finally, spatial variations may play some role; for example, deposition into some of the basins may reflect sediment focusing. Despite all these difficulties, it is clear that the diverse data sets exhibit substantial consistency with BC fluxes in the order of $g_{BC}/m^2$ per year for this region.

*3.5. Radiocarbon measurements of BC and OC*

Radiocarbon ($^{14}C$) measurements of the BC in selected samples were used to test for POC charring artifacts and to assess whether fossil fuel combustion was the dominant source of BC in the GoM seawater. In no case did the $^{14}C$ signature of the BC match the $^{14}C$ of the same sample's POC, implying that the data did not simply reflect charring of POC. Rather, it appears that the fossil fuel contributions ranged widely from only about 15 to as much as 90% (Fig. 4). The highest fossil fuel-contribution to the BC was observed for the sample closest to Boston near the Massachusetts Water Resources Authority sewage discharge site, indicating the importance

of fossil fuel-combustion for soot inputs in this area. The samples with lower fossil fuel-derived BC content were distant from urban centers (Georges Bank, Penobscot Bay and Wilkinson Basin). Therefore, if charring was not present, the relatively modern $^{14}C$ content of these BC samples indicates they were substantially affected by biomass burning (e.g., forest fires or use of wood for home heating).

The importance of biomass burning appears reasonable. Energy use data from the Energy Information Administration (http://www.eia.doe.gov/), combined with a technology based emission factor approach (Bond et al., 2004), suggests that within New England 30% of the soot BC (<1 um) is produced from biofuel or biomass combustion, while 70% comes from petroleum, coal, and natural gas combustion (Table S1 and S2). Moreover, in the summer of 2004, large plumes of smoke deriving from intense boreal forest fires were observed in the GoM during August of 2004 (e.g. Martin et al., 2006; Quinn et al., 2006). Long distance transport selects for smaller, soot-like BC particles formed during biomass/biofuel combustion (Garstang, et al., 1997). Therefore, our August/September cruise samples (Fig 5) may have been especially affected by distant forest fires.

Stable carbon isotope ($\delta^{13}C$) data were also collected for some of our samples (Table S5). However, since BC sources from biomass combustion in the New England area have contributions from a wide mix of sources (tundra-like communities, coniferous forests, and hardwood forests; Magee and Ahles (1999)), uncertainty in the source signatures (Table S6) prevented us from making a simple mixing interpretation of this data.

*3.6. BC mass balance in the GoM*

To characterize the fate of BC emanating from the Northeast United States coastline, we calculated the various BC sources and sinks into and out of the GoM (Fig. 1 C, Tables S3 and S4). Atmospheric deposition (mainly wet) was the main BC input into the GoM. In contrast to previous reports (Masiello and Druffel, 2001), rivers only contribute minor inputs to this coastal system, despite having elevated BC concentrations in slow-flowing urban systems like the Charles River (Table S4). The chief output of BC from the GoM was sedimentation, although there was significant water-borne transport offshore (i.e., Maine Surface Water and Maine Intermediate Water have higher concentrations than Scotian Shelf Water and Slope Water). The residence time of BC in the water column was about two months. This residence time is consistent with our observed changes in BC concentrations between April and August.

An imbalance in our inputs and outputs in the GoM mass balance suggests that either we are underestimating our BC sources or that we are not accounting for an important source. It is possible that atmospheric concentrations of BC in the central Gulf are higher than we estimated based on data from land or open ocean measurements (Table 4). Non-local or intermittent pollution plumes may be important sources to this area, as well as the transit of ships across the GoM. However, ocean-based measurements for this area are not readily available.

Using the estimated surface-ocean export fluxes from this study, we inferred that the GoM captured about 80% of the BC carried offshore by aeolian transport from the Northeastern USA. Extrapolating this view of BC cycling to a global scale suggests that annual BC deposition rates ($1 - 10$ g/m$^2$·yr) into coastal areas ($3.15 \times 10^6$ km$^2$; Sverdrup et al., 1946) between 16 - 275 Tg BC/yr can account for most of the estimated annually produced BC (4 - 270 Tg BC/yr; Hendricks et al., 2004; Kuhlbusch, 1995; Penner et al., 1993; Reddy and Boucher, 2004).

## 4. Summary

These BC data allowed a much better understanding of the impacts of BC suspended in coastal seawater. First, the BC concentrations imply these particles would substantially affect the speciation of high molecular weight pollutants like PAH and PCDD in GoM seawater (Lohmann et al., 2005; Accardi-Dey et al., 2002). BC-sorption of these toxic substances limits their degradation as well as their toxic effects. Secondly, BC contributed, on average, 6% of the POC carbon suspended in the GoM, implying that about half of the previously chemically unidentifiable POC (Eglinton and Repeta, 2004) may simply be these combustion-derived particles. The recognized presence of this recalcitrant BC carbon may well explain why some POC is not recycled to $CO_2$ during its transport to depth and even within the sediment beds below. Hwang and Druffel (2002) previously reported that an important fraction of the unidentifiable POC in the Northeast Pacific could correspond to a lipid-like material found in the marine environment. However, they also pointed out that additional old and terrestrial sources were needed to explain the previously reported $^{13}$CNM spectra (Hedges et al., 2001) and stable and radioisotope characteristics of the unidentifiable POC. Finally, the contributions of the fossil fuel-derived BC to POC can explain the $^{14}$C-depleted nature of the reported uncharacterized material previously reported in POC and sedimentary OC (Masiello and Druffel; 1998; Eglinton and Repeta, 2004); in contrast to the hypothesis that century- and millennia-scale transport processes are contributing weathered organic matter off the continents. This result suggests that efforts to control BC in the atmosphere over the Northeast USA must be concerned with biomass burning activities as well as fossil fuel uses.

Recognizing the importance of BC in environments beyond the atmosphere strongly suggests that environmental scientists, engineers, and policy makers need to assess the presence and

impacts of combustion processes in all environmental compartments (soils, lakes, oceans, coastal sediments).

## 5. Acknowledgments

We thank the captains and crews and CTD technicians of RV Oceanus and RV Cape Hatteras, and R. K. Nelson, K. Pangallo, E. Peacock, E. Roosen, S. Silva, E. Tauten, and L. Xu, members of C. Reddy's lab, for their help in sample collection. L. Xu and A. McNichol are gratefully acknowledged for $^{13}C$ and $^{14}C$ analyses. We are also grateful for support from NFS grants (OCE-0223441 and BES-0607136) and CONACYT and MSFS fellowships to D. X. F.

## 6. References

Accardi-Dey, A.M. 2003. Black carbon in marine sediments: quantification and implications for the sorption of polycyclic aromatic hydrocarbons. MIT-WHOI: Cambridge, MA.

Accardi-Dey, A., Gschwend, P.M., 2002. Assessing the combined roles of natural organic matter and black carbon as sorbants in sediments. Environ. Sci. Technol. 36, 21-29.

Birch, M.E., Cary, R.A., Elemental carbon-based method for monitoring occupational exposures to particulate diesel exhaust. Aerosol Sci. Technol. 25(3), 221-241

Bond, T.I., Streets, D.G., Yarber, K.F., Nelson, S.M., Woo, J., Klimont, Z., 2004. A technology-based global inventory of black and organic carbon emissions from combustion. J. Geophys. Res. 109, D14203.

Brown, W.S., Irish, J.D., 1993. The annual variation of water mass structure in the Gulf of Maine: 1986-1987. J. Mar. Res. 51, 53-107.

Bucheli, T.D., Gustafsson, Ö., 2000. Quantification of the soot-water distribution coefficient of PAHs provide mechanistic basis for enhanced sorption observations. Environ. Sci. Technol. 34, 5144-5151.

Buesseler, K.O., Cochran, J.K., Bacon, M.P., Livingstone, H.D., Casso, A., Hirschberg, D., Hartman, M.C., Fleer, A.P., 1992. Determination of thorium isotopes in seawater by non-destructive and radiochemical procedures. Deep-Sea Res., 39, 1102-1114.

Cachier, H., Brémond, M-P., Buat-Ménard, 1990. Organic carbon and black carbon aerosols over marine regions of the Northern Hemisphere. Proceedings of International Conference on Atmospheric Chemistry, Brookhaven National Lab., Upton, NY.

Charette, M.A., Moran, S.B., Pike, S.M., 2001. Investigating the carbon cycle in the Gulf of Maine using the natural tracer thorium 234. J. Geophys. Res, 106, C6, 11.553-11.579.

Chen, J.H., Edwards, R.L., Wasserburg, G.J, 1986. 238U, 234U and 232Th in seawater. Earth Planet Sci. Lett. 80, 241-251.

Chylek, P., Kou, L., Johnson, B., Boudala, F., Lesins, G., 1999. Black carbon concentrations in precipitation and near surface air in and near Halifax, Nova Scotia. Atmospheric Environment, 33, 2269-2277.

Cooke, W.F., Ramaswamy, V., Kasibhatla, P., 2002. Construction of a 1x1 fossil fuel emission data set for carbonaceous aerosols and implementation and radiative impact in the ECHAM4 model. J. Geophys. Res. doi: 10.1029/2001JD001274.

Currie, L.A., 2000. Evolution and multidisciplinary frontiers of 14C aerosol science. Radiocarbon 42, 115-126.

Dai, M.H., Benitez-Nelson, C.R., 2001. Colloidal organic carbon and 234Th in the Gulf of Maine. Mar. Chem. 2001, 74, 181-196.

Daggupaty, S.M., Banic, C.M., Cheung, P., Ma, J., 2006. Numerical simulation of air concentration and deposition of particulate metals around a copper smelter in northern Québec, Canada. Geochemistry: Exploration, Environment, Analysis, 6, 139–146.

DFO (Department of Fisheries and Oceans, Canada), 2004. Chemical and Biological Oceanographic conditions in 2002-Gulf of Maine, Bay of Fundy, Scotian Shelf and the Southern Gulf of St. Lawrence. In DFO Science Ecosystem Status Report 2004/2003.

Dockery, D.W., Pope, C.A., Xu, X.P., Spengler, J.D., Ware J.H., Fay, M.E., Ferris, B.G., Speize, F.E., 1993. An association between air pollution and mortality in six United States cities. N. Engl. J. Med. 329, 1753-1759.

Durbin, E., 1996. In The Gulf of Maine Ecosystem Dynamics; Wallace, G. T. and E. F. Braasch, Ed. Regional Association for Research on the Gulf of Maine: St. Andrews, New Brunswick.

Eglinton, T.I., Eglinton, G., Dupont, L., Scholkovitz, E.R., Montlucon, D., Reddy, C.M., 2002. Composition, age, and provenance of organic matter in NW African dust over the Atlantic Ocean. Geochem. Geophys. Geosys., 3, 1525-2027.

Eglinton, T.I., Repeta, D.J., 2004. Organic matter in the contemporary ocean. Treatise Geochem. 6, 145.

Flores-Cervantes, D.X., Reddy, C.M., Gschwend, P.M., 2008. Inferring black carbon concentrations in coastal seawater by observing pyrene fluorescence losses. To be submitted.

Garstang, M., Tyson, P.D., Cachier, H., Radke, L., 1997. Atmospheric transports of particulate and gaseous products by fire. In Sediment Records of Biomass Burning and Global Change, Clark, J. S., Cachier, H., Goldammer, J. G., and Stocks Brian, Ed. Springer-Verlag, Berlin, Heildelberg.

Goldberg, E.D., 1985. Black Carbon in the Environment. John Wiley & Sons, New York, 198 pp.

Gustafsson, Ö., Haghseta, F., Chan, C., MacFarlane, J, Gschwend, P.M., 1997. Quantification of the dilute sedimentary soot phase: implications for PAH speciation and bioavailability. Environ. Sci. Technol. 31, 203-209.

Gustafsson, Ö., Gschwend, P.M., Buesseler, K.O., 1997b. Settling removal rates of PCBs into the Northwestern Atlantic derived from 238U-234Th disequilibria. Environ. Sci. Technol. 31, 3544-3550.

Gustafsson, Ö., Gschwend, P.M., 1998. The flux of black carbon to surface sediments on the New England continental shelf. Geochim. Cosmochim. Acta, 62, 465-472.

Gustafsson, Ö., Buesseker, K.O., Geyer, W.R., Moran, S.B., Gschwend, P.M., 1998. An assessment of the relative importance of horizontal and vertical transport of particle-reactive chemicals in the coastal ocean. Cont. Shelf Res. 18, 805-829.

Griffin, J,J., Goldberg, E.E., 1995. The fluxes of elemental carbon in coastal marine sediments. Limnol. Oceanogr. 20, 456-463.

Gryparis, A., Coull, B.A., Schwartz, J., Suh, H.H., 2006. Semiparametric Latent Variable Regression Models for Spatio-temporal Modeling of Mobile Source Particles in the Greater Boston Area. Harvard University Biostatistics Working Paper Series. Working Paper 41. http://www.bepress.com/harvardbiostat/paper41.

Hammes, K., et al., 2007. Comparison of black carbon quantification methods using reference materials form soil, water, sediment and the atmosphere, and implications for the global carbon cycle. Global Biogeochem. Cycles 21, doi: 10.1029/2006GB002914.

Hedges, J.I., Keil, R.G., 1995. Sedimentary organic matter preservation: an assessment and speculative synthesis. Mar. Chem., 49, 81-115.

Herdge, J.I., Baldock, J.A., Gelinas, Y., Lee, C., Peterson, M., Wakeham, S. G., 2001. Evidence of non-selective preservation of organic matter in sinking marine particles. Nature 409, 801-804.

Hendricks, J., Kächer, B., Döpelheuer, A., Feichter, J., Lohmann, U., 2004. Simulating the global atmospheric black carbon cycle: a revisit to the contribution of aircraft emissions. Atmos. Chem. And Phys. Discuss., 4, 3485-3533.

Jacobson, M.Z., 2004. Climate response of fossil fuel and biofuel soot, accounting for soot's feedback to snow and sea ice albedo and emissivity. J. Geophys. Res. doi:10.1029/2004JD004945.

Kaufman, Y.J., Fraser, R.S., 1997. The effect of smoke particles on clouds and climate forcing. Science 277, 1636-1639.

Kuhlbusch, T.A., 1995. Method for determining black carbon in residues of vegetation fires. Environ. Sci. Technol. 29, 2695-2702.

Kuhlbusch, T.A.J., Crutzen, P.J., 1995b. Toward a global estimate of black carbon in residues of vegetation fires representing a sink of atmospheric CO2 and a source of O2. Global Biogeochem. Cycles, 9, 491-501.

Kuhlbusch, T.A., 1998. Black Carbon and the Carbon Cycle. Science, 280, 1903-1904.

Künzli, N., et al., 2000. Public-health impact of outdoor and traffic-related air pollution: a European assessment. Lancet 356, 795-801.

Incze, L., Jakobbson, M., 2008. Hypsometric characterization of the Gulf of Maine, Georges Bank, Scotian Shelf and neighboring continental slope. http://www.usm.maine.edu/gulfofmaine-census/ (accessed October, 2004).

Liousse, C., Cachier, H., Jennings, S.G., 1993. Optical and thermal measurements of black carbon aerosol content in different environments: Variation of the specific cross section, sigma. Atmos. Environ. 27A, 1203-1211.

Liousse, C., Penner, J.E., Chuang, C., Walton, J.J., Eddleman, H., 1996. A global three-dimensional study of carbonaceous aerosols. J. Geophys. Res. 101, D14, 19,411-19,423.

Lohmann, R., MacFarlane, J.K., Gschwend, P.M., 2005. Importance of black carbon to sorption of native PAHs, PCBs, and PCDDs in Boston and New York Harbor sediments. Environ. Sci. Technol. 39, 141-148.

Magee, D.W., Ahles, H. E., Flora of the Northeast. A manual of the vascular flora of New England and adjacent New York. University of Massachusetts Press, Amherst, MA.

Mannino, A., Harvey, H.R., 2004. Black carbon in estuarine and coastal ocean dissolved organic matter. Limnol. Oceanogr. 49, 735 (2004).

Martin, M.V., Honrath, R.E., Owen, R.C., Pfister, G., Fialho, P., Barata, F., 2006. Significant enhancement of nitrogen oxides, black carbon, and ozone in the North Atlantic lower free troposphere resulting from North Amercian boreal wildfires. J. Geophys. Res., doi:10.1029/2006JD007530

Masiello, C.A., Druffel, E.R.M., 1998. Black carbon in deep-sea sediments. Science 280, 1911-1913.

Masiello, C.A., Druffel, E.R.M., 2001. Carbon isotope geochemistry of the Santa Clara River. Global Biogeochem. Cycles 15, 407-416.

Menon, S., Hansen, J., Nazarenko, L., Luo, Y., 2002. Climate effects of black carbon aerosols in China and India. Science 297, 2250-2253

McNichol, A.P., Osbourne, E.A., Gagnon, A.R., Fry, B., Jones, G.A., 1994. TIC, TOC, DIC, DOC, PIC, POC – unique aspects in the preparation of oceanographic samples for 14CAMS. Nuclear Instruments and Methods in Physics Research B 92, 162–165.

Middleburg, J.J., Nieuwenhuize, J., Can Breuge, P., 1999. Black carbon in marine sediments. Mar. Chem. 65, 245-252.

Mitra, S., Bianchi, T.S., Mckee, B.A., Sutula, M., 2002. Black carbon from the Mississippi Rive: quantities, sources, and potential implications for the global carbon cycle. Environ. Sci. Technol. 36, 2296.

Ogren, J.A., Groblicki, P.J., Charlson, R.J., 1984. Measurement of the removal rate of elemental carbon from the atmosphere. Science of the Total Environment, 36, 329-338.

Park, R.J., Jacob, D.J., Chin, M., Martin, R.V., 2003. Sources of carbonaceous aerosols over the United States and implications for natural visibility. J. Geophys. Res. 108, doi:10.1029/2002JD003190.

Pedersen, D.U., 2002. Human cell mutagenicity of respirable airborne particles (PM2.5) in northeastern United States. MIT: Cambridge, MA.

Penner, J.E., Eddleman, H., Novakov, T., 1993. Towards the development of a global inventory for black carbon emissions. Atmos. Environ., 27A, 1277-1295.

Quinn, P.K., Bates, T.S., Coffman, D., Onasch, T.B., Worsnop, D., Baynard, T., de Gouw, J.A., Goldan, P.D., Kuster, W.C., Williams, E., Roberts, J.M., Lerner, B., Stohl, A., Pettersson, A., Lovejoy, E.R., 2006. Impacts of sources and aging on submicrometer aerosol properties in the marine boundary layer across the Gulf of Maine. J. Geophys. Res., doi:10.1029/2006JD007582.

Reddy, C.M., Pearson, A., Xu, L., McNichol, A.P., Benner Jr, B.A., Wise, S.A., Klouda, G.A., Currie, L.A., Eglinton, T., 2002. Radiocarbon as a tool to apportion the sources of polycyclic aromatic hydrocarbons and black carbon in environmental samples. Environ. Sci. Technol. 36, 1774-1782.

Reddy, M.S., Boucher, O., 2004. A study of global cycle of carbonaceous aerosols in the LMDZT general circulation model. J. Geophys. Res., 109, D14203.

Schmidt, M.W., Noack, A.G., 2000. Black carbon in soils and sediments: analysis, distribution, implications, and current challenges. Global Biogeochem. Cycles 14, 777-793.

Seinfeld, J.H., Pandis, S.N., 1998. Atmospheric chemistry and physics: From air pollution to climate change. Wiley-Interscience: USA.

Smetacek, V., von Bröckel, K., Zeitzschel, B., Zenk, W., 1978. Sedimentation of particulate matter during a phytoplankton spring bloom in relation to the hydrographical regime. Mar. Biology 47, 211-226.

Suman, D.O., Kuhlbusch, T.A.J., Lim, B., 1997. Marine sediments: a reservoir for black carbon and their use as spatial and temporal records of combustion. In Sediment Records of Biomass Burning and Global Change H. C. J. S. Clark, J. G. Goldammer, B. J. Stocks, Ed. (Springer-Verlag, Berlin) pp. 489.

Seiler, W., Crutzen, P.J., 1980. Estimates of gross and net fluxes of carbon between the biosphere and the atmosphere from biomass burning. Climate Change, 2, 207-247.

Smith, D.M., Griffin, J.J., Goldberg, E.D., 1973. Elemental carbon in marine sediments: a baseline for burning. Nature, 241, 233-238.

Stuiver, M., Polach, H.A., 1977. Reporting of $^{14}C$ data. Radiocarbon 19, 355-363.

Sverdrup, H.U., Johnson, M.W., Fleming, R.H., 1946. The oceans: Their physics, chemistry, and general biology. Prentice Hall, Englewood Cliffs, NJ.

Townsend, D.W., 1996. In The Gulf of Maine Ecosystem Dynamics; Wallace, G. T. and E. F. Braasch, Eds. Regional Association for Research on the Gulf of Maine: St. Andrews, New Brunswick.

Van Dingenen, R., Raes, F., Jensen, N.R., 1995. Evidence for anthropogenic impact on number concentration and sulfate content of cloud-processed aerosol particles over the North Atlantic. J. Geophys. Res. 100, D10, 21,057-21,067.

Venkatachari, P., Zhou, L., Hopke, P.K., Felton, D., Rattigan, O.V., Schwab, J.J., Dmerjian, K.L., 2006. Spatial and temporal variability of black carbon in New York City. J. Geophys. Res., doi: 10.1029/2005JD006314.

Windsor, J.G., Hites, R.A., 1979. Polycyclic aromatic hydrocarbons in Gulf of Maine sediments and Nova Scotia soils. Geochim. Cosmochim. Acta 43, 27 (1979).

## Figure Captions

**Figure 1**. **A**. GoM bathymetry and station locations. **B**. BC concentrations (μg/L) in the GoM. Upper and lower values represent mixed layer (typically *ca.* 6 m) and sub-mixed layer (typically *ca.* 60 m) samples, respectively (see Table 1). Black (left) and blue (right) data represent April and August samples, respectively. **C**. Mass balance model of BC in the GoM (Gg = $10^9$ g). Size of BC reservoir and water column flux estimates were calculated using detailed bathymetric data collected by Incze and Jakobbson (2008) from http://pubs.usgs.gov/ and our measured BC concentrations and fluxes (Table S3); BC inputs and outputs from water currents and river flows were calculated using water volumetric flows from Townsend (1996) and BC concentrations estimated from this study (Table S4); BC atmospheric deposition was estimated using average deposition rates of 1 and 0.3 g/m$^2$·yr (see Table 4) for the coastal (28,000 km$^2$; regions 5 and 6 on Table S3) and central GoM (122,000 km$^2$; regions 2, 3, 7-10 on Table S3) areas, respectively; and BC sedimentation was calculated using average BC sediment fluxes of 2 and 1 g/m$^2$·yr (see Table 4) for the coastal (28,000 km$^2$) and central GoM (122,000 km$^2$) areas, respectively.

**Figure 2**. Sorption isotherm for the Jordan Basin surface sample. Filled diamonds represent the experimental results. Open squares represent the linear $f_{oc}K_{oc}$ sorption model. Best fit $K_{BC}$ and Freundlich parameter, *n*, obtained from the linear regression of Log $_{pys}$ vs Log $C_{pyw}$, and Log $K_d$ vs Log $C_{iw}$ were 5.95 ± 0.10 and 0 .66±0.04, respectively.

**Figure. 3**. Log PAH and BC concentrations vs distance from Boston. Comparison of (A) observations by Windsor and Hites (1981) of logarithmic decrease of total PAHs concentrations with distance with logarithmic decrease of shallow, and (B) BC concentrations collected during 2004 (data set include Charles River (59 ± 7 μg/L; n=3) and Boston Harbor (51 ± 6 μg/L; n=2) collected from shore during May-June 2004, and MWRA and EPB collected on board of *R/V Oceanus* during April 2004).

**Figure 4**. $\Delta^{14}C$ and fraction modern ($f_m$) of BC and OC in the GoM. Open squares represent OC, and solid symbols represent BC. End members used for this calculations were $\Delta^{14}C$= -1000 and $f_m$= 0 for fossil fuel combustion, and ; $\Delta^{14}C$= +100 and $f_m$> 1 for biomass combustion. April 2004 samples: Georges Bank shallow (GB); August 2004 samples: Inner Penobscot Bay shallow (IPB), Massachusetts Water Resources Authority shallow (MWRA) and Wilkinson Basin shallow ($WB_{shallow}$) and deep ($WB_{deep}$).

## Table Captions

**Table 1.** Gulf of Maine sampling stations site characterization.

**Table 2.** Concentrations of BC in POC > 53 μm (Nitex) and 53 μm > POC >0.7 μm (GFF/Quartz filter).

**Table 3.** $^{234}Th$ and $^{238}U$ radionuclide activities in the GoM.

**Table 4.** Comparison of estimated BC fluxes ($g_{BC}/m^2$ yr) at different distances from shore and urban sites.

**Table 1**. Gulf of Maine sampling stations site characterization.

| Sample name[a] (depth) | Lat. +N/- S | Long. +E/- W | Approx. Water depth (m) | APRIL 2004 | | | | | | AUGUST/SEPTEMBER 2004 | | | | | |
|---|---|---|---|---|---|---|---|---|---|---|---|---|---|---|---|
| | | | | Mixed layer depth (m) | Temp (°C) | Salinity (PSU) | Chl *a* (µg/L) | $O_2$ (mg/L) | POC (µg/L) | Mixed layer depth (m) | Temp (°C) | Salinity (PSU) | Chl *a* (µg/L) | $O_2$ (mg/L) | POC (µg/L) |
| MWRA (6 m) | 42.37 | -70.81 | 33 | 10 | 5.7 | 30.7 | 3.0 | 10.2 | 322 | 15 | 13.7 | 31.5 | 0.6 | 8.5 | 144 |
| MWRA (20 m) | 42.37 | -70.81 | 33 | 10 | 3.8 | 32.0 | 6.6 | 10.6 | 248 | 15 | 8 | 31.8 | 0.3 | 9.6 | 103 |
| NMB (6 m) | 42.52 | -70.45 | 90 | 21 | 4.6 | 31.3 | 10.1 | 10.5 | 296 | - | - | - | - | - | - |
| NMB (50 m) | 42.52 | -70.45 | 90 | 21 | 3.5 | 32.8 | 1.2 | 10.7 | 35.6 | - | - | - | - | - | - |
| MER (6 m) | 42.81 | -70.73 | 35 | 10 | 5.6 | 31.4 | 7.8 | 10.3 | 288 | 15 | 15 | 31.4 | 0.6 | 8.3 | 129 |
| MER (20 m) | 42.81 | -70.73 | 35 | 10 | 3.8 | 32.0 | 2.4 | 10.6 | 258 | 15 | 9.6 | 31.9 | 0.9 | 9.2 | 93.8 |
| CB (6 m) | 43.56 | -70.05 | 180 | 24 | 5.2 | 30.8 | 6.3 | 10.4 | 324 | 10 | 12.4 | 31.7 | 1.0 | 8.7 | 145 |
| CB (15 m) | 43.56 | -70.05 | 180 | 24 | 3.1 | 32.1 | 0.5 | 10.8 | 64.3 | 10 | 10.5 | 31.9 | 0.8 | 9.1 | 190 |
| WB 1 (6 m) | 42.99 | -69.90 | 200 | 50 | 3.2 | 32.1 | 2.4 | 10.7 | 148 | 50 | 18.2 | 31.1 | 0.2 | 8 | 63.2 |
| WB 1 (80 m) | 42.99 | -69.90 | 200 | 50 | 4 | 33.3 | 0.8 | 10.5 | n.m. | 50 | 4.7 | 32.7 | 0.1 | 10.3 | 16.7 |
| WB 2 (8 m) | 43.37 | -69.89 | 170 | 50 | 4.1 | 31.8 | 4.7 | 10.6 | 280 | - | - | - | - | - | - |
| WB 2 (30 m) | 43.37 | -69.89 | 170 | 50 | 2.9 | 32.7 | 1.4 | 10.8 | 71.1 | - | - | - | - | - | - |
| EPB (6 m) | 43.11 | -69.18 | 50 | 63 | 3.8 | 32.2 | 1.2 | 10.6 | 88.5 | 50 | 16.2 | 31.9 | 0.3 | 8.5 | 55.6 |
| EPB (35 m) | 43.11 | -69.18 | 50 | 63 | 3.5 | 32.2 | 0.8 | 10.7 | 81.5 | - | - | - | - | - | - |
| EPB (80 m) | 43.11 | -69.18 | 50 | - | - | - | - | - | - | 50 | 6.8 | 32.8 | 0.1 | 9.9 | 28.9 |
| IPB (3 m) | 44.42 | -68.83 | 25 | 6 | 3.9 | 22.8 | 1.6 | 11.2 | 286 | 4 | 13.1 | 29.0 | 0.8 | 8.7 | 291 |
| IPB (6 m) | 44.42 | -68.83 | 25 | 6 | 2.8 | 30.5 | 1.3 | 11 | 205 | 4 | 11.6 | 30.8 | 0.6 | 9 | 209 |
| JB (8 m) | 43.41 | 67.41 | 285 | 50 | 2.8 | 31.9 | 1 | 10.9 | 127 | 50 | 18.1 | 32.1 | 0.4 | 7.9 | 72.1 |
| JB (60 m) | 43.41 | 67.41 | 285 | 50 | 2.4 | 32.1 | 0.2 | 11 | 37.0 | - | - | - | - | - | - |
| JB (80 m) | 43.41 | 67.41 | 285 | - | - | - | - | - | - | 50 | 5.1 | 32.8 | 0.1 | 10.2 | 19.9 |
| GB (8 m) | 41.75 | -68.00 | 195 | 50 | 5.3 | 32.9 | 7.2 | 10.2 | 155 | 50 | 18.2 | 32.0 | 0.2 | 7.6 | 52.9 |
| GB (60 m) | 41.75 | -68.00 | 195 | 50 | 4.5 | 33.2 | 2.7 | 10.4 | 45.2 | 50 | 5 | 32.6 | 0.1 | 10.3 | 51.8 |
| GSC (8 m) | 41.83 | -69.67 | 198 | 50 | 5.1 | 32.7 | n.m. | 10.3 | 149 | 32 | 17.3 | 31.5 | 0.3 | 7.9 | 188 |
| GSC (60 m) | 41.83 | -69.67 | 198 | 50 | 3.5 | 33.1 | n.m. | 10.6 | n.m. | 32 | 4.4 | 32.5 | 0.0 | 7.9 | 23.4 |
| CCB 1 (6 m) | 41.80 | -70.05 | 20 | 13 | 6 | 31.8 | 1.2 | 10.1 | 240 | - | - | - | - | - | - |
| CCB 2 (6 m) | 41.92 | -70.17 | 27 | 13 | 5.2 | 32.2 | 5.4 | 10.3 | 169 | 15 | 17.4 | 31.3 | 0.3 | 8.0 | 114 |
| CCB 2 (20 m) | 41.92 | -70.17 | 27 | 13 | 5.1 | 32.2 | 5.7 | 10.3 | n.m. | 15 | 7.4 | 32.0 | 0.2 | 9.9 | 114 |

[a]Massachusetts Water Reservoir Authority (MWRA); North Mass Bay (NMB); Merrimack River (MER); Casco Bay (CB); Wilkinson Basin I (WB1); Wilkinson Basin II (WB2); East Plats Bay (EPB); Inner Penobscot Bay (IPB); Jordan Basin (JB); Georges Bank (GB); Great South Channel (GS); Cape Cod Bay I (CCB1); Cape Cod Bay II (CCB2); n.m. not measured; the mixed layer depth for this study was selected as the depth up to which temperature, salinity and oxygen saturation remained relatively homogeneous.

**Table 2.** Concentrations of BC in POC > 53 μm (Nitex) and 53 μm> POC >0.7 μm (GFF/Quartz filter).

| | APRIL 2004 | | | | AUGUST/SEPTEMBER 2004 | | | | SUM | | SUM | | | |
|---|---|---|---|---|---|---|---|---|---|---|---|---|---|---|
| | GFF | | NITEX | | QUARTZ | | NITEX | | April | +/- | August | +/- | Average | +/- |
| Station (depth) | C (μg/L) | +/- | C (μg/L) | +/- | C (μg/L) | +/- | C (μg/L) | +/- | | | | | | |
| MWRA (6 m) | 4.0 | 0.4 | 0.18 | 0.08 | 7.1 | 0.4 | 0.27 | 0.09 | 4.2 | 0.4 | 7.3 | 0.5 | 5.8 | 0.6 |
| MWRA (20 m) | 6.5 | 2.8 | <0.07 | - | 0.80 | 0.26 | <3.5 | - | 6.5 | 2.8 | 0.8 | 0.3 | 3.6 | 2.8 |
| NMB (6 m) | 3.0 | 1.7 | <0.05 | - | | | | | 3.0 | 1.7 | | | 3.0 | 1.7 |
| NMB (50 m) | <0.3 | | <0.05 | - | | | | | <0.3 | - | | | <0.3 | - |
| MER (6 m) | 3.9 | 2.4 | 2.8 | 0.3 | 5.4 | 0.1 | <0.24 | - | 6.6 | 2.4 | 5.4 | 0.1 | 6.0 | 2.4 |
| MER (20 m) | 16 | 7.1 | <0.6 | - | 7.3 | 0.2 | <0.01 | - | 16 | 7.1 | 7.3 | 0.2 | 12 | 7.1 |
| CB (6 m) | 3.5 | 1.2 | 0.30 | 0.09 | 1.8 | 1.1 | 0.19 | 0.03 | 3.8 | 1.3 | 2.0 | 1.1 | 2.9 | 1.7 |
| CB (15 m) | 3.6 | 1.5 | 2.2 | 0.1 | 3.8 | 0.5 | <1.6 | - | 5.8 | 1.5 | 3.8 | 0.5 | 4.8 | 1.6 |
| WB 1 (6 m) | 3.3 | 1.5 | <0.4 | - | 0.81 | 0.04 | 0.03 | 0.01 | 3.3 | 1.5 | 0.8 | 0.0 | 2.1 | 1.5 |
| WB 2 (80 m) | | | | | <0.4 | | <2.2 | - | | | <2.6 | - | <2.6 | - |
| WB 2 (8 m) | 0.4 | 1.6 | <0.2 | - | | | | | 0.4 | 1.6 | | | 0.4 | 1.6 |
| WB 2 (30 m) | 15 | 4.5 | <1 | - | | | | | 15 | 4.5 | | | 15 | 4.5 |
| EPB (6 m) | 2.8 | 1.2 | 0.07 | 0.01 | 1.5 | 0.1 | 0.04 | 0.01 | 2.8 | 1.2 | 1.5 | 0.1 | 2.2 | 1.2 |
| EPB (35 m) | 2.1 | 1.5 | <0.4 | - | | | | | 2.1 | 1.5 | | | 2.1 | 1.5 |
| EPB (80 m) | | | | | 5.6 | 0.1 | <0.9 | - | | | 5.6 | 0.1 | 5.6 | 0.1 |
| IPB (3 m) | 6.1 | 3.0 | 0.79 | 0.2 | 6.9 | 0.1 | 0.43 | 0.05 | 6.9 | 3.0 | 7.3 | 0.1 | 7.1 | 3.0 |
| IPB (6 m) | 8.4 | 2.4 | <1 | - | 3.4 | 0.1 | <0.01 | - | 8.4 | 2.4 | 3.4 | 0.1 | 5.9 | 2.4 |
| JB (8 m) | 4.5 | 1.8 | 0.41 | 0.12 | 1.6 | 0.0 | 0.06 | 0.01 | 4.9 | 1.8 | 1.6 | 0.0 | 3.2 | 1.8 |
| JB (60 m) | 0.1 | 1.7 | <0.5 | - | | | | | 0.1 | 1.7 | | | 0.1 | 1.7 |
| JB (80 m) | | | <0.01 | - | 1.3 | 0.1 | <0.01 | - | | | 1.3 | 0.1 | 1.3 | 0.1 |
| GB (8 m) | 5.6 | 0.9 | <0.2 | | 2.8 | 0.1 | <2.0 | - | 5.6 | 0.9 | 2.8 | 0.1 | 4.2 | 0.9 |
| GB (60 m) | <0.3 | - | <0.2 | - | 2.1 | 0.2 | <0.11 | - | <0.5 | | 2.1 | 0.2 | 2.1 | 0.2 |
| GSC (8 m) | 6.6 | 0.9 | <0.2 | - | 12 | 0.2 | <0.44 | - | 6.6 | 0.9 | 11.6 | 0.2 | 9.1 | 0.9 |
| GSC (60 m) | | | | | <0.6 | - | <0.01 | - | | | <0.6 | - | <0.6 | - |
| CCB 1 (6 m) | 1.1 | 3.2 | 0.08 | | | | | | 1.1 | 3.2 | | | 1.1 | 3.2 |
| CCB 2 (6 m) | 8.7 | 2.5 | <0.35 | - | 2.2 | 0.1 | <0.01 | - | 8.7 | 2.5 | 2.2 | 0.1 | 5.4 | 2.5 |
| CCB 2 (20 m) | | | | | 0.54 | 0.16 | 0.3 | 0.06 | | | 0.86 | 0.17 | | |

Note 1: < x if signal to noise raitio is less than 3:1

Note 2: Absolute uncertainty calculated using error propagation (including sampling and analytical error)

**Table 3.** $^{234}$Th and $^{238}$U radionuclide activities in the GoM.

| Station | $^{238}$U (dpm/L) | | | | Total $^{234}$Th (dpm/L) | | | | Nitex $^{234}$Th (mdpm[c]/L) | | | $^{234}$Th/$^{238}$U % | | | |
|---|---|---|---|---|---|---|---|---|---|---|---|---|---|---|---|
| | April | May[a] | Aug/Sept | Sept[a,b] | April | May[a] | Aug/Sept | Sept | April | Aug/Sept | Sept | April | May[a] | Aug/Sept | Sept |
| CCB1 | 2.12 ± 0.02 | | 2.11 ± 0.02 | | 0.83 ± 0.02 | | 1.04 ± 0.02 | | 2.4 ± 0.1 | 1.1 ± 0.1 | | 39 | | 50 | |
| CCB2 | 2.14 ± 0.02 | | n.m. | | 0.49 ± 0.02 | | n.m. | | 3.7 ± 0.2 | n.m. | | 23 | | | |
| MWRA | 2.05 ± 0.02 | 1.92 ±0.02 | 2.09 ± 0.02 | 2.20 ± 0.02[a] | 0.37 ± 0.02 | 0.50 ± 0.03 | 1.39 ± 0.01 | 0.12 ± 0.02[a] | 13 ± 1 | 1.7 ± 0.1 | n.m. | 18 | 26 | 66 | 5[a] |
| NMB | 2.09 ± 0.02 | | n.m. | | 0.91 ± 0.03 | | n.m. | | 33 ± 2 | n.m. | | 43 | | | |
| MER | 2.07 ± 0.02 | | 2.09 ± 0.02 | | 1.47 ± 0.06 | | 0.79 ± 0.01 | | 35 ± 2 | 1.7 ± 0.1 | | 71 | | 38 | |
| WB1 | 2.14 ± 0.02 | | 2.08 ± 0.02 | 2.24[b] | 1.93 ± 0.10 | | 0.89 ± 0.01 | 1.03[b] | 21 ± 1 | 0.71 ± 0.04 | 6.4[b] | 90 | | 43 | 46[b] |
| WB2 | 2.11 ± 0.02 | | n.m | 2.30[b] | 1.87 ± 0.10 | | n.m. | 0.95[b] | 200 ± 10 | n.m. | 25.2[b] | 89 | | | 41[b] |
| OCB | 2.07 ± 0.02 | 2.04 ± 0.02 | 2.08 ± 0.02 | 2.24 ± 0.02[a] | 0.66 ± 0.04 | 0.78 ± 0.04 | 0.84 ± 0.01 | 0.22 ± 0.04[a] | 2.6 ± 0.1 | 1.3 ± 0.1 | n.m. | 32 | 38 | 40 | 10[a] |
| IPB | 1.86 ± 0.02 | | 1.97 ± 0.02 | | 0.16 ± 0.01 | | 0.03 ± 0.00 | | 7.4 ± 0.4 | 1.0 ± 0.1 | | 9 | | 1 | |
| EPB | 2.14 ± 0.02 | 2.20 ± 0.02 | 2.13 ± 0.02 | n.m. | 1.91 ± 0.11 | 1.81 ± 0.05 | 1.00 ± 0.01 | n.m. | 18 ± 1 | 0.89 ± 0.04 | n.m. | 90 | 82 | 47 | |
| JB | 2.12 ± 0.02 | | 2.14 ± 0.02 | 2.30[b] | 2.05 ± 0.12 | | 1.99 ± 0.02 | 1.14[b] | 46 ± 2 | 1.5 ± 0.1 | 1.3[b] | 97 | | 93 | 49[b] |
| GB | 2.19 ± 0.02 | | 2.13 ± 0.02 | 2.29[b] | 1.62 ± 0.06 | | 1.87 ± 0.02 | 0.72[b] | 12 ± 1 | 3.5 ± 0.2 | 8[b] | 74 | | 88 | 32[b] |
| GSC | 2.17 ± 0.02 | | 2.11 ± 0.02 | | 1.85 ± 0.08 | | 1.17 ± 0.01 | | 42 ± 2 | 2.9 ± 0.1 | | 85 | | 55 | |

[a]Gustafsson et al. (1997b); [b]Charette et al. (2001); n.m. not measured; [c]mdpm = $10^{-3}$ dpm

**Table 4.** Comparison of estimated BC fluxes ($g_{BC}/m^2 \cdot yr$) at different distances from shore and urban sites.

| Near Urban Sites | | Non-urban/Near-shore sites | | Continental Shelf Regimes[s] | | Open Ocean[s] | |
|---|---|---|---|---|---|---|---|
| | | | *Atmospheric deposition* | | | | |
| Thompson Farm, NH[a, c] | 0.13 | Arcadia National Park, ME[b,l] | 0.21 | Gulf of Maine[a, m] | 0.001 | Pacific open ocean[a, n] | 0.002-0.01 |
| Halifax, NS[a, d] | 0.41 | Brockport, NY (rural)[a, f] | 0.28 | Pacific coast[a, n] | 0.04 - 0.08 | | |
| Sable Island, NS[a, e] | 0.09 | Quabbin State Park, MA[a, f] | 0.19 | Northern Sweden[b, o] | 0.02 | | |
| Kenmore, MA (urban)[a, f] | 0.56 | | | Southern Sweden[b, o] | 0.06 | | |
| Queens, NY[a, g] | 0.1 - 3.0 | | | North Atlantic[b, p] | 0.30 | | |
| Greater Boston, MA[a, h] | 0.02 - 1.7 | | | | | | |
| | | | *Water column export (Gulf of Maine)* | | | | |
| | April Aug/Sept | | April Aug/Sept | | April Aug/Sept | | |
| MWRA, MA[i] | 2.9 ± 1.3 20 ± 7 | Inner Pennobscot Bay[j] | 26 ± 6 36 ± 5 | Great South Channel[i] | <1.4 <11 | | |
| | | Merrimack River Bay[j] | 6.0 ± 0.5 <15 | Georges Bank[i] | <6.3 <8.7 | | |
| | | Cape Cod Bay[j] | 6.9 ± 0.9 <26 | Jordan Basin[i] | 1.2 ± 0.4 11 ± 2 | | |
| | | Casco Bay[j] | 31 ± 9 21 ± 4 | Wilkinson Basin[i] | <2.4 16 ± 6 | | |
| | | | | East Platts Bank[i] | 0.7 ± 0.1 20 ± 5 | | |
| | | | *Sediment fluxes* | | | | |
| Fort Point Channel, MA[j] | 23 | Mouth of Providence River, RI[j] | 14 | Santa Barbara Basin, CA[q] | 0.4 | N. and S. Pacific Ocean[l] | 0.0001-0.001 |
| Spectacle Island, ME[j] | 4.7 | Palos Verdes Shelf, CA[j] | 7-10 | Saanich Inlet, BC[q] | 0.7 | | |
| Portland Harbor, ME[j] | 6.5 | New England Harbors[j] | 5-23 | W. Med. Sea[n] | 1 | | |
| MWRA, MA[k] | 1.1 | Gulf of Maine | | Gulf of Maine | | | |
| | | Inner Penobscot Bay[k] | 1.7 | Wilkinson Basin[j] | 1.2[j], 0.8[k] | | |
| | | Cape Cod Bay I | 1.9[j], 0.9[k] | Jordan Basin[k] | 1.7 | | |
| | | Cape Cod Bay II[j] | 1.0 | | | | |
| | | Casco Bay[k] | 0.9 | | | | |

[a] Under-cloud scavenging fluxes estimated from atmospheric concentrations according to Seinfield and Spiros (1998) and scavenging coefficients from Daggupaty et al (2006), and a dry deposition rate of 0.1 cm/s was assumed; [b]Measured atmospheric flux; [c]airmap.nhu.edu; [d]Chylek et al., (1999); [e]Cooke et al. (2002); [f]Pedersen (2002); [g]Venkatachari et al (2006); [h]Gryparis et al (2006); [i]This study; [j]Gustafsson et al. (1998); [k]Flores-Cervantes et al. (2008); [l]Cachier et al. (1990); [m]Liousse et al. (1996); [n]Suman et al. (1997); [o]Ogren et al. (1984); [p]Van Dingenenen et al. (1995); [q]Griffin and Goldberg (1975); [r]Smith et al. (1973); [s] Atmospheric deposition in remote areas may be uderestimated by a factor of four (Liousse et al., 1993).

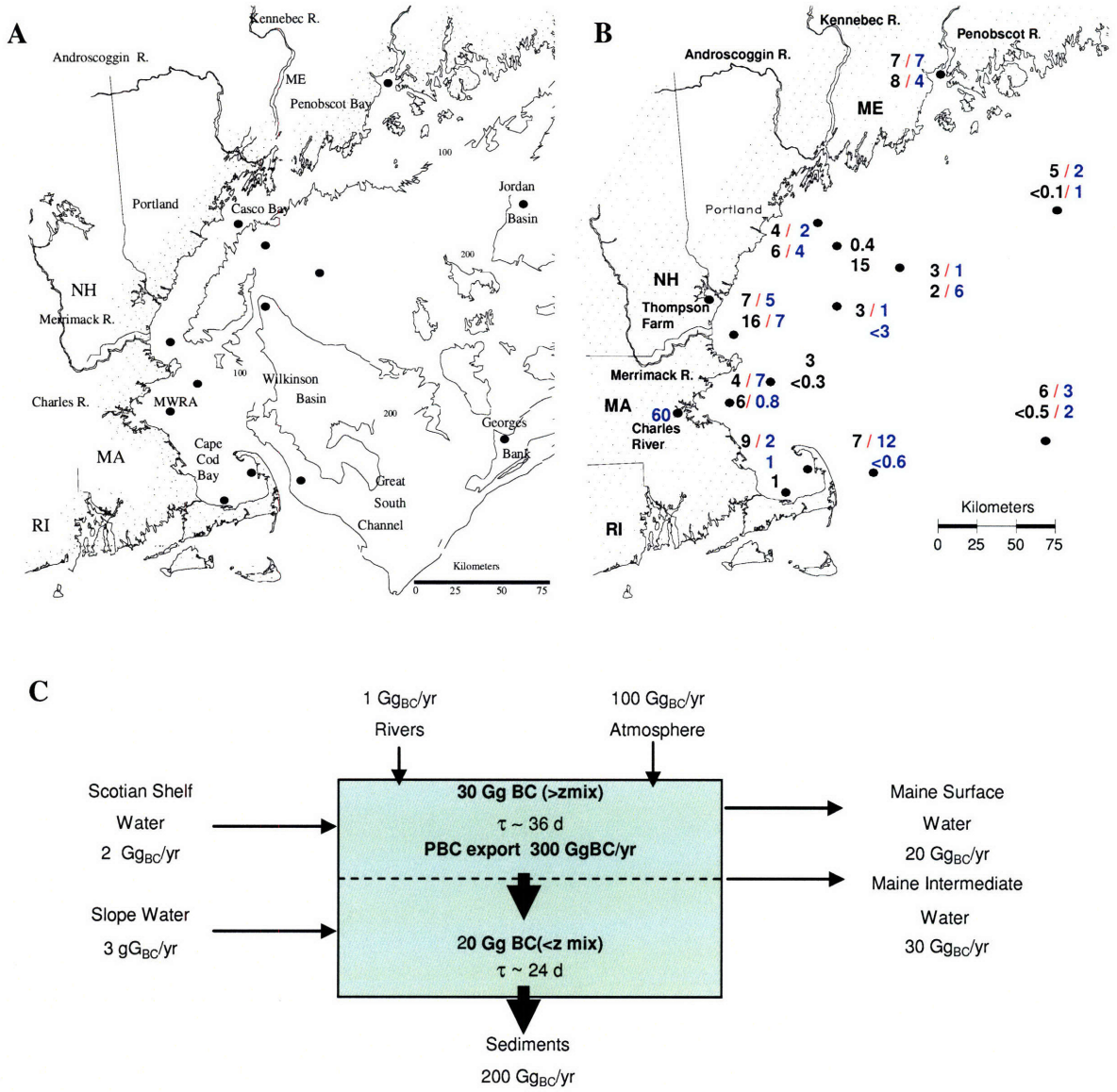


**Figure 1**. **A**. GoM bathymetry and station locations. **B**. BC concentrations (μg/L) in the GoM. Upper and lower values represent mixed layer (typically *ca.* 6 m) and sub-mixed layer (typically *ca.* 60 m) samples, respectively (see Table 1). Black (left) and blue (right) data represent April and August samples, respectively. **C**. Mass balance model of BC in the GoM (Gg = $10^9$ g). Size of BC reservoir and water column flux estimates were calculated using detailed bathymetric data collected by Incze and Jakobbson (2008) from http://pubs.usgs.gov/ and our measured BC concentrations and fluxes (Table S3); BC inputs and outputs from water currents and river flows were calculated using water volumetric flows from Townsend (1996) and BC concentrations estimated from this study (Table S4); BC atmospheric deposition was estimated using average deposition rates of 1 and 0.3 g/m$^2$·yr (see Table 4) for the coastal (28,000 km$^2$; regions 5 and 6 on Table S3) and central GoM (122,000 km$^2$; regions 2, 3, 7-10 on Table S3) areas, respectively; and BC sedimentation was calculated using average BC sediment fluxes of 2 and 1 g/m$^2$·yr (see Table 4) for the coastal (28,000 km$^2$) and central GoM (122,000 km$^2$) areas, respectively.

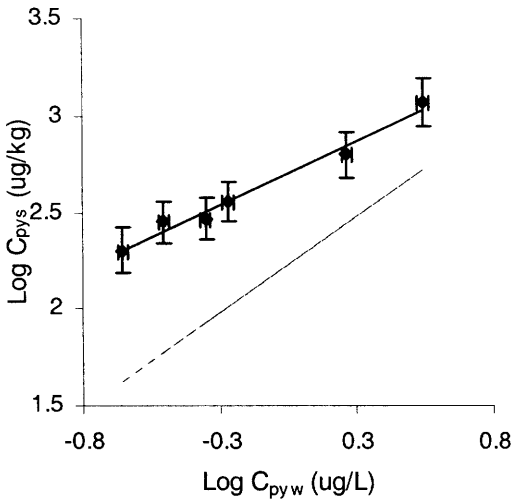


**Figure 2. Sorption isotherm for the Jordan Basin surface sample.** Filled diamonds represent experimental results. Dashed line represents the linear $f_{oc}K_{oc}$ sorption model. Best fit $K_{BC}$ and Freundlich parameter, *n*, obtained from the linear regression of Log $_{pys}$ vs Log $C_{pyw}$, and Log $K_d$ vs Log $C_{iw}$ were 5.95 ± 0.10 and 0 .66±0.04, respectively (Flores-Cervantes et al., manuscript in preparation, 2008).

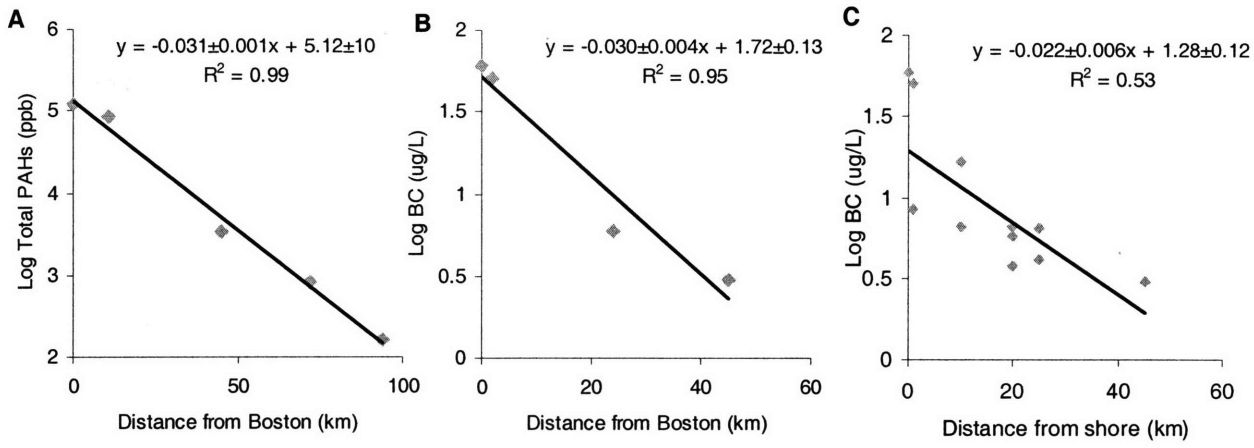


**Figure. 3. Log PAH and BC concentrations vs distance from Boston.** Comparison of (A) observations by Windsor and Hites (1981) of logarithmic decrease of total PAHs concentrations with distance with logarithmic decrease of shallow, and (B) BC concentrations collected during 2004 (data set include Charles River (59 ± 7 μg/L; n=3) and Boston Harbor (51 ± 6 μg/L; n=2) collected from shore during May-June 2004, and MWRA and EPB collected on board of *R/V Oceanus* during April 2004).

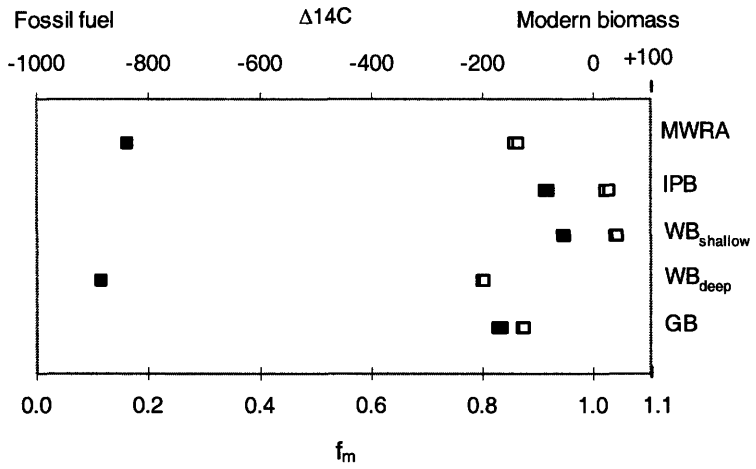


**Figure 4. $\Delta^{14}C$ and fraction modern ($f_m$) of BC and OC in the GoM.** Open squares represent OC, and solid symbols represent BC. End members used for these calculations were $\Delta^{14}C$= -1000 for fossil fuel combustion, and $\Delta^{14}C$= 100 for biomass combustion. April 2004 samples: Georges Bank shallow (GB); August 2004 samples: Inner Penobscot Bay shallow (IPB), Massachusetts Water Resources Authority shallow (MWRA) and Wilkinson Basin shallow ($WB_{shallow}$) and deep ($WB_{deep}$).

**Supplementary Information for:**

**"Black carbon in the ocean: New insights into inputs and cycling of highly recalcitrant organic carbon"**

D. Xanat Flores-Cervantes[1], Desiree L. Plata[1, 2], John K. MacFarlane[1], Christopher M. Reddy[2], and Philip M. Gschwend[1].

[1]R.M. Parsons Laboratory, MIT 48-413, Department of Civil and Environmental Engineering, Massachusetts Institute of Technology, Cambridge, Massachusetts 02139, USA

[2]Department of Marine Chemistry and Geochemistry, Woods Hole Oceanographic Institution, Woods Hole, Massachusetts, 02543

xanatf@mit.edu, dplata@whoi.edu, jmac@mit.edu, creddy@whoi.edu, pmgschwe@mit.edu.

This document includes:

Tables S1, S2, S3, S4, S5.

## Table Captions

**Table S1**. Summary of New England BC ($Gg_{BC}$) emissions estimated from energy use (http://www.eia.doe.gov/) and technology-based BC emission factors (Bond et al., 2004).

**Table S2**. Detailed energy consumption estimates (2004, trillion Btu) and BC ($Gg_{BC}$) emission estimates for New England by sector.

**Table S3**. Estimation of BC mass in regions of the GoM using detailed (every 10 m) bathymetric data collected by Incze and Jakobbson (2008) from http://pubs.usgs.gov/.

**Table S4**. BC inputs and outputs from water currents and river flows in the GoM.

**Table S5.** Stable and radiocarbon isotope signatures of seawater samples in the GoM.

**Table S6**. Possible sources of stable and radiocarbon isotopes in natural environments.

**Table S1.** Summary of New England BC ($Gg_{BC}$) emissions estimated from energy use (http://www.eia.doe.gov/) and technology-based BC emission factors (Bond et al., 2004).

| Sector | Coal | Natural Gas | Petroleum | Biomass[d] | Ethanol | Total |
|---|---|---|---|---|---|---|
| Residential | 0.000 | 0.003 | 6.80 | 1.86 | 0.000 | 8.674 |
| Commercial | 0.005 | 0.002 | 0.08 | 0.230 | 0.000 | 0.318 |
| Industrial | 0.025 | 0.001 | 0.10 | 1.98 | 0.000 | 2.105 |
| Transportation | 0.000 | 0.000 | 4.15 | 0.00 | 0.022 | 4.173 |
| Power generation | 0.109 | 0.006 | 0.073 | 0.397 | 0.000 | 0.585 |
| **Total** | 0.139 | 0.012 | 11.22 | 5.14 | 0.022 | 15.855 |

[d] Wood and biomass waste. BC from forest fires of 0.67 $Gg_{BC}$ were added to the total; $Gg = 10^9$ g

**Table S2.** Detailed energy consumption estimates (2004, trillion Btu) and BC ($Gg_{BC}$) emission estimates for New England by sector.

Residential Sector Energy Consumption Estimates (2004, trillion Btu) and BC ($Gg_{BC}$) Emission Estimates

| State | Coal | Natural Gas [a] | Petroleum | | | | Wood | Geo-thermal | Solar/ PV [b] | Retail Electricity Sales | Net Energy | Electrical System Energy Losses [c] | Total |
|---|---|---|---|---|---|---|---|---|---|---|---|---|---|
| | | | Distillate Fuel | Kerosene | LPG | Total | | | | | | | |
| New England | 0.1 | 193.5 | 338.8 | 19.1 | 30.3 | 388 | 28.5 | 0 | 0.8 | 159.4 | 770.5 | 354.6 | 1125.3 |
| Gg BC | 0.000 | 0.003 | 6.692 | 0.051 | 0.065 | 6.808 | 1.863 | 0.000 | 0.000 | 0.000 | 0.000 | 0.000 | 8.674 |

Commercial Sector Energy Consumption Estimates (2004, trillion Btu) and BC ($Gg_{BC}$) Emission Estimates

| State | Coal | Natural Gas [a] | Petroleum | | | | | | Hydro-electric Power [c] | Biomass [d] | Geo-thermal | Retail Electricity Sales | Net Energy | Electrical System Energy Losses [e] | Total [f] |
|---|---|---|---|---|---|---|---|---|---|---|---|---|---|---|---|
| | | | Distillate Fuel | Kerosene | LPG [b] | Motor Gasoline | Residual Fuel | Total | | | | | | | |
| New England | 1 | 124 | 87.8 | 3.4 | 5.4 | 2.4 | 30.2 | 129 | 0 | 9.5 | 0.3 | 183.2 | 447.2 | 407.6 | 854.9 |
| Gg BC | 0.005 | 0.002 | 0.054 | 0.002 | 0.005 | 0.002 | 0.017 | 0.080 | 0.000 | 0.230 | 0.000 | 0.000 | 0.000 | 0.000 | 0.318 |

Industrial Sector Energy Consumption Estimates (2004, trillion Btu) and BC ($Gg_{BC}$) Emission Estimates

| Region | Coal | Nat. Gas [a] | Petroleum | | | | | | | | | Hydro electrical power | Bio-mass [d] | Geothermal | Retail Electri-city Sales | Net Energy [e] | Electri-cal System Energy Losses [f] | Total [g] |
|---|---|---|---|---|---|---|---|---|---|---|---|---|---|---|---|---|---|---|
| | | | Asphalt and Road Oil | Distillate Fuel | Kero-sene | LPG | Lubricants | Motor Gaso-line | Resi-dual Fuel | Other [b] | Total | | | | | | | |
| New England | 4.5 | 85.1 | 36.1 | 35.7 | 2.1 | 5.5 | 3.9 | 13.5 | 36.5 | 18.5 | 152.2 | 5.9 | 81.5 | 0 | 82.8 | 412.1 | 184.3 | 596.2 |
| Gg BC | 0.025 | 0.001 | 0.022 | 0.022 | 0.001 | 0.005 | 0.00 | 0.013 | 0.031 | 0.011 | 0.105 | 0.00 | 1.975 | 0 | 0.000 | 0.000 | 0.000 | 2.105 |

Transportation Sector Energy Consumption Estimates (2004, trillion Btu) and BC ($Gg_{BC}$) Emission Estimates

| State | Coal | Natural Gas [a] | Petroleum | | | | | | | | Ethanol [b] | Retail Electricity Sales | Net Energy | Electrical System Energy Losses [c] | Total |
|---|---|---|---|---|---|---|---|---|---|---|---|---|---|---|---|
| | | | Aviation Gasoline | Distillate Fuel | Jet Fuel | LPG | Lubricants | Motor Gasoline | Residual Fuel | Total | | | | | |
| New England | 0 | 6.7 | 1.5 | 169.8 | 79.2 | 0.2 | 5.5 | 822.9 | 0.3 | 1093.7 | 14.4 | 2 | 1102.5 | 4.5 | 1107.1 |
| Gg BC | 0.000 | 0.000 | 0.000 | 3.354 | 0.000 | 0.000 | 0.000 | 0.796 | 0.000 | 4.151 | 0.022 | 0.000 | 0.000 | 0.000 | 4.173 |

**Table S2 (continuation).** Energy consumption estimates (2004, trillion Btu) and BC ($Gg_{BC}$) emission estimates for New England.

| Electric Power Sector Energy Consumption Estimates (2004, trillion Btu) and BC ($Gg_{BC}$) Emission Estimates | | | | | | | | | | | | | | |
|---|---|---|---|---|---|---|---|---|---|---|---|---|---|---|
| | | Natural | Petroleum | | | | Nuclear | Hydro- | | | | | Electricity | |
| State | Coal | Gas [a] | Residual Fuel [b] | Distillate Fuel [c] | Petroleum Coke | Total | Electric Power | electric Power [d] | Biomass | Geo-thermal | Solar /PV [f] | Wind | Net Imports [g] | Total |
| New England | 194.3 | 365.2 | 110.6 | 6.4 | 0 | 116.9 | 380.7 | 68.2 | 117.2 | 0 | 0 | 0.1 | 27 | 1269.9 |
| Gg BC | 0.109 | 0.006 | 0.070 | 0.004 | 0.000 | 0.073 | 0.000 | 0.000 | 0.397 | 0.000 | 0.000 | 0.000 | 0.000 | 0.585 |

Note: BC emission estimates are different for the same fuel in each different sector due to differences in the Technology used. See Bond et al. (2004) for a detailed description of the BC emission factors.

[a]End-use sector data include electricity sales and associated electrical system energy losses.

[b]U.S. total energy and U.S. industrial sector include 137.8 trillion Btu of net imports of coal coke not allocated to the States.

[c]Includes supplemental gaseous fuels.

[d]Conventional hydroelectric power. Does not include pumped-storage hydroelectricity.

[e]Wood and waste.

[f]"Other" is geothermal, wind, photovoltaic, solar thermal energy, and net imports of electricity.

[g]Net interstate flow of electricity is the difference between the amount of energy in the electricity sold within a State (including associated losses) and the energy input at the electric utilities within the State. A positive number indicates that more electricity (including associated losses) came into the State than went out of the State during the year; conversely, a negative number indicates that more electricity (including associated

(s) = Value less than 0.05 trillion Btu.

Sources: Energy consumption estimates from U.S. Department of Energy (DOE) http://tonto.eia.doe.gov/; BC emission factors to calculate BC emissions from Bond et al. (2004)

**Table S3**. Estimation of BC mass in regions of the GoM using detailed (every 10 m) bathymetric data collected by Incze and Jakobbson, (2008) from http://pubs.usgs.gov/.

| Region[1] | Name | Surface Area ($km^2$) | Total Vol ($km^3$) | $z_{mix}$ | Surface Vol ($km^3$) | Deep Vol ($km^3$) | Surface [BC] (μg/L) | deep [BC] (μg/L) | Total BC (Gg) | Surface BC (Gg) | Deep BC (Gg) | Export[1] area ($km^2$) | Export[2] ($g/m^2 \cdot yr$) | Total Export (Gg/yr) |
|---|---|---|---|---|---|---|---|---|---|---|---|---|---|---|
| 2 | Browns Bank | 1,780 | 160 | 50 | 106 | 54 | 3.64 | 0.63 | 0.4 | 0.4 | 0.0 | 1,743 | 0.1 | 0.17 |
| 3 | Eastern Coastal Shelf | 13,794 | 1,165 | 50 | 712 | 453 | 1.1 | 0.14 | 0.8 | 0.8 | 0.1 | 10,628 | 0.7 | 7.0 |
| 5 | Northern Coastal Shelf | 19,311 | 1,435 | 20 | 517 | 918 | 3.79 | 5.66 | 7.2 | 2 | 5.2 | 16,541 | 9.8 | 160 |
| 6 | Southern Costal Shelf | 8,239 | 466 | 20 | 221 | 246 | 6.45 | 1.68 | 1.8 | 1.4 | 0.4 | 7,133 | 12 | 82 |
| 7 | Great South Channel | 5,202 | 511 | 40 | 260 | 251 | 6.68 | 0.57 | 1.9 | 1.7 | 0.1 | 5,200 | 0.2 | 0.78 |
| 8 | Georges Bank | 38,471 | 2,846 | 40 | 2,109 | 737 | 4.24 | 2.09 | 10 | 9 | 1.5 | 30,017 | 0.2 | 6.8 |
| 9 | Georges Basin | 4,104 | 1,224 | 50 | 246 | 978 | 4.24 | 2.09 | 3.2 | 1.1 | 2.1 | 4,104 | 0.3 | 1.2 |
| 10 | Jordan Basin | 6,696 | 1,494 | 50 | 402 | 1,092 | 3.64 | 0.06 | 1.5 | 1.5 | 0.1 | 6,696 | 6.1 | 41 |
| 11 | Wilkinson Basin | 7,076 | 1,623 | 60 | 495 | 1,128 | 1.22 | 0.4 | 1 | 0.6 | 0.4 | 7,076 | 0.1 | 1.0 |
| 12 | Central Gulf of Maine | 44,799 | 8,127 | 40 | 2,236 | 5,891 | 3.22 | 2.05 | 21 | 9 | 12 | 44660 | 0.9 | 42 |
| Total | | 149,100 | 18,940 | | 9,500 | 15,000 | | | 49 | 27 | 22 | | | 342 |

[1]See Appendix IV for description of region and detailed bathymetric data.

**Table S4**. BC inputs and outputs from water currents and river flows in the GoM.

| **Water Currents** | **Annual Total** | **μg BC/L** | **GgBC/yr** |
|---|---|---|---|
| Scotian Shelf Water | $6.3x10^{12}m^3/yr$ | 0.3 | 1.8 |
| Slope Water | $8.7x10^{12}m^3/yr$ | 0.3 | 2.5 |
| Maine Surface Water | $5.0x10^{12}m^3/yr$ | 3.7 | 19 |
| Maine Intermediate Water | $10x10^{12}m^3/yr$ | 3.7 | 37 |
| | **Rivers** | | |
| **Province/State** | **Annual Total** | **μg BC/L** | **GgBC/yr** |
| Nova Scotia[a] | $0.1x10^{10}m^3/yr$ | 10 | 0.01 |
| New Brunswick[a] | $3.4x10^{10}m^3/yr$ | 15 | 0.52 |
| Maine[b] | $3.3x10^{10}m^3/yr$ | 7 | 0.23 |
| New Hampshire[b] | $0.5x10^{10}m^3/yr$ | 4 | 0.02 |
| Massachusetts[a,b] | $0.7x10^{10}m^3/yr$ | 60 | 0.45 |
| **Total rivers** | **$8.0x10^{10}m^3/yr$** | | **1.22** |

[a]BC concentrations estimated from measured concentrations; [b]Concentrations estimated from measured concentrations and two end member salinity mass balance

**Table S5.** Stable and radiocarbon isotope signatures of seawater samples in the GoM.

| Sample | OC | | BC | |
|---|---|---|---|---|
| | $\delta^{13}C$ | $\Delta^{14}C$ | $\delta^{13}C$ | $\Delta^{14}C$ |
| Aug/Sep IPB-3 | -21.73 | 18 | -21.59 | -91 |
| Aug/Sep MWRA-20 | -27.70 | -147 | -45.44 | -842 |
| Aug/Sep WB-10 | -22.27 | 34 | -24.49 | -60 |
| Aug/Sep WB-80 | -28.81 | -205 | -48.22 | -889 |
| April GB-8 | -26.00 | -132 | -25.00 | -175 |

**Table S6**. Possible sources of stable and radiocarbon isotopes in natural environments.

| | Possible sources | |
|---|---|---|
| Source | $d^{13}C$ | $\Delta^{14}C$ |
| Graphitic BC | -19.4 to -21.3[a] | -895 to -989[a] |
| Marine plankton | -18 to -23[a] | 0 to -100[a] |
| C4 grasses | -12 to -16[a] | |
| C3 terrestrial | -23.5 to -27.7[a] | -9 to -240[a] |
| Fossil fuel | | -1000[b] |
| Biomass burning | | >-50[b] |
| Pure marine | -19 to -21[b] | |
| BC samples | -23.9 and 18.6[b] | |
| Oceanic DOC | -20 to -22[b] | |
| Pine wood | -19.5[c] | |
| Oak wood | -25[c] | |
| SRM 1650 | -27[c] | |
| Natural gas | -27 to -44 | |

[a]Dickens et al. (2004); [b]Masiello and Druffel (2003); [c]Currie (2000); [d]Prinzhofer et al. (2000).

**References**

Bond, T.I., Streets, D.G., Yarber, K.F., Nelson, S.M., Woo, J., Klimont, Z., 2004. A technology-based global inventory of black and organic carbon emissions from combustion. J. Geophys. Res. 109, D14203.

Dickens, A.F., Gelinas, Y., Masiello, C.A., Wakeham, S., Hedges, J., 2004. Reburial of fossil organic carbon in marine sediments. Nature 427, 336-339.

Incze, L., Jakobbson, M., 2008. Hypsometric characterization of the Gulf of Maine, Georges Bank, Scotian Shelf and neighboring continental slope. http://www.usm.maine.edu/gulfofmaine-census/ (accessed October, 2004).

Masiello, C.A., Druffel, E.R.M., 2003. Organic and black carbon 13C and 14C through the Santa Monica Basin sediment oxic-anoxic transition. Geophys. Res. Lett. 30, 1185.

Townsend, D.W., 1996. In The Gulf of Maine Ecosystem Dynamics; Wallace, G. T. and E. F. Braasch, Ed. Regional Association for Research on the Gulf of Maine: St. Andrews, New Brunswick.

Currie, L.A., 2000. Evolution and multidisciplinary frontiers of 14C aerosol science. Radiocarbon 42, 115-126.

Prinzhofer, A., Rocha-Mello, M., Takaki, T., 2000. Geochemical characterization of natural gas: A physical multivariable approach and its applications in maturity and migration estimates. AAPG Bulletin 84, 1152-1171.

# Inferring black carbon concentrations in coastal seawater by observing pyrene fluorescence losses

*D. Xanat Flores-Cervantes[1], Christopher M. Reddy[2], and Philip M. Gschwend[1]**

[1]R.M. Parsons Laboratory, MIT 48-413, Department of Civil and Environmental Engineering, Massachusetts Institute of Technology, Cambridge, Massachusetts 02139, USA.

[2]Department of Marine Chemistry and Geochemistry, Woods Hole Oceanographic Institution, Woods Hole, Massachusetts, 02543, USA.

xanatf@mit.edu, creddy@whoi.edu, pmgschwe@mit.edu

**Journal format**

*Corresponding author phone: (617)2531638; fax: (617)2537395; e-mail: pmgschwe@mit.edu.

**Abstract**

Black carbon (BC), the soot and char formed during incomplete combustion of fossil and biomass fuels, is ubiquitous and been implicated in diverse environmental processes and human health. However, uncertainty persists regarding how accurately the present BC-measurement methods quantify such roles. Focusing on the influence of BC on pollutant fates, we developed a new, low-sample-manipulation methodology that effectively differentiates BC from other non-BC organic carbon (OC) due to its sorbent properties. We measured BC concentrations in seawater particulate organic matter (POM), collected in a coastal area downwind of important BC sources, by observing the decrease in fluorescence from pyrene spiked into samples, referred to as the pyrene fluorescence loss (PFL) method. Sorption isotherms obtained with this PFL approach were non-linear. Average BC concentrations of 4 μg BC/L were able to explain such observations. Correspondence between measured concentrations using the PFL method and an extensively evaluated thermal oxidation approach (CTO-375) validated the usage of this technique to measure BC. Such BC levels indicate that pollutants such as polycyclic aromatic hydrocarbons (PAHs) and polychlorinated dibenzodioxins (PCDDs) would be mainly sorbed to BC-containing solid particles, and therefore less bioavailable.

## Introduction

Research on black carbon (BC), a term given to a range of thermally altered carbonaceous materials produced by the incomplete combustion of fossil fuels and biomass, is diversifying as new observations suggest that BC has potential implications to human health (1,2), climate change (3,4), global carbon cycling (5), and pollutant fates (6). This diversification has resulted in a wide variety of analytical methodologies, terminologies, and conceptual approaches, with various scientific communities interested in different characteristics. For example, most atmospheric scientists are interested in the "blackness" of aerosols and the resultant effect on the radiative heat balance (3, 7), while oceanographers and geologists are interested in the refractory properties of BC in soils and sediments influencing its role in carbon cycling.

Concurrently, environmental engineers are investigating the impact of BC on contaminant mobility and bioavailability. Studies since the late 1970s and early 1980s have suggested that sorption into organic matter is a key process controlling the fate and effects of hydrophobic organic pollutants in the environment (8, 9), and this process could be described using a linear sorption model:

$$K_d = f_{TOC} K_{TOC} \qquad (1)$$

where $K_d$ is the solid-water distribution coefficient ($L/kg_{solid}$), and is characterized by the product of the total organic carbon (TOC) fraction ($f_{TOC}$, $kg_{TOC}/kg_{sediment}$) and the TOC-normalized distribution coefficient ($K_{TOC}$, $L/kg_{oc}$). However, in many previous observations polycyclic aromatic hydrocarbons (PAHs) sorbed more strongly to sediments than predicted using this model (10-12). Recent studies (e.g. 13,14) refined this view by modeling sorption of PAHs and polychlorinated dibenzodioxins (PCDDs), especially at low concentrations, using (1) an

*absorption* term that is the product of the TOC fraction minus its BC contents ($f_{OC}$, $kg_{OC}/kg_{sediment}$, where OC=TOC - BC) and the OC-normalized distribution coefficient ($K_{OC}$, $L/kg_{OC}$); and (2) an *adsorption* term that is the product of the BC fraction ($f_{BC}$, $kg_{BC}/kg_{sediment}$), the BC-normalized distribution coefficient ($K_{BC}$, $(\mu g/kg_{BC})/(\mu g/L)^n$), and a function of $C_w$, the truly dissolved concentration (μg/L) to the (*n-1*) power, where *n* is the Freundlich exponent that describes the adsorption site distribution:

$$K_d = f_{OC}K_{OC} + f_{BC}K_{BC}C_w^{n-1} \qquad (2)$$

Unfortunately, none of the existing methodologies to measure BC specifically quantify this carbonaceous material with respect to its sorbent character.

The main objective of this work was to test a new method for measuring BC in environmental samples suited to accurately quantifying this phase as a sorbent. To this end, we sought to quantify pyrene fluorescence losses (PFL) in pyrene-spiked samples to which materials potentially containing BC sorbents were added. We made the assumption that pyrene would sorb in a manner as previously described by Accardi-Dey and Gschwend ((14), Eq. 2 with $K_{OC} = 10^{4.7}$ and $K_{BC} = 10^{6.25}$), and together with measures of the TOC (OC + BC), used this model to infer BC content in seawater, sediment, and a group of reference materials previously used in BC literature (15). The values we determined using this simple, inexpensive, and low-sample-manipulation method demonstrated the importance of considering a BC sorbent phase for estimating the fates of contaminants like PAHs and PCDDs.

**Methods**

**Seawater sample collection.** Different size fractions of particulate organic matter (POM) were collected during two cruises to the Gulf of Maine (GoM) (Figure 1) in April 2004 (*R/V Oceanus*) and in August/September 2004 (*R/V Cape Hatteras*). At each station, between 100 and 800 L of seawater were pumped on-board using positive-displacement gear pumps (Fultz Pump Inc., Lewis Town, NJ) from shallow (<20 m to be in the surface layer) and deeper depths (>20 m to be below the surface layer). The absolute depths at each location were guided by measurements of salinity, temperature, and fluorescence. The pumps were connected to a 142-mm diameter filter holder with a 53-μm mesh pre-cleaned Nitex screen (TETKO, Depew, NY), followed by a 293-mm stainless steel filter holder with a 0.7-μm pre-combusted GFF or quartz filter (Pall Gellman Sciences, Ann Arbor, MI). To remove inorganic carbon after collection and while still in the filter holder, all the samples were acidified with 100 mL of 10 mM $H_2SO_3$ for 5 min followed by a 100 mL rinse of low-carbon water (Aries Vaporics, Rockland, MA). Sample blanks were collected throughout the sampling procedure and consisted of "wetting" the filtration devices by pumping only 1 L of seawater from the sampling station. All collected samples were kept frozen in pre-combusted aluminum envelopes until analysis. The POM fraction analyzed in this BC study was the one collected on the GFF/quartz filter; i.e., 0.7 μm < POM < 53 μm.

**South Dorchester Bay (SDB) sediment sample collection.** Grab samples of surface sediments (about 12 cm deep) were previously collected by A. M. Accardi-Dey and J. K. MacFarlane (Gschwend lab, MIT) from a littoral site in Boston Harbor, at south Dorchester Bay (SDB) near Quincy, MA (42° 18.0' N 71° 1.8' W) in December 1999. The samples were kept in zip-lock bags and stored at 4 °C in dark. BC concentrations in this sample have been previously measured (14) using the chemothermal oxidation method (CTO 375; (6)).

**Reference materials.** Twelve reference materials, previously utilized in an international BC-method intercomparison study (15), were also examined with our new method. This suite of samples provides materials with varying amounts of BC and characteristics including: (1) four laboratory produced BC-rich and non-BC materials (hexane soot, wood char, grass char, and melanoidin), and (2) eight environmental matrices (Suwannee River dissolved organic matter (DOM), shale, lignite coal, bituminous coal, urban dust, German soil, Australian soil, and marine sediments).

**TOC quantification.** Single samples of the POM collected from seawater (0.7 μm < POM < 53 μm) and triplicate subsamples of the sediment and reference materials were weighed dry, acidified with 0.6 % by volume sulfurous acid ($H_2SO_3$), and dried overnight at 60 °C. TOCs of the dry samples were measured using a commercial CHN analyzer (Vario EL, Elementar Americas, Inc., NJ) at a combustion temperature of 950 °C. Daily response factors were determined using acetanilide standards (Elemental Microanalysis, Manchester, MA), and the detection limit of the analyzer was 0.6 μg of C. Response factors for all elements remained stable throughout the experiment (± 0.5 % for nitrogen, ± 0.07 % for carbon, and ± 0.6 % for hydrogen). Instrument blanks (no sample introduced in CHN analyzer) were run after every sample to verify that the previous sample combustion was complete, and at least two sample preparation blanks were included every three samples. Blanks were subtracted from raw sample data.

**BC quantification using pyrene fluorescence losses.** BC content was inferred by observing the decrease in fluorescence from a pyrene solution. Known masses of dry samples (between 12 and 16 mg of the dried GFF or quartz filters or about 5 mg of the SDB sediment and reference materials) were introduced into 25-mL, precombusted, volumetric flasks containing an aqueous

solution of pyrene at about 1 μg/L, and a sodium azide ($NaN_3$) concentration of 10 mM made up in low carbon water (Aries Vaporic System, Rockland, MA). Procedural blanks consisted of processing our sample blanks (1 L of seawater) collected during our sampling campaigns in the same manner as our samples. Each batch of observations included a pyrene-spiked control flask without a sample (or filter) and a control flask with only water, $NaN_3$, and the sample (no pyrene spike). All flasks were closed with glass stoppers, completely covered with aluminum foil, and placed in a wrist-action shaker to encourage sorptive equilibration. A preliminary kinetics experiment using a piece of the filter from our Jordan Basin surface sample showed that dissolved pyrene concentrations in the flasks continued to change up to 15 d. However, no changes were detectable after 22 d. In order to ensure equilibrium, we ran our experiments for 30 d. To test for method precision, we examined triplicates and estimated BC concentrations at three or more concentrations for some of our POM samples collected in April 2004.

The choice of pyrene as the chemical probe for our analysis was based on observations by Rudnick and collaborators (16, 17), previous work in our research group (14, 18. 19), and our own experience in the lab. Rudnick (16) examined four of the most soluble PAHs on the priority pollutant list, expecting these PAHs to be the ones found in the greatest amounts in seawater environments: pyrene, fluoranthene, anthracene, and phenanthrene. However, he found out that the spectral signature of fluoranthene could not be distinguished from that of terrestrial humic substances; anthracene presented a lower relative fluorescence than the absorbencies would indicate; and phenanthrene had a very low molar absorbancy and was not reliably detected at reasonable environmental levels. Previous studies in our research group have used pyrene as a probe for aqueous sorption studies due to its relatively high solubility in water, its high solid-to-water partitioning constant, and especially due to its uniquely long fluorescence lifetime (14, 18,

19). Finally, our own experimentation with another aromatic compound, *p*-terphenyl, showed that its fluorescence peaks were less sharp and, especially at lower concentrations, more difficult to differentiate from background signals.

To measure dissolved pyrene concentrations, a Perkin-Elmer KS50B Luminescence Spectrofluorometer (Buckinghamshire, England) was used. Aliquots of the solutions were transferred to a Sterna quartz cell (1 cm path length, Atascadero, CA) for fluorescence analysis using a synchronous scan with a ΔEnergy of -3000 $cm^{-1}$, excitation and emission slits of 5.0 nm, and a scan speed of 100 nm/min. These parameters, although different from the ones used by Accardi-Dey and Gschwend (14), provided the sharpest peak at the lowest concentrations used in this study. At the beginning of every sample run, the spectrofluorometer lamp was allowed to warm up for about 30 min and a set of calibration standards between 0.5 and 3.0 $\mu g_{pyr}/L$, as well as water without pyrene, was used to check for any shifts in the calibration curve created at the beginning of the experiment. After sample analysis, aliquots were returned to their original flasks. Background fluorescence signals were subtracted from the pyrene signals for each sample. With these parameters the detection limit was 0.20 μg pyrene/L (signal-to-noise ratio 2:1).

Ambient pyrene concentrations are usually well below μg/L levels. For example, Rudnick et al. (17) observed dissolved pyrene concentrations at 100 ng/L or less in Boston Harbor seawater. Thus, to increase our signal-to-noise ratio, decrease the instrumental error (<4%), and decrease the influence of the Freundlich exponent on the truly dissolved water function ($C_w^{n-1}$), we spiked our samples with concentrations in the vicinity of 1 μg pyrene/L (i.e., $1^{n-1} \sim 1$, independent of the value of $n$).

To test the accuracy of our observations below 0.5 μg/L, we compared our measured concentrations with those found on the same samples using time-gated laser induced fluorescence spectroscopy (TGLIF, 16-18). TGLIF triggers a time-gated mechanism that allows the system to filter out short-lived fluorescence signals from fluorophores other than pyrene, by imposing a time delay for the detection of the emitted photons (18 and references therein). The concentrations using both instruments were highly consistent (TGLIF = (0.90 ± 0.07) Specfluo + (0.01 ± 0.02); $r^2$=0.97; $n$ = 15) and indicated that other chromophores (if present) were usually not substantially affecting our fluorescence signal. Some exemptions required us to make inner filter effect corrections, and these are discussed below.

The fraction of the dissolved pyrene remaining in the water ($f_w = C_{wf}/C_{wi}$; where $C_{wi}$ was the initial pyrene concentration at day zero and $C_{wf}$ is the final pyrene concentration at day thirty) together with the solid-to-water ratio ($r_{sw}$ = weight of filter with sample/volume of solution in flask ($kg_{filter}/L$)), allowed us to estimate the distribution coefficient, $K_d$ (eq.3), in each incubation.

$$K_d = \frac{(1 - f_w)}{f_w r_{sw}} \qquad (3)$$

**Sorption isotherms.** Sorption isotherms were developed for the seawater POM samples and the SDB sediment. For the seawater POM samples from five of the stations sampled during April 2004, GFF/quartz filters (about 12 mg) were added to solutions with a range of initial pyrene concentrations (0.2–2.5 μg/L). Similarly, for SDB sediments, known masses (about 7 mg) were added to the same range of initial pyrene concentrations (0.2–2.5 μg/L). After 30 d, dissolved pyrene concentrations were measured in aliquots of the solutions, and sorbed concentrations were estimated by subtracting the final dissolved concentration from the initial dissolved concentrations.

**South Dorchester Bay (SDB) sediment BC quantification using the chemo-thermal oxidation (at 375 °C) method (CTO 375).** Following a similar procedure to the one described by Gustafsson et al. (6), triplicate subsamples of dry and ground SDB sediment were placed into pre-tared, crucible-shaped, Ag capsules (D2029 8 x 5 mm; Elemental Microanalysis Limited, EMAL Tech, Ohio). The samples were then combusted in a F47915 Thermolyne muffle furnace (Barnstead Thermolyne International, Dubuque, IA) at 375 °C for 24 h under excess air. After cooling, 25 μL of low carbon (Aries Vaporics, Rockland, Massachusetts) water were added to each capsule, followed by 25 μL of $H_2SO_3$ 6 % by vol. (Fisher Chemicals). The samples were allowed to sit at room temperature for 1 h and then they were dried in an oven at 60 °C. This procedure was repeated until no effervescence was observed after acid addition. Finally, the samples were dried overnight at 60 °C (~ 15 h). The remaining reduced carbon contents in the oxidized and acidified samples were determined using a commercial CHN analyzer (Vario EL, Elementar America, Inc., NJ) as described previously.

## Results and Discussion

**Inferred $K_d$ values for pyrene sorption to GoM seawater POM.** Observed $K_d$ values of our seawater POM samples almost always exceeded $f_{OC}K_{OC}$ estimates (Figure 2), suggesting that absorption to TOC on the filters was not the only sorption mechanism. Please note that here and for the rest of this paper we refer to OC as the difference, TOC – BC. Dissolved concentration decreases for pyrene in the flasks containing the seawater POM samples were between 10 and 40%, while the losses of pyrene in the control flasks were always less than 5% in the first 30 d. Differences in concentrations measured after 6 mo for two of the April cruise

samples (MWRA and GSC), as well as for two control flasks, remained below 10%. Losses from procedural blanks were always less than 7% with the exception of one of the GoM stations in April (at the Massachusetts Water Reservoir Authority, MWRA, outfall site, Figure 1) where the procedural blank loss was 12%. The relative standard deviation for the measured TOC values of nine subsamples from a single filter of our POM seawater samples (April-JB-shallow) from the center to the rim was 8.8%, with the piece closest to the rim accounting for 23 % of this standard deviation (Figure S1). Most of the pieces taken for our experiments were taken from the center of the filter, where our own observation and pictures from our samples (Figure S2 (a)) revealed that the filters appeared to be homogenously covered. However, it is important to mention that in five our samples (April-shallow-MER April-shallow-CB, April-deep-IPB, August-shallow-CB, and August-shallow-IPB), our filters had lighter patches at the middle of the filter (Figure S2 (b)), and, therefore, the BC concentrations at these stations may be mis-estimated by filter subsampling.

**GoM sorption isotherms.** All pyrene sorption isotherms showed a non-linear behavior, indicating the presence of an *ad*sorptive material with decreasing sorption strength at higher sorbate concentrations (Figure 3). Freundlich exponents, *n*, obtained from the linear regressions of log $K_d$ against log $C_{iw}$ (Figure S3) were 0.72 ± 0.14. Since the $K_d$ values exceed the product, $f_{OC}K_{OC}$, by so much in many of these cases (i.e., $C_s = f_{OC}K_{OC}C_w + f_{BC}K_{BC}C_w^n \sim f_{BC}K_{BC}C_w^n$), this best-fit Freundlich parameter may be close to, although a little larger than, the value reflecting just the adsorptive phase. $K_{BC}$s (more than an order of magnitude larger than $K_{OC}$) obtained from the linear regression of $C_{is}$ against $C_{iw}$ (at $C_{iw}$ = 1 μg/L) further corroborated this high-sorptive non-linear scenario (Figure 3). Moreover, these *n* and $K_{BC}$ values were similar to those reported previously (13,14,19). Variability, within our samples and between this and previous studies,

may be due to experimental error, and/or differences between the isolated materials due to their formation process (e.g., soot vs char) or surface transformations during transport.

**Testing of the Pyrene-Fluorescence-Loss (PFL) Method for Quantifying $f_{BC}$.** As a first test of the method, we utilized SDB sediment, which has previously been examined for its ability to sorb pyrene and its TOC and BC contents (14). Estimating $f_{BC}$ from the isotherm data required an iterative process. As a first approximation, $f_{OC}$ ($f_{OC1}$) of a sample was assumed to be equal to the measured TOC concentrations and introduced in eq. 2. Using values of $K_{oc}$ ($10^{4.7}$, (20)), $K_{BC}$ ($10^{6.25}$, (14)), and $K_d$ at $C_{pyw}$ = 1 μg/L ($K_{d1\mu g/L}$; from the intercepts in Figure 3, i.e., $K_d = 10^{intercept}/C_{pyw}$), we were then able to obtain a first estimate of $f_{BC}$ ($f_{BC1}$):

$$f_{BC1} = \frac{\left[K_{d1\mu g/L} - (f_{OC1}) \cdot (10^{4.7})\right]}{10^{6.25}} \qquad (4)$$

For the second iteration, $f_{OC2}$ was calculated from $f_{OC1}$-$f_{BC1}$. The process was repeated until $f_{BC}$ did not change, usually within three iterations. Using this approach on the SDB sediment, we found $f_{BC} = 0.0016 \pm 0.0005$ and $f_{OC} = 0.0104 \pm 0.0014$. If we had assumed $K_{BC}$ was $10^{6.4}$ (19), we would have estimated $f_{BC} = 0.0011$, while if we had taken $K_{OC}$ to be $10^{4.8}$, we would have calculated $f_{BC}$ to be 0.0015. All of these outcomes are reasonably close to our CTO 375-measured $f_{OC}$ and $f_{BC}$ values ($0.012 \pm 0.001$ and $0.0007 \pm 0.0001$, respectively), and those reported previously by Accardi-Dey and Gschwend (14) for this site ($f_{OC} = 0.0146 \pm 0.0013$ and $f_{BC} = 0.0026 \pm 0.0007$). Differences in the measured BC could be due to heterogeneity of the sample (roots and darker patches were visible in the grab sample) or methodology variations (we used smaller sample sizes to avoid charring).

As a second test of this pyrene-fluorescence-loss method, we used a standards addition approach. Increasing amounts of SDB sediment were added to different flasks, each containing the same initial pyrene concentrations of about 1 μg/L and shallow seawater POM collected on a piece of GFF filter (at the Jordan Basin (JB)). For each SDB addition to the test flask containing our GoM filter sample, we observed an increasing loss of pyrene fluorescence after the 1-month incubation. The results (Figure 4) showed that the PFL method tracked the added BC increments (slope = 1.09 ± 0.16 $\mu g_{BC}$/mg sediment added) and that interfering matrix effects were minimal for all but the greatest addition. The increased interfering matrix effects at larger concentration may indicate the presence of a non-particulate-OC material (e.g., dissolved organic carbon) present in high enough amounts to quench pyrene fluorescence (21, 22). Moreover, without considering the last increment (where matrix effects might have interfered with the signal), the intercept (1.66 ± 0.76) indicates an $f_{BC}$ of 0.00018 ± 0.00006 (average filter mass = 10.4 ± 1.4 mg), or a particulate BC concentration in seawater of 4.1 ± 2.0 $\mu g_{BC}$/L for this Jordan Basin station. This result is very close to the CTO 375 values (4.5± 1.8 $\mu g_{BC}$/L) previously reported by Flores-Cervantes et al (23). The standards addition approach also showed that for SDB sediment differences between the expected BC content measured with CTO 375 and the inferred BC content from pyrene fluorescence losses at low concentrations were minimal.

**Application of the PFL method to GoM POM samples.** Utilizing the PFL method on our POM seawater samples collected from the GoM, we found that BC concentrations for the 0.7 μm < POM < 53 μm fractions in April and August ranged from <0.01 to 17 μg/L (Table 1). These estimated BC concentrations indicate that between 0.5 and 8.9 % of the POM organic carbon was BC, and that the percentage of BC in POM increases with depth. All but one of the deep samples collected in August 2004 had higher percentages than the shallow samples (Table 1). This

observation is consistent with the expectation that BC is more recalcitrant than non-BC TOC, and therefore, the percentage of BC-to-TOC should increase as organic carbon is remineralized while it travels deeper through the water column and into the sediment bed.

BC values deduced with PFL were generally higher in April and closer to shore (Massachusetts Water Reservoir Authority, MWRA; Inner Penobscot Bay, IPB; Casco Bay, CB; Cape Cod Bay, CCB) than in August/September and at distant from shore locations (Wilkinson Basin , WB; East Plats Bay, EPB; Jordan Basin, JB; Georges Bank, GB; and Great South Channel, GSC) (Table 1). Van Dingenen et al. (24) also reported decreasing atmospheric concentrations of BC with distance from shore in the same coastal ocean and the North Atlantic. Since atmospheric wet and dry depositions largely depend on concentration and particle size (25), our observations suggest that atmospheric deposition is an important removal mechanism for BC in the GoM, and that higher BC concentrations closer to shore consist of both smaller (nm to μm) and larger (μm to mm) size airborne particles, while lower concentrations further away from shore will consist mainly of smaller (nm to μm) BC containing particles. The observed differences between BC concentrations in April and August/September might reflect both variations in atmospheric BC concentrations and also variations in the type of fuel and technology used in this area. Liquid or gas fuel (e.g., fuel used for heating during the winter and early spring) burn at higher temperatures and produce more soot-like materials (μm to nm size particles) with higher sorptive properties than char-like materials (mm to μm size particles) produced from solid fuels (e.g., wood combustion from forest fires during the summer and early fall) at lower temperatures (26,27). Higher concentrations observed during April might indicate higher amounts of a sooty BC in our samples during that time of the year than in August/September.

Comparison between BC concentrations estimated using PFL and those reported by Flores-Cervantes et al. (23) for the same samples using CTO 375 (between <0.3 and 16 μg/L) indicated that, although within the same range of values (Figure 5a), PFL generally estimated higher BC values than CTO 375 for samples closer to the shore and lower for samples further away from shore. Consistent with our previous discussion, these observations suggest that BC values closer to shore included both soot-like (CTO-resistant) and char-like (CTO-labile) material. For our PLF-estimated BC calculations, we assumed $K_{BC}$ to be $10^{6.25}$, since this partitioning constant was derived by Accardi-Dey and Gschwend (14) for coastal sediment samples collected within the GoM. However, higher CTO 375-estimated BC concentrations further away from shore may indicate that the overall $K_{BC}$ of the isolated material (that includes both char- and soot-like BC) was different from the one estimated using only the soot-like BC ($10^{6.25}$ (14)), leading to a PFL-BC underestimation. Exemptions to these observations were the August/September samples taken from the Merrimack River (MER) at both depths, and the shallow Inner Penobscot Bay (IPB) and Massachusetts Water Reservoir Authority (MWRA) samples, where, although close to shore, our PFL-estimated BC concentrations were lower than the ones reported using CTO 375 (23). These observations may indicate that the sources of the collected material included an important proportion of distant (soot-like) sources (e.g., Boston, MA, Portland, ME, or large plumes of forest fires from Alaska observed during June-September 2004 (28)), or that local soot-like BC sources (e.g. near shore boat exhaust) were present.

**Comparison of the PFL method with CTO-375 measures of BC.** To examine biases of our PFL method, we compared our PFL-inferred BC concentrations with previously reported BC values measured using CTO 375 for twelve standard reference materials (15, Figure 5b). In the case of melanoidin and DOM, due to high concentrations of other shorter-lived fluorophores,

we used TGLIF (16-17) to confirm that fluorescence background signals were not adding to our pyrene signal, and we corrected for inner filter effects following the same procedure as Kuo et al. (18). The observed results suggested that our samples could be divided in three distinct groups. The first group consisted of samples for which BC concentrations were the same using both methodologies, indicating that the isolated material was both, resistant to thermal oxidation and highly sorptive. This group included soot and bituminous coal (mature coal (29)), and both of these materials are considered to be highly sorptive and resistant (15, 6, 27, 29). The second group included samples with labile, but highly sorptive BC and, thus, PFL-estimated concentrations were higher than those measured using CTO 375. Samples included in this second group included DOM, German soil, Australian soil, wood char, and grass char. As mentioned before, CTO 375 is thought to preferentially isolate soot-like BC material as opposed to char-like or more labile BC material (15, 30), and therefore, a higher PFL-estimated BC content in DOM, Australian soil, German soil, wood char, and grass char may indicate the presence of highly sorptive but labile-to-thermal-oxidation materials (for example, chars). Finally, the third group included BC that was CTO 375-resistant, but whose sorptive properties might be lower than the ones estimated on a mass basis by Accardi Dey and Gschwend (14) and, therefore, PFL-estimated BC concentrations were lower than those measured using CTO 375. This last group included shale, lignite coal (immature and more labile coal (6, 29)), urban dust, and marine sediment. All of these are environmental samples with a complex matrix that may involve a mixture of soot- and char-like material resistant to CTO 375, but whose sorptive strength could lead to an underestimation of BC using PFL if, for example, their overall $K_{BC}$ was different from $10^{6.25}$ (14; see also 15).

Melanoidin was not included in any of the groups mentioned above as BC concentrations in this material were below PFL detection limits (< 0.06 $g_{BC}/kg_{dw}$). This synthetic material was included in the international BC-method comparison study (15) to act as negative control, yet non zero BC concentrations were reported by other methods, including CTO 375 (15). PFL-estimated BC values below detection limits for melanoidin were indicative of the lack of interferences with this synthetic material, and provide confidence in our BC measurements using PFL.

By developing this method we were mainly interested in the characterization of a highly sorptive material. The thermal oxidation method mainly isolates a refractory material. The fact that the PFL method detects comparable amounts of carbon to the ones isolated using CTO 375 in our POM seawater samples suggests that the detected material is similar in both approaches, and that it has the following characteristics: (1) it is a soot-like material with planar hydrophobic surfaces (as described by Sergides et al. (33)) responsible of the enhanced sorption of hydrophobic organic pollutants; (2) it travels long distances through aeolian transport, and therefore is within the < 100 um sized particles, (3), it is refractory and resistant to natural degradation processes and thermal oxidation.

The estimated BC concentrations of about 1 to 10 $\mu g_{BC}/L$ in seawater (of average 4% of the POM TOC) have important implications for the pollutant fate or hydrophobic organic pollutants and the carbon cycling in this coastal ecosystem. First, the BC measured is a more recalcitrant form of POM that degrades at slower rates, explaining why a percentage of POM TOC is not recycled into $CO_2$ during its transport to the sediments (34). Second, these $\mu g_{BC}/L$ concentrations indicate that an important fraction of OC present in POM, that has not been molecularly characterized (35), may represent the highly-sorptive and highly-refractory material

that we were able to characterize. And finally, planar hydrophobic organic pollutants (e.g., PAHs and PCDDs) at relatively low concentrations (ng/L – μg/L) would be mainly sorbed to BC-containing POM.

In summary, we have developed a low-sample-manipulation and simple technique able to measure BC concentrations of a recalcitrant carbonaceous material with enhanced sorptive nature. Some of the disadvantages of this technique include the period of 30 d required to allow the system to come to equilibrium, and the potential artifacts present in matrices containing pyrene fluorescence quenchers. However, this method allows us to overcome some of the limitations of previous methodologies: (1) sample manipulation and transfers are kept to a minimal; (2) it is able to use a wide range of environmental samples (any sample that can be placed on a filter); and (3) it measures a material with a specific characteristic of interest for sorption studies.

**Acknowledgments**

The authors are grateful for support from NFS grants (OCE-0223441 and BES-0607136) and CONACYT and MFSF fellowships to D. X. F. We thank the captains, crews, and CTD technicians of *R/V Oceanus* and *R/V Cape Hatteras*, and J. MacFarlane, D. Plata, R. K. Nelson, and S. Silva for their help in sample collection. We also thank J. MacFarlane for providing the SDB sediment sample. Dave Kuo is gratefully acknowledged for TGLIF measurements and inspiring discussions.

## Supporting Information Available

Log $K_d$ (L/Kg) vs Log $C_{iw}$ linear regression for the estimation of Freundlich exponents, *n*, in the SI.

## Literature Cited

(1) Dockery, D. W., Pope, C. A., Xu, X. P., Spengler, J. D., Ware, J. H., Fay, M. E., Ferris, B. G., Speize, F. E., An association between air pollution and mortality in six United States cities. *N. Engl. J. Med.* **1993**, *329*, 1753-1759.

(2) Künzli, N., Kaise, R., Medina, S., Studnicka, M., Chanel, O., Filliger, P., Herrz, M., Horak Jr, F., Puybonniewux-Texier, V., Quénel, P., Schneider, J., Seethaler, R., Vergnaud, J-C., Sommer, H., Public-health impact of outdoor and traffic-related air pollution: a European assessment. *Lancet* **2000**, *356*, 795-801.

(3) Park, R. L., Jacob, D. J., Chin, M., Martin, R. V., Sources of carbonaceous aerosols over the United States and implications for natural visibility. *J. Geophys. Res.* **2003**, *108*, doi:10.1029/2002JD003190.

(4) Bond, T. I., Streets, D. G., Yarber, K. F., Nelson, S. M., Woo, J., Klimont, Z., A technology-based global inventory of black and organic carbon emissions from combustion. *J. Geophys. Res.* **2004**, *109*, D14203.

(5) Schmidt, M. W., Noack, A.G., Black Carbon in soils and sediments: analysis, distribution, implications, and current challenges. *Global Biogeochem. Cycles* **2000**, *14*, 777-793.

(6) Gustafsson, Ö., Haghsete, F., Chan, C., MacFarlane, J., Gschwend, P. M., Quantification of the dilute sedimentary soot phase: implications for PAH speciation and bioavailability. *Environ. Sci. Technol.* **1997**, *31*, 203-209.

(7) Cooke, W. F., Wilson, J. J. N., A global black carbon aerosol model. *J. Geophys. Res.* **1993**, *101*, 19.292-19.409.

(8) Chiou, C. T., Peters, L. J., Freed, V. H., A physical concept of soil-water equilibria for nonionic organic compounds. *Science* **1979**, *206*, 831-832.

(9) Karickoff, S. W., Semi-empirical estimation of sorption of hydrophobic pollutants on natural sediments and soils. *Chemosphere* **1981**, *10*, 833-846.

(10) McGroddy, S., Farrington, J. W., Sediment porewater partitioning of polycyclic aromatic hydrocarbons in three cores from Boston Harbor, Massachusetts. *Environ. Sci. Technol.* **1995**, *29*, 1542-1550.

(11) Gustafsson, Ö., Gschwend, P.M. Soot as a strong partition medium for polycyclic aromatic hydrocarbons in aquatic systems. In *Molecular Markers in Environmental Geochemistry*; Erganhouse, R. P., Ed.; ACS Symposium Series 671: American Chemical Society: Washington, D. C., 1997; pp 365-381.

(12) Jonker, M. T. O., Smedes, F., Preferential sorption of planar contaminants in sediments from Lake Ketekmeer, The Netherlands. *Environ. Sci. Technol.* **2000**, *34*, 1620-1626.

(13) Cornelissen, G., Gustafsson, Ö., Bucheli, T. D., Koelmans, A. A., and Van Noort, P. C. M., Extensive Sorption of Organic Compounds to black carbon, coal and kerogen in sediments

and soils: mechanisms and consequences for distribution, bioaccumulation, and biodegradation. *Environ. Sci. Technol.* **2005**, *39*, 6881-6895.

(14) Accardi-Dey, A., Gschwend, P. M., Assessing the combined roles of natural organic matter and black carbon as sorbants in sediments. *Environ. Sci. Technol.* **2002**, *36*, 21-29.

(15) Hammes, K., Schmidt, M. W., Curri, L. A., Ball, W. P., Nguyen, T. H., Louchouarn, P., Houel, S., Gustafsson, O., Elmquist, M., Cornelissen, G., Smernik, R. J., Skjemstad, J. O., Masiello, C. A., Comparison of black carbon quantification methods using reference materials form soil, water, sediment and the atmosphere, and implications for the global carbon cycle. *Global Biogeochem. Cycles* **2007**, *21*, doi:10.1029/2006GB002914.

(16) Rudnick, S. M., 1998. *In-situ* fluorescence of polycyclic aromatic hydrocarbons (PAH) in the marine environment. Ph. D. Thesis, University of Massachusetts, Boston, MA.

(17) Rudnick, S. M., Chen, R. F., Laser-induced fluorescence of pyrene and other polycyclic aromatic hydrocarbons (PAH) in seawater. *Talanta* **1998**, *47*, 907-919.

(18) Kuo, D. T. F., Adams, R. G., Rudnick, S. M., Chen, R. F., Gschwend, P. M., Investigating desorption of native pyrene from sediment on minute-to-month-timescales by time-gated fluorescence spectroscopy. *Environ. Sci. Technol.* **2007**, *41*, 7752-7758.

(19) Lohmann, R., MacFarlane, J. K., and Gschwend, P. M., Importance of Black Carbon to Sorption of Native PAHs, PCBs, and PCDDs in Boston and New York Harbor Sediments. *Environ. Sci. Technol.* **2005**, *39*, 141-148.

(20) Gawlik, B. M., Sotiriou, N., Feicht, E. A., Schulte-Hostede, S., and Kettrup, A., Alternatives for the determination of the soil adsorption coefficient, Koc, of non-ionic compounds-a review. *Chemosphere* **1997**, *34*, 2525-2551.

(21) MacDonald, B. C., Lvin, S. J., Patterson, H., Correction of fluorescence inner filter effects and partitioning of pyrene to dissolved organic carbon. *Anal. Chim. Acta* **1997**, *338*, 155-162.

(22) Mitra, S., Dickhut, R. M., Three-phase modeling of polycyclic aromatic hydrocarbon association with pore-water dissolved organic carbon. *Environ. Toxicol. Chem.* **1999**, *18*, 1144-1148.

(23) Flores-Cervantes, D. X., Plata, D., McFarlane, J. K., Reddy, C. M., Gschwend, P. M., Black carbon in the ocean: New insights into inputs and cycling of highly recalcitrant organic carbon. *Mar. Chem.* **2008.** To be submitted for publication.

(24) Van Dingenen, R. F., Raes, F., Jensen, N. R., Evidence for anthropogenic impact on number concentration and sulfate content of cloud-processed aerosol particles over the North Atlantic. *J. Geophys. Res.* **1995**, 100, 21,057-21,067.

(25) Seinfeld, J. H., Pandis, S. N., *Atmospheric chemistry and physics: From air pollution to climate change*; Willey-Interscience: USA, 1998.

(26) Czimczik, C. I., Preston, C. M., Schmidt, W. I., Werner, R. A., Schulze, E., Effects of charring on mass, organic carbon, and stable isotope composition of wood. *Org. Geochem.* **2002**, *33*, 1207-1223.

(27) Jonker, M. T., Koelmans A. A., Sorption of PAHs and PCBs to soot and soot-like materials in the aqueous environment: mechanistic consideration. *Environ. Sci. Technol.* **2002**, *36*, 3725-3734.

(28) Quinn, P. K., Bates, T. S., Coffman, D., Onasch, T. B., Worsnop, D., Baynard, T., de Gouw, J. A., Goldan, P. D., Kuster, W. C., Williams, E., Roberts, J. M., Lerner, B., Stohl, A., Pettersson, A., Lovejoy, E. R., 2006. Impacts of sources and aging on submicrometer aerosol properties in the marine boundary layer across the Gulf of Maine. *J. Geophys. Res.*, doi:10.1029/2006JD007582.

(29) Vorres, K., The Argonne Premium Coal Sample Program, *Energy Fuels*, **1990**, *4*, 420-426.

(30) Currie, L. A., Benner, B.A., Kessler, J. D., Klinedinst, D. B., Klouda, G.A., Marolf, J. V., Slater, J. F., Wise, S. A., Cachier, H., Cary, R., Chow, J. C., Watson, J., Druffel, E. R. M., Masiello, C. A., Eglinton, T. I., Pearson, A., Reddy, C. M., Gustafsson, Ö., Quinn, J. G., Hartmann, P. C., Hedges, J. I., Prentice, K. M., Kirchstetter, T. W., Novakow, T., Puxbaum, H., and Schmid, H. A, A critical evaluation of interlaboratory data on total, elemental, and isotopic carbon in the carbonaceous particle reference material, NIST SRM 1649a. *J. Res. Natl. Inst. Stand. Technol.* **2002**, *107*, 279-298.

(31) Gauthier, T. D., Shane, E.C., Guerin, W. F., Seitz, W. R., Grant, C. L., Fluorescence quenching method for determining equilibrium constants for polycyclic aromatic hydrocarbons binding to dissolved humic materials. *Environ. Sci. Technol.* **1986**, *20*, 1162-1166.

(32) Peuravuori, J., Binding of pyrene on lake aquatic humic matter: the role of structural descriptors. *Anal. Chim. Acta* **2001**, 429, 75-89.

(33) Sergides, C. A., Jassim, J.A., Chughtai, A.R., Smith, D.M., The structure of hexane soot. Part III: ozonation studies. *Applied Spectroscopy* **1987**, *41*, 482-492.

(34) Hedges, J. I., Keil, R. G., Sedimentary organic matter preservation: an assessment and speculative synthesis. *Mar. Chem.* **1995**, *49*, 81-115.

(35) Eglinton, T. I., and Repeta, D. J., Organic matter in the contemporary ocean. *Teatrise Geochem.* **2004**, *6*, 145-180.

## Figure Captions

**Figure 1.** Sampling stations in the Gulf of Maine (GoM).

**Figure 2.** Solid-water distribution coefficients ($K_d$) observed for pyrene sorption to particles collected from GoM seawater vs expectations from the linear model: $K_d = f_{oc}K_{oc}$.

**Figure 3.** Sorbed ($C_{pys}$) vs dissolved ($C_{pyw}$) pyrene concentrations for GoM seawater samples. SDB sediments (panel a, previously investigated by Accardi-Dey and Gschwend, (14)) were used as a control. Filled diamonds represent observations. Dashed line represents the expected $C_s$ concentrations using a linear sorption model $C_s=K_{TOC}\, f_{TOC}C_{iw}$, where $f_{TOC}$ is the measured total organic carbon (TOC) and $K_{TOC}= 10^{4.7}$ (20). $K_{BC}$ is obtained from the intercept B (log $C_{is}$= A log $C_{iw}$ + B). At $C_{iw}$ = 1 μg/L, log $C_{iw}$=0 and in B= log ($f_{oc}K_{oc}$ + $f_{bc}K_{BC}$). $f_{BC}$ values for SDB sediments and GoM seawater were those measured using CTO 375 in this study and previously reported. The standard deviation associated with $C_{iw}$ was ± 5 % and the propagated uncertainty associated with $C_{is}$ was ± 30 %.

**Figure 4.** Standard additions. BC increments (μg) by adding a certain amount of SDB sediment (mg) to a piece of filter containing filtered seawater (April-JB-shallow). Inferred BC content by observing pyrene fluorescence losses (PFL; filled diamonds) and expected BC content based on CTO 375 measurements (open squares). Dashed line represents linear increments of BC with increasing amounts of SDB sediment.

**Figure 5.** (a) BC concentrations in GoM POM seawater samples, and (b) twelve standard reference materials using CTO 375 (grey) and pyrene fluorescence loss (PFL) (white). Error bars represent propagated uncertainties according to Harris (1995). OC and CH followed by a number after the abbreviated name of the station indicate the time of collection of the sample (OC (*R/V*

*Oceanus*) for April and CH (*R/V Cape Hatteras*) for August) and the depth at which the sample was collected.

**Table Captions**

**Table 1.** TOC and BC seawater concentrations for 0.7 μm < POM < 53 μm in the GoM measured using the PFL method.

**Table 1**. TOC and BC seawater concentrations for 0.7 μm < POM < 53 μm in the GoM measured using the PFL method.

| Name Station | April | | | August/September | | | |
|---|---|---|---|---|---|---|---|
| | TOC (μg/L)[1] | BC (μg/L)[2] | %BC/TOC | TOC (μg/L)[1] | BC (μg/L)[2] | %BC/TOC | Shallow/Deep BC/TOC Ratio |
| Mass. Water Res. Authority (6m) | 233 | 13 | 5.7 | 131 | 2.4 | 1.9 | 0.4 |
| Mass. Water Res. Authority (20m) | 214 | n.m. | | 82.2 | 6.8 | 8.3 | |
| Merrimack River (6m) | 241 | 1.1 | 0.5 | 119 | 2.7 | 2.3 | 0.8 |
| Merrimack River (20m) | 234 | n.m. | | 93.8 | 3.4 | 3.6 | |
| Casco Bay (15m) | 289 | n.m. | | 133 | <0.01 | - | - |
| Casco Bay (24m) | 41 | n.m. | | 167 | 6.9 | 4.1 | |
| Wilkinson Basin (10m) | 80.4 | 7.2 | 8.9 | 61.4 | 0.46 | 0.8 | 0.4 |
| Wilkinson Basin (80m) | 49.9 | n.m. | | 14.3 | 1.2 | 8.3 | |
| East Platts Bay (10m) | 69.5 | 1.6 | 2.2 | 119 | 0.32 | 0.3 | 0.2 |
| East Platts Bay (80m) | 73.3 | n.m. | | 93.8 | 1.7 | 1.9 | |
| Inner Penobscott Bay (3m) | 280 | 17 | 6.2 | 270 | 2.2 | 0.8 | 0.5 |
| Inner Penobscott Bay (6m) | 196 | n.m. | | 185 | 4.8 | 2.6 | |
| Jordan Basin (10m) | 87.5 | 4.2 | 4.8 | 67.0 | 1.1 | 1.7 | 0.5 |
| Jordan Basin (80m) | 26.3 | n.m. | | 19.9 | 2.3 | 12 | |
| Georges Bank (10m) | 132 | n.m. | | 49.4 | 1.4 | 2.9 | 0.8 |
| Georges Bank (80m) | <3 | <0.01 | | 51.8 | 1.9 | 3.6 | |
| Great South Channer (10m) | 120 | 1.3 | 1.1 | 167 | 2.4 | 1.5 | 1.3 |
| Great South Channer (60m) | n.m. | n.m. | | 23.4 | 1.9 | 8.3 | |
| Cape Cod Bay (6m) | 176 | n.m. | | 94.8 | 2.7 | 2.8 | 0.4 |
| Cape Cod Bay (20m) | 230 | n.m. | | 85.2 | 6.9 | 8.0 | |

[1]Propagated uncertainties POC ± 0.1%; [2]Propagated uncertainties BC ± 20%; n.m.=not measured.

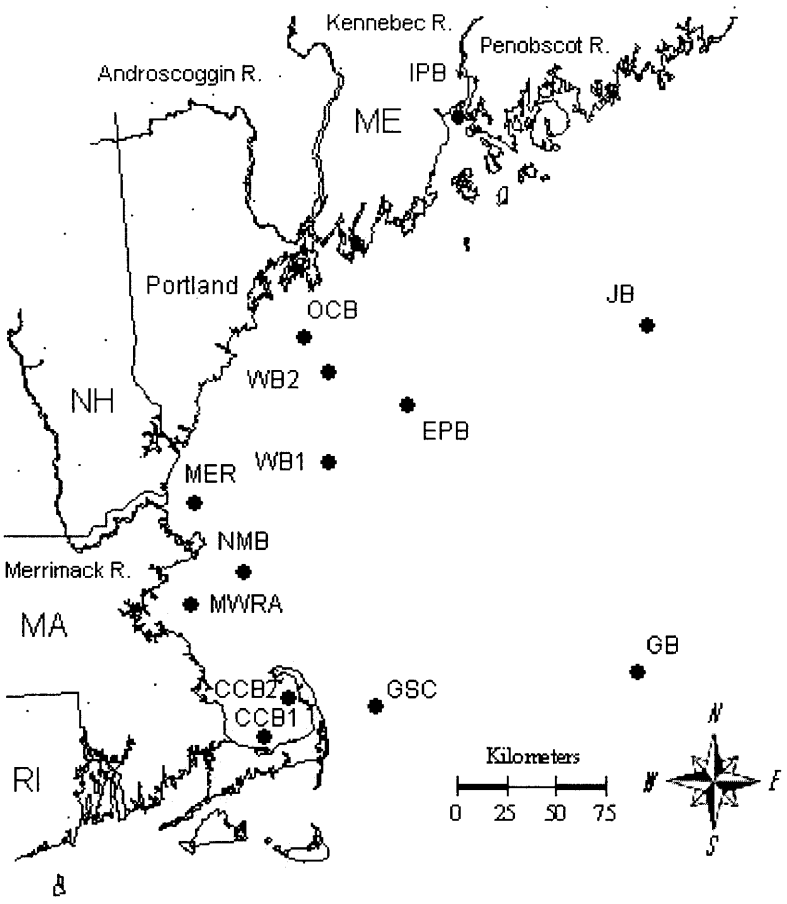


**Figure 1.** Particulate organic carbon (POC) sampling stations in the Gulf of Maine (GoM).

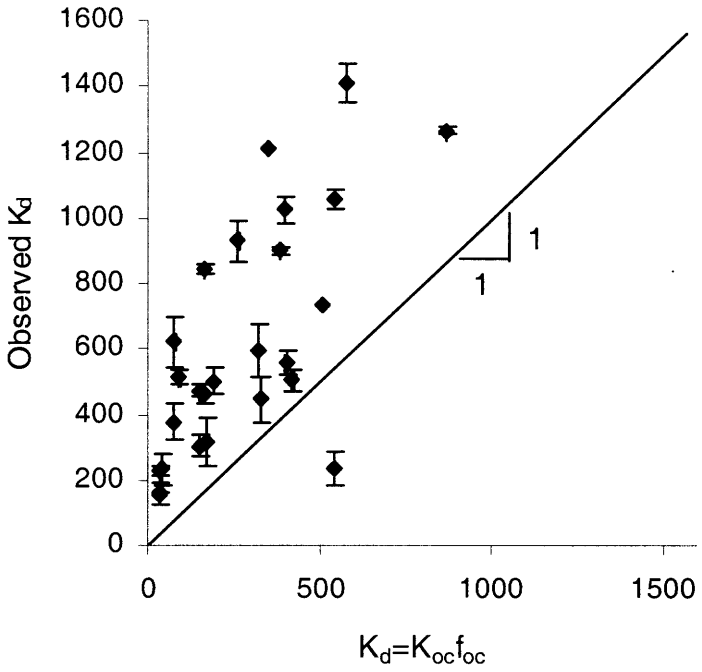


**Figure 2.** Solid-water distribution coefficients ($K_d$) observed for pyrene sorption to particles collected from GoM seawater vs expectations from the linear model: $K_d = f_{oc}K_{oc}$.

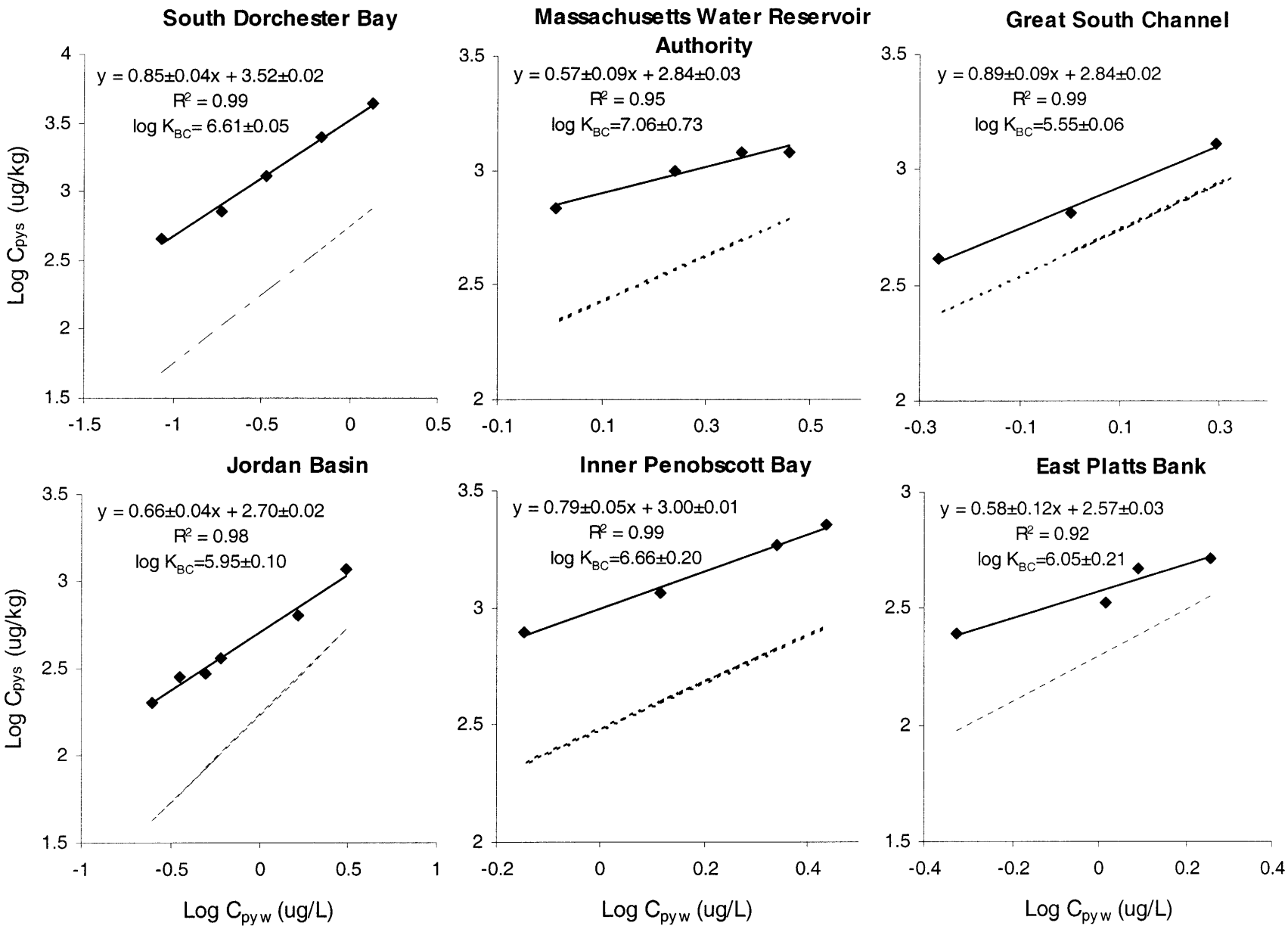
South Dorchester Bay
y = 0.85±0.04x + 3.52±0.02
R² = 0.99
log K_BC= 6.61±0.05
Massachusetts Water Reservoir Authority
y = 0.57±0.09x + 2.84±0.03
R² = 0.95
log K_BC=7.06±0.73
Great South Channel
y = 0.89±0.09x + 2.84±0.02
R² = 0.99
log K_BC=5.55±0.06
Jordan Basin
y = 0.66±0.04x + 2.70±0.02
R² = 0.98
log K_BC=5.95±0.10
Inner Penobscott Bay
y = 0.79±0.05x + 3.00±0.01
R² = 0.99
log K_BC=6.66±0.20
East Platts Bank
y = 0.58±0.12x + 2.57±0.03
R² = 0.92
log K_BC=6.05±0.21
Log C_pys (ug/kg)
Log C_pyw (ug/L)

**Figure 3.** Sorbed ($C_{pys}$) vs dissolved ($C_{pyw}$) pyrene concentrations for GoM seawater samples. SDB sediments (panel a, previously investigated by Accardi-Dey and Gschwend, (14)) were used as a control. Filled diamonds represent observations. Dashed line represents the expected $C_s$ concentrations using a linear sorption model $C_s=K_{TOC}\ f_{TOC}C_{iw}$, where $f_{TOC}$ is the measured total organic carbon (TOC) and $K_{TOC}= 10^{4.7}$ (20). $K_{BC}$ is obtained from the intercept B ($\log C_{is}= A \log C_{iw} + B$). At $C_{iw}$ = 1 μg/L, $\log C_{iw}=0$ and in $B= \log (f_{oc}K_{oc} + f_{bc}K_{BC})$. $f_{BC}$ values for SDB sediments and GoM seawater were those measured using CTO 375 in this study and previously reported. The standard deviation associated with $C_{iw}$ was ± 5 % and the propagated uncertainty associated with $C_{is}$ was ± 30 %.

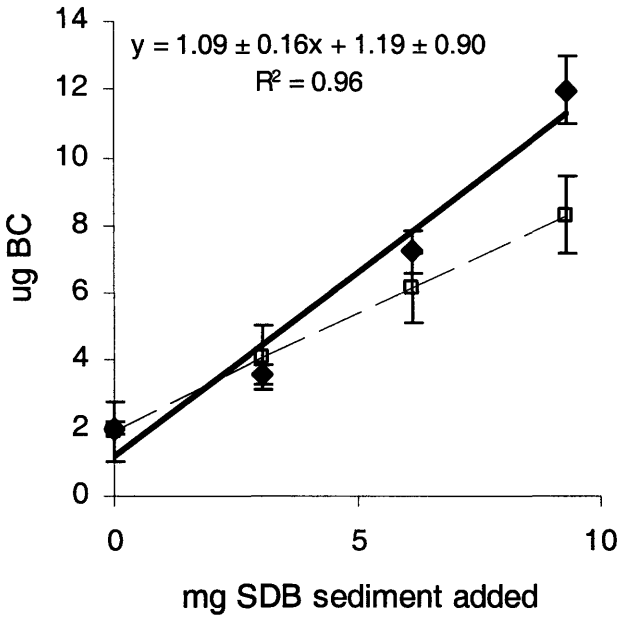


**Figure 4.** Standard additions. BC increments (μg) by adding a certain amount of SDB sediment (mg) to a piece of filter containing filtered seawater (April-JB-shallow). Inferred BC content by observing pyrene fluorescence losses (PFL; filled diamonds) and expected BC content based on CTO 375 measurements (open squares). Dashed line represents linear increments of BC with increasing amounts of SDB sediment.

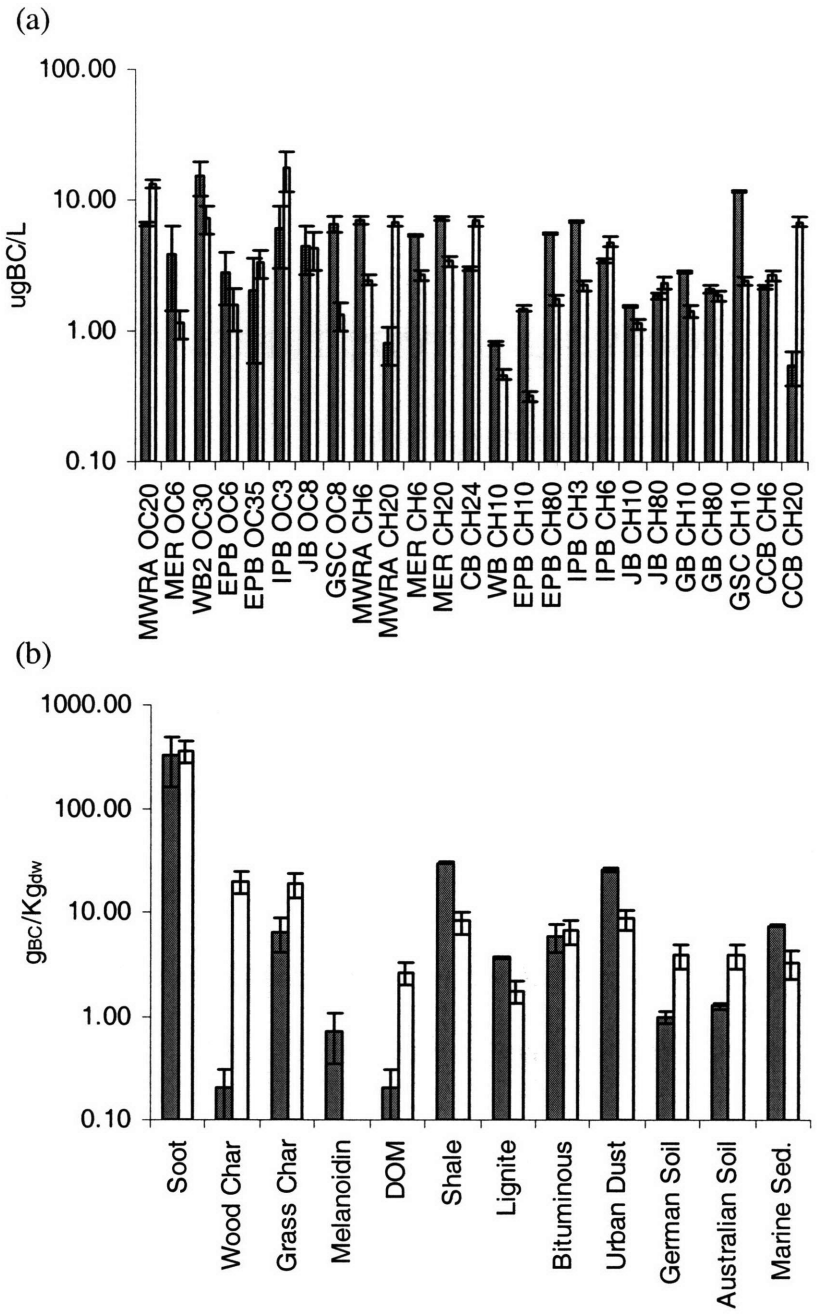


**Figure 5.** (a) BC concentrations in GoM POM seawater samples, and (b) twelve standard reference materials using CTO 375 (grey) and pyrene fluorescence loss (PFL) (white). Error bars represent propagated uncertainties according to Harris (1995). OC and CH followed by a number after the abbreviated name of the station indicate the time of collection of the sample (OC (*R/V Oceanus*) for April and CH (*R/V Cape Hatteras*) for August) and the depth at which the sample was collected.

# Supplementary Information for:

# "Inferring black carbon concentrations in coastal seawater by observing pyrene fluorescence losses"

*D. Xanat Flores-Cervantes[1], Christopher M. Reddy[2], and Philip M. Gschwend[1].*

[1]R.M. Parsons Laboratory, MIT 48-413, Department of Civil and Environmental Engineering, Massachusetts Institute of Technology, Cambridge, Massachusetts 02139, USA

[2]Department of Marine Chemistry and Geochemistry, Woods Hole Oceanographic Institution, Woods Hole, Massachusetts, 02543, USA.

xanatf@mit.edu, creddy@whoi.edu, pmgschwe@mit.edu.

This document includes:

Figure S1, S2, S3.

## Figure Captions

**Figure S1**. TOC values for our April-JB-shallow filter with increasing distance from the center.

**Figure S2**. Example of (a) an homogeneous (April-shallow-WB) and (b) a heterogeneous (April-deep-IPB) filter.

**Figure S3. Log $K_d$ (L/Kg) vs Log $C_{iw}$ for SDB sediments and GoM seawater samples.** The slope A of the linear regression (log $K_d$= A log $C_{iw}$ + B) is $n$-1. The standard deviation associated with $C_{iw}$ was ± 5 % and the propagated uncertainty associated with $K_d$ was ± 7 %.

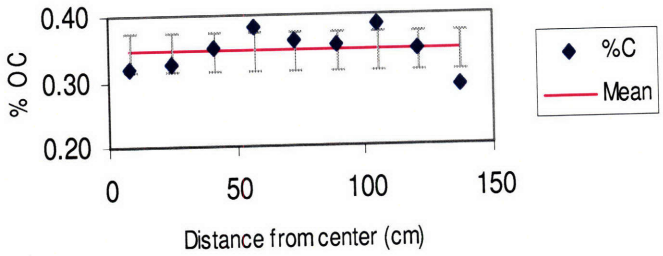


**Figure S1**. TOC values for our April-JB-shallow filter with increasing distance from the center.

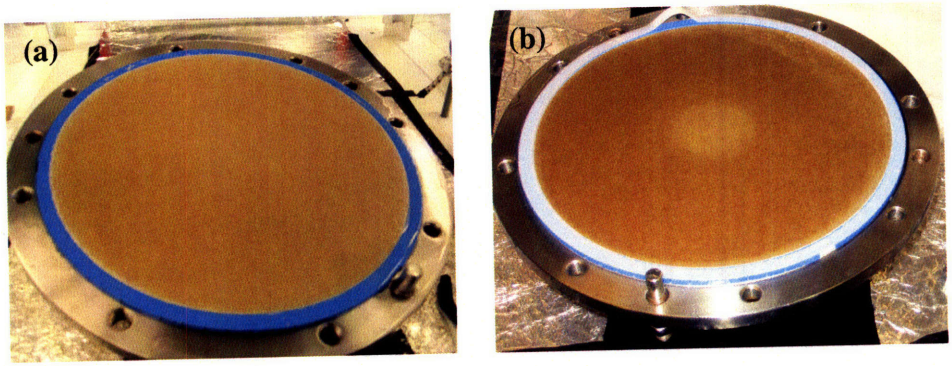


**Figure S2**. Example of (a) an homogeneous (April-shallow-WB) and (b) a heterogeneous (April-deep-IPB) filter.

**South Dorchester Bay**

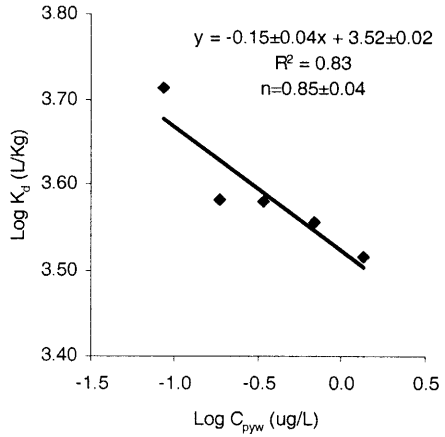


**Massachusetts Water Reservoir Authority**

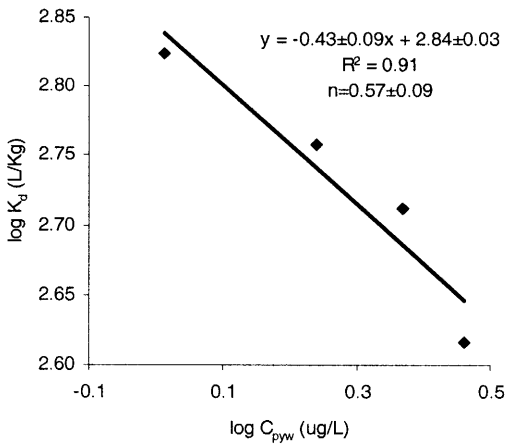


**Great South Channel**

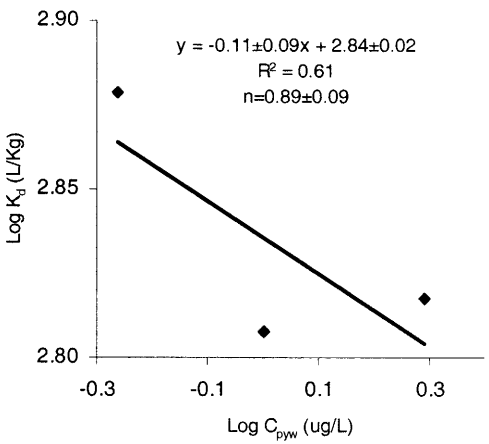


**Jordan Basin**

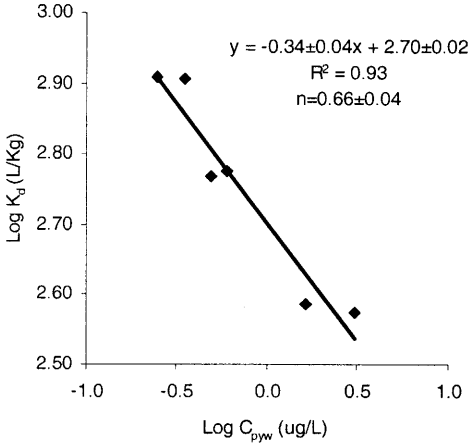


**Inner Penobscott Bay**

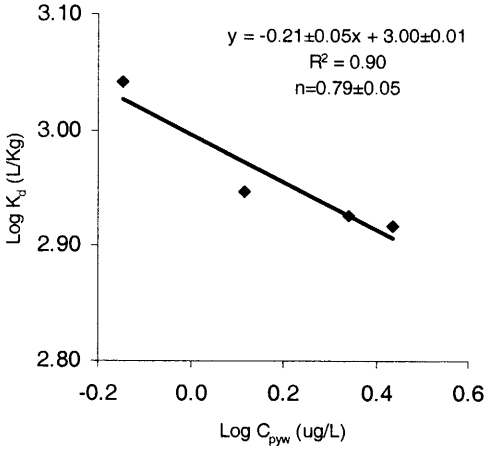


**East Platts Bank**

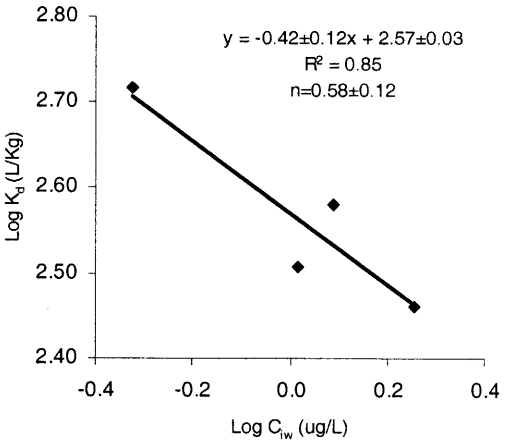

**Figure S3. Log $K_d$ (L/Kg) vs Log $C_{iw}$ for SDB sediments and GoM seawater samples.** The slope A of the linear regression (log $K_d$= A log $C_{iw}$ + B) is $n$-1. The standard deviation associated with $C_{iw}$ was ± 5 % and the propagated uncertainty associated with $K_d$ was ± 7 %.

# Spatial and temporal variations of black carbon and polycyclic aromatic hydrocarbons inputs to the Gulf of Maine in the last 100 years

D. Xanat Flores-Cervantes[1], Kristin J. Pangallo, Christopher M. Reddy[2], and Philip M. Gschwend[1*]

[1]R.M. Parsons Laboratory, MIT 48-413, Department of Civil and Environmental Engineering, Massachusetts Institute of Technology, Cambridge, Massachusetts 02139, USA

[2]Department of Marine Chemistry and Geochemistry, Woods Hole Oceanographic Institution, Woods Hole, Massachusetts, 02543

xanatf@mit.edu, ksmith@whoi.edu, creddy@whoi.edu, pmgschwe@mit.edu.

**Journal format**

*Corresponding author email pmgschwe@mit.edu, tel. +1-617-253-1638.

**Abstract**

To evaluate the effects of historic changes in fuel usage, combustion technologies, and emission regulations, sedimentation fluxes of black carbon (BC), a combustion-derived contaminant, were measured in five sediment cores from the Gulf of Maine. In addition, loadings of polycyclic aromatic hydrocarbons (PAHs), co-produced with BC, were also reconstructed for two of these cores, one close to shore and the other one further away (150 km). Both BC and PAH fluxes increased in the past 100 years, peaking at different times during the second half of the 20$^{th}$ century. Difference in BC and PAH fluxes between sampling stations indicate that these sites were influenced by changes in fossil and biomass fuels emissions, as much as by hydrographic and climatological variations in this area. Fluxes of BC and PAHs in the past 100 years were higher in sediments closer to shore (3.1 ± 1.1 g BC $m^{-2}$ $yr^{-1}$; 5.4 ± 2.8 mg ΣPAH $m^{-2}$ $yr^{-1}$) than further away from shore (0.57 ± 0.24 gBC $m^{-2}$ $yr^{-1}$; 0.30 ± 0.12 mg ΣPAH $m^{-2}$ $yr^{-1}$). Three of our cores recorded the 1947 fire disaster in Maine, while decreases in BC and PAH fluxes seen in other cores during the 1970s and the 1990s were consistent with the introduction of Clean Air Act of 1970 and the Clean Air Act Amendments in 1990. PAH source apportionment ratios suggest that combustion of a mixture of coal and biomass were the main sources of the PAHs and BC, and that atmospheric transport was the main route of transportation for these contaminants to distant areas. A decrease in BC and PAH fluxes to this area during the later part of the 20$^{th}$ century was evidence of the effects of more stringent environmental regulation, and strongly encourages the transfer of science and technology to fast-growing economies like India and China, two of the major BC producers with lower environmental standards.

## Introduction

Apart from their effects on global climate change, combustion processes account for some of the most toxic components released into the atmosphere. Black carbon (BC) and polycyclic aromatic hydrocarbons (PAHs), emitted during the incomplete combustion of fossil and biomass fuels, can negatively affect human health. BC is believed to be responsible for respiratory and cardiac hospital admissions (Dockery et al., 1993; Grigg, 2002) and about 400,000 deaths among women and children in developing countries (Smith, 2005; Pachauri, 1998), while some PAHs are known or suspected carcinogens to humans and animals (Menzie, 1992; Moore, 1995). In addition, PAHs may also bioaccumulate in shellfish and other benthic organisms (Bierman, 1990; Lohmann et al., 2004; Tracey and Hansen, 1996) consumed by humans, creating an additional exposure pathway.

To diminish these negative consequences, improvements in technology to have cleaner combustion processes and different governmental regulations have taken place. However, the local effects of these actions are in many cases unknown. While there are current estimates of atmospheric BC and PAH concentrations based on fuel consumption and fuel- and technology specific emission factors (Bond et al., 2004; Lee et al., 2005; Rogge et al., 1993), this approach is not able to address historical changes in the composition of fuel and improvements in engine and emission control technologies, fuel usage, and emission regulations. For example, measurements of air quality in the Los Angeles basin, CA, reveal decreasing concentrations of all six air pollutants regulated by the Clean Air Act (CAA) since its introduction in 1970 (Kahn, 1996; Künzli et al., 2003). However, the effect of such regulations in rural areas or off-shore sites, where air quality monitoring is not available, remains unknown.

Sediment records of BC and PAHs can provide a historical record of deposition of combustion-derived carbonaceous aerosols over the past century, a period characterized by accelerated industrialization and major changes in fuel usage and combustion technology. Sediment records in different urban lakes and coastal areas have shown good agreement between both PAHs and BC concentrations and energy consumption, improvements in combustion technologies, and air quality regulations. For example, decreases in oil consumption during the Great Depression and the Organization of Petroleum Exporting Countries (OPEC) oil embargo were captured in a sediment core collected in the Pettaquamscutt River basin, RI (Lima, et al., 2003); while sediment records of Central Park and Prospect Park Lakes in New York City recorded the shift from coal to oil and gas for space heating in the 1920s (Louchouarn et al., 2007). Similarly, sediment profiles in Europe (Elmquist et al., 2007) and the USA (Louchouarn et al., 2007) recorded decreasing BC concentrations in the second part of the $20^{th}$ due to more stringent regulations on particulate control, such as the Clean Air Act Amendments (CAAA). However, previous studies of sedimentary records have showed mixed results regarding correlations between PAH and BC fluxes into the sediments. While some researchers have shown similar trends for PAHs and BC in sediment cores (Gustafsson et al., 1997; Wakeham et al., 2004), others have reported decoupled trends between these two contaminants (Lima, 2004; Elmquist et al., 2007, Louchouarn et al., 2007). Therefore, differences between these previous studies suggest there may have been regional variability in combustion fuel and combustion conditions (i.e., temperature, oxygen, technology used), differential transport and transformations of PAHs and BC after their emission, and/or hydrographic and climatological differences between the studied depositional basins.

In this study we present reconstructed loadings of BC from five sediment cores collected in the Gulf of Maine, a coastal area located off the Northeastern coast of the United States (Figure 1). PAH loadings from two of these cores; one close to shore and another one further away from shore, are also examined. Unlike previous studies, this study was able to provide additional information regarding the influence of spatial, hydrographic, and climatological variations on combustion emissions. Furthermore, as far as we know, this is the first joint reconstruction of BC and PAH records in coastal sediments.

## Methods

### *Sediment sampling*

Sediment cores were collected using an MC-800 multicorer sediment sampler (Ocean Instruments, San Diego, CA) deployed off the end of the research vessels (with help from crew staff) from five different locations in the Gulf of Maine (GoM, Figure 1) downwind of important combustion emission sources (such as Boston, MA and New York, NY), during April (*R/V Oceanus*) and August/September (*R/V Cape Hatteras*) of 2004 (see Table 1). The multicorer was able to recover up to eight replicate samples of undisturbed surface sediments with an effective penetration of more than 45 cm. Upon retrieval, the cores were extruded after siphoning off overlying water and sliced in sections by pushing out the cores from below. The outer sediment that had been in contact with the barrel was discarded, and the remainder was placed in pre-combusted glass jars with aluminum foil-lined screw caps, and stored in chest freezers (-18 °C). With the exemption of MWRA, the cores were sliced on board into 0.5 cm sections from 0 to 2 cm, 1 cm sections from 2 to 6 cm, 2 cm sections from 6 to 10 cm; 4 cm sections from 10 to 22 cm, and 8 cm sections for the remainder of the cores. MWRA was sliced

into 0.5 cm sections from 0 to 2 cm, and 1 cm sections for the remainder of the core. Before analysis, the sediments were freeze dried and homogenized with mortar and pestle. Due to demands in sample size and to avoid contamination, different parallel cores were used for BC, PAH, and radionuclide dating.

Measurements of porosity and density were made at each station on a sister core. About 10 mg of wet sediment were weighed (WWS) on an aluminum pan, and allowed to dry overnight. The dry sediment was again weighed (WDS) and introduced into a pre-weighted 50 mL glass cylinder. Methanol was added to the cylinder and the total (methanol + sediment) weight (TW) and total volume (TV) were recorded when no more air bubbles were observed coming out from the sediment. The volume of methanol added (VM) was calculated by weigh difference of TW before and after adding the methanol. The density of the sediment was then calculated from the salt-corrected (using CTD-measured salinity at the site) WDS and the difference between the TV and VM. The volume occupied by water (VW) in the sediment was $(WWS - WDS)/\rho_{water}$, and the porosity of the sediment $\Phi$ was $VW/(VW + TV - VW)$.

*Sediment dating*

Radionuclide depth profiles were determined for $^{137}Cs$ and unsupported $^{210}Pb$ ($^{210}Pb_{xs} = {}^{210}Pb_{total} - {}^{214}Pb$). Dry sediments (5 – 20 g) were placed in plastic jars, stored for more than three weeks to allow for the in-growth of $^{214}Pb$ and analyzed by gamma spectrometry for $^{210}Pb$ (46.5 keV), $^{214}Pb$ (295.2 and 351.9 keV) and $^{137}Cs$ (661 keV) using a high-purity germanium detector (Canberra model GL2020). Relative counting efficiencies were between of 0.36 and 0.49 for $^{210}Pb$, and 1.34 and 1.60 for $^{214}Pb$, based on readings from adding Environmental Protection Agency (EPA) standard Pitch Blend Ore to our samples. These efficiencies changed depending

on the amount of sample analyzed (geometry of the sample). The $^{210}Pb$ and $^{137}Cs$ activities for every sediment sample were calculated in disintegrations and counts per minute per gram of salt-free sediment, respectively. Activities were decay-corrected to the sample collection date.

With the exemption of IPB, where disagreement between the calculated chronology and the appearance of $^{137}Cs$ was observed, sedimentation rates were determined using the constant rate of supply model (CRS; Appleby and Oldfield, 1978) with salinity-corrected density and porosity (Appendix III). To derive a more consistent chronology between sedimentation rates and $^{137}Cs$ appearance in the IPB core (using CRS, the appearance of $^{137}Cs$ was observed in 1920), IPB sedimentation rates were calculated using the constant initial concentration model (CIC), where the sedimentation rate was calculated from the slope of a straight line in a plot of ln $^{210}Pb$ vs depth of the sediment sample.

We caution the reader that although mixing in the upper layer due to bioturbation may be present in our cores, the CRS model used in our calculations neglects this effect.

*Black carbon (BC) analysis*

BC was analysed using the chemothermal oxidation at 375 °C method (CTO-375; Gustafsson et al., 1997). The CTO-375 method is particularly suited to analysis of the soot of both fossil fuel and biomass, as opposed to more labile combustion-derived charred residues (Gustafsson et al, 1997; Hammes et al.., 2007), and it has been evaluated against potential interferences from biogenic/diagenetic organic matter (Reddy et al., 2002; Hammes et al., 2007). Triplicate samples of about 5 mg of dry sediments were ground and weighed into manually shaped mortar Ag capsules placed in precombusted Petri dishes and combusted at 375 °C for 24 hr under air in a F47915 Thermolyne muffle furnace (Barnstead Thermolyne International, Dubuque, IA) to

remove labile organic carbon. The samples were then *in situ* acidified with about 200 µl of 6% by volume $H_2SO_3$ (Fisher Chemicals, Fairlawn, NJ), before being dried at 60 °C overnight. The carbon content of the remaining material was determined using a CHN analyzer (Vario EL, Elementar America, Inc., NJ), with a detection limit of 1 µg C for a signal-to-noise ratio larger than 3:1. All samples were blank corrected and variation between replicates was less than 10%.

*Polycyclic aromatic hydrocarbons (PAHs) extraction and analysis*

Dry sediment samples (~1 mg) were spiked with deuterated PAHs (acenaphthene-*d10*, phenenthrene-*d10*, pyrene-*d10*, *m*-terphenyl, chrysene-*d12*, and perylene-*d12* or benzo[*b*]fluoranthene-*d12*) and pressurized fluid extracted (Dionex ASE-200) three times with 10 % methanol in methylene chloride at 7,000 kPa at 100 °C The extracts were reduced to 1 ml aliquots under a nitrogen gas stream, and spiked with deuterated PAH injection standards (anthracene-*d10*, fluoranthene-*d10*, and benz[*a*]anthracene-*d12*) before gas chromatography-mass spectrometry (GC-MS) analysis. For quantification, the analytes were separated on a capillary column (J & W Scientific, Folsom, CA) in an HP 6890 GC connected to a JEOL GC mate MS. Samples (1 µL) were auto injected in the splitless mode with the injection port held at 280 °C, and the mass spectrometer operating in full scan mode. Recoveries for lighter PAHs (*m/z*=164, 188) were 72.5 ± 19.1%, for medium PAHs (*m/z*=212) 87.4 ± 20.0%, and 92.8 ± 18.0% for heavier PAHs (*m/z*=230-252). Procedural blanks consisted of analyzing pre-combusted Ottawa quartz sand (S23-3, Fischer Scientific, Fair Lawn, NJ) which was processed in the same manner as our sediment samples, and the sample results were blank-procedure corrected. To assess accuracy and precision, we did replicates of three of our samples in each core, and extracted and analyzed 1.0 g of NIST Standard Reference Material 1941a (Organics in

Marine Sediment; NIST SRM 1941a). Variations between replicates were less than 20%, and our measured PAH concentrations were within 21% of the certified NIST SRM 1941a values. Here we report ΣPAH as the sum of 13 out of the 16 parent PAHs on the EPA priority pollution list (fluorene, phenanthrene, anthracene, fluoranthene, pyrene, benz[*a*]anthracene, chrysene, benzo[*b*]fluoranthene, benzo[*k*]fluoranthene, benzo[*e*]pyrene, benzo[*a*]pyrene, indeno[1,2,3-*c,d*]pyrene, and dibenz[*a,h*]anthracene). Naphthalene, acenaphthene, and acenathylene were not reported due to the low recoveries of the spiked acenaphthene-*d10* in some of our samples. In our samples we also measured the sum of methyl-phenanthrenes (ΣMP) for purposes of PAH source identification.

## Results and Discussion

*Sediment dating*

Observed unsupported $^{210}$Pb radionuclide profiles (Figure S1) were for the most part relatively uniform, suggesting that mechanical or biological turbation for this area was low below the first few centimeters (Appleby, 2001). One clear exception was the bottom section of the MWRA sediment core (at 11, 12 and 16 cm from the surface; Figure S1), where, in order to provide a better estimate, we interpolated unsupported $^{210}$Pb values from above and below the given depth (see Appendix III). Age assignments of the unsupported $^{210}$Pb radionuclide profiles calculated using either the CRS or CIC dating models were consistent with the initial activity increase of $^{137}$Cs in the same core (Figures S2, and Appendix III). In all cores, increased $^{137}$Cs activity was detected in the late 1940s/early 1950s, and a larger activity increase corresponded to the mid 1960s, consistent with the increased nuclear weapon testing that occurred in the United States between 1961 and 1963 (Norris and Cochran, 1994). Previous studies have also reported

a second peak in the mid 1980s corresponding to the Chernobyl reactor fire in the former Soviet Union in 1986 (Appleby, 2001; Lima et al., 2003). However, we only saw this second peak in three of our cores (JB, CCB and WB; Fig. S2).

Granstein and Turekian (1986) reported deposition inventories of $^{210}$Pb in New Haven of 38.6 dpm cm$^{-2}$. Assuming a relatively uniform $^{210}$Pb atmospheric deposition in the northeastern USA region, our depth-integrated $^{210}$Pb sediment inventories (Table 1) showed significant sediment focusing occurred in the JB sediment core (factor of 2.4), but not in the other cores. Deep basins tend to exhibit sediment focusing due to inputs from the basin periphery. Therefore a focusing factor of 2.4 at JB, a large and deep basin, is not surprising and has been also previously reported (focusing factor of ~ 4; Hites et al., 1980). To be consistent, all of the sediment fluxes discussed below were corrected for focusing.

*BC and ΣPAH fluxes*

Average BC burial fluxes between 0.57 and 3.1 g m$^{-2}$ yr$^{-1}$ (Figure 2 and 3) agreed well with conclusions previously reported for this area (Gustafsson and Gschwend, 1998). Observations of decreasing deposition fluxes with increasing distance from shore (i.e., IPB > CCB2 > MWRA > WB2 > JB) indicated that atmospheric deposition might be the main source of BC to these areas. Similarly, average ΣPAH fluxes at IPB (5,400 ± 2,800 μg ΣPAH m$^{-2}$ yr$^{-1}$) were also substantially higher than those observed at JB (350 ± 120 μg ΣPAH m$^{-2}$ yr$^{-1}$). These fluxes and spatial distributions are consistent with PAH atmospheric deposition (Golomb et al., 2001), sedimentation fluxes (Gschwend and Hites, 1981), and concentrations (Hites at al., 1980; Windsor and Hites, 1979) previously observed in this coastal area. Due to their recalcitrant and hydrophobic nature, we expect minimal chemical or biological degradation and mobility of BC.

Lower molecular weight PAHs (less than four aromatic rings) tend to degrade at faster rates than higher molecular weight PAHs (Hinga, 2003 and references therein). Therefore, the relative constant molecular ratio observed in our sediment samples between a low and a high molecular weigh PAH, anthracene-to-indeno[1,2,3-c,d]pyrene (Figure S3), further supported our hypothesis of minimal biological or chemical degradation at these sites. We reserved ourselves from interpreting the first centimeter depth in our cores due to the propensity of this first layer of sediment to mechanical or biological turbation.

PAH and BC are both produced during pyrogenic processes and are thought to have similar transport pathways (Gustafsson et al., 1997). However, as mentioned before, their relative emissions can vary significantly, depending on the fuel and the technology used (Table S1). Also, before their final sedimentation, PAHs' and BC's transport and transformation pathways may differ (e.g. Lima et al., 2003; Elmquist et al., 2007; Miguel et al., 1998; Novakov et al., 2004). Therefore, in the following section we discuss the observed changes of BC and ΣPAHs in our sediment cores without assuming a strong correlation between them.

*Massachusetts Water Reservoir Authority Outfall Area (MWRA)*

The record of BC fluxes into the sediments near the MWRA outfall followed a trend consistent with fuel use in Massachusetts and similar to what others have seen for lake sediment (Gustafsson et al., 1997; Louchouarn et al, 2007) for the Northeastern USA (Figure 2a). With the onset of industrialization, BC fluxes sharply increased during the first decades of the 20$^{th}$ century until the early 1930s, possibly reflecting a decrease in energy consumption during the Great Depression (EIA, 2007). During the 1940s and the 1950s, energy consumption in the U.S. continued to increase (EIA, 2007), but, during this time, changes in fuel from coal to petroleum

also occurred. BC emissions from oil are usually lower than from coal (Bond et al., 2004), and the relatively unchanged BC fluxes observed in the MWRA sediment core may reflect this shift. However, the rapid increase in energy consumption was eventually reflected in the sharp increase in BC fluxes from the early 1950s to the late 1960s, when changes in regulations and the technology influenced contaminant emissions into the atmosphere. Decreased BC fluxes throughout the 1970s may have recorded the effects of the introduction of the EPA CAA, the introduction of catalytic converters, and the OPEC oil embargo in the mid 1970s (EIA, 2007; Lima et al., 2003; Schneider et al., 2001; Van Metre et al., 2000). In our core we see an additional increase in the early 1980s that has not been previously reported and that may correspond to a shift back to coal for energy use in the state of Massachusetts (EIA, 2007; Figure S3) during that period of time. A decrease in BC fluxes observed in the early 1990s in this and all of the other sampled sites (Figure 2 and 3) coincides with the introduction of the 1990 CAAA, and this has also been reported for two New York City lakes (Louchouarn, 2007). Furthermore, an increased use since the early 1990s of natural gas, a low emission fuel, in Massachusetts may be responsible for the decrease in BC fluxes in the last decade of the 20$^{th}$ century (EIA, 2007; Figure S4).

*Cape Cod Bay (CCB2)*

Downcore changes in fluxes of BC at CCB also show peaks in the early 1970s and mid 1980s (Figure 2b). However, different from MWRA there is apparently no increase in the earlier years of the 20$^{th}$ century. This observation is not surprising, since the population of Cape Cod remained relatively low and constant until the early 1950s, but increase rapidly in the following decades tripling it size by 1980 (WHRC, 2007). The decrease in BC fluxes after 1978 may

represent the after-effects of the introduction of the CAA and the OPEC oil embargo, and the sharp increase following that period a continuous population growth and energy use in that area until the mid 1990s, when population growth sharply decreased. In addition, the observed increase in BC fluxes in the 1980s and decrease in the 1990s, may reflect, as in the MWRA core, changes in fuel from petroleum, to coal, to natural gas (EIA, 2007; Figure S4).

*Wilkinson Basin (WB2)*

This core is further away from shore (~150 km from Boston) and may not be as sensitive to local changes as the previous two cores. Different from the previous two cores, in this core we see a peak maximum early in the 20$^{th}$ century and no further BC flux increases until later in the 1980s. Furthermore, BC fluxes in the early 1980s returned to pre-industrialization values (Figure 2c). Elmquist et al. (2007) reported a similar pattern with a BC flux maxima in the mid 1920s and decrease to pre-industrialization values during the late 1980s, and they observed that this shift was consistent with the substitution of wood with coal and coke in Europe. In the US the shift from wood to coal/coke was reported earlier, and instead, the peak observed in the 1930s and 1940s might represent increases in coal consumption in the early 1900s and the subsequent decrease during the Depression years (EIA, 2007; Figure S4). It may also correspond to the worst fire on record in the history of Maine and New England in the late 1940s (October through September 1947; 200,000 acres burned; Butler, 1997; NIFC, 2007). The relatively low BC fluxes in the following years at this site point out to differences between close to shore and further away from shore sites due to changes in fuel use and/or technology. Particulate emissions from coal are higher and have larger mean particle sizes than for petroleum (Bond et al., 2004). Therefore, increases in BC fluxes due to increases in coal use might not be as evident

at distance from shore sites. The eventual increase in BC fluxes in the 1980s and subsequent decrease in the 1990s are consistent with energy use trends (EIA, 2007) and the introduction of the CAAA. Although major commercial trawling events have been reported in this area of the GoM (Pilskaln et al., 1998), a continuous $^{210}$Pb sediment profile suggests minimum sediment disturbance (Figure S1).

*Inner Penobscott Bay (IPB)*

The sediment record in this core only dates back to the early 1940s and does not provide information regarding changes in fuel usage and consumption in this area during the early 1900s (Figure 3a). Nonetheless, a very fast increase of both BC and ΣPAH fluxes in the late 1940s indicated the record of the devastating fire in Maine in 1947 (NIFC, 2007). ΣPAH fluxes peaked in the late 1940s, yet BC fluxes continued to increase through the early 1950s. Subsequent runoff and soil erosion containing high concentrations of BC promoted by a decrease in vegetation that resulted from the fire could be responsible for the observed increase in BC fluxes. A faster increase in ΣPAH fluxes compared to BC fluxes during the 1960s is consistent with a shift from wood to fossil fuel (~ 5 fold difference in ΣPAH-to-BC emissions ratio between wood and diesel fuel combustion; Table S1) observed in Maine (EIA, 2007; Figure S4). Like in previous cores and observations made by other researchers (Lima et al., 2003; Louchouarn, 2007, Elmquist and Gustafsson, 2006), both BC and ΣPAH fluxes presented a peak-maxima in the late 1970s. This increase and subsequent decrease is consistent with trends in energy use (EIA, 2007; Figure S4) in the 20$^{th}$ century, and the latter introduction of the CAA, changes in combustion technology, and the OPEC oil embargo in the 1970s. A second decoupling of BC from ΣPAH observed in the early 1980s may represent the introduction of catalytic converters in

motor vehicles a lower ΣPAH-to-BC emission ratio (Table S1). ΣPAH fluxes continued to decrease for the remainder of the 20th century. However, consistent with trends in energy use in Maine (and the whole New England area; EIA, 2007), BC fluxes again increased in the early late 1980s and early 1990s, before their eventual decrease in the middle and late 1990s, which coincides with the enactment of the CAAA. Although the CAA promoted the development of new combustion technologies that improved air quality, the CAAA were more stringent regarding particulate matter and promoted the used of cleaner fuels such as low sulfur coal and natural gas. Our findings suggest that the CAAA were more successful at reducing BC emissions than the previous CAA.

*Jordan Basin (JB)*

JB, a site located about 270 km from Boston (Figure 1), presented the lowest concentrations and fluxes of BC and ΣPAH (Figure 3b). At this site, both BC and ΣPAH fluxes have dramatically departed from pre-industrial concentrations. BC and ΣPAH fluxes started to increase with the turn of the past century (assuming $^{210}$Pb-based sedimentation rates can be extrapolated back past 1900) and the onset of the industrial revolution, and similar to IPB, presented a peak in 1940s. JB is about 80 km from IPB and is possible that the peak observed in this sediment core in the 1940s was also representative of the 1947 Maine fire disaster. Similar to the WB site, at this core we were unable to identify the 1960-1970s peak seen in other studies. Instead we see that fluxes of BC and ΣPAHs remained low until the early 1980s when they started to increase again. This later increase continued until the 1990s, and followed the trends in New England's energy use (EIA, 2007; Figure S4) and coincides with the enactment of the CAAA.

Sediment records of BC fluxes at JB were similar to the ones observed at WB, another distant-from-shore site, and differed from observations at close-to-shore stations (i.e., MWRA, CCB, and IPB), probably due to differences in transport processes. Closer similarities between BC and ΣPAHs at JB than at IPB, further suggests that variations in the sediment record will be affected by the transformations that BC and PAHs may undergo before their final burial.

*PAH source ratios*

Analyses of PAH ratios have proven to be good indicators of source and delivery routes of PAHs (Gschwend and Hites, 1981; Gustafsson and Gschwend, Yunker et al., 2002). In order to differentiate petrogenic from pyrogenic sources, as well as fossil fuel combustion from coal, softwood and grass combustion, we used fluoranthene-to (pyrene plus fluoranthene) (Fla/(Fla+Py)) (petrogenic<0.4; 0.4 <fossil fuel combustion<0.6; coal, softwood, grass combustion >0.6; Yunket et al., 2003), and ∑methyl-phenanthrenes to phenanthrene ratios (ΣMP/P) (~0.5 for petrogenic and ~5 for pyrogenic; Yunker et al., 2003). The IPB and JB PAH source diagnostic ratios (Figure 4) indicate that for the main sources of PAHs to both of these sites were mixtures of combustion sources. In addition, higher than 0.6 Fla/(Fla+Py) ratios suggest that these sites were mainly influenced by coal, wood, and/or grass combustion. These findings are not surprising since Maine is one of the top US producers of electricity from wood and wood waste, and Massachusetts heavily relies on coal for energy production (EIA, 2007). Searsport is an oil seaport close to IPB, and possible oil spills could explain the high ΣMP/P ratio observed in 1949 and 1960. However, we were not able to trace back any specific oil spill events in this area. PAH ratios of benzo[*a*]pyrene to benzo[*e*]pyrene (B[*a*]P/B[*e*]P) are indicative of the distance from the emission source, as well as the travel route (i.e., atmospheric

or aeolian transport) of the pyrogenic compounds (Gschwend and Hites, 1981). B[*a*]P photo degrades at a faster rate than B[*e*]P in the atmosphere. As a result, higher ratios of B[*a*]P to B[*e*]P indicate closeness to the source, whereas lower ratios indicate that the PAH have travelled a distance long enough to see a decrease in the more sensitive PAH due to photo degradation. In our cores we see a decreased B[*a*]P/B[*e*]P ratio in JB as compared to IPB. This indicates that PAHs found in IPB are probably produced locally; whereas PAHs from JB travelled a certain distance before its final deposition.

Abundances of individual PAHs of different molecular weight can also provide valuable information regarding changes in energy use or transport processes. For example, the higher anthracene-to-ideno[1,2,3-c,d]pyrene ratio observed at IPB than JB (Figure S3), may indicate different transportation routes between these two sampling sites. Smaller PAHs (such as anthracene) are vaporized and dissolved more readily from particles than larger PAHs (such as ideno[1,2,3-c,d]pyrene), and are more sensitive to reactions with OH radicals present in the atmosphere and direct photochemical reactions (Schwarzenbach et al., 2003). In addition, larger PAHs are predominantly particle-bound, due to their stronger affinities for BC containing aerosols (Gustafsson et al., 1997), reducing significantly the losses by these mechanisms in the atmosphere. This observation implies that atmospheric transport was the main route of the BC and ΣPAHs found at JB.

The different influences of each one of the locations, more importantly in the distant from shore locations, may be influenced by different pyrogenic events and regional weather patterns. WB and JB are generally north of the area of the 1947 fire disaster in Maine, yet based on the observations from the sediment cores, both of these sites may have been more heavily impacted

by this mayor event than historical changes in fuel usage in urban areas (e.g. Boston, MA and New Your, NY).

Sediment records of BC and ΣPAHs fluxes provided valuable information regarding historic sources and transportation mechanisms of atmospheric contaminants. This study allowed us to identify spatial and temporal patterns of BC and ΣPAH fluxes reflecting combustion sources, technology, and emission regulations, as well as transport processes. Sedimentation fluxes of BC and ΣPAHs were higher for sites closer to shore, and where available, PAH source ratios and relative abundances suggest that atmospheric transport is the main route for these materials to off shore sites. Larger variability was observed in sites closer to shore, probably due stronger influences from nearby sources. Nevertheless, all studied sites are able to show a finger print of human influences based on society, industry and government regulated decisions, as well as economic activity and, in the case of wildfires, meteorological conditions. These reconstructed fingerprints provide useful information to address the effects of regulations and constrain historical human exposure of combustion derived pollutants.

**Acknowledgments**

We are very thankful to the captains and crews of RV Oceanus and RV Cape Hatteras, and D. Plata, R. K. Nelson, E. Roosen, E. Peacock, S. Silva, E. Tauten, and L. Xu, members of C. Reddy's lab, for all their help slicing the sediment cores on board. We are especially thankful to Emily Peacock for the PAH extraction of the IPB sediment core. We are also grateful for the financial support from NFS grants (OCE-0223441 and BES-0607136) and CONACYT and MFSF fellowships to D. X. F.

## References


Appleby, P. G., 2001. Chronostratigraphic techniques in recent sediments. In: W. Last, Smol, J. (Editor), Tracking environmental change using lake sediments. Kluwer Academic Publishers, Dordrecht, The Netherlands, pp. 171-203.

Appleby, P. G., Oldfield, F., 1978. The calculation of lead-2 10 dates assuming a constant rate of supply of unsupported 210Pb to the sediment. Catena, 5: 1-8.

Bierman, V. J. Jr., 1990. Equilibrium partitioning and magnification of organic chemicals in benthic animals. Envriron. Sci. Technol. 24, 1407-1412.

Bond, T. I., D. G. Streets, K. F. Yarber, S. M. Nelson, J. Woo, Z. Klimont, 2004. A technology-based global inventory of black and organic carbon emissions from combustion. J. Geophys. Res., 109: D14203.

Butler, J., 1997. Wildfire loose. The week Maine Burned. Down East Books, Camden, Maine.

Dockery, D. W., C. A. Pope, X. P. Xu, J. D. Spengler, J. H. Ware, M. E. Fay, B. G. Ferris, F. E. Speize, 1993. An association between air pollution and mortality in six United States cities. N. Engl. J. Med., 329(24): 1753-1759.

EIA (Energy Information Administration). Official Energy Statistics from the U.S. Government. http://www.eia.doe.gov (accessed multiple times during 2007).

Elmquist, M., Z. Sencak, Ö. Gustafsson, 2007. A 700 year sediment record of black carbon and polycyclic aromatic hydrocarbons near the EMEP air monitoring station in Aspvreten, Sweden. Environ. Sci. Technol., 41: 6926-6932.

Golomb, D., D. Ryan, J. Underhill, T. Wades, S. Zemba, 1997. Atmospheric deposition of toxics onto Massachusetts Bay-II. Polycyclic aromatic hydrocarbons. Atmos. Environ., 31(9): 1361-1368.

Grigg, J., 2002. The health effects of fossil fuel derived particles. Arch. Dis. Child., 86(2): 79-83.

Gschwend, P. M., Hites, R. A., 1981. Fluxes of polycyclic aromatic hydrocarbons to marine and lacrustine sediments in the northeastern United States. Geochim. Cosmochim.Acta, 35(2359-2367).

Gustafsson, Ö., and Gschwend, P. M., 1998. The flux of black carbon to surface sediments on the New England continental shelf. Geochim. Cosmochim. Acta, 62(3): 465-472.

Gustafsson, Ö., F. Haghsete, C. Chan, J. MacFarlane, P. M. Gschwend, 1997. Quantification of the dilute sedimentary soot phase: implications for PAH speciation and bioavailability. Environ. Sci. Technol., 31: 203-209.

Hammes, K., Schmidt, M. W., Curri, L. A., Ball, W. P., Nguyen, T. H., Louchouarn, P., Houel, S., Gustafsson, O., Elmquist, M., Cornelissen, G., Smernik, R. J., Skjemstad, J. O., Masiello, C. A., 2007. Comparison of black carbon quantification methods using reference materials form soil, water, sediment and the atmosphere, and implications for the global carbon cycle. Global Biogeochem. Cycles, 21: doi:10.1029/2006GB002914.

Hinga, K. R., 2003. Degradation rates of low molecular weight PAH correlate with sediment TOC in marine subtidal sediments. Marine Pollution Bulletin, 46: 466-476.

Hites, R. A., R. E. Laflamme, and J. G. Windsor, Jr., 1980. Polycyclic aromatic hydrocarbons in marine/aquatic sediments and their ubiquity. In: L.P.a.F.T. Weiss (Editor), Petroleum in the Marine Environment. American Chemical Society, Washington DC.

Kahn, M., 1996. New evidence on trends in vehicle emissions. Rand Journal of Economics, Spring.

Künzli, N., McConnell, R., Bates, D., Bastain, T., Hricko, A., Lurmann, F., Avol, E., Gilliland, F., Peters, J., 2003. Breathless in Los Angeles: The Exhausting Search for Clean Air. American Journal of Public Health, 93(9): 1494-1499.

Lee, R. G. M., P. Coleman, J. L. Jones, K. C. Jones, R. Lohman, 2005. Emission factors and importance of PCDD/Fs, PCBs, PCNs, PAHs and PM10 from domestic burning of coal and wood in the UK. Environ. Sci. Technol., 39: 1426-1447.

Lima, A. L., 2004. Molecular and isotopic records of combustion inputs to the environment over the last 250 years, Massachusetts Institute of Technology/Woods Hole Oceanographic Institution, Woods Hole, 267 pp.

Lima, A. L. C., Eglinton, T. I., and Reddy, C., 2003. High-resolution record of pyrogenic polycyclic aromatic hydrocarbon deposition during the 20th century. Environ. Sci. Technol., 37: 53-61.

Lohmann, R., Burguess, R. M., Cantwell, M. G., Ryba, S. A., MacFarlane, J. K., Gschwend, P. M., 2004. Dependendency of polychlorinated biphenyl and polycyclic aromatic hydrocarbon bioaccumulation in *mya arenaria* on both water column and sediment bed chemical activities. Environ. Toxicol. Chem. 23, 2551-2562.

Louchouarn, P., S. N. Chillrud, S. Houel, B. Yan, D. Chaky, C. Rumpel, C. Largeau, G. Bardoux, D. Walsh, R. F. Bopp, 2007. Elemental and molecular evidence of soot- and char-derived black carbon inputs to New York City's atmosphere during the 20th century. Environ. Sci. Technol., 41: 82-87.

Menzie, C. A., Potocki, B. B., Santodonato, J., 1992. Exposure to carcinogenic PAHs in the environment. Environ. Sci. Technol., 26: 1278-1284.

Miguel, A. H., T. W. Kirchstetter, R. A. Harley, 1998. On-road emissions of particulate polycyclic aromatic hydrocarbons and black carbon from gasoline and diesel vehicles. Environ. Sci. Technol., 32: 450-455.

Moore, M., 1995. Mutagenesis and carcinogenesis of PAHs in the marine environment., In Sources, fate and effects of PAHs in Massachusetts Bay. Massachusetts Bay Program, US Environmental Protection Agency, Boston, MA.

NIFC (National Interagency Fire Center). Nation's Logistic Support Center. http://www.nifc.gov (accessed multiple times during 2007)

Norris, R. S., T. B. Cochran, 1994. United States Nuclear Tests; July 1945 to 31 December 1992. NWD, 94-1.

Novakov, T., V. Ramanathan, J. E. Hansen, T. W. Kirchstetter,1 M. Sato, J. E. Sinton, J. A. Sathaye, 2003. Large historical changes of fossil-fuel black carbon aerosols. Geophys. Res. Lett., 30: doi:10.1029/2002GL016345.

Pachauri, R. K., Sridharan, P. V., 1998. Looking back to think ahead, GREEN India 2047: Growth with resource enhancement of environment and nature. Tata Energy Research Institute: New Dehli.

Pilskaln, C., Churchil, J. H., Mayer, L. W., 1998. Resuspension of Sediment by Bottom Trawling in the Gulf of Maine and Potential Geochemical Consequences. Conservation Biology, 12(6): 1223-1229.

Reddy, C. M., Pearson, A., Xu, L., McNichol, A. P., Benner Jr, B. A., Wise, S. A., Klouda, G. A., Currie, L. A., and Eglinton, T., 2002. Radiocarbon as a tool to apportion the sources of polycyclic aromatic hydrocarbons and black carbon in environmental samples. Environ. Sci. Technol., 36(1774-1782).

Rogge, W. F., L. M. Hildemann, M. A. Mazurek, G. R. Cass, B. R. T. Simoneit, 1993. Sources of fine organic aerosol. 2. Noncatalyst and catalyst equipped automobiles and heavy duty diesel trucks. Environ. Sci. Technol., 27: 636-651.

Schneider, A. R., H. M. Stapleton, J. Cornwell J. E. Baker, 2001. Recent declines in PAH, PCB, and tocaphene levels in the northern Great Lakes as determined from high resolution cores. Environ. Sci. Technol., 35: 3809-3815.

Schwarzenbach, R. P., Gschwend, P. M., Imboden, D. M., 2003. Environmental Organic Chemistry. John Wiley and Sons, Inc., Hoboken.

Smith, K. R., 2005. National burden of disease in India from indoor air pollution. Proc. Natl Acad. Sci. USA, 97: 13286-13293.

Tracey, G. A., Hansen, D. J., 1996. Use of biota-sediment accumulation factors to assess similarity of non-ionic organic chemical exposure to benthically-coupled organisms of different trophic mode. Arch. Environ. Toxicol. Contam. 30, 467-475.

Van Metre, P. C., B. J. Mahler, and E. T. Furlong, 2000. Urban sprawl leaves its PAH signature. Environ. Sci. Technol., 34: 4064-4070.

Windsor, J. G., and Hites, R. A., 1979. Polycyclcic aromatic hydrocarbons in Gulf of Maine sediments and Nova Scotia soils. Geochim. Cosmochim. Acta, 43(1): 27-33.

WHRC (Woods Hole Research Center). Land cover and population changes in Cape Cod. http://www.whrc.org (accessed multiple times during 2007).

Yunker, M. B., Macdonald, R. W., Vingarzan, R., Mitchell, R. H., Gayette, D., Sylvestre, S., 2002. PAHs in the Fraser River basin: a critical appraisal of PAH ratios as indicators of PAH source and composition. Org. Geochem., 33: 489-515.

## Figure Captions

**Figure 1**. Sediment sampling locations in the Gulf of Maine (GoM).

**Figure 2.** BC sediment fluxes for (a) MWRA, (b) CCB2 and (c) WB2.

**Figure 3.** BC and ΣPAH sedimentation fluxes in (a) IPB and (b) JB.

**Figure 4.** Source apportionment PAH ratios: Sum of methyl phenanthrenes to phenanthrene (ΣMP/P), fluoranthene to fluoranthene plus pyrene (Fla/(Fla+Py)), and benzo[*a*]pyrene to benzo[*e*]pyrene for (a) IPB and (b) JB.

## Table Captions

**Table 1.** Description of sampling station in the GoM.

**Table 1.** Description of sampling stations in the GoM.

| Name | Date of collection | Water Depth (m) | Latitude | Longitude | Sediment Depth (cm) | $^{210}$Pb inventory (dpm $m^{-2}$) |
|---|---|---|---|---|---|---|
| MA Water Resources Authority (MWRA) | 9/02/2004 | 71 | 42° 27.21 N | 70° 39.11 W | 15 | 43 |
| Cape Cod Bay (CCB2) | 4/18/2004 | 30 | 41°56.28 N | 70°10.89 W | 38 | 26 |
| Wilkinson Basin (WB2) | 4/20/2004 | 167 | 43°22.53 N | 69°53.21 W | 47 | 33 |
| Inner Penobscot Bay (IPB) | 4/21/2004 | 17 | 44° 25.87 N | 68° 50.31 W | 33 | 26 |
| Jordan Basin (JB) | 4/22/2004 | 287 | 43°28.98 N | 67°52.96 W | 56 | 94 |

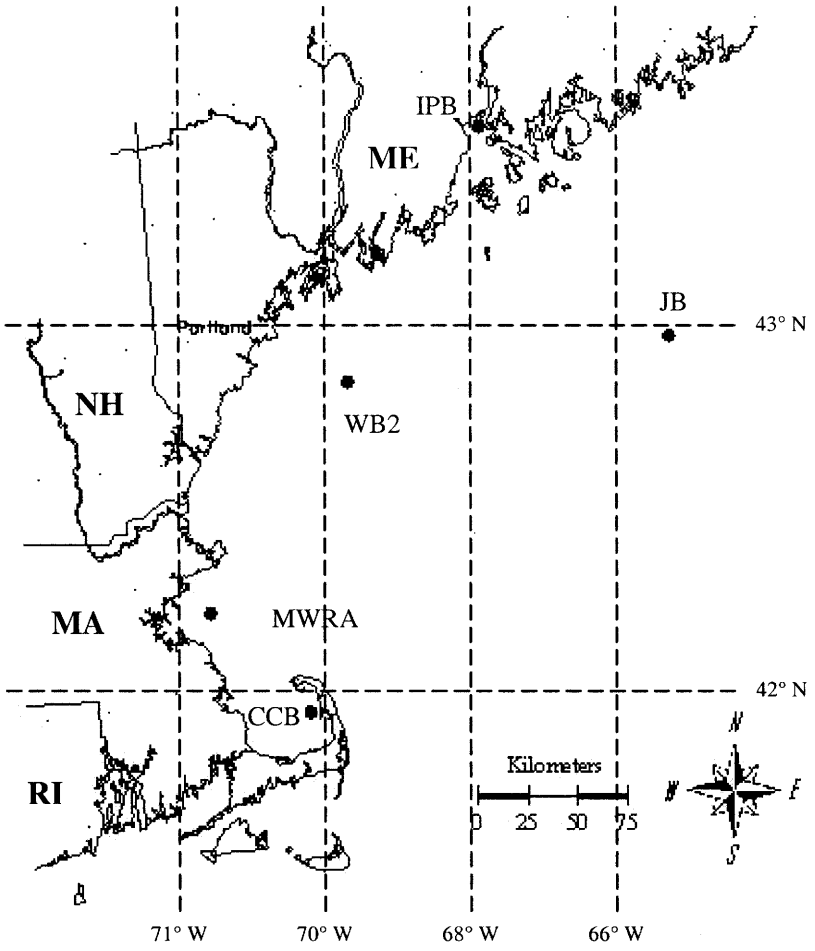


**Figure 1**. Sediment sampling locations in the Gulf of Maine (GoM).

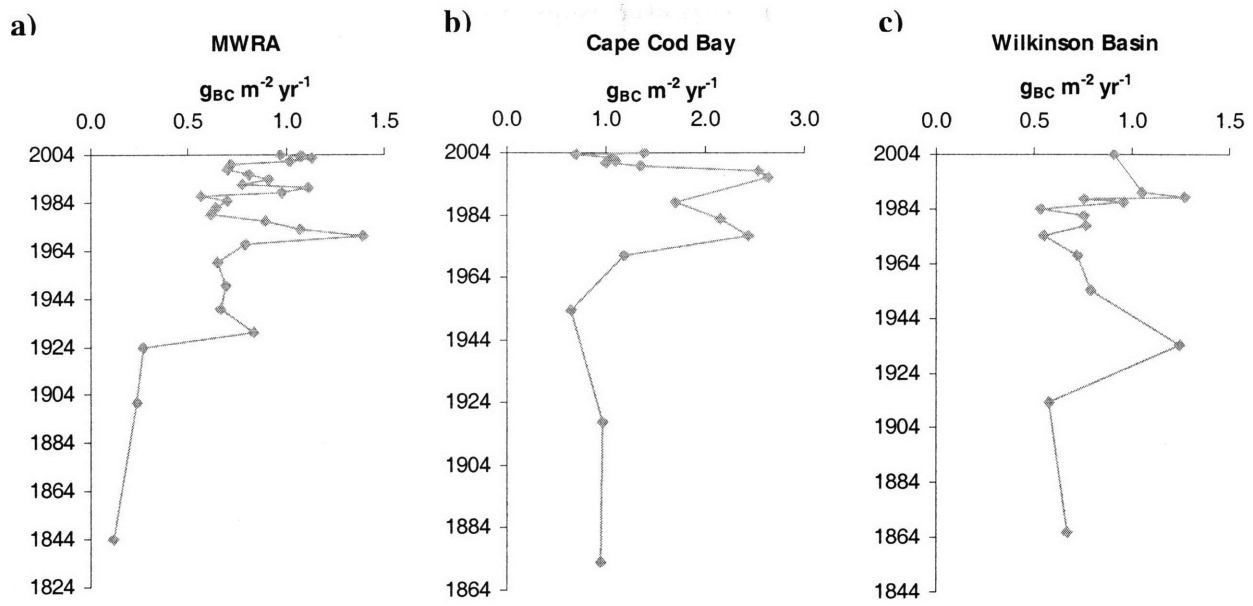


**Figure 2.** BC sediment fluxes for (a) MWRA, (b) CCB2 and (c) WB2.

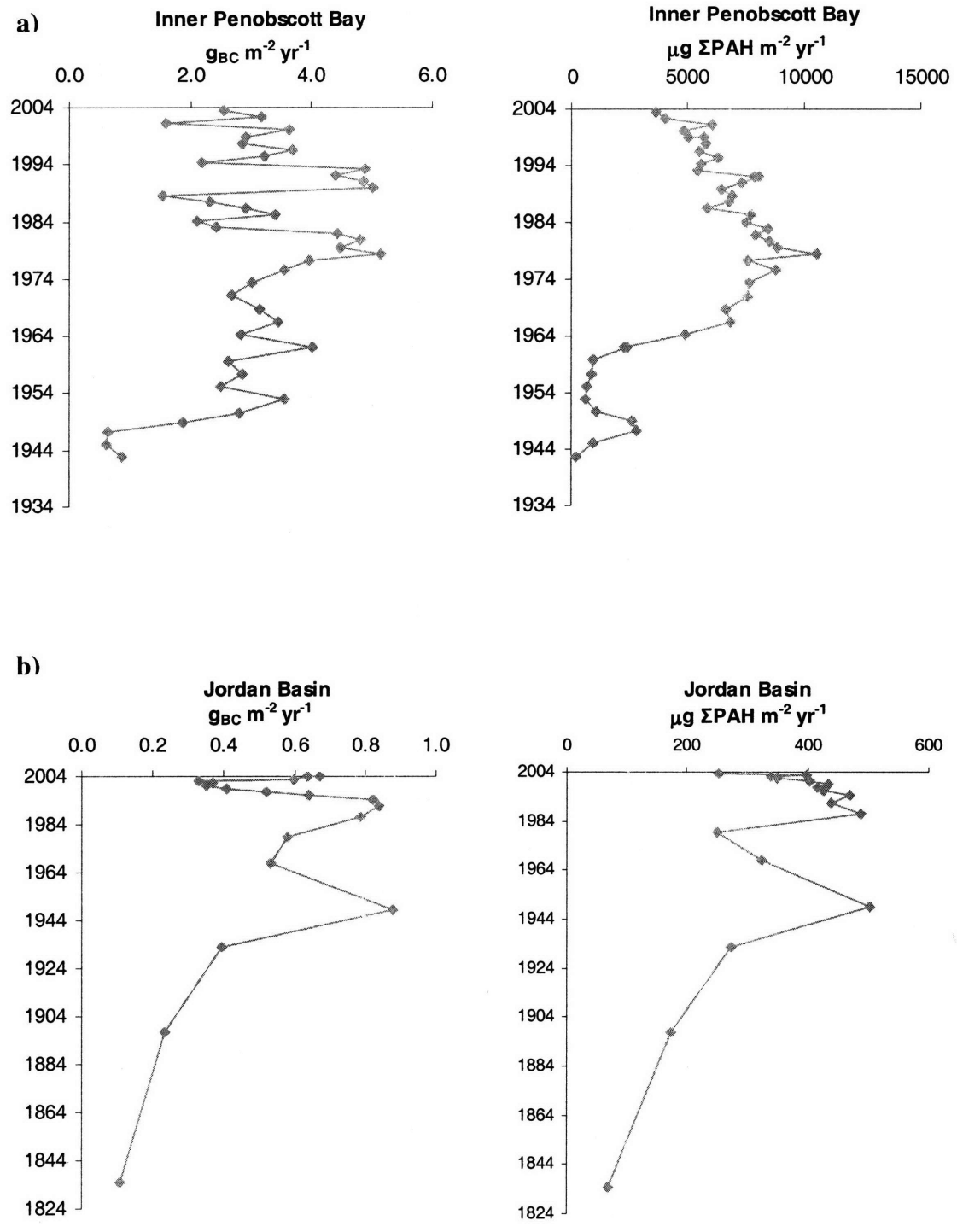


**Figure 3**. BC and ΣPAH sedimentation fluxes in (a) IPB and (b) JB.

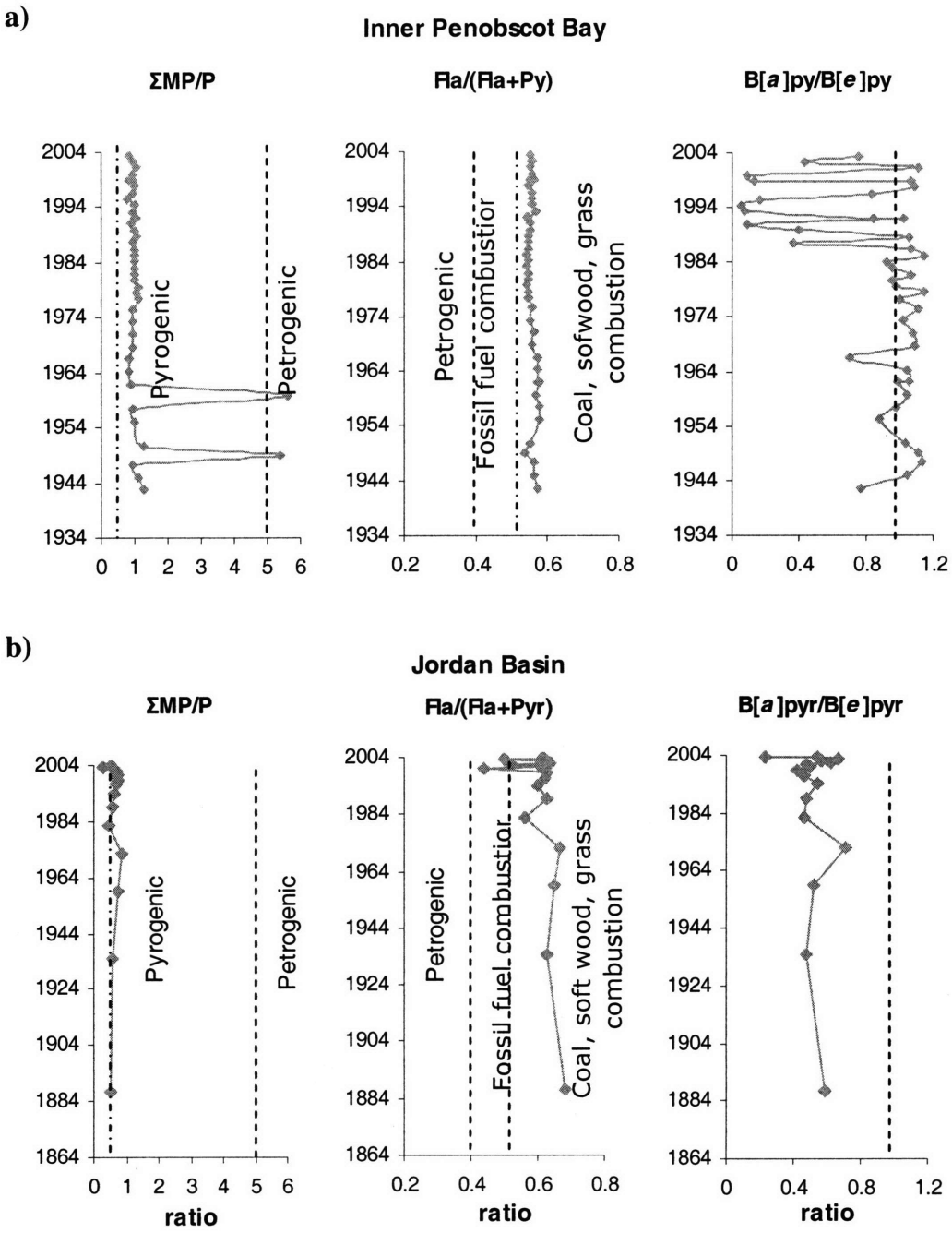


**Figure 4.** Source apportionment PAH ratios: Sum of methyl phenanthrenes to phenanthrene (ΣMP/P), fluoranthene to fluoranthene plus pyrene (Fla/(Fla+Py)), and benzo[*a*]pyrene to benzo[*e*]pyrene (B[*a*]P/B[*e*]P) for (a) IPB and (b) JB.

**Supporting Information for:**

# "Spatial and temporal variations of black carbon and polycyclic aromatic hydrocarbons inputs to the Gulf of Maine in the last 100 years"

D. Xanat Flores-Cervantes[1], Christopher M. Reddy[2], and Philip M. Gschwend[1].

[1]R.M. Parsons Laboratory, MIT 48-413, Department of Civil and Environmental Engineering, Massachusetts Institute of Technology, Cambridge, Massachusetts 02139, USA

[2]Department of Marine Chemistry and Geochemistry, Woods Hole Oceanographic Institution, Woods Hole, Massachusetts, 02543

xanatf@mit.edu, creddy@whoi.edu, pmgschwe@mit.edu.

This document includes:

Table S1.

Figures S1, S2, S3, S4.

## Figure Captions

**Figure S1.** Depth profiles of unsupported $^{210}Pb$ for all cores vs. depth (data on Appendix III).

**Figure S2.** Depth profiles of $^{137}Cs$ for all cores vs. year of deposition as estimated by the $^{210}Pb$ CRS and CIC models (see text and Appendix III).

**Figure S3.** Anthracene-to-indeno[1,2,3-c,d]pyrene ratio for Inner Penobscot Bay (IPB) and Jordan Basin (JB).

**Figure S4.** Historical energy use in (a) the USA, (b) the New England area, (c) Connecticut, (d) Maine, (e) Massachusetts, (f) New Hampshire, (g) Rhode Island, (h) Vermont. Data from EIA, 2007.

## Table Captions

**Table S1.** Range of PAH-to-BC emission ratios based on fuel and technology used.

**Table S1.** Range of PAH-to-BC emission ratios based on fuel and technology used.

| Sector | Fuel | $\Sigma PAH_8$[a] mg $kg^{-1}$ | BC (mg kg-1) | | PAH/BC | |
|---|---|---|---|---|---|---|
| | | | low | high | $mg_{PAH}/mg_{BC}$ | |
| Industry | Diesel fuel | 1.1[b] | 3.4[c] | 4.4[c] | 0.32 | 0.25 |
| | Brown coal | 0.002[d] | 0.01[c] | 1.2[c] | 0.15 | 0.00 |
| Transportation | Gasoline (non-catalyst) | 3.2[e] | 0.43[c] | | 7.4 | |
| | | 2.2[fg] | 8.3f[g] | | 0.3 | |
| | Gasoline (catalyst) | 0.24[e] | 0.08[c] | 0.43[c] | 3.0 | 0.6 |
| | | 0.05[hi] | 0.03[h] | | 1.5 | |
| | | 0.04[fg] | 0.77[fg] | | 0.05 | |
| | Diesel (heavy-duty) | 0.27[e] | 1.3[c] | 3.6[c] | 0.21 | 0.08 |
| | | 1.40[hi] | 1.4[h] | | 1.0 | |
| | | 0.46[gjk] | 57[gj] | | 0.01 | |
| Residential | Diesel fuel | 32[l] | 0.06[c] | 4.0[c] | 533 | 8 |
| | Wood | 30[m] | 0.3[c] | 1.4[c] | 100 | 21 |
| | Wood pine | 37[n] | 0.13[n] | | 279 | |
| | Wood oak | 20[n] | 0/16[n] | | 123 | |
| | Wood eucalyptus | 20[n] | 0.22[n] | | 89 | |
| | Hardwood in fireplace | 30[o] | 0.65[c] | | 46 | |
| | Hardwood in stove | 14[o] | 0.30[c] | | 46 | |
| | Coal briquette | 8.8[p] | 0.15[c] | | 59 | |
| | Charcoal | 6.1[p] | 1.0[c] | | 6.1 | |
| | Hard coal | 111[q] | 0.76[c] | 5.4[c] | 146 | 21 |
| | Brown coal | 57.8 – 136[q] | 0.18[c] | | 321 | 756 |
| Natural fires/ agricultural burning | Pine wood | 5.7[r] | 0.56[c] | 0.61[c] | 10.18 | 9.34 |
| | Agricultural waste | 3.8[r] | 0.69[c] | | 5.4 | |

[a]$SPAH_8$: phenanthrene, anthracene, fluoranthene, pyrene, chrysene/triphenylene, benzo(*a*)anthracene, benzo(*b+k*)fluoranthene, benzo(*a*)pyrene; [b]US EPA (1993); [c]Bond et al. (2004); [d]US EPA (1998); [e]Rogge et al. (1993); [f]Shauer et al. (2002); [g]units mg km-1; [h]Miguel et al. (1998); [i]phenanthrene and anthracene were not measured; [j]Schauer et al. (1999); [k]benzo(*b+k*)fluoranthene, benzo(*a*)pyrene were not measured; [l]Johansson et al. (2004); [m]Oanh et al. (2002); [n]Schauer et al. (2001); [o]McDonald et al. (2000); [p]Oanh et al. (1999); [q]Chen et al. (2005); [r]Jenkins et al. (1996)

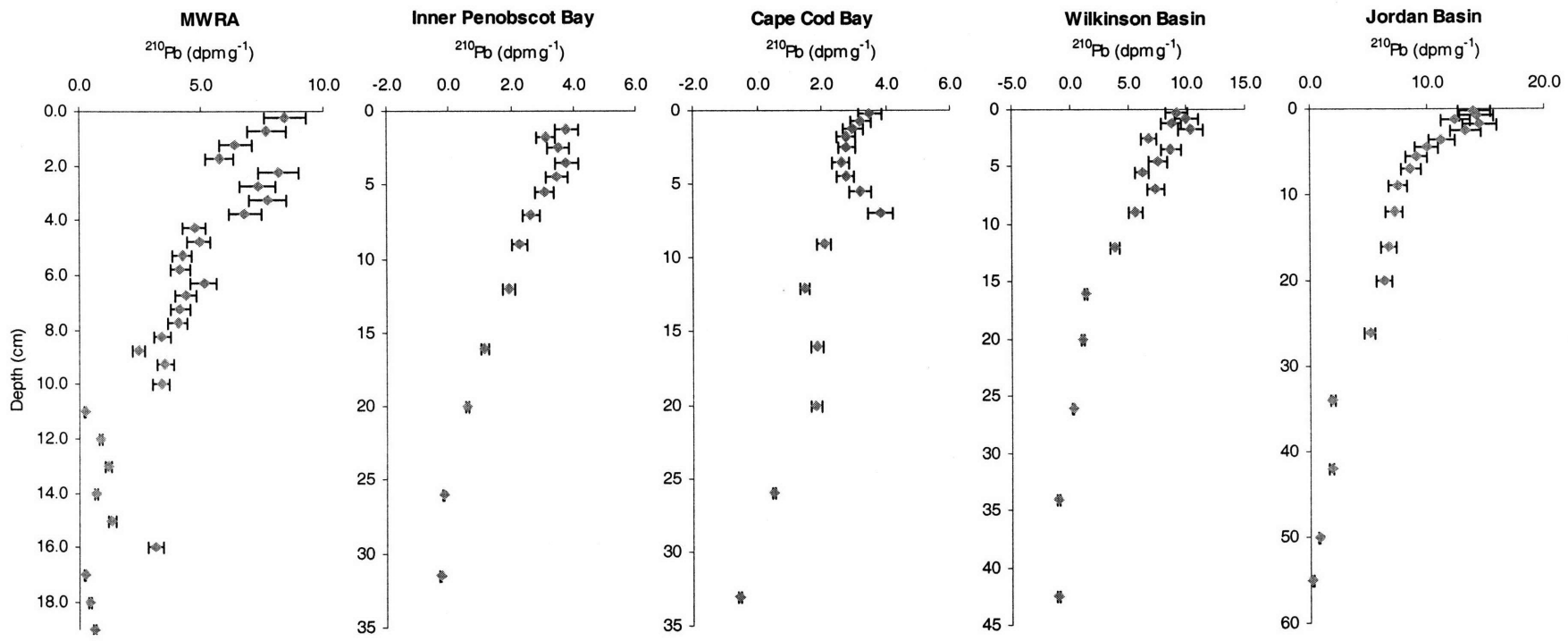


**Figure S1.** Depth profiles of unsupported $^{210}$Pb for all cores vs. depth (data in Appendix III).

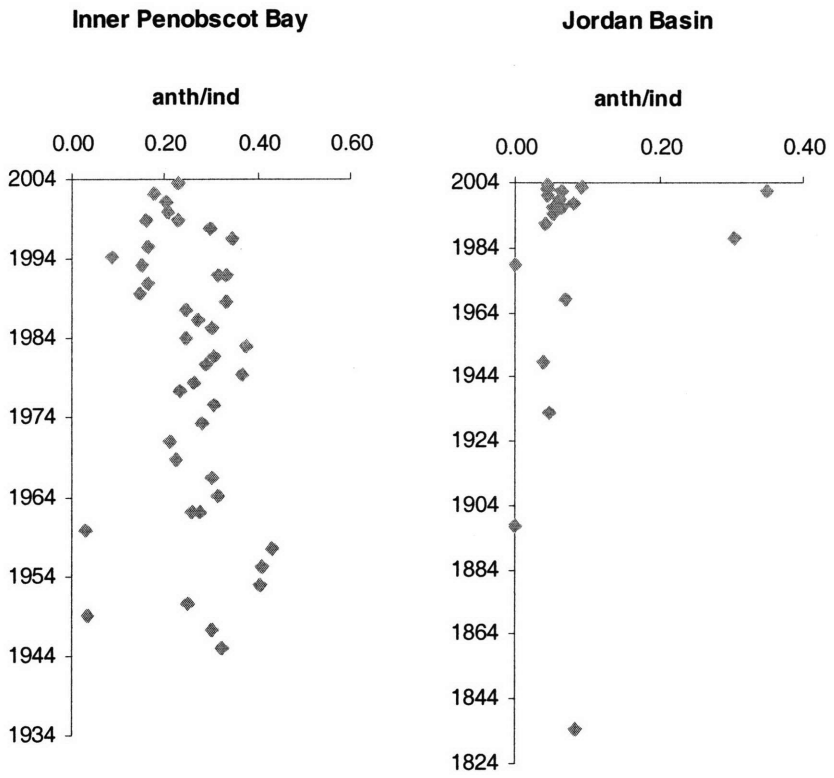


**Figure S3.** Anthracene-to-indeno[1,2,3-c,d]pyrene ratio for Inner Penobscot Bay (IPB) and Jordan Basin (JB).

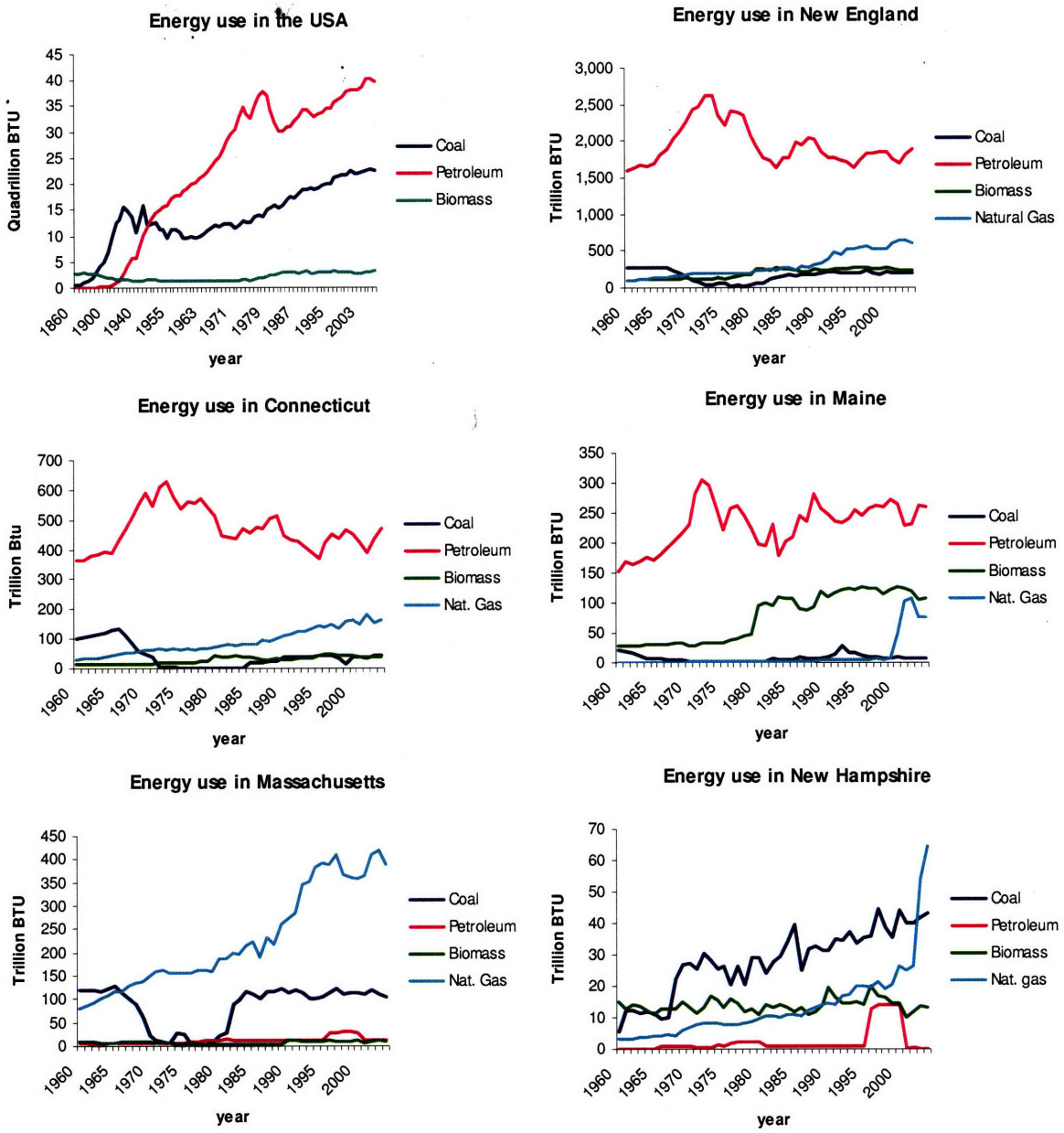


**Figure S4**. Historical energy use in (a) the USA, (b) the New England area, (c) Connecticut, (d) Maine, (e) Massachusetts, (f) New Hampshire, (g) Rhode Island, (h) Vermont. Data from EIA, 2007.

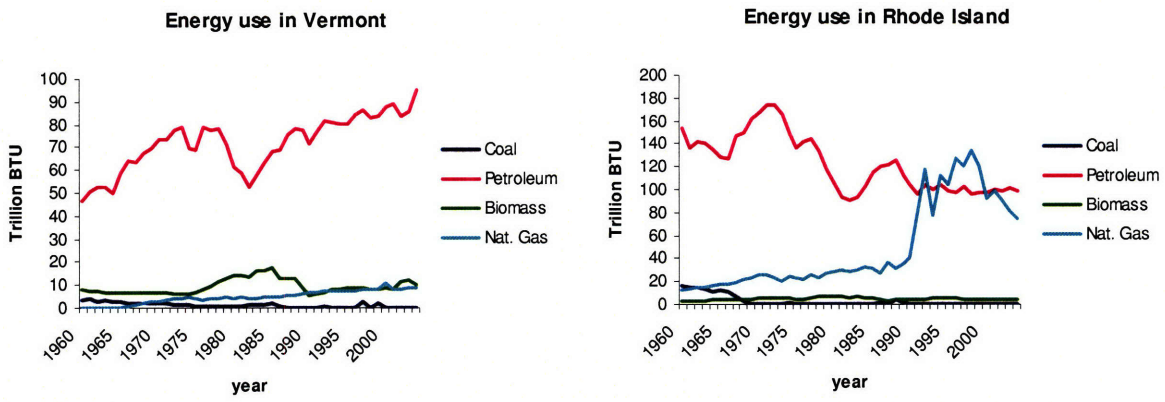


**Figure S4 (continuation)**. Historical energy use in (a) the USA, (b) the New England area, (c) Connecticut, (d) Maine, (e) Massachusetts, (f) New Hampshire, (g) Rhode Island, (h) Vermont. Data from EIA, 2007.

## References


Bond, T. I., Streets, D. G., Yarber, K.F., Nelson, S.M., Woo, J., Klimont, Z., 2004. A technology-based global inventory of black and organic carbon emissions from combustion. J. Geophys. Res. 109, D14203.

Chen, Y. J., Sheng, G. Y., Bi, X. H., Feng, Y. L., Mai, B. X., Fu, J. M., 2005. Emission factors for carbonaceous particles and polycyclic aromatic hydrocarbons from residential coal combustion in China. Environ. Sci. Technol. 39, 1861-1867.

Johansson, L. S., Leckener, B., Gustavsson, L., Cooper, D., Tullin, C., Potter, A., 2004. Emission characteristics of modern and old-type residential boilers fired with wood logs and wood pellets. Atmos. Environ. 38, 4183-4195.

Jenkins, B. M., Jones, A. D., Turn, S. Q., Williams, R. B., 1996. Emission factors for polycyclic aromatic hydrocarbons from biomass burning. Environ. Sci. Technol. 30, 2462-2469.

McDonald, R. D., Zilinska, B., Fujita, E. M., Sagabiel, J. C., Chow, J. C., Watson, J. G., 2000. Fine particulate and gaseous emission rates from residential wood combustion. Environ. Sci. Technol, 34, 2080-2091.

Miguel, A. H., T. W. Kirchstetter, R. A. Harley, 1998. On-road emissions of particulate polycyclic aromatic hydrocarbons and black carbon from gasoline and diesel vehicles. Environ. Sci. Technol. 32, 450-455.

Oanh, N. T. L., Reutergardh, L. B., Dung, N. T., 1999. Emission of polycyclic aromatic hydrocarbons and particulate matter from domestic combustion of selected fuels. Environ. Sci. Technol. 33, 2703-2709.

Oanh, N. T. K., Nghiem, L., Phyu, Y. L., 2002. Emission of polycyclic aromatic hydrocarbons, toxicity, and mutagenicity from domestic cooking using sawdust briquettes, wood, and kerosene. Environ. Sci. Technol. 36, 833-839.

Rogge, W. F., Hildemann, L. M., Mazurek, M. A., Cass, G. R., Simonet, B. R. T., 1993. Sources of fine organic aerosol. 2. Noncatalyst and catalyst-equipped automobiles and heavy-duty diesel trucks. Environ. Sci. Tecnol. 27, 636-651.

Schauer, J. J., Kleeman, M. J., Cass, G. R., Simonet, B. R. T., 1999. Measurements of emissions from air pollution sources. 1. C1 through C30 organic compounds from medium duty diesel trucks. Environ. Sci. Technol. 33, 1578-1587.

Schauer, J. J., Kleeman, M. J., Cass, G. R., Simonet, B. R. T., 2001. Measurements of emissions from air pollution sources. 1. C1 through C29 organic compounds from fireplace combustion of wood. Environ. Sci. Technol. 35, 1716-1728.

Schauer, J. J., Kleeman, M. J., Cass, G. R., Simonet, B. R. T., 2002. Measurements of emissions from air pollution sources. 5. C1 through C32 organic compounds from gasoline-powered motor vehicles. Environ. Sci. Technol. 36, 1169-1180.

US EPA (US Environmental Protection Agency), 1993. Emission factor documentation for AP-42 section 3.4, large stationary and all stationary duel fuel engines. Office of Air Quality Planning and Standards, US Environmental Protection Agency, Research Triangle Park, NC.

# CHAPTER 7. CONCLUSIONS

## Summary

Two different techniques, a modified chemothermal oxidation at 375 °C method (CTO-375) and pyrene fluorescence losses (PFL), were applied to measure BC in seawater particulate organic carbon (POC). In both cases, the data indicate that BC contributes, on average, 5% of the POC. The modified CTO-375 method is a strong oxidative method that retains only the most recalcitrant carbon, while the PFL method distinguishes BC from other materials due to its strong sorption properties. The resemblance in concentrations between both methodologies suggests that the isolated material is both recalcitrant and highly sorptive. The observed concentrations imply that up to half of the previously chemically unidentifiable POC in seawater (Aluwihare et al., 1997; Eglinton and Repeta, 2004) may simply be these combustion-derived particles. Furthermore, the recognized presence of this recalcitrant BC carbon may well explain why some POC is not recycled to $CO_2$ during its transport to depth and even within the sediment beds below. Finally, the observed BC concentrations of this highly sorptive material imply that BC substantially affects the speciation of high molecular weight pollutants like polycyclic aromatic hydrocarbons (PAHs) and polychlorinated dibenzo dioxins (PCDD) in GoM seawater, by limiting their degradation and toxic effects.

The use of the CTO-375, adapted to measure BC in seawater samples with additional sample manipulations, was found to be appropriate to measure BC in seawater POC. The application of the methodology with positive and negative controls as well as seawater phytoplankton, provided additional confidence in the use of the method in a given setting, and called to attention certain manipulations that might increase or decrease interferences in our measurements. Of special

interest for this study was to learn that some seawater phytoplankton species may be more prone to charring than others and that measurements of BC concentrations in seawater may be compromised when cryopreservant or theca-containing phytoplankton are present at high concentrations. Results from testing, of the modified CTO-375 in phytoplankton species commonly observed in the Gulf of Maine, indicated that samples of POC taken during spring and fall, when diatoms are dominant species, may not compromise the measured BC concentrations. However, our findings indicate that caution should be taken for BC measurements during the summer, when theca-containing dinoflagellates are the dominant species in the surface waters in this coastal area. Further research of the CTO-375 method and its adaptations to different media should continue to test different scenarios where BC measurements using this methodology would be compromised due to both over- and under-detection.

The study of organic carbon cycling in the GoM provided useful information regarding physical processes that influence the fate of BC, and its similarities and differences with non-BC organic carbon (OC). Larger fluxes of particulate matter out of the water column in August/September than in April, and positioned closer or further away from shore, influence the export of both of these fractions of organic carbon from the surface water. However, primary productivity was found to be the main source of organic carbon to the GoM, while atmospheric transport appeared to be the main transport mechanism of BC to this area. In addition, decreasing OC concentrations and relatively constant BC levels with increasing depth in the water column indicated that BC is a more recalcitrant form of OC that degrades at much slower rates. Since there are no previous estimates of BC in coastal water, comparison between the processes that govern both non-BC OC and BC with previous studies of carbon cycling allowed us to build confidence in our calculations.

Similarities between the measured BC concentrations by observing pyrene fluorescence losses (PFL) and the modified CTO-375, two methodologies with very different set of principles, further builds confidence in our results. Results using these methods suggest that the isolated material is both recalcitrant and highly sorptive. PFL is designed to measure concentrations of a carbonaceous material with enhanced sorptive nature, while CTO-375 measures the recalcitrant carbonaceous material that survives a chemothermal oxidation. Both of these characteristics conform well with the BC model proposed by Sergides et al (1987). Although this new methodology has not been as thoroughly tested as CTO-375, it allows us to overcome some of the limitations of previous methodologies: (1) sample manipulation and transfers are kept to a minimal; (2) it is able to use a wide range of environmental samples (any sample that can be placed on a filter); (3) it measures a material with a specific characteristic of our interest for sorption studies; and (4) it might be able to see both char and soot BC..

Finally, sediment records of BC fluxes suggested that BC emissions in the past 100 years were largely influenced by anthropogenic activities. More strict regulations, improvements in fuel combustion technologies, and the use of cleaner fuels (such as natural gas) were largely responsible for the observed decreases towards the end of the past century. However, with today's growing need for new alternative sources, and plans to replace gasoline with diesel in on-road vehicles and fossil fuels with coal in industry and electricity production, there are debates about whether BC emissions will continue to decrease (Miguel et al., 1998). Furthermore, with increasing evidence that local events of aerosol pollution can affect other distant places in the globe (e.g., Eglinton et al., 2002), these observations strongly encourage the transfer of science and technology to fast-growing economies like India and China, two of the major BC producers with lower environmental standards.

Recognition of water bodies as atmospheric BC sinks, and acknowledging that aerosol BC is the main transport mechanism to distant from shore sites, identifies the oceans as potential large BC reservoirs. Extrapolating our measured BC fluxes to a global scale, BC in coastal POC can account for most of the estimated annually produced biomass and fossil fuels BC (Bond et al., 2004). This work shows that the importance of BC in water bodies has been underestimated, that BC concentrations in water are needed to fully understand the transport and transformation processes of BC, and that BC concentrations in water play an active role in other important geochemical cycles. Recognizing the importance of BC in environments beyond the atmosphere strongly suggests that environmental scientists, engineers, and policy makers need to assess the presence and impacts of combustion processes. Hopefully this work will encourage more intense campaigns to measure BC in seawater, as well as collaboration between different science fields that focus on the study of BC.

**Additional implications of the thesis**

With increasing evidence that BC might be the second largest contributor to current global climate change (Ramanathan and Carmichael, 2008), measurements of BC fluxes provide information to reduce uncertainties in the atmospheric concentrations, by constraining the amount of BC that leaves the atmosphere to be incorporated into water bodies. Furthermore, BC fluxes in seawater POC can also constrain sediment and soil inputs of BC, providing a better estimate of the recalcitrant carbon potentially sequestered in these pools. If we are able to know how much BC is in the rivers and oceans of the world, we will be able to constrain how much is in the atmosphere, the sediments, and the soils, and vice versa.

**Future work**

The work presented here opens several new pathways of future research. However, here I will only mention some of the ones that I find most interesting.

Although this thesis addresses the importance of BC in POC, there are indications that BC may also be present in the methodology-defined dissolved organic carbon (DOC; Kim et al., 2004; Mannino and Harvery, 2004; Masiello and Druffel, 1998; Simpson and Hatcher, 2004) and would likely be present in the colloidal (COC) organic carbon fraction as well. If recalcitrant BC is present in seawater, as the non-BC material is recycled within the water column, it is reasonable to assume that BC-containing particles will tend to coagulate with other smaller particles present in the water column on its way to the ocean's floor. POC represents less than 20% of the total organic carbon (TOC). Therefore, the BC ocean reservoir could be much larger than expected if only BC in POC is considered. Future work in that direction would provide very important findings regarding the source of "old" ($^{14}$C-depleted ) dissolved organic carbon in the deep ocean; one of the most intriguing challenges of marine organic biochemists. Consequences of this future research would be most useful to estimate the potential of large water bodies to sequester anthropogenic carbon emissions from the atmosphere. However, further testing of the applicability of the present methodologies to measure BC in these organic carbon fractions involves a new line of research by itself.

Since these are some of the first measurements of BC in water bodies, this work leaves an open pathway for future studies to address spatial and temporal variations, especially in the open ocean, where up to now, measurements of BC in POC seawater have yet to be made. What are the concentrations of BC in open oceans? How did BC get to the most remote parts of the ocean? Is BC transported to these remote areas mainly by major episodic events, or are there

continuous inputs of BC to these areas? Are there any parts of the oceans where BC is accumulating? These are some of the unanswered questions that still need to be resolved.

One of the major difficulties of the study of black carbon is that although many different fields of science are studying this carbonaceous material, different definitions and methodologies create great gaps between researchers from different lines of research. Discrepancies in BC concentrations measured by atmospheric scientists or oceanographers, due to differences in the methodology used, stress the need to investigate the applicability and interchangeability between BC concentrations using one or another method. In addition, this line of research will require the need to continue to develop methods to unequivocally identify and quantify BC, such as transmission electron microscope (TEM) and scanning electron microscope (SEM) techniques. The later could then serve as the basis to normalize measurements made using other techniques.

## References


Aluwihare, L.I., Repeta, D. J. and Chen, R. F., 1997. A major biopolymeric component to dissolved organic carbon in seawater. Nature, 387: 166-169.

Bond, T.I., D. G. Streets, K. F. Yarber, S. M. Nelson, J. Woo, Z. Klimont, 2004. A technology-based global inventory of black and organic carbon emissions from combustion. J. Geophys. Res., 109: D14203.

Eglinton, T.I., and Repeta, D. J., 2004. Organic matter in the contemporary ocean. Teatrise Geochem., 6: 145-180.

Eglinton, T.I., G. Eglinton, L. Dupont, E. R. Scholkovitz, D. Montlucon, C. M. Reddy, 2002. Composition, age, and provenance of organic matter in NW African dust over the Atlantic Ocean. Geochem. Geophys. Geosys., 3(8): 1525-2027.

Kim, S., R. W. Kramer, P. G. Hatcher, 2003. Graphical method for analysis of ultrahigh-resolution broadband mass spectra of natural organic matter, the Van Krevelen Diagram. Anal. Chem., 75: 5336-5344.

Mannino, A., H. R. Harvey, 2004. Black carbon in estuarine and coastal ocean dissolved organic matter. Limnol. Oceanogr., 49(3): 735-740.

Masiello, C.A., and Druffel, E. R. M., 1998. Black carbon in deep-sea sediments. Science, 280: 1911-1913.

Miguel, A.H., T. W. Kirchstetter, R. A. Harley, 1998. On-road emissions of particulate polycyclic aromatic hydrocarbons and black carbon from gasoline and diesel vehicles. Environ. Sci. Technol., 32: 450-455.

Ramanathan, V., Carmichael, G., 2008. Global and regional climate changes due to black carbon. Nature Geoscience, 1: 221-228.

Sergides, C.A., Jassim, J.A., Chughtai, A.R., Smith, D.M., 1987. The structure of hexane soot. Part III: ozonation studies. Applied Spectroscopy, 41: 482-492.

Simpson, M., Hatcher, P., 2004. Determination of black carbon in natural organic matter by chemical oxidation and solid-state 13C nuclear magnetic resonance spectroscopy. Org. Chem., 35: 923-935.

# APPENDIX II

# $^{238}U$ AND $^{234}Th$ RADIONUCLIDE DISEQUILIBRIA

**Table 1.** $^{238}U$ and $^{234}Th$ radionuclide disequilibria in seawater during April 2004

| | | NISKIN | | | | | NITEX | |
|---|---|---|---|---|---|---|---|---|
| Station Name | depth | Salinity expected $^{238}U$ (dpm/m$^3$) | net error +/- dpm/m$^3$ | $^{234}Th$ dpm at collection (dpm/m$^3$) | net error +/- dpm/m$^3$ | $^{234}Th/^{238}U$ | $^{234}Th$ dpm at collection (dpm/m$^3$) | net error +/- dpm/m$^3$ |
| CCB1 | 6.4 | 2118 | 21 | 831 | 25 | 0.39 | 2.4113 | 0.1213 |
| | 9.3 | 2114 | 21 | 907 | 27 | 0.43 | | |
| | 13.1 | 2114 | 21 | 863 | 20 | 0.41 | | |
| CCB2 | 6.4 | 2143 | 21 | 489 | 19 | 0.23 | 3.6785 | 0.1847 |
| | 12.5 | 2143 | 21 | 635 | 23 | 0.30 | | |
| MWRA | 3.5 | 2045 | 20 | 373 | 15 | 0.18 | 13.0774 | 0.4884 |
| | 6.14 | 2047 | 20 | 390 | 18 | 0.19 | | |
| | 10 | 2092 | 21 | 329 | 13 | 0.16 | | |
| | 20 | 2185 | 22 | 477 | 17 | 0.22 | 9.4614 | 0.3189 |
| NMB | 2.4 | 2093 | 21 | 905 | 30 | 0.43 | | |
| | 6 | 2102 | 21 | 1070 | 29 | 0.51 | 32.5833 | 1.6293 |
| | 9.3 | 2136 | 21 | 1114 | 38 | 0.52 | | |
| | 14 | 2151 | 22 | 1591 | 73 | 0.74 | | |
| | 21 | 2156 | 22 | 1007 | 48 | 0.47 | | |
| | 24 | 2167 | 22 | 1516 | 57 | 0.70 | | |
| | 29 | 2169 | 22 | 1350 | 65 | 0.62 | | |
| | 50 | 2174 | 22 | 1655 | 79 | 0.76 | 4.4197 | 0.2218 |
| | | | 0 | | | | | |
| MER | 3 | 2072 | 21 | 1468 | 56 | 0.71 | | |
| | 6.1 | 2112 | 21 | 1552 | 96 | 0.73 | 35.4917 | 1.7748 |
| | 10.5 | 2119 | 21 | 1523 | 63 | 0.72 | | |
| | 20.2 | 2128 | 21 | 1717 | 73 | 0.81 | 11.0014 | 0.5522 |
| | | | 0 | | | | | |
| WB1 | 6 | 2136 | 21 | 1929 | 104 | 0.90 | 21.0840 | 1.0544 |
| | 25 | 2140 | 21 | 1834 | 99 | 0.86 | | |
| | 38 | 2170 | 22 | 2190 | 118 | 1.01 | | |
| | 50 | 2183 | 22 | 1581 | 87 | 0.72 | | |
| | 60 | 2186 | 22 | 2011 | 111 | 0.92 | | |
| | 80 | 2188 | 22 | 1961 | 108 | 0.90 | | |
| | 97.5 | 2203 | 22 | 1909 | 105 | 0.87 | | |
| | 140 | 2213 | 22 | 1974 | 109 | 0.89 | | |
| | | | 0 | | | | | |
| WB2 | 6 | 2113 | 21 | 1875 | 101 | 0.89 | 201.1258 | 10.0565 |
| | 11 | 2132 | 21 | 2096 | 113 | 0.98 | | |
| | 16.5 | 2135 | 21 | 2029 | 110 | 0.95 | | |
| | 25 | 2135 | 21 | 2056 | 111 | 0.96 | | |
| | 30 | 2139 | 21 | 2021 | 109 | 0.94 | 3.7057 | 0.1865 |
| | 50 | 2158 | 22 | 1792 | 99 | 0.83 | | |
| | 65 | 2171 | 22 | 1887 | 104 | 0.87 | | |
| | 100 | 2175 | 22 | 1735 | 95 | 0.80 | | |

**Table 1 (continuation).** $^{238}U$ and $^{234}Th$ radionuclide disequilibria in seawater during April 2004

| Station Name | depth | Salinity expected $^{238}U$ (dpm/m$^3$) | NISKIN net error +/- dpm/m$^3$ | NISKIN $^{234}Th$ dpm at collection (dpm/m$^3$) | NISKIN net error +/- dpm/m$^3$ | $^{234}Th/^{238}U$ | NITEX $^{234}Th$ dpm at collection (dpm/m$^3$) | NITEX net error +/- dpm/m$^3$ |
|---|---|---|---|---|---|---|---|---|
| OCB | 6 | 2072 | 21 | 662 | 38 | 0.32 | 2.5928 | 0.1298 |
| | 12 | 2093 | 21 | 691 | 40 | 0.33 | 13.5807 | 0.6792 |
| | 24 | 2134 | 21 | 747 | 43 | 0.35 | 35.5566 | 1.7779 |
| | 36 | 2145 | 21 | 904 | 52 | 0.42 | | |
| | | | 0 | | | | | |
| IPB | 3 | 1857 | 19 | 165 | 7 | 0.09 | 7.4383 | 0.3728 |
| | 6 | 2055 | 21 | 591 | 26 | 0.29 | 10.8626 | 0.4652 |
| | | | 0 | | | | | |
| EPB | 6 | 2139 | 21 | 1915 | 105 | 0.90 | 18.2691 | 0.9136 |
| | 13 | 2139 | 21 | 1937 | 107 | 0.91 | | |
| | 27 | 2139 | 21 | 2066 | 114 | 0.97 | | |
| | 35 | 2139 | 21 | 1969 | 108 | 0.92 | 6.4472 | 0.3228 |
| | 63 | 2178 | 22 | 2078 | 114 | 0.95 | | |
| | 93 | 2200 | 22 | 2193 | 121 | 1.00 | | |
| | 120 | 2210 | 22 | 2199 | 121 | 0.99 | | |
| | 160 | 2214 | 22 | 1627 | 90 | 0.73 | | |
| | | | 0 | | | | | |
| JB | 6 | 2119 | 21 | 2201 | 132 | 1.04 | 46.4811 | 2.3242 |
| | 20 | 2119 | 21 | 2049 | 123 | 0.97 | | |
| | 40 | 2129 | 21 | 1829 | 110 | 0.86 | | |
| | 60 | 2143 | 21 | 2243 | 135 | 1.05 | 0.5395 | 0.0272 |
| | 80 | 2155 | 22 | 2023 | 121 | 0.94 | | |
| | 120 | 2192 | 22 | 780 | 49 | 0.36 | | |
| | 145 | 2215 | 22 | 2387 | 48 | 1.08 | | |
| | 200 | 2262 | 23 | 1615 | 32 | 0.71 | | |
| | | | 0 | | | | | |
| GB | 6 | 2186 | 22 | 1616 | 56 | 0.74 | 15.3900 | 0.5788 |
| | 13 | 2193 | 22 | 594 | 26 | 0.27 | | |
| | 20 | 2196 | 22 | 1407 | 50 | 0.64 | | |
| | 35 | 2201 | 22 | 1361 | 49 | 0.62 | | |
| | 60 | 2208 | 22 | 1408 | 51 | 0.64 | 12.4286 | 0.6276 |
| | 100 | 2216 | 22 | 1564 | 77 | 0.71 | | |
| | 140 | 2219 | 22 | 1009 | 64 | 0.45 | | |
| GSC | 6 | 2170 | 22 | 1846 | 81 | 0.85 | 42.3551 | 2.1178 |
| | 20 | 2181 | 22 | 2003 | 88 | 0.92 | | |
| | 30 | 2188 | 22 | 1797 | 79 | 0.82 | | |
| | 60 | 2197 | 22 | 1867 | 82 | 0.85 | | |
| | 85 | 2200 | 22 | 1832 | 99 | 0.83 | | |
| | 120 | 2211 | 22 | 1816 | 98 | 0.82 | | |
| | 140 | 2216 | 22 | 1999 | 108 | 0.90 | | |
| | 180 | 2225 | 22 | 1504 | 70 | 0.68 | | |

**Table 2.** $^{238}U$ and $^{234}Th$ radionuclide disequilibria in seawater during April 2004

| | | NISKIN | | | | | NITEX | |
|---|---|---|---|---|---|---|---|---|
| Station Name | depth | Salinity expected $^{238}U$ (dpm/m$^3$) | net error +/- dpm/m$^3$ | $^{234}Th$ dpm at collection (dpm/m$^3$) | net error +/- dpm/m$^3$ | $^{234}Th/^{238}U$ | $^{234}Th$ dpm at collection (dpm/m$^3$) | net error +/- dpm/m$^3$ |
| GSC | 5 | 2107 | 21 | 1166.27 | 11.84 | 0.55 | 2.86 | 0.14 |
| | 9.9 | 2109 | 21 | 1171.13 | 12.38 | 0.56 | | |
| | 15 | 2131 | 21 | 1400.17 | 13.51 | 0.66 | | |
| | 19 | 2147 | 21 | 1741.40 | 16.67 | 0.81 | | |
| | 32 | 2159 | 22 | 1715.14 | 14.60 | 0.79 | | |
| | 57 | 2169 | 22 | 1746.18 | 16.72 | 0.81 | 0.60 | 0.03 |
| | 79 | 2174 | 22 | 2456.66 | 23.52 | 1.13 | | |
| | 97 | 2173 | 22 | 1856.48 | 17.38 | 0.85 | | |
| | 122 | 2191 | 22 | 2260.41 | 21.16 | 1.03 | | |
| | 141 | 2202 | 22 | 2475.70 | 23.17 | 1.12 | | |
| GB | 4 | 2130 | 21 | 1868.36 | 17.49 | 0.88 | 3.49 | 0.17 |
| | 9 | 2137 | 21 | 1557.55 | 16.57 | 0.73 | | |
| | 17 | 2137 | 21 | 1677.15 | 15.66 | 0.78 | | |
| | 46 | 2163 | 22 | 2226.79 | 21.32 | 1.03 | | |
| | 77 | 2201 | 22 | 283.99 | 2.73 | 0.13 | 1.13 | 0.06 |
| | 98 | 2207 | 22 | 2147.42 | 20.56 | 0.97 | | |
| | 121 | 2251 | 23 | 1969.27 | 18.85 | 0.88 | | |
| | 146 | 2273 | 23 | 1749.22 | 16.75 | 0.77 | | |
| JB | 5 | 2140 | 21 | 1990.91 | 18.91 | 0.93 | 1.54 | 0.08 |
| | 15 | 2144 | 21 | 545.51 | 5.00 | 0.25 | | |
| | 29.8 | 2166 | 22 | 2193.12 | 18.66 | 1.01 | | |
| | 44 | 2184 | 22 | 2245.21 | 19.11 | 1.03 | | |
| | 79 | 2218 | 22 | 2031.74 | 20.75 | 0.92 | 0.28 | 0.01 |
| | 112 | 2236 | 22 | 1361.18 | 13.90 | 0.61 | | |
| | 147 | 2242 | 22 | 2267.58 | 23.16 | 1.01 | | |
| | 196 | 2262 | 23 | 1840.49 | 18.80 | 0.81 | | |
| EPB | 4.6 | 2128 | 21 | 1002.77 | 7.92 | 0.47 | 0.89 | 0.04 |
| | 9.5 | 2141 | 21 | 1118.08 | 9.28 | 0.52 | | |
| | 24 | 2168 | 22 | 1737.09 | 14.42 | 0.80 | | |
| | 49 | 2177 | 22 | 1605.36 | 12.30 | 0.74 | | |
| | 78 | 2196 | 22 | 1740.67 | 13.70 | 0.79 | 1.38 | 0.07 |
| | 98 | 2186 | 22 | 1569.43 | 11.02 | 0.72 | | |
| | 147 | 2199 | 22 | 2112.27 | 21.57 | 0.96 | | |
| IPB | 1.4 | 1969 | 20 | 25.75 | 0.24 | 0.01 | 1.01 | 0.05 |
| | 2.5 | 2030 | 20 | 372.54 | 3.58 | 0.18 | | |
| | 5.4 | 2063 | 21 | 451.25 | 4.31 | 0.22 | 1.22 | 0.06 |
| | 8.6 | 2055 | 21 | 408.50 | 3.76 | 0.20 | | |

**Table 2 (continuation).** $^{238}U$ and $^{234}Th$ radionuclide disequilibria in seawater during April 2004

| | | NISKIN | | | | | NITEX | |
|---|---|---|---|---|---|---|---|---|
| Station Name | depth | Salinity expected $^{238}U$ (dpm/m$^3$) | net error +/- dpm/m$^3$ | $^{234}Th$ dpm at collection (dpm/m$^3$) | net error +/- dpm/m$^3$ | $^{234}Th/^{238}U$ | $^{234}Th$ dpm at collection (dpm/m$^3$) | net error +/- dpm/m$^3$ |
| CB | 1.8 | 2079 | 21 | 837.89 | 7.07 | 0.40 | 1.31 | 0.07 |
| | 4 | 2109 | 21 | 855.64 | 5.13 | 0.41 | | |
| | 9.4 | 2118 | 21 | 825.66 | 6.76 | 0.39 | | |
| | 18.8 | 2127 | 21 | 895.87 | 7.06 | 0.42 | 1.53 | 0.08 |
| | 29 | 2134 | 21 | 835.06 | 6.58 | 0.39 | | |
| WB | 4.5 | 2084 | 21 | 892 | 4 | 0.43 | | |
| | 9.8 | 2111 | 21 | 1347 | 6 | 0.64 | 0.71 | 0.04 |
| | 24 | 2154 | 22 | 1591 | 7 | 0.74 | | |
| | 49 | 2165 | 22 | 1758 | 7 | 0.81 | | |
| | 78 | 2176 | 22 | 1988 | 8 | 0.91 | 1.05 | 0.05 |
| | 107 | 2185 | 22 | 2241 | 18 | 1.03 | | |
| | 155 | 2207 | 22 | 2246 | 18 | 1.02 | | |
| | 207 | 2230 | 22 | 1994 | 8 | 0.89 | | |
| MER | 1.8 | 2086 | 21 | 795 | 7 | 0.38 | 1.68 | 0.08 |
| | 5.5 | 2098 | 21 | 913 | 7 | 0.44 | | |
| | 11.8 | 2112 | 21 | 821 | 7 | 0.39 | | |
| | 19.6 | 2126 | 21 | 907 | 7 | 0.43 | 1.21 | 0.06 |
| | 24 | 2127 | 21 | 1029 | 8 | 0.48 | | |
| MWRA | 1.8 | 2089 | 21 | 1385 | 14 | 0.66 | | |
| | 5.7 | 2105 | 21 | 1290 | 13 | 0.61 | 1.73 | 0.09 |
| | 12 | 2117 | 21 | 1190 | 12 | 0.56 | | |
| | 19.6 | 2121 | 21 | 1419 | 11 | 0.67 | 0.40 | 0.02 |
| CCB | 5.8 | 2106 | 21 | 1043 | 11 | 0.50 | 1.11 | 0.06 |
| | 11.8 | 2121 | 21 | 1145 | 12 | 0.54 | | |
| | 19.5 | 2130 | 21 | 1577 | 17 | 0.74 | 5.93 | 0.30 |
| | 25.4 | 2129 | 21 | 773 | 6 | 0.36 | | |

# APPENDIX III

## SEDIMENT CRS MODEL CALCULATIONS AND $^{210}Pb$, $^{214}Pb$, AND $^{137}Cs$ DATA

**Constant rate of supply (CRS) model and calculations.**

The constant rate of supply model (CRS; Appleby and Oldfield, 1978; Appleby, 2001) assumes that the rate of deposition of unsupported $^{210}$Pb from the atmosphere is constant, but that sedimentation rates and compaction change throughout the sediment core.

The activity of excess/unsupported $^{210}$Pb ($^{210}Pb_{exc}$) in sediment deposits at a given depth ($C_{(x)}$; dpm/g) decays with time $t$ according to its natural radioactive decay

$$C_{(t)} = C_{(0)} \cdot \exp^{-\lambda t} \qquad (1)$$

where $C_{(0)}$ is the $^{210}Pb_{exc}$ activity at the sediment-water interface (dpm/g) and $\lambda$ is the decay constant of $^{210}$Pb (0.03114 1/yr). After decay, the remaining $^{210}Pb_{exc}$ in the sediment record from past inputs at time $\tau$, after a small interval time d$\tau$, can be expressed in terms of the $^{210}$Pb rate of supply ($P$),

$$Pe^{-\lambda\tau}d\tau. \qquad (2)$$

Assuming $P$ to be constant, the amount of $^{210}$Pb present in the sediment at an age $t$ or greater, can then be expressed as

$$A = \int_t^{\infty} Pe^{\lambda\tau}d\tau = \frac{P}{\lambda}e^{-\lambda t}, \qquad (3)$$

where $A_{(0)} = P/\lambda$ is the total $^{210}Pb_{exc}$ inventory when equation (2) is integrated from $t = 0$ to $\infty$, and the residual $^{210}Pb_{exc}$ in sediments below a depth $x$ can then be calculated as

$$A_{(x)} = A_{(0)} \cdot e^{\lambda t}. \qquad (4)$$

$A_{(x)}$ and $A_{(0)}$ at each sediment layer can be calculated by integrating the $^{210}Pb_{exc}$ sediment concentration below a depth ($x$) and the whole depth profile, respectively,

$$A = \int_x^{\infty} C_{(x)}dx, \qquad A_{(o)} = \int_0^{\infty} C_{(x)}dx. \qquad (5)$$

Equation (5) can be estimated by numerical integration by multiplying the concentration of $^{210}Pb_{exc}$ ($C_{(x)}$) by the dry mass ($m_{(x)}$; g/cm$^2$) at that given depth ($x$).

$$A = \sum_{x}^{\infty} C_{(x)} \cdot m_{(x)}, \qquad A_{(o)} = \sum_{0}^{\infty} C_{(x)} \cdot m_{(x)}. \quad (6)$$

Where $m_{(x)}$ can be estimated as the dry bulk density (DBD, g/cm$^3$) times the thickness of the sediment layer ($T_{(x)}$)

$$DBD_{(X)} = (1 - \phi_{(x)}) \cdot \rho_{sed(x)} \quad (7)$$

$$m_{(x)} = DBD_{(x)} \cdot T_{(x)}, \quad (8)$$

and $\rho(x)$ and $\Phi(x)$ are the density and porosity at a given depth.

The age of the sediment at a given depth (x) can then be calculated by rearranging equation (4),

$$t = \frac{1}{\lambda} \ln\left(\frac{A_{(0)}}{A_{(x)}}\right). \quad (9)$$

Since sediments below the sediment-water interface, will be of age $t = m/r$, where $r$ is the dry mass sedimentation rate (g/cm$^2$·yr), equation (1) can then be expressed as

$$C_{(x)} = C_{(0)} \cdot \exp^{-\lambda \frac{m}{r}} \quad (10)$$

where $C_{(0)} = P/r$, and equation (10) can then be written as

$$r = \frac{P}{C_{(x)}} \cdot \exp^{-\lambda t}. \quad (11)$$

Calculating $P$ from substituting (4) and (9) into (11), we can then estimate $r$ (g/cm$^2$·yr)

$$r = \frac{\lambda A_{(x)}}{C_{(x)}}. \quad (10)$$

Sedimentation rate in cm/yr would then be $r/DBD$.

**Table 1.** Massachusetts Water Resources Authority (MWRA) sediment CRS model.

| Midpoint depth cm | | $\rho_{sed}$ (g/cm$^3$) | Porosity | DBD g/cm$^3$ | m g/cm$^2$ | $^{210}Pb_{exc}$ dpm/g | $^{210}Pb_{exc}$ Inventory dpm/cm$^2$ | CRS (cm/yr) | t yr | Model Date |
|---|---|---|---|---|---|---|---|---|---|---|
| 0.25 | 0-0.5 | 1.67 | 0.81 | 0.31 | 0.08 | 8.46 | 44.62 | 0.53 | 0.00 | 2004 |
| 0.75 | 0.5-1.0 | 0.52 | 0.76 | 0.12 | 0.06 | 7.69 | 43.96 | 1.45 | 0.48 | 2004 |
| 1.25 | 1.0-1.5 | 1.27 | 0.75 | 0.32 | 0.16 | 6.45 | 43.49 | 0.66 | 0.82 | 2003 |
| 1.75 | 1.5-2.0 | 2.43 | 0.79 | 0.51 | 0.25 | 5.79 | 42.46 | 0.45 | 1.59 | 2002 |
| 2.25 | 2-2.5 | 2.18 | 0.77 | 0.51 | 0.25 | 8.16 | 41.00 | 0.31 | 2.72 | 2001 |
| 2.75 | 2.5-3.0 | 2.10 | 0.71 | 0.61 | 0.31 | 7.33 | 38.93 | 0.27 | 4.38 | 2000 |
| 3.25 | 3.0-3.5 | 1.52 | 0.61 | 0.58 | 0.29 | 7.72 | 36.68 | 0.25 | 6.29 | 1998 |
| 3.75 | 3.5-4.0 | 1.86 | 0.64 | 0.66 | 0.33 | 6.82 | 34.43 | 0.24 | 8.33 | 1996 |
| 4.25 | 4.0-4.5 | 1.93 | 0.65 | 0.68 | 0.34 | 4.77 | 32.16 | 0.31 | 10.52 | 1993 |
| 4.75 | 4.5-5.0 | 1.92 | 0.65 | 0.68 | 0.34 | 4.95 | 30.55 | 0.28 | 12.17 | 1992 |
| 5.25 | 5.0-5.5 | 1.76 | 0.62 | 0.66 | 0.33 | 4.26 | 28.88 | 0.32 | 13.97 | 1990 |
| 5.75 | 5.5-6.0 | 1.99 | 0.64 | 0.72 | 0.36 | 4.16 | 27.47 | 0.29 | 15.58 | 1988 |
| 6.25 | 6.0-6.5 | 1.74 | 0.60 | 0.69 | 0.34 | 5.13 | 25.97 | 0.23 | 17.38 | 1987 |
| 6.75 | 6.5-7.0 | 2.47 | 0.68 | 0.79 | 0.40 | 4.39 | 24.21 | 0.22 | 19.64 | 1984 |
| 7.25 | 7.0-7.5 | 2.46 | 0.65 | 0.87 | 0.43 | 4.16 | 22.47 | 0.19 | 22.04 | 1982 |
| 7.75 | 7.5-8.0 | 2.71 | 0.67 | 0.91 | 0.45 | 4.06 | 20.66 | 0.17 | 24.73 | 1979 |
| 8.25 | 8.0-8.5 | 2.54 | 0.55 | 1.13 | 0.57 | 3.42 | 18.81 | 0.15 | 27.74 | 1976 |
| 8.75 | 8.5-9.0 | 2.54 | 0.55 | 1.13 | 0.57 | 2.44 | 16.87 | 0.19 | 31.23 | 1973 |
| 9.25 | 9.0-9.5 | 1.94 | 0.52 | 0.94 | 0.47 | 3.53 | 15.49 | 0.15 | 33.99 | 1970 |
| 10 | 9.5-10.5 | 2.25 | 0.49 | 1.16 | 0.87 | 3.37 | 13.83 | 0.11 | 37.61 | 1966 |
| 11 | 10.5-11.5 | 2.47 | 0.48 | 1.29 | 1.29 | 2.21[a] | 10.91 | 0.12 | 45.22 | 1959 |
| 12 | 11.5-12.5 | 1.90 | 0.43 | 1.08 | 1.08 | 1.93[a] | 8.07 | 0.12 | 54.92 | 1949 |
| 13 | 12.5-13.5 | 2.34 | 0.46 | 1.26 | 1.26 | 1.19 | 5.98 | 0.12 | 64.55 | 1939 |
| 14 | 13.5-14.5 | 2.45 | 0.48 | 1.27 | 1.27 | 0.67 | 4.47 | 0.16 | 73.87 | 1930 |
| 15 | 14.5-15.5 | 2.26 | 0.40 | 1.35 | 1.35 | 1.34 | 3.62 | 0.06 | 80.62 | 1923 |
| 16 | 15.5-16.5 | 2.26 | 0.40 | 1.35 | 1.35 | 1.12[a] | 1.81 | 0.04 | 102.85 | 1901 |
| 17 | 16.5-17.5 | 2.14 | 0.40 | 1.27 | 1.27 | 0.24 | 0.31 | 0.03 | 159.87 | 1844 |

[a]Data points interpolated due to uncertainties in actual data points. See Table 2.

**Table 2.** Massachusetts Water Resources Authority (MWRA) sediment $^{210}Pb$ and $^{214}Pb$.

| $^{210}Pb$ Lead-210 Excess only (already subtracted supported) | | | | | $^{214}Pb$ Lead-214 | | | | |
|---|---|---|---|---|---|---|---|---|---|
| counts/min | dpm/g | avg depth | min | max | counts/min | dpm/g | avg depth | min | max |
| 0.11 | 8.5 | 0.25 | 0.0 | 0.5 | 0.09 | 1.7 | 0.25 | 0.0 | 0.5 |
| 0.11 | 7.7 | 0.75 | 0.5 | 1.0 | 0.10 | 2.2 | 0.75 | 0.5 | 1.0 |
| 0.10 | 6.4 | 1.25 | 1.0 | 1.5 | 0.10 | 2.1 | 1.25 | 1.0 | 1.5 |
| 0.10 | 5.8 | 1.75 | 1.5 | 2.0 | 0.13 | 2.8 | 1.75 | 1.5 | 2.0 |
| 0.11 | 8.2 | 2.25 | 2.0 | 2.5 | 0.10 | 2.1 | 2.25 | 2.0 | 2.5 |
| 0.22 | 7.3 | 2.75 | 2.5 | 3.0 | 0.17 | 1.9 | 2.75 | 2.5 | 3.0 |
| 0.20 | 7.7 | 3.25 | 3.0 | 3.5 | 0.08 | 0.8 | 3.25 | 3.0 | 3.5 |
| 0.19 | 6.8 | 3.75 | 3.5 | 4.0 | 0.09 | 0.9 | 3.75 | 3.5 | 4.0 |
| 0.15 | 4.8 | 4.25 | 4.0 | 4.5 | 0.15 | 1.6 | 4.25 | 4.0 | 4.5 |
| 0.16 | 4.9 | 4.75 | 4.5 | 5.0 | 0.16 | 1.8 | 4.75 | 4.5 | 5.0 |
| 0.15 | 4.3 | 5.25 | 5.0 | 5.5 | 0.17 | 1.8 | 5.25 | 5.0 | 5.5 |
| 0.15 | 4.2 | 5.75 | 5.5 | 6.0 | 0.18 | 2.1 | 5.75 | 5.5 | 6.0 |
| 0.16 | 5.1 | 6.25 | 6.0 | 6.5 | 0.14 | 1.5 | 6.25 | 6.0 | 6.5 |
| 0.14 | 4.4 | 6.75 | 6.5 | 7.0 | 0.12 | 1.3 | 6.75 | 6.5 | 7.0 |
| 0.15 | 4.2 | 7.25 | 7.0 | 7.5 | 0.17 | 1.9 | 7.25 | 7.0 | 7.5 |
| 0.14 | 4.1 | 7.75 | 7.5 | 8.0 | 0.15 | 1.7 | 7.75 | 7.5 | 8.0 |
| 0.13 | 3.4 | 8.25 | 8.0 | 8.5 | 0.16 | 1.8 | 8.25 | 8.0 | 8.5 |
| 0.10 | 2.4 | 8.75 | 8.5 | 9.0 | 0.16 | 1.7 | 8.75 | 8.5 | 9.0 |
| 0.14 | 3.5 | 9.25 | 9.0 | 9.5 | 0.20 | 2.3 | 9.25 | 9.0 | 9.5 |
| 0.14 | 3.4 | 10.00 | 9.5 | 10.5 | 0.22 | 2.5 | 10.00 | 9.5 | 10.5 |
| 0.07 | 2.2 | 11.00 | 10.5 | 11.5 | 0.22 | 2.5 | 11.00 | 10.5 | 11.5 |
| 0.08 | 1.9 | 12.00 | 11.5 | 12.5 | 0.21 | 2.4 | 12.00 | 11.5 | 12.5 |
| 0.09 | 1.2 | 13.00 | 12.5 | 13.5 | 0.22 | 2.5 | 13.00 | 12.5 | 13.5 |
| 0.08 | 0.7 | 14.00 | 13.5 | 14.5 | 0.22 | 2.5 | 14.00 | 13.5 | 14.5 |
| 0.09 | 1.3 | 15.00 | 14.5 | 15.5 | 0.19 | 2.1 | 15.00 | 14.5 | 15.5 |
| 0.13 | 1.1 | 16.00 | 15.5 | 16.5 | 0.21 | 2.4 | 16.00 | 15.5 | 16.5 |
| 0.06 | 0.2 | 17.00 | 16.5 | 17.5 | 0.20 | 2.2 | 17.00 | 16.5 | 17.5 |
| 0.07 | 0.4 | 18 | 17.5 | 18.5 | 0.20 | 2.2 | 18 | 17.5 | 18.5 |
| 0.07 | 0.6 | 19 | 18.5 | 19.5 | 0.20 | 2.2 | 19 | 18.5 | 19.5 |

**Table 3**. Massachusetts Water Resources Authority (MWRA) sediment $^{137}C$.

| $^{137}Cs$ | Cesium-137 | | | |
|---|---|---|---|---|
| counts/min/g | cpm/g (x$10^3$) | avg depth | min | max |
| -4.53E-04 | 0.0 | 0.25 | 0.0 | 0.5 |
| 8.85E-04 | 0.9 | 0.75 | 0.5 | 1.0 |
| -6.07E-04 | 0.0 | 1.25 | 1.0 | 1.5 |
| 4.40E-04 | 0.4 | 1.75 | 1.5 | 2.0 |
| -8.71E-05 | 0.0 | 2.25 | 2.0 | 2.5 |
| 1.16E-05 | 0.0 | 2.75 | 2.5 | 3.0 |
| -6.85E-05 | 0.0 | 3.25 | 3.0 | 3.5 |
| 2.47E-04 | 0.2 | 3.75 | 3.5 | 4.0 |
| 1.55E-03 | 1.5 | 4.25 | 4.0 | 4.5 |
| -6.40E-04 | 0.0 | 4.75 | 4.5 | 5.0 |
| -4.59E-05 | 0.0 | 5.25 | 5.0 | 5.5 |
| -1.38E-05 | 0.0 | 5.75 | 5.5 | 6.0 |
| 3.11E-05 | 0.0 | 6.25 | 6.0 | 6.5 |
| 0.00E+00 | 0.0 | 6.75 | 6.5 | 7.0 |
| 1.03E-03 | 1.0 | 7.25 | 7.0 | 7.5 |
| 1.41E-04 | 0.1 | 7.75 | 7.5 | 8.0 |
| -6.40E-05 | 0.0 | 8.25 | 8.0 | 8.5 |
| -1.04E-04 | 0.0 | 8.75 | 8.5 | 9.0 |
| -1.03E-04 | 0.0 | 9.25 | 9.0 | 9.5 |
| 1.74E-03 | 1.7 | 10.00 | 9.5 | 10.5 |
| -4.13E-04 | 0.0 | 11.00 | 10.5 | 11.5 |
| -9.55E-04 | 0.0 | 12.00 | 11.5 | 12.5 |
| -1.17E-04 | 0.0 | 13.00 | 12.5 | 13.5 |
| -2.40E-05 | 0.0 | 14.00 | 13.5 | 14.5 |
| -8.25E-04 | 0.0 | 15.00 | 14.5 | 15.5 |
| -6.00E-05 | 0.0 | 16.00 | 15.5 | 16.5 |
| 1.60E-05 | 0.0 | 17.00 | 16.5 | 17.5 |
| 3.45E-05 | 0.0 | 18 | 17.5 | 18.5 |
| -5.88E-04 | 0.0 | 19 | 18.5 | 19.5 |

**Table 4**. Wilkinson Basin (WB) sediment CRS model.

| Midpoint depth cm | $\rho_{sed}$ (g/cm$^3$) | Porosity | DBD g/cm$^3$ | m g/cm$^2$ | $^{210}Pb_{exc}$ dpm/g | $^{210}Pb_{exc}$Invent dpm/cm$^2$ | CRS (cm/yr) | t yr | Model Date |
|---|---|---|---|---|---|---|---|---|---|
| 0.25 | 0.96 | 0.83 | 0.16 | 0.04 | 9.2 | 32.77 | 0.68 | 13.86 | 2004 |
| 0.75 | 1.67 | 0.85 | 0.26 | 0.13 | 10.0 | 32.39 | 0.39 | 14.22 | 1990 |
| 1.25 | 1.46 | 0.84 | 0.23 | 0.12 | 8.8 | 31.10 | 0.48 | 15.54 | 1988 |
| 1.75 | 0.76 | 0.70 | 0.23 | 0.12 | 10.3 | 30.08 | 0.39 | 16.60 | 1987 |
| 2.50 | 2.36 | 0.86 | 0.34 | 0.26 | 6.8 | 28.89 | 0.39 | 17.90 | 1986 |
| 3.50 | 1.48 | 0.82 | 0.27 | 0.27 | 8.7 | 27.15 | 0.36 | 19.89 | 1984 |
| 4.50 | 1.76 | 0.82 | 0.32 | 0.32 | 7.6 | 24.81 | 0.31 | 22.78 | 1981 |
| 5.50 | 1.97 | 0.81 | 0.37 | 0.37 | 6.2 | 22.35 | 0.30 | 26.14 | 1978 |
| 7.00 | 2.93 | 0.87 | 0.38 | 0.58 | 7.3 | 20.06 | 0.22 | 29.61 | 1974 |
| 9.00 | 2.77 | 0.84 | 0.45 | 0.90 | 5.6 | 15.83 | 0.19 | 37.22 | 1967 |
| 12.00 | 2.36 | 0.82 | 0.43 | 1.30 | 3.9 | 10.73 | 0.20 | 49.71 | 1954 |
| 16.00 | 2.64 | 0.80 | 0.53 | 2.11 | 1.3 | 5.72 | 0.26 | 69.88 | 1934 |
| 20.00 | 2.96 | 0.82 | 0.52 | 2.08 | 1.1 | 2.99 | 0.16 | 90.70 | 1913 |
| 26.00 | 1.60 | 0.71 | 0.46 | 2.75 | 0.3 | 0.69 | 0.19 | 137.86 | 1866 |

**Table 5.** Wilkinson Basin (WB) sediment $^{210}Pb$ and $^{214}Pb$.

| $^{210}Pb$ Lead-210 Excess only (already subtracted supported) | | | | | $^{214}Pb$ Lead-214 | | | | |
|---|---|---|---|---|---|---|---|---|---|
| counts/min | dpm/g | avg depth | min | max | counts/min | dpm/g | avg depth | min | max |
| 0.28 | 9.2 | 0.25 | 0 | 0.5 | 0.16 | 1.6 | 0.25 | 0 | 0.5 |
| 0.29 | 10.0 | 0.75 | 0.5 | 1 | 0.13 | 1.2 | 0.75 | 0.5 | 1 |
| 0.28 | 8.8 | 1.25 | 1.0 | 1.5 | 0.16 | 1.8 | 1.25 | 1.0 | 1.5 |
| 0.30 | 10.3 | 1.75 | 1.5 | 2.0 | 0.14 | 1.3 | 1.75 | 1.5 | 2.0 |
| 0.22 | 6.8 | 2.50 | 2.0 | 3.0 | 0.16 | 1.7 | 2.50 | 2.0 | 3.0 |
| 0.26 | 8.7 | 3.50 | 3.0 | 4.0 | 0.13 | 1.2 | 3.50 | 3.0 | 4.0 |
| 0.24 | 7.6 | 4.50 | 4.0 | 5.0 | 0.15 | 1.5 | 4.50 | 4.0 | 5.0 |
| 0.22 | 6.2 | 5.50 | 5.0 | 6.0 | 0.17 | 1.9 | 5.50 | 5.0 | 6.0 |
| 0.24 | 7.3 | 7.00 | 6.0 | 8.0 | 0.16 | 1.8 | 7.00 | 6.0 | 8.0 |
| 0.19 | 5.6 | 9.00 | 8.0 | 10.0 | 0.15 | 1.5 | 9.00 | 8.0 | 10.0 |
| 0.15 | 3.9 | 12.00 | 10.0 | 14.0 | 0.15 | 1.5 | 12.00 | 10.0 | 14.0 |
| 0.10 | 1.3 | 16.00 | 14.0 | 18.0 | 0.16 | 1.8 | 16.00 | 14.0 | 18.0 |
| 0.08 | 1.1 | 20.00 | 18.0 | 22.0 | 0.14 | 1.3 | 20.00 | 18.0 | 22.0 |
| 0.07 | 0.3 | 26.00 | 22.0 | 30.0 | 0.16 | 1.7 | 26.00 | 22.0 | 30.0 |
| 0.05 | -1.0 | 34.00 | 30.0 | 38.0 | 0.17 | 2.0 | 34.00 | 30.0 | 38.0 |
| 0.04 | -1.0 | 42.50 | 38.0 | 47.0 | 0.16 | 1.8 | 42.50 | 38.0 | 47.0 |

**Table 6**. Wilkinson Basin (WB) sediment $^{137}C$

| $^{137}Cs$ | Cesium-137 | | | |
|---|---|---|---|---|
| counts/min/g | cpm/g (x$10^3$) | avg depth | min | max |
| -3.69E-04 | 0.00 | 0.25 | 0 | 0.5 |
| 2.01E-03 | 0.00 | 0.75 | 0.5 | 1 |
| 8.98E-04 | 0.90 | 1.25 | 1.0 | 1.5 |
| 1.98E-03 | 1.98 | 1.75 | 1.5 | 2.0 |
| 4.38E-03 | 4.38 | 2.50 | 2.0 | 3.0 |
| 2.60E-03 | 2.60 | 3.50 | 3.0 | 4.0 |
| 2.50E-03 | 2.50 | 4.50 | 4.0 | 5.0 |
| 1.80E-03 | 1.80 | 5.50 | 5.0 | 6.0 |
| 2.56E-03 | 2.56 | 7.00 | 6.0 | 8.0 |
| 3.18E-04 | 0.32 | 9.00 | 8.0 | 10.0 |
| 5.45E-04 | 0.55 | 12.00 | 10.0 | 14.0 |
| 8.41E-04 | 0.00 | 16.00 | 14.0 | 18.0 |
| 1.73E-03 | 0.00 | 20.00 | 18.0 | 22.0 |
| 3.20E-04 | 0.00 | 26.00 | 22.0 | 30.0 |
| 8.55E-04 | 0.00 | 34.00 | 30.0 | 38.0 |
| 1.52E-04 | 0.00 | 42.50 | 38.0 | 47.0 |

**Table 7**. Jordan Basin (JB) sediment CRS calculation

| Midpoint depth cm | | $\rho_{sed}$ (g/cm$^3$) | Porosity | DBD g/cm$^3$ | m g/cm$^2$ | $^{210}Pb_{exc}$ dpm/g | $^{210}Pb_{exc}$Invent dpm/cm$^2$ | CRS (cm/y) | t yr | Model Date |
|---|---|---|---|---|---|---|---|---|---|---|
| 0.25 | 0-0.5 | 2.05 | 0.87 | 0.26 | 0.07 | 14.08 | 93.87 | 0.79 | 0.00 | 2004 |
| 0.75 | 0.5-1.0 | 1.96 | 0.86 | 0.27 | 0.13 | 14.28 | 92.94 | 0.76 | 0.32 | 2004 |
| 1.25 | 1.0-1.5 | 2.67 | 0.88 | 0.32 | 0.16 | 12.48 | 91.05 | 0.72 | 0.98 | 2003 |
| 1.75 | 1.5-2.0 | 3.56 | 0.90 | 0.34 | 0.17 | 14.60 | 89.08 | 0.56 | 1.68 | 2002 |
| 2.50 | 2-3 | 3.17 | 0.91 | 0.29 | 0.22 | 13.38 | 86.60 | 0.69 | 2.59 | 2001 |
| 3.50 | 3-4 | 2.32 | 0.87 | 0.29 | 0.29 | 11.26 | 83.69 | 0.79 | 3.69 | 2000 |
| 4.50 | 4-5 | 2.09 | 0.84 | 0.33 | 0.33 | 10.01 | 80.38 | 0.76 | 4.98 | 1999 |
| 5.50 | 5-6 | 2.74 | 0.87 | 0.36 | 0.36 | 9.15 | 77.09 | 0.72 | 6.32 | 1998 |
| 7.00 | 6-8 | 2.53 | 0.87 | 0.33 | 0.50 | 8.63 | 73.76 | 0.81 | 7.74 | 1996 |
| 9.00 | 8-10 | 3.21 | 0.89 | 0.37 | 0.73 | 7.55 | 69.48 | 0.78 | 9.66 | 1994 |
| 12.00 | 10-14 | 2.16 | 0.82 | 0.39 | 1.17 | 7.25 | 63.95 | 0.70 | 12.32 | 1992 |
| 16.00 | 14-18 | 2.78 | 0.84 | 0.45 | 1.81 | 6.74 | 55.48 | 0.57 | 16.89 | 1987 |
| 20.00 | 18-22 | 3.23 | 0.85 | 0.49 | 1.97 | 6.40 | 43.26 | 0.43 | 24.88 | 1979 |
| 26.00 | 22-30 | 2.47 | 0.82 | 0.45 | 2.71 | 5.11 | 30.66 | 0.41 | 35.93 | 1968 |
| 34.00 | 30-38 | 2.28 | 0.81 | 0.44 | 3.54 | 1.87 | 16.84 | 0.63 | 55.18 | 1949 |
| 42.00 | 38-46 | 2.44 | 0.81 | 0.46 | 3.72 | 1.83 | 10.22 | 0.37 | 71.20 | 1933 |
| 50.00 | 46-54 | 2.65 | 0.81 | 0.50 | 4.01 | 0.73 | 3.42 | 0.29 | 106.39 | 1898 |
| 55.00 | 54-56 | 3.12 | 0.84 | 0.50 | 2.52 | 0.19 | 0.49 | 0.16 | 169.03 | 1835 |

**Table 8.** Jordan Basin (JB) sediment $^{210}Pb$ and $^{214}Pb$

| $^{210}Pb$ Lead-210 Excess only (already subtracted supported) | | | | | $^{214}Pb$ Lead-214 | | | | |
|---|---|---|---|---|---|---|---|---|---|
| counts/min | dpm/g | avg depth | min | max | counts/min | dpm/g | avg depth | min | max |
| 0.18 | 14.1 | 0.07 | 0.0 | 0.5 | 0.08 | 0.5 | 0.07 | 0.0 | 0.5 |
| 0.19 | 14.3 | 0.20 | 0.5 | 1.0 | 0.11 | 1.2 | 0.20 | 0.5 | 1.0 |
| 0.17 | 12.5 | 0.36 | 1.0 | 1.5 | 0.12 | 1.5 | 0.36 | 1.0 | 1.5 |
| 0.19 | 14.6 | 0.53 | 1.5 | 2.0 | 0.09 | 0.9 | 0.53 | 1.5 | 2.0 |
| 0.72 | 13.4 | 0.74 | 2.0 | 3.0 | 0.27 | 1.2 | 0.74 | 2.0 | 3.0 |
| 0.63 | 11.3 | 1.04 | 3.0 | 4.0 | 0.29 | 1.3 | 1.04 | 3.0 | 4.0 |
| 0.55 | 10.0 | 1.37 | 4.0 | 5.0 | 0.24 | 1.1 | 1.37 | 4.0 | 5.0 |
| 0.52 | 9.2 | 1.73 | 5.0 | 6.0 | 0.26 | 1.2 | 1.73 | 5.0 | 6.0 |
| 0.50 | 8.6 | 2.23 | 6.0 | 8.0 | 0.28 | 1.3 | 2.23 | 6.0 | 8.0 |
| 0.45 | 7.5 | 2.96 | 8.0 | 10 | 0.29 | 1.3 | 2.96 | 8.0 | 10 |
| 0.42 | 7.2 | 4.13 | 10 | 14 | 0.25 | 1.1 | 4.13 | 10 | 14 |
| 0.41 | 6.7 | 5.94 | 14 | 18 | 0.29 | 1.4 | 5.94 | 14 | 18 |
| 0.40 | 6.4 | 7.91 | 18 | 22 | 0.27 | 1.2 | 7.91 | 18 | 22 |
| 0.33 | 5.1 | 10.61 | 22 | 30 | 0.27 | 1.2 | 10.61 | 22 | 30 |
| 0.17 | 1.87 | 14.15 | 30 | 38 | 0.26 | 1.1 | 14.15 | 30 | 38 |
| 0.17 | 1.8 | 17.87 | 38 | 46 | 0.26 | 1.2 | 17.87 | 38 | 46 |
| 0.12 | 0.7 | 21.88 | 46 | 54 | 0.27 | 1.2 | 21.88 | 46 | 54 |
| 0.10 | 0.2 | 24.40 | 54 | 56 | 0.30 | 1.4 | 24.40 | 54 | 56 |

**Table 9**. Jordan Basin (JB) sediment $^{137}Cs$.

| $^{137}Cs$ | Cesium-137 | | | | |
|---|---|---|---|---|---|
| counts/min/g | cpm/g ($x10^3$) | avg depth | min | max | grams Sed. |
| 1.94E-03 | 1.94 | 0.25 | 0 | 0.5 | 2.0 |
| 4.19E-04 | 0.42 | 0.75 | 0.5 | 1.0 | 2.0 |
| 1.45E-03 | 1.45 | 1.25 | 1.0 | 1.5 | 2.0 |
| -1.06E-03 | 0.00 | 1.75 | 1.5 | 2.0 | 2.0 |
| 1.53E-03 | 1.53 | 2.5 | 2.0 | 3.0 | 10.0 |
| 1.17E-03 | 1.17 | 3.5 | 3.0 | 4.0 | 10.0 |
| 9.48E-04 | 0.95 | 4.5 | 4.0 | 5.0 | 10.0 |
| 2.45E-03 | 2.45 | 5.5 | 5.0 | 6.0 | 10.0 |
| 7.89E-04 | 0.79 | 7.0 | 6.0 | 8.0 | 10.0 |
| 8.05E-04 | 0.81 | 9.0 | 8.0 | 10 | 10.0 |
| 3.79E-04 | 0.38 | 12 | 10 | 14 | 10.0 |
| 9.21E-04 | 0.92 | 16 | 14 | 18 | 10.0 |
| 6.75E-04 | 0.67 | 20 | 18 | 22 | 10.0 |
| 1.23E-03 | 1.23 | 26 | 22 | 30 | 10.0 |
| 1.28E-04 | 0.13 | 34 | 30 | 38 | 10.0 |
| -1.05E-04 | 0.00 | 42 | 38 | 46 | 10.0 |
| -3.02E-04 | 0.00 | 50 | 46 | 54 | 10.0 |
| -5.53E-04 | 0.00 | 55 | 54 | 56 | 10.0 |

**Table 10.** Cape Cod Bay (CCB) sediment CRS calculation.

| Midpoint depth cm | $\rho_{sed}$ ($g/cm^3$) | Porosity | DBD $g/cm^3$ | m $g/cm^2$ | $^{210}Pb_{exc}$ dpm/g | $^{210}Pb_{exc}$ Inventory $dpm/cm^2$ | CRS (cm/y) | t yr | Model Date |
|---|---|---|---|---|---|---|---|---|---|
| 0.25 | 1.60 | 0.82 | 0.29 | 0.07 | 3.51 | 25.67 | 0.78 | 0.00 | 2004 |
| 0.75 | 2.84 | 0.86 | 0.40 | 0.30 | 3.21 | 25.42 | 0.62 | 0.32 | 2004 |
| 1.25 | 1.25 | 0.71 | 0.36 | 0.18 | 2.98 | 24.46 | 0.70 | 1.56 | 2002 |
| 1.75 | 2.48 | 0.81 | 0.47 | 0.23 | 2.78 | 23.92 | 0.57 | 2.28 | 2002 |
| 2.5 | 1.78 | 0.79 | 0.38 | 0.29 | 2.79 | 23.27 | 0.68 | 3.16 | 2001 |
| 3.5 | 1.77 | 0.76 | 0.43 | 0.43 | 2.61 | 22.47 | 0.63 | 4.28 | 2000 |
| 4.5 | 2.94 | 0.85 | 0.45 | 0.45 | 2.75 | 21.36 | 0.54 | 5.91 | 1998 |
| 5.5 | 2.39 | 0.42 | 1.38 | 1.38 | 3.21 | 20.13 | 0.14 | 7.82 | 1996 |
| 7 | 2.31 | 0.83 | 0.40 | 0.61 | 3.81 | 15.70 | 0.32 | 15.80 | 1988 |
| 9 | 2.92 | 0.83 | 0.49 | 0.97 | 2.09 | 13.39 | 0.41 | 20.90 | 1983 |
| 12 | 2.74 | 0.82 | 0.48 | 1.45 | 1.47 | 11.36 | 0.50 | 26.17 | 1978 |
| 16 | 2.50 | 0.79 | 0.53 | 2.12 | 1.84 | 9.24 | 0.29 | 32.83 | 1971 |
| 20 | 1.95 | 0.75 | 0.49 | 1.95 | 1.83 | 5.32 | 0.19 | 50.52 | 1953 |
| 26 | 2.49 | 0.77 | 0.58 | 3.47 | 0.50 | 1.75 | 0.19 | 86.26 | 1918 |

**Table 11**. Cape Cod Bay (CCB) sediment $^{210}Pb$.

| $^{210}Pb$ Lead-210 Excess only (already subtracted supported) | | | | | $^{214}Pb$ Lead-214 | | | | |
|---|---|---|---|---|---|---|---|---|---|
| counts/min | dpm/g | avg depth | min | max | counts/min | dpm/g | avg depth | min | max |
| 0.16 | 3.5 | 0.25 | 0 | 0.5 | 0.16 | 1.2 | 0.25 | 0 | 0.5 |
| 0.14 | 3.2 | 0.75 | 0.5 | 1 | 0.13 | 0.8 | 0.75 | 0.5 | 1 |
| 0.15 | 3.0 | 1.25 | 1.0 | 1.5 | 0.16 | 1.2 | 1.25 | 1.0 | 1.5 |
| 0.14 | 2.8 | 1.75 | 1.5 | 2.0 | 0.15 | 1.1 | 1.75 | 1.5 | 2.0 |
| 0.13 | 2.8 | 2.50 | 2.0 | 3.0 | 0.14 | 0.9 | 2.50 | 2.0 | 3.0 |
| 0.13 | 2.6 | 3.50 | 3.0 | 4.0 | 0.16 | 1.2 | 3.50 | 3.0 | 4.0 |
| 0.13 | 2.7 | 4.50 | 4.0 | 5.0 | 0.14 | 0.9 | 4.50 | 4.0 | 5.0 |
| 0.15 | 3.2 | 5.50 | 5.0 | 6.0 | 0.15 | 1.1 | 5.50 | 5.0 | 6.0 |
| 0.17 | 3.8 | 7.00 | 6.0 | 8.0 | 0.15 | 1.2 | 7.00 | 6.0 | 8.0 |
| 0.12 | 2.1 | 9.00 | 8.0 | 10.0 | 0.16 | 1.2 | 9.00 | 8.0 | 10.0 |
| 0.11 | 1.5 | 12.00 | 10.0 | 14.0 | 0.19 | 1.6 | 12.00 | 10.0 | 14.0 |
| 0.12 | 1.8 | 16.00 | 14.0 | 18.0 | 0.17 | 1.4 | 16.00 | 14.0 | 18.0 |
| 0.12 | 1.8 | 20.00 | 18.0 | 22.0 | 0.17 | 1.4 | 20.00 | 18.0 | 22.0 |
| 0.09 | 0.5 | 26.00 | 22.0 | 30.0 | 0.19 | 1.7 | 26.00 | 22.0 | 30.0 |
| 0.05 | -0.5 | 33.00 | 30.0 | 36.0 | 0.19 | 1.6 | 33.00 | 30.0 | 36.0 |

**Table 12.** Cape Cod Bay (CCB) sediment $^{137}Cs$.

| $^{137}Cs$ | Cesium-137 | | | |
|---|---|---|---|---|
| counts/min/g | cpm/g (x$10^3$) | avg depth | min | max |
| 9.32E-04 | 0.93 | 0.25 | 0 | 0.5 |
| -2.11E-03 | 0.00 | 0.75 | 0.5 | 1 |
| -2.60E-04 | 0.00 | 1.25 | 1.0 | 1.5 |
| -3.49E-04 | 0.00 | 1.75 | 1.5 | 2.0 |
| -6.58E-04 | 0.00 | 2.50 | 2.0 | 3.0 |
| 1.01E-03 | 1.01 | 3.50 | 3.0 | 4.0 |
| -1.34E-04 | 0.00 | 4.50 | 4.0 | 5.0 |
| -2.30E-04 | 0.00 | 5.50 | 5.0 | 6.0 |
| 2.59E-03 | 2.59 | 7.00 | 6.0 | 8.0 |
| -4.93E-04 | 0.00 | 9.00 | 8.0 | 10.0 |
| 1.22E-05 | 0.01 | 12.00 | 10.0 | 14.0 |
| 8.02E-04 | 0.80 | 16.00 | 14.0 | 18.0 |
| -2.36E-04 | 0.00 | 20.00 | 18.0 | 22.0 |
| -4.79E-04 | 0.00 | 26.00 | 22.0 | 30.0 |
| -1.37E-03 | 0.00 | 34.00 | 30.0 | 38.0 |

**Table 13**. Inner Penobscot Bay (IPB) sediment CRS calculation.

| Midpoint depth cm | | ρsed (g/cm$^3$) | Porosity | DBD g/cm$^3$ | m g/cm$^2$ | $^{210}Pb_{exc}$ dpm/g | $^{210}Pb_{exc}$ Inventory dpm/cm$^2$ | CRS (cm/y) | t yr | Model Date |
|---|---|---|---|---|---|---|---|---|---|---|
| 0.25 | 0-0.5 | 3.11 | 0.91 | 0.28 | 0.07 | 4.25 | 26.32 | 0.70 | 0.00 | 2004 |
| 0.75 | 0.5-1.0 | 3.15 | 0.89 | 0.34 | 0.17 | 4.11 | 26.02 | 0.58 | 0.36 | 2004 |
| 1.25 | 1.0-1.5 | 2.54 | 0.87 | 0.34 | 0.17 | 3.96 | 25.33 | 0.58 | 1.23 | 2003 |
| 1.75 | 1.5-2.0 | 1.82 | 0.80 | 0.36 | 0.18 | 3.83 | 24.65 | 0.56 | 0.87 | 2002 |
| 2.50 | 2-3 | 2.46 | 0.86 | 0.34 | 0.26 | 3.63 | 23.96 | 0.60 | 1.78 | 2001 |
| 3.50 | 3-4 | 3.11 | 0.86 | 0.42 | 0.42 | 3.38 | 23.03 | 0.50 | 3.05 | 2000 |
| 4.50 | 4-5 | 3.66 | 0.87 | 0.47 | 0.47 | 3.15 | 21.61 | 0.45 | 5.10 | 1998 |
| 5.50 | 5-6 | 3.60 | 0.85 | 0.53 | 0.53 | 2.94 | 20.12 | 0.40 | 7.39 | 1995 |
| 7.00 | 6-8 | 2.91 | 0.83 | 0.49 | 0.74 | 2.64 | 18.57 | 0.44 | 9.97 | 1993 |
| 9.00 | 8-10 | 2.28 | 0.78 | 0.50 | 0.99 | 2.29 | 16.61 | 0.45 | 13.56 | 1989 |
| 12.00 | 10-14 | 2.73 | 0.79 | 0.58 | 1.75 | 1.86 | 14.33 | 0.41 | 18.29 | 1984 |
| 16.00 | 14-18 | 2.39 | 0.74 | 0.63 | 2.52 | 1.40 | 11.08 | 0.39 | 26.56 | 1976 |
| 20.00 | 18-22 | 2.42 | 0.72 | 0.67 | 2.68 | 1.06 | 7.54 | 0.33 | 38.89 | 1964 |
| 26.00 | 22-30 | 2.70 | 0.74 | 0.70 | 4.22 | 0.69 | 4.71 | 0.30 | 53.99 | 1949 |
| 31.50 | 30-32 | 2.88 | 0.76 | 0.70 | 3.83 | 0.47 | 1.80 | 0.17 | 84.95 | 1918 |

**Table 14**. Inner Penobscot Bay (IPB) sediment $^{210}Pb$ and $^{214}Pb$

| $^{210}Pb$ Lead-210 Excess only (already subtracted supported) | | | | | $^{214}Pb$ Lead-214 | | | | |
|---|---|---|---|---|---|---|---|---|---|
| counts/min | dpm/g | avg depth | min | max | counts/min | dpm/g | avg depth | min | max |
| 0.27 | 3.8 | 1.25 | 1.0 | 1.5 | 0.31 | 1.8 | 1.25 | 1.0 | 1.5 |
| 0.15 | 3.1 | 1.75 | 1.5 | 2.0 | 0.23 | 2.5 | 1.75 | 1.5 | 2.0 |
| 0.36 | 3.5 | 2.50 | 2.0 | 3.0 | 0.35 | 1.3 | 2.50 | 2.0 | 3.0 |
| 0.37 | 3.8 | 3.50 | 3.0 | 4.0 | 0.33 | 1.2 | 3.50 | 3.0 | 4.0 |
| 0.35 | 3.5 | 4.50 | 4.0 | 5.0 | 0.33 | 1.2 | 4.50 | 4.0 | 5.0 |
| 0.34 | 3.1 | 5.50 | 5.0 | 6.0 | 0.39 | 1.5 | 5.50 | 5.0 | 6.0 |
| 0.30 | 2.6 | 7.00 | 6.0 | 8.0 | 0.38 | 1.4 | 7.00 | 6.0 | 8.0 |
| 0.28 | 2.3 | 9.00 | 8.0 | 10.0 | 0.39 | 1.5 | 9.00 | 8.0 | 10.0 |
| 0.25 | 1.9 | 12.00 | 10.0 | 14.0 | 0.37 | 1.4 | 12.00 | 10.0 | 14.0 |
| 0.20 | 1.2 | 16.00 | 14.0 | 18.0 | 0.41 | 1.5 | 16.00 | 14.0 | 18.0 |
| 0.16 | 0.6 | 20.00 | 18.0 | 22.0 | 0.39 | 1.5 | 20.00 | 18.0 | 22.0 |
| 0.11 | -0.2 | 26.00 | 22.0 | 30.0 | 0.42 | 1.6 | 26.00 | 22.0 | 30.0 |
| 0.11 | -0.3 | 31.50 | 30.0 | 33.0 | 0.44 | 1.6 | 31.50 | 30.0 | 33.0 |

**Table 15**. Inner Penobscot Bay (IPB) sediment $^{137}Cs$.

| $^{137}Cs$ | Cesium-137 | | | | |
|---|---|---|---|---|---|
| counts/min/g | cpm/g ($x10^3$) | avg depth | min | max | grams sed. |
| 1.34E-03 | 1.34 | 1.25 | 1.0 | 1.5 | 2.0 |
| -1.31E-03 | 0.00 | 1.75 | 1.5 | 2.0 | 2.0 |
| 2.78E-03 | 2.78 | 2.5 | 2.0 | 3.0 | 10.0 |
| 2.86E-03 | 2.86 | 3.5 | 3.0 | 4.0 | 10.0 |
| 4.00E-03 | 4.00 | 4.5 | 4.0 | 5.0 | 10.0 |
| 3.28E-03 | 3.28 | 5.5 | 5.0 | 6.0 | 10.0 |
| 2.70E-03 | 2.70 | 7.0 | 6.0 | 8.0 | 10.0 |
| 2.93E-03 | 2.93 | 9.0 | 8.0 | 10 | 10.0 |
| 2.82E-03 | 2.82 | 12 | 10 | 14 | 10.0 |
| 2.42E-03 | 2.42 | 16 | 14 | 18 | 10.0 |
| 7.47E-04 | 0.75 | 20 | 18 | 22 | 10.0 |
| -5.79E-05 | 0.00 | 26 | 22 | 30 | 10.0 |
| -5.20E-04 | 0.00 | 32 | 30 | 33 | 10.0 |

## References


Appleby, P. G., 2001. Chronostratigraphic techniques in recent sediments. In: W. Last, Smol, J. (Editor), Tracking environmental change using lake sediments. Kluwer Academic Publishers, Dordrecht, The Netherlands, pp. 171-203.

Appleby, P. G., Oldfield, F., 1978. The calculation of lead-2 10 dates assuming a constant rate of supply of unsupported 210Pb to the sediment. Catena, 5: 1-8.

# APPENDIX IV

## DETAILED BATHYMETRIC DATA USED FOR MASS BALANCE CALCULATIONS

Source: Incze, L., Jakobbson, M., 2008. Hypsometric characterization of the Gulf of Maine, Georges Bank, Scotian Shelf and neighboring continental slope. http://www.usm.maine.edu/gulfofmaine-census/ (accessed October, 2004).

**Fig.1.** Gulf of Maine study area and physiographic sub regions defined for this study.

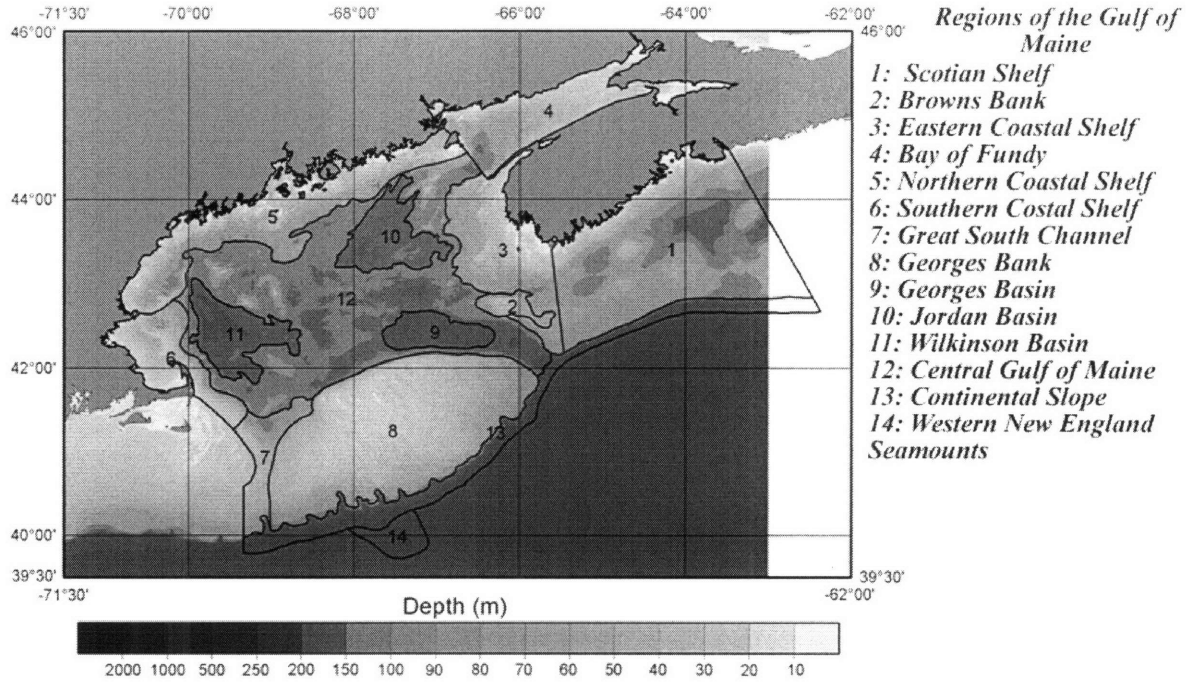


**Table 1**. Regions used for this study

| Region | Name | Surface Area (km^2) |
|---|---|---|
| 1 | Scotian Shelf | 36,242.00 |
| 2 | Browns Bank | 1,780.30 |
| 3 | Eastern Coastal Shelf | 13,794.00 |
| 4 | Bay of Fundy | 12,518.00 |
| 5 | Northern Coastal Shelf | 19,311.00 |
| 6 | Southern Costal Shelf | 8,239.10 |
| 7 | Great South Channel | 5,202.30 |
| 8 | Georges Bank | 38,471.00 |
| 9 | Georges Basin | 4,103.70 |
| 10 | Jordan Basin | 6,695.80 |
| 11 | Wilkinson Basin | 7,075.60 |
| 12 | Central Gulf of Maine | 44,799.00 |
| Total | | 198,231.80 |

**Table 2.** Detailed bathymetric data

| Scotian Shelf (Area 1) | | | Browns Bank (Area 2) | | |
|---|---|---|---|---|---|
| Sea level | Volume (km^3) | Area (km^2) | Sea level | Volume (km^3) | Area (km^2) |
| 0 | 357.99 | 36242 | 0 | 17.803 | 1780.3 |
| -10 | 351.145 | 35356 | -10 | 17.803 | 1780.3 |
| -20 | 346.68 | 34873 | -20 | 17.803 | 1780.3 |

| | | | | | |
|---|---|---|---|---|---|
| -30 | 342.27 | 34463 | -30 | 17.799 | 1780.3 |
| -40 | 337.275 | 33991 | -40 | 17.613 | 1779.5 |
| -50 | 331.955 | 33464 | -50 | 16.798 | 1743.1 |
| -60 | 325.58 | 32927 | -60 | 14.465 | 1616.5 |
| -70 | 317.745 | 32189 | -70 | 11.92 | 1276.5 |
| -80 | 307.49 | 31360 | -80 | 8.893 | 1107.5 |
| -90 | 286.44 | 30138 | -90 | 5.591 | 671.1 |
| -100 | 253.23 | 27150 | -100 | 4.0605 | 447.1 |
| -110 | 216.98 | 23496 | -110 | 3.298 | 365 |
| -120 | 183.72 | 19900 | -120 | 2.6105 | 294.6 |
| -130 | 156.68 | 16844 | -130 | 1.922 | 227.5 |
| -140 | 130.49 | 14492 | -140 | 1.16 | 156.9 |
| -150 | 102.3235 | 11606 | -150 | 0.4555 | 75.1 |
| -160 | 77.588 | 8858.7 | -160 | 0.0885 | 16 |
| -170 | 59.6695 | 6658.9 | -170 | 0.0085 | 1.7 |
| -180 | 46.651 | 5275 | -180 | 0 | 0 |
| -190 | 35.457 | 4055.2 | | | |
| -200 | 26.8735 | 3036.2 | | | |
| -210 | 20.5085 | 2338.5 | | | |
| -220 | 14.6915 | 1763.2 | | | |
| -230 | 8.7005 | 1175.1 | | | |
| -240 | 4.256 | 565 | | | |
| -250 | 2.262 | 286.2 | | | |
| -260 | 1.546 | 166.2 | | | |
| -270 | 1.367 | 143 | | | |
| -280 | 1.251 | 130.4 | | | |
| -290 | 1.1475 | 119.8 | | | |
| -300 | 1.0545 | 109.7 | | | |
| -310 | 0.9735 | 101.2 | | | |
| -320 | 0.8995 | 93.5 | | | |
| -330 | 0.83 | 86.4 | | | |
| -340 | 0.763 | 79.6 | | | |
| -350 | 0.6985 | 73 | | | |
| -360 | 0.6365 | 66.7 | | | |
| -370 | 0.577 | 60.6 | | | |
| -380 | 0.522 | 54.8 | | | |
| -390 | 0.4735 | 49.6 | | | |
| -400 | 0.4315 | 45.1 | | | |
| -410 | 0.3935 | 41.2 | | | |
| -420 | 0.358 | 37.5 | | | |
| -430 | 0.3255 | 34.1 | | | |
| -440 | 0.2955 | 31 | | | |
| -450 | 0.269 | 28.1 | | | |
| -460 | 0.249 | 25.7 | | | |
| -470 | 0.2355 | 24.1 | | | |
| -480 | 0.2245 | 23 | | | |
| -490 | 0.2135 | 21.9 | | | |
| -500 | 0.203 | 20.8 | | | |

| | | | | | |
|---|---|---|---|---|---|
| -510 | 0.193 | 19.8 | | | |
| -520 | 0.1835 | 18.8 | | | |
| -530 | 0.1745 | 17.9 | | | |
| -540 | 0.1655 | 17 | | | |
| -550 | 0.1565 | 16.1 | | | |
| -560 | 0.148 | 15.2 | | | |
| -570 | 0.1395 | 14.4 | | | |
| -580 | 0.131 | 13.5 | | | |
| -590 | 0.123 | 12.7 | | | |
| -600 | 0.1155 | 11.9 | | | |
| -610 | 0.108 | 11.2 | | | |
| -620 | 0.1005 | 10.4 | | | |
| -630 | 0.0935 | 9.7 | | | |
| -640 | 0.087 | 9 | | | |
| -650 | 0.0805 | 8.4 | | | |
| -660 | 0.074 | 7.7 | | | |
| -670 | 0.068 | 7.1 | | | |
| -680 | 0.0625 | 6.5 | | | |
| -690 | 0.057 | 6 | | | |
| -700 | 0.0515 | 5.4 | | | |
| -710 | 0.0465 | 4.9 | | | |
| -720 | 0.0415 | 4.4 | | | |
| -730 | 0.037 | 3.9 | | | |
| -740 | 0.0325 | 3.5 | | | |
| -750 | 0.0285 | 3 | | | |
| -760 | 0.025 | 2.7 | | | |
| -770 | 0.021 | 2.3 | | | |
| -780 | 0.0175 | 1.9 | | | |
| -790 | 0.0145 | 1.6 | | | |
| -800 | 0.0115 | 1.3 | | | |
| -810 | 0.009 | 1 | | | |
| -820 | 0.007 | 0.8 | | | |
| -830 | 0.005 | 0.6 | | | |
| -840 | 0.0035 | 0.4 | | | |
| -850 | 0.002 | 0.3 | | | |
| -860 | 0.001 | 0.1 | | | |
| -870 | 0.0005 | 0.1 | | | |
| -880 | 0 | 0 | | | |

| Eastern Coastal Shelf (Area 3) | | | Bay of Fundy (Area 4) | | | Northern Coastal Shelf (Area 5) | | |
|---|---|---|---|---|---|---|---|---|
| Sea level | Volume (km^3) | Area (km^2) | Sea level | Volume (km^3) | Area (km^2) | Sea level | Volume (km^3) | Area (km^2) |
| 0 | 135.175 | 13794 | 0 | 118.755 | 12518 | 0 | 185.68 | 19311 |
| -10 | 129.04 | 13241 | -10 | 108.22 | 11233 | -10 | 171.83 | 17825 |
| -20 | 121.775 | 12567 | -20 | 100.7975 | 10411 | -20 | 159.295 | 16541 |
| -30 | 114.52 | 11788 | -30 | 93.0335 | 9748.5 | -30 | 146.62 | 15318 |
| -40 | 108.72 | 11116 | -40 | 82.0685 | 8858.2 | -40 | 133.98 | 14006 |
| -50 | 103.0315 | 10628 | -50 | 70.636 | 7555.5 | -50 | 121.41 | 12790 |
| -60 | 95.351 | 9978.3 | -60 | 60.687 | 6571.7 | -60 | 108.835 | 11492 |
| -70 | 86.373 | 9091.9 | -70 | 50.5915 | 5565.7 | -70 | 95.6945 | 10275 |
| -80 | 77.459 | 8182.7 | -80 | 40.936 | 4552.6 | -80 | 80.97 | 8863.9 |
| -90 | 64.382 | 7309.1 | -90 | 32.197 | 3634.6 | -90 | 65.6585 | 7330.1 |
| -100 | 48.154 | 5567.3 | -100 | 24.6575 | 2804.8 | -100 | 52.548 | 5801.6 |
| -110 | 34.2775 | 4063.5 | -110 | 19.002 | 2126.7 | -110 | 41.501 | 4708 |
| -120 | 22.6085 | 2792 | -120 | 15.0665 | 1673.7 | -120 | 30.7415 | 3592.2 |
| -130 | 13.1835 | 1729.7 | -130 | 11.584 | 1339.6 | -130 | 20.7125 | 2556.1 |
| -140 | 6.573 | 907 | -140 | 9.0195 | 977.2 | -140 | 11.4345 | 1586.4 |
| -150 | 2.835 | 407.6 | -150 | 7.5315 | 826.7 | -150 | 4.8435 | 700.5 |
| -160 | 0.9895 | 159.4 | -160 | 6.082 | 679.6 | -160 | 1.905 | 268.2 |
| -170 | 0.31 | 38.5 | -170 | 4.63 | 536.8 | -170 | 0.734 | 112.8 |
| -180 | 0.1625 | 23.5 | -180 | 3.2435 | 389.2 | -180 | 0.2075 | 34 |
| -190 | 0.064 | 9 | -190 | 1.7485 | 259.5 | -190 | 0.042 | 7.5 |
| -200 | 0.0305 | 3.8 | -200 | 0.541 | 90.2 | -200 | 0.005 | 0.9 |
| -210 | 0.013 | 2.3 | -210 | 0.093 | 18 | -210 | 0.0005 | 0.1 |
| -220 | 0.0015 | 0.3 | -220 | 0.003 | 0.6 | -220 | 0 | 0 |
| -230 | 0 | 0 | -230 | 0 | 0 | | | |

| Southern Coastal Shelf (Area 6) | | | Great South Channel (Area 7) | | | Georges Bank (Area 8) | | |
|---|---|---|---|---|---|---|---|---|
| Sea level | Volume (km^3) | Area (km^2) | Sea level | Volume (km^3) | Area (km^2) | Sea level | Volume (km^3) | Area (km^2) |
| 0 | 79.689 | 8239.1 | 0 | 52.023 | 5202.3 | 0 | 384.71 | 38471 |
| -10 | 74.157 | 7698.7 | -10 | 52.023 | 5202.3 | -10 | 384.3 | 38471 |
| -20 | 66.811 | 7132.7 | -20 | 52.023 | 5202.3 | -20 | 380.375 | 38389 |
| -30 | 56.215 | 6229.5 | -30 | 52.01 | 5202.3 | -30 | 361.32 | 37686 |
| -40 | 46.1225 | 5013.5 | -40 | 51.6555 | 5199.7 | -40 | 322.975 | 34578 |
| -50 | 38.3825 | 4211 | -50 | 49.659 | 5131.4 | -50 | 275.28 | 30017 |
| -60 | 31.2175 | 3465.5 | -60 | 45.3135 | 4800.4 | -60 | 220.06 | 25039 |
| -70 | 24.2725 | 2778 | -70 | 38.3965 | 4262.3 | -70 | 165.04 | 18973 |
| -80 | 17.352 | 2076.5 | -80 | 30.653 | 3417 | -80 | 118.2865 | 14035 |
| -90 | 12.07 | 1393.9 | -90 | 23.7285 | 2713.6 | -90 | 75.3635 | 9622.3 |
| -100 | 8.6345 | 1020.1 | -100 | 18.056 | 2032.1 | -100 | 46.6505 | 5450.4 |
| -110 | 5.694 | 706.8 | -110 | 14.6155 | 1579.1 | -110 | 33.815 | 3879.7 |
| -120 | 3.2665 | 432 | -120 | 12.3455 | 1344 | -120 | 25.415 | 2883.3 |
| -130 | 1.605 | 221.3 | -130 | 9.6265 | 1125.1 | -130 | 19.0635 | 2199.7 |
| -140 | 0.6325 | 99.7 | -140 | 5.703 | 800.2 | -140 | 13.1985 | 1613 |
| -150 | 0.1775 | 26.8 | -150 | 2.1655 | 340.4 | -150 | 8.3655 | 1026.7 |
| -160 | 0.0495 | 8.7 | -160 | 0.618 | 92.7 | -160 | 5.2765 | 646.4 |
| -170 | 0.006 | 1.2 | -170 | 0.2295 | 30.9 | -170 | 3.232 | 408.9 |
| -180 | 0 | 0 | -180 | 0.112 | 15 | -180 | 1.7605 | 237.5 |
| | | | -190 | 0.055 | 7.4 | -190 | 0.8285 | 114.6 |
| | | | -200 | 0.026 | 3.6 | -200 | 0.3285 | 51.1 |
| | | | -210 | 0.015 | 1.6 | -210 | 0.089 | 14.6 |
| | | | -220 | 0.013 | 1.4 | -220 | 0.019 | 3.2 |
| | | | -230 | 0.0115 | 1.2 | -230 | 0.003 | 0.6 |
| 466.3545 | | | -240 | 0.0105 | 1.1 | -240 | 0 | 0 |
| | | | -250 | 0.0095 | 1 | | | |
| | | | -260 | 0.0085 | 0.9 | | | |
| | | | -270 | 0.0075 | 0.8 | | | |
| | | | -280 | 0.0065 | 0.7 | | | |
| | | | -290 | 0.0055 | 0.6 | | | |
| | | | -300 | 0.0045 | 0.5 | | | |
| | | | -310 | 0.0035 | 0.4 | | | |
| | | | -320 | 0.003 | 0.3 | | | |
| | | | -330 | 0.0025 | 0.3 | | | |
| | | | -340 | 0.002 | 0.2 | | | |
| | | | -350 | 0.0015 | 0.2 | | | |
| | | | -360 | 0.001 | 0.1 | | | |
| | | | -370 | 0.001 | 0.1 | | | |
| | | | -380 | 0.0005 | 0.1 | | | |
| | | | -390 | 0 | 0 | | | |

| Georges Basin (Area 9) | | | Jordan Basin (Area 10) | | | Wilkinson Basin (Area 11) | | |
|---|---|---|---|---|---|---|---|---|
| Sea level | Volume (km^3) | Area (km^2) | Sea level | Volume (km^3) | Area (km^2) | Sea level | Volume (km^3) | Area (km^2) |
| 0 | 41.037 | 4103.7 | 0 | 66.958 | 6695.8 | 0 | 70.756 | 7075.6 |
| -10 | 41.037 | 4103.7 | -10 | 66.958 | 6695.8 | -10 | 70.756 | 7075.6 |
| -20 | 41.037 | 4103.7 | -20 | 66.958 | 6695.8 | -20 | 70.756 | 7075.6 |
| -30 | 41.037 | 4103.7 | -30 | 66.958 | 6695.8 | -30 | 70.756 | 7075.6 |
| -40 | 41.037 | 4103.7 | -40 | 66.958 | 6695.8 | -40 | 70.756 | 7075.6 |
| -50 | 41.037 | 4103.7 | -50 | 66.958 | 6695.8 | -50 | 70.756 | 7075.6 |
| -60 | 41.037 | 4103.7 | -60 | 66.958 | 6695.8 | -60 | 70.756 | 7075.6 |
| -70 | 41.037 | 4103.7 | -70 | 66.958 | 6695.8 | -70 | 70.756 | 7075.6 |
| -80 | 41.037 | 4103.7 | -80 | 66.958 | 6695.8 | -80 | 70.756 | 7075.6 |
| -90 | 41.037 | 4103.7 | -90 | 66.958 | 6695.8 | -90 | 70.756 | 7075.6 |
| -100 | 41.037 | 4103.7 | -100 | 66.958 | 6695.8 | -100 | 70.756 | 7075.6 |
| -110 | 41.037 | 4103.7 | -110 | 66.958 | 6695.8 | -110 | 70.756 | 7075.6 |
| -120 | 41.037 | 4103.7 | -120 | 66.958 | 6695.8 | -120 | 70.756 | 7075.6 |
| -130 | 41.037 | 4103.7 | -130 | 66.958 | 6695.8 | -130 | 70.756 | 7075.6 |
| -140 | 41.037 | 4103.7 | -140 | 66.958 | 6695.8 | -140 | 70.756 | 7075.6 |
| -150 | 41.037 | 4103.7 | -150 | 66.958 | 6695.8 | -150 | 70.754 | 7075.6 |
| -160 | 41.037 | 4103.7 | -160 | 66.9505 | 6695.8 | -160 | 70.7375 | 7075.2 |
| -170 | 41.037 | 4103.7 | -170 | 66.8575 | 6694.3 | -170 | 70.689 | 7072.3 |
| -180 | 41.037 | 4103.7 | -180 | 66.3875 | 6677.2 | -180 | 70.5255 | 7065.5 |
| -190 | 41.037 | 4103.7 | -190 | 64.7285 | 6600.3 | -190 | 69.52 | 7039.6 |
| -200 | 41.037 | 4103.7 | -200 | 57.2765 | 6345.4 | -200 | 62.285 | 6864.4 |
| -210 | 41.037 | 4103.7 | -210 | 44.175 | 5109.9 | -210 | 48.673 | 5592.6 |
| -220 | 41.037 | 4103.7 | -220 | 29.5735 | 3725.1 | -220 | 36.078 | 4142 |
| -230 | 41.031 | 4103.7 | -230 | 15.98 | 2189.6 | -230 | 26.05 | 3073.6 |
| -240 | 40.788 | 4102.5 | -240 | 6.8875 | 1006.4 | -240 | 17.388 | 2136.4 |
| -250 | 38.6525 | 4055.1 | -250 | 2.5385 | 371.1 | -250 | 10.246 | 1341.2 |
| -260 | 34.641 | 3675.4 | -260 | 0.9355 | 136.6 | -260 | 5.331 | 708 |
| -270 | 30.0725 | 3252.8 | -270 | 0.316 | 50.5 | -270 | 2.479 | 358.2 |
| -280 | 25.366 | 2761.7 | -280 | 0.0885 | 12.7 | -280 | 0.8075 | 137.6 |
| -290 | 21.039 | 2311.5 | -290 | 0.0285 | 5 | -290 | -0.1 | 23.9 |
| -300 | 16.9655 | 1896.3 | -300 | 0.0035 | 0.7 | | | |
| -310 | 13.0935 | 1496.8 | -310 | 0 | 0 | | | |
| -320 | 9.488 | 1121.9 | | | | | | |
| -330 | 5.9865 | 775.7 | | | | | | |
| -340 | 2.6995 | 421.6 | | | | | | |
| -350 | 0.633 | 118.3 | | | | | | |
| -360 | 0.0415 | 8.3 | | | | | | |
| -370 | 0 | 0 | | | | | | |

| Central Gulf of Maine (Area 12) | | |
|---|---|---|
| Sea level | Volume (km^3) | Area (km^2) |
| 0 | 447.835 | 44799 |
| -10 | 447.505 | 44768 |
| -20 | 447.155 | 44733 |
| -30 | 446.79 | 44698 |
| -40 | 446.4 | 44660 |
| -50 | 445.94 | 44620 |
| -60 | 445.135 | 44568 |
| -70 | 443.655 | 44459 |
| -80 | 441.71 | 44272 |
| -90 | 439.51 | 44070 |
| -100 | 436.48 | 43832 |
| -110 | 431.855 | 43464 |
| -120 | 425.905 | 42907 |
| -130 | 416.525 | 42274 |
| -140 | 401.315 | 41031 |
| -150 | 374.76 | 39232 |
| -160 | 331.575 | 35720 |
| -170 | 271.96 | 30595 |
| -180 | 203.615 | 23797 |
| -190 | 141.21 | 16926 |
| -200 | 93.121 | 11316 |
| -210 | 60.933 | 7308.2 |
| -220 | 40.21 | 4878.4 |
| -230 | 24.2955 | 3163.6 |
| -240 | 11.959 | 1695.5 |
| -250 | 4.866 | 696.3 |
| -260 | 2.1295 | 276.9 |
| -270 | 1.192 | 149 |
| -280 | 0.719 | 89.4 |
| -290 | 0.4185 | 54.4 |
| -300 | 0.2225 | 29.3 |
| -310 | 0.1125 | 15.2 |
| -320 | 0.053 | 7.3 |
| -330 | 0.02 | 3.3 |
| -340 | 0.0035 | 0.7 |
| -350 | 0 | 0 |

# APPENDIX V

## ENERGY CONVERSION FACTORS USED FOR BLACK CARBON EMISSION ESTIMATES

**Table 1.** Energy conversion factors used for black carbon emission estimates.

| Average Energy Content of Various Fuels | | |
|---|---|---|
| Fuel | Average | |
| 1 kilowatt-hour of electricity | 3,413 | Btu |
| 1 cubic foot of natural gas | 5,521 | Btu |
| 1 therm natural gas | 100,000 | Btu |
| 1 gallon of liquefied petroleum gas (LPG) | 95,475 | Btu |
| 1 gallon of crude oil | 138,095 | Btu |
| 1 barrel of crude oil | 5,800,000 | Btu |
| 1 gallon of kerosene or light distillate oil | 135,000 | Btu |
| 1 gallon od middle distillate or diesel fuel oil | 138,690 | Btu |
| 1 gallon of residual fuel oil | 149,690 | Btu |
| 1 gallon of gasoline | 125,000 | Btu |
| 1 gallon of ethanol | 84,400 | Btu |
| 1 gallon of methanol | 62,800 | Btu |
| 1 gallon of gasohol | 120,900 | Btu |
| 1 pound of coal | 10,550 | Btu |
| 1 ton of coal | 21,100,000 | Btu |
| 1 ton of coke | 26,000,000 | Btu |
| 1 ton of wood | 13,000,000 | Btu |
| 1 standard cord of wood | 21,000,000 | Btu |
| 1 face cord of wood | 14,000,000 | Btu |
| 1 pound of low pressure steam | 1,000 | Btu |
| | | |
| 1 barrel lubricant | 6,065,000,000 | Btu |
| 1 barrel motor gasoline | 5,253,000,000 | Btu |
| 1 barrel aviation gasoline | 5,048,000,000 | Btu |
| 1 barrel jet fuel kerosene type | 5,670,000,000 | Btu |
| 1 barrel jet fuel naphtha type | 5,355,000,000 | Btu |
| | | |
| Aviation fuel density | 6.02 | lb/US gallon |
| | 2.73 | kg/US gallon |
| | 721.36 | $kg/m^3$ |
| Jet Fuel | 0.775-0.840 | kg/L |
| | 0.81 | kg/L |
| | 3.06 | kg/gallon |
| | 807.50 | $kg/m^3$ |
| Motor gasoline | 737.22 | $kg/m^3$ |
| Diesel | 850.00 | $kg/m^3$ |
| Kerosene | 810.00 | $kg/m^3$ |
| Ethanol | 789.00 | $kg/m^3$ |
| Residual oil | 940.00 | $kg/m^3$ |
| Lubricant | 945.75 | $kg.m^3$ |

Source: http://www.eia.doe.gov/emeu/states/sep_use/notes/use_b.pdf

# APPENDIX VI

## BLACK CARBON EMISSION CONVERSION FACTORS

Source: Bond et al. (2004)

**Table 1.** Black carbon (BC) emission conversion factors ($EF_{BC}$).

| Fuel | Technology | $EF_{PM}$ g/kg | $F_{1.0}$ | $F_{BC}$ |
|---|---|---|---|---|
| Biofuel | stoker | 2.2 | 0.86 | 0.05 |
| Biofuel | traditional | 1 | 0.85 | 0.1 |
| Briquettes | stoker | 2.5 | 0.25 | 0.01 |
| Brown coal | cyclone | 33 | 0.17 | 0.006 |
| Brown coal | pulverized | 29 | 0.09 | 0.006 |
| Brown coal | stoker | 17 | 0.11 | 0.05 |
| Hard coal | cyclone | 1.3 | 0.15 | 0.006 |
| Hard coal | pulverized | 12 | 0.09 | 0.006 |
| Hard coal | stoker | 4.2 | 0.33 | 0.2 |
| Hard coal | traditional brick kiln | 10 | 0.9 | 0.5 |
| Coking coal | coke oven | 5.8 | 0.35 | 0.48 |
| Coking coal | coke oven (uncaptured) | 20 | 0.5 | 0.48 |
| Coke | blast furnace | 0.4 | 0.28 | 0.28 |
| Heavy fuel oil (Residual fuel oil) | all | 1.1 | 0.45 | 0.08 |
| Middle dist oil | industry/power | 0.49 | 0.18 | 0.3 |
| Middle dist oil | generator | 6 | 0.86 | 0.66 |
| Mid/light dist | external combustion | 0.25 | 0.9 | 0.29 |
| Kerosene Residentila | residential | 0.9 | 1 | 0.13 |
| LPG Residential | residential | 0.52 | 1 | 0.13 |
| Natural Gas all | all | 0.002 | 1 | 0.06 |
| Solid Waste | all | 12.6 | 0.1 | 0.035 |
| Solid Waste | open burning | 30 | 0.5 | 0.37 |
| | **Conditions** | | | |
| Aviation fuel | all | 0.14 | - | 0.7 |
| Diesel, on road genera | standards in place | 1.5 | 0.86 | 0.66 |
| Diesel, on road genera | standards beginning | 3.5 | 0.86 | 0.66 |
| Diesel, superemitter | all | 12 | 0.86 | 0.66 |
| Diesel, farm vehicles | all | 4 | 0.86 | 0.66 |
| Diesel, nonfarm off-road vehicles | all | 5.5 | 0.86 | 0.66 |
| Diesel and heavy oil, ships | all | 1.8 | 0.86 | 0.66 |
| Diesel, railroad | all | 2.7 | 0.86 | 0.66 |
| Gasoline, all vehicles | standard in place | 0.15 | 0.85 | 0.34 |
| Gasoline, all vehicles | standards beginning | 0.5 | 0.85 | 0.34 |
| Gasoline super emitter | - | 2 | 0.85 | 0.34 |
| Gasoline, two stroke | standard | 15 | 0.95 | 0.05 |
| Gasoline, two stroke | high-emission practice | 30 | 0.95 | 0.05 |
| | **Sector** | | **$EF_{BC}$** | |
| Animal wastes | Residential | | 0.53 | |
| Charcoal | Residential | | 1.0 | |
| Agricultural residues | Residential | | 1.0 | |
| Wood | Power | | 0.044 | |
| | Industry | | 0.08-0.55 | |
| | Residential | | 0.3-1.4 | |
| Biomass burning | Savanna | | 0.48 | |
| | Crop Residues | | 0.69 | |
| | Forest | | 0.56-0.61 | |

$EF_{BC} = EF_{PM} * F_{1.0} * F_{BC}$. Source: Tables 5, 7, and 9 from Bond, T.I., Streets, D.G., Yarber, K.F., Nelson, S.M., Woo, J., Klimont, Z., 2004. A technology-based global inventory of black and organic carbon emissions from combustion. J. Geophys. Res. 109, D14203.

# APPENDIX VII

# INNER FILTER EFFECT CORRECTION FOR FLUORESCENCE MEASUREMENTS OF MELANOIDIN AND DISSOLVED ORGANIC MATTER (DOM)

**Inner filter effect corrections for fluorescence measurements in solutions containing melanoidin and dissolved organic matter (DOM)**

The inner filter effects in fluorescence measurements of pyrene for aqueous solutions containing melanoidin and dissolved organic matter (DOM) at the concentrations used in chapter 4 of this thesis (212 and 131 mg/L, respectively), were assessed. The absorbance of these solutions at excitation ($\lambda_{exc}$: 337 nm) and emission ($\lambda_{em}$: 387 nm) wavelengths was determined using a Beckman DU600 spectrophotometer. Due to the presence of other flourophores in these aqueous solutions, pyrene fluorescence measurements in aqueous solutions containing melanoidin and DOM were made using time-gated, laser-induced fluorescence (TGLIF) spectroscopy (Kuo et al., 2007; Rudnick, 1998; Rudnick and Chen, 1998). To correct for the absorbance of melanoidin and DOM considering the illumination geometry of the TGLIF system, we corrected our inner filter effects according to Kuo et al. (2007):

$$\frac{F_{filter}}{F_{nofil}} = \frac{\int_0^L 10^{-(\alpha_{exc}+\alpha_{em})x} G(x)dx}{\int_0^L 10^{-(\varepsilon_{exc}+\varepsilon_{em})C_{pyr}\cdot x} G(x)dx} \quad , \qquad (1)$$

where $\alpha_{exc}$ and $\alpha_{em}$ are excitation and emission attenuation coefficients ($cm^{-1}$) of the melanoidin or DOM aqueous solutions; $\varepsilon_{exc}$ and $\varepsilon_{em}$ are the excitation and emission extinction coefficients of pyrene ($M^{-1}\cdot cm^{-1}$) in aqueous solutions; $C_{pyr}$ is the concentration of pyrene (M); $G(x)$ is the geometric factor for illumination volume variation as a function of distance ($x$) from the illumination source.

We used a numerical integration approach to correct for inner filter effect and followed the same approximation that Kuo et al. (2007) used to estimate G(x):

$$G(x) = \frac{reception\_area_{x=o}}{area\_of\_illum.\_sphere} = \frac{\pi r_0^2}{4\pi r^2}, \qquad (2)$$

where $r_0$ is the radius at the reception probe tip (0.05 cm) and $r$ (cm) is the distance between the probe tip and a fluorescent dissolve pyrene molecule with a function radius $r = 0.44 \cdot x$.

**Table 1.** Light absorption properties of melanoidin, DOM, and pyrene solutions.

| | λ=337 $\alpha_{ex}$ ($cm^{-1}$) | λ=387 $\alpha_{em}$ ($cm^{-1}$) |
|---|---|---|
| Melanoidin | 3.7 | 3.1 |
| DOM | 0.9 | 0.6 |
| | $\varepsilon_{ex}$ ($M^{-1}cm^{-1}$) | $\varepsilon_{em}$ ($M^{-1}cm^{-1}$) |
| Pyrene | 32,591 | 704 |

Note: An initial pyrene concentration close to the uncorrected value was used for the first estimate. However, as can be seen in Table 1 and Table 2, the calculations were not sensitive to the pyrene concentration used and no further correction or iterative processes were needed.

**Table 2.** Numerical integration for the inner filter effect correction of pyrene fluorescence measurements in melanoidin considering the illumination geometry of the TGLIF system.

| $x$ (cm) | $10^{-(\alpha ex+\alpha em)x}$ | $G(x)$ | $\Sigma 10^{-(\alpha ex+\alpha em)x} \cdot G(x) \cdot \Delta x$ | $10^{-(\varepsilon ex+\varepsilon em)Cpyr \cdot x}$ | $\Sigma 10^{-(\varepsilon aex+\varepsilon em)\,Cpyr \cdot x} \cdot G(x) \cdot \Delta x$ |
|---|---|---|---|---|---|
| 0.1 | 2.09E-01 | 3.24E-01 | 6.76E-03 | 1.00E+00 | 3.24E-02 |
| 0.2 | 4.37E-02 | 8.09E-02 | 3.53E-04 | 1.00E+00 | 8.09E-03 |
| 0.3 | 9.12E-03 | 3.60E-02 | 3.28E-05 | 1.00E+00 | 3.60E-03 |
| 0.4 | 1.91E-03 | 2.02E-02 | 3.86E-06 | 1.00E+00 | 2.02E-03 |
| 0.5 | 3.98E-04 | 1.29E-02 | 5.16E-07 | 1.00E+00 | 1.29E-03 |
| 0.6 | 8.32E-05 | 8.99E-03 | 7.48E-08 | 1.00E+00 | 8.99E-04 |
| 0.7 | 1.74E-05 | 6.61E-03 | 1.15E-08 | 1.00E+00 | 6.61E-04 |
| 0.8 | 3.63E-06 | 5.06E-03 | 1.84E-09 | 1.00E+00 | 5.06E-04 |
| 0.9 | 7.59E-07 | 4.00E-03 | 3.03E-10 | 1.00E+00 | 4.00E-04 |
| 1.0 | 1.58E-07 | 3.24E-03 | 5.13E-11 | 1.00E+00 | 3.24E-04 |
| 1.1 | 3.31E-08 | 2.68E-03 | 8.86E-12 | 1.00E+00 | 2.68E-04 |
| 1.2 | 6.92E-09 | 2.25E-03 | 1.56E-12 | 1.00E+00 | 2.25E-04 |
| 1.3 | 1.45E-09 | 1.92E-03 | 2.77E-13 | 1.00E+00 | 1.92E-04 |
| 1.4 | 3.02E-10 | 1.65E-03 | 4.99E-14 | 1.00E+00 | 1.65E-04 |
| 1.5 | 6.31E-11 | 1.44E-03 | 9.08E-15 | 1.00E+00 | 1.44E-04 |
| 1.6 | 1.32E-11 | 1.26E-03 | 1.67E-15 | 1.00E+00 | 1.26E-04 |
| 1.7 | 2.75E-12 | 1.12E-03 | 3.09E-16 | 1.00E+00 | 1.12E-04 |
| 1.8 | 5.75E-13 | 9.99E-04 | 5.75E-17 | 1.00E+00 | 9.99E-05 |
| 1.9 | 1.20E-13 | 8.97E-04 | 1.08E-17 | 1.00E+00 | 8.97E-05 |
| 2.0 | 2.51E-14 | 8.09E-04 | 2.03E-18 | 1.00E+00 | 8.09E-05 |
| 2.1 | 5.25E-15 | 7.34E-04 | 3.85E-19 | 1.00E+00 | 7.34E-05 |
| 2.2 | 1.10E-15 | 6.69E-04 | 7.33E-20 | 1.00E+00 | 6.69E-05 |
| 2.3 | 2.29E-16 | 6.12E-04 | 1.40E-20 | 1.00E+00 | 6.12E-05 |
| 2.4 | 4.79E-17 | 5.62E-04 | 2.69E-21 | 1.00E+00 | 5.62E-05 |
| 2.5 | 1.00E-17 | 5.18E-04 | 5.18E-22 | 1.00E+00 | 5.18E-05 |
| 2.6 | 2.09E-18 | 4.79E-04 | 1.00E-22 | 1.00E+00 | 4.79E-05 |
| 2.7 | 4.37E-19 | 4.44E-04 | 1.94E-23 | 1.00E+00 | 4.44E-05 |
| 2.8 | 9.12E-20 | 4.13E-04 | 3.77E-24 | 1.00E+00 | 4.13E-05 |
| 2.9 | 1.91E-20 | 3.85E-04 | 7.33E-25 | 1.00E+00 | 3.85E-05 |
| 3.0 | 3.98E-21 | 3.60E-04 | 1.43E-25 | 1.00E+00 | 3.60E-05 |
| 3.1 | 8.32E-22 | 3.37E-04 | 2.80E-26 | 1.00E+00 | 3.37E-05 |
| 3.2 | 1.74E-22 | 3.16E-04 | 5.49E-27 | 1.00E+00 | 3.16E-05 |
| 3.3 | 3.63E-23 | 2.97E-04 | 1.08E-27 | 1.00E+00 | 2.97E-05 |
| 3.4 | 7.59E-24 | 2.80E-04 | 2.12E-28 | 1.00E+00 | 2.80E-05 |
| 3.5 | 1.58E-24 | 2.64E-04 | 4.19E-29 | 1.00E+00 | 2.64E-05 |
| 3.6 | 3.31E-25 | 2.50E-04 | 8.27E-30 | 1.00E+00 | 2.50E-05 |
| 3.7 | 6.92E-26 | 2.36E-04 | 1.64E-30 | 1.00E+00 | 2.36E-05 |
| 3.8 | 1.45E-26 | 2.24E-04 | 3.24E-31 | 1.00E+00 | 2.24E-05 |
| 3.9 | 3.02E-27 | 2.13E-04 | 6.43E-32 | 1.00E+00 | 2.13E-05 |
| 4.0 | 6.31E-28 | 2.02E-04 | 1.28E-32 | 1.00E+00 | 2.02E-05 |
| **SUM** | | | **7.15E-03** | | **5.24E-02** |
| **$F_{obs}/F_{corr}$** | | **0.14** | | | |

**Table 3.** Numerical integration for the inner filter effect correction of pyrene fluorescence measurements in dissolved organic matter (DOM) considering the illumination geometry of the TGLIF system.

| $x$ (cm) | $10^{-(\alpha ex+\alpha em)x}$ | $G(x)$ | $\Sigma 10^{-(\alpha ex+\alpha em)x} \cdot G(x) \cdot \Delta x$ | $10^{-(\varepsilon ex+\varepsilon em)Cpyr \cdot x}$ | $\Sigma 10^{-(\varepsilon ex+\varepsilon em)\,Cpy \cdot x} \cdot G(x) \cdot \Delta x$ |
|---|---|---|---|---|---|
| 0.1 | 7.08E-01 | 3.24E-01 | 2.29E-02 | 1.00E+00 | 3.24E-02 |
| 0.2 | 5.01E-01 | 8.09E-02 | 4.06E-03 | 1.00E+00 | 8.09E-03 |
| 0.3 | 3.55E-01 | 3.60E-02 | 1.28E-03 | 1.00E+00 | 3.60E-03 |
| 0.4 | 2.51E-01 | 2.02E-02 | 5.08E-04 | 1.00E+00 | 2.02E-03 |
| 0.5 | 1.78E-01 | 1.29E-02 | 2.30E-04 | 1.00E+00 | 1.29E-03 |
| 0.6 | 1.26E-01 | 8.99E-03 | 1.13E-04 | 1.00E+00 | 8.99E-04 |
| 0.7 | 8.91E-02 | 6.61E-03 | 5.89E-05 | 1.00E+00 | 6.60E-04 |
| 0.8 | 6.31E-02 | 5.06E-03 | 3.19E-05 | 1.00E+00 | 5.06E-04 |
| 0.9 | 4.47E-02 | 4.00E-03 | 1.79E-05 | 9.99E-01 | 3.99E-04 |
| 1 | 3.16E-02 | 3.24E-03 | 1.02E-05 | 9.99E-01 | 3.24E-04 |
| 1.1 | 2.24E-02 | 2.68E-03 | 5.99E-06 | 9.99E-01 | 2.67E-04 |
| 1.2 | 1.58E-02 | 2.25E-03 | 3.56E-06 | 9.99E-01 | 2.25E-04 |
| 1.3 | 1.12E-02 | 1.92E-03 | 2.15E-06 | 9.99E-01 | 1.91E-04 |
| 1.4 | 7.94E-03 | 1.65E-03 | 1.31E-06 | 9.99E-01 | 1.65E-04 |
| 1.5 | 5.62E-03 | 1.44E-03 | 8.09E-07 | 9.99E-01 | 1.44E-04 |
| 1.6 | 3.98E-03 | 1.26E-03 | 5.03E-07 | 9.99E-01 | 1.26E-04 |
| 1.7 | 2.82E-03 | 1.12E-03 | 3.16E-07 | 9.99E-01 | 1.12E-04 |
| 1.8 | 2.00E-03 | 9.99E-04 | 1.99E-07 | 9.99E-01 | 9.98E-05 |
| 1.9 | 1.41E-03 | 8.97E-04 | 1.27E-07 | 9.99E-01 | 8.96E-05 |
| 2 | 1.00E-03 | 8.09E-04 | 8.09E-08 | 9.99E-01 | 8.08E-05 |
| 2.1 | 7.08E-04 | 7.34E-04 | 5.20E-08 | 9.99E-01 | 7.33E-05 |
| 2.2 | 5.01E-04 | 6.69E-04 | 3.35E-08 | 9.99E-01 | 6.68E-05 |
| 2.3 | 3.55E-04 | 6.12E-04 | 2.17E-08 | 9.99E-01 | 6.11E-05 |
| 2.4 | 2.51E-04 | 5.62E-04 | 1.41E-08 | 9.99E-01 | 5.61E-05 |
| 2.5 | 1.78E-04 | 5.18E-04 | 9.21E-09 | 9.98E-01 | 5.17E-05 |
| 2.6 | 1.26E-04 | 4.79E-04 | 6.03E-09 | 9.98E-01 | 4.78E-05 |
| 2.7 | 8.91E-05 | 4.44E-04 | 3.96E-09 | 9.98E-01 | 4.43E-05 |
| 2.8 | 6.31E-05 | 4.13E-04 | 2.61E-09 | 9.98E-01 | 4.12E-05 |
| 2.9 | 4.47E-05 | 3.85E-04 | 1.72E-09 | 9.98E-01 | 3.84E-05 |
| 3 | 3.16E-05 | 3.60E-04 | 1.14E-09 | 9.98E-01 | 3.59E-05 |
| 3.1 | 2.24E-05 | 3.37E-04 | 7.54E-10 | 9.98E-01 | 3.36E-05 |
| 3.2 | 1.58E-05 | 3.16E-04 | 5.01E-10 | 9.98E-01 | 3.16E-05 |
| 3.3 | 1.12E-05 | 2.97E-04 | 3.34E-10 | 9.98E-01 | 2.97E-05 |
| 3.4 | 7.94E-06 | 2.80E-04 | 2.22E-10 | 9.98E-01 | 2.79E-05 |
| 3.5 | 5.62E-06 | 2.64E-04 | 1.49E-10 | 9.98E-01 | 2.64E-05 |
| 3.6 | 3.98E-06 | 2.50E-04 | 9.94E-11 | 9.98E-01 | 2.49E-05 |
| 3.7 | 2.82E-06 | 2.36E-04 | 6.66E-11 | 9.98E-01 | 2.36E-05 |
| 3.8 | 2.00E-06 | 2.24E-04 | 4.47E-11 | 9.98E-01 | 2.24E-05 |
| 3.9 | 1.41E-06 | 2.13E-04 | 3.01E-11 | 9.98E-01 | 2.12E-05 |
| 4 | 1.00E-06 | 2.02E-04 | 2.02E-11 | 9.98E-01 | 2.02E-05 |
| **SUM** | | | **2.92E-02** | | **5.24E-02** |
| **$F_{obs}/F_{corr}$** | | **0.56** | | | |

## References

Kuo, D. T. F., Adams, R. G., Rudnick, S. M., Chen, R. F., Gschwend, P. M., Investigating desorption of native pyrene from sediment on minute-to-month-timescales by time-gated fluorescence spectroscopy. *Environ. Sci. Technol.* **2007**, *41*, 7752-7758.

Rudnick, S. M., 1998. *In-situ* fluorescence of polycyclic aromatic hydrocarbons (PAH) in the marine environment. Ph. D. Thesis, University of Massachusetts, Boston, MA.

Rudnick, S. M., Chen, R. F., Laser-induced fluorescence of pyrene and other polycyclic aromatic hydrocarbons (PAH) in seawater. *Talanta* **1998**, *47*, 907-919.

# APPENDIX VIII

## PAH CONCENTRATIONS FOR INNER PENOBSCOT BAY (IPB) AND JORDAN BASIN (JB) SEDIMENTS

**Table 1.** Concentrations of PAHs in Inner Penobscot Bay (IPB) sediment samples.

| Depth Interval (cm) | concentration (ng/g)[a] | | | | | | | | | | |
|---|---|---|---|---|---|---|---|---|---|---|---|
| | naph | naph-C1 | aceny | acen | fluo | phen | anth | phen-C1 | phen-C2 | fla | pyr |
| 0-0.5 | 35 | 20 | 18 | 9 | 21 | 254 | 43 | 218 | 165 | 421 | 340 |
| 0.5-1.0 | 45 | 24 | 17 | 9 | 20 | 229 | 29 | 217 | 212 | 395 | 315 |
| 1.0-1.5 | 51 | 29 | 30 | 12 | 20 | 279 | 65 | 291 | 241 | 526 | 428 |
| 1.5-2.0 | 42 | 24 | 20 | 12 | 23 | 261 | 36 | 243 | 199 | 493 | 396 |
| 2.0-2.5 | 46 | 21 | 23 | 9 | 24 | 278 | 38 | 227 | 184 | 522 | 411 |
| 2.0-2.5b | 42 | 21 | 30 | 11 | 27 | 313 | 59 | 289 | 224 | 517 | 424 |
| 2.5-3.0 | 46 | 27 | 27 | 15 | 25 | 280 | 80 | 286 | 230 | 516 | 429 |
| 3.0-3.5 | 38 | 21 | 19 | 11 | 20 | 232 | 55 | 220 | 182 | 429 | 344 |
| 3.5-4.0 | 37 | 23 | 20 | 18 | 26 | 297 | 41 | 238 | 206 | 499 | 398 |
| 4.0-4.5 | 32 | 19 | 15 | 9 | 14 | 241 | 17 | 235 | 233 | 412 | 327 |
| 4.5-5.0 | 22 | 14 | 16 | 7 | 16 | 221 | 25 | 203 | 212 | 422 | 319 |
| 5.0-5.5 | 40 | 20 | 21 | 10 | 21 | 255 | 59 | 250 | 257 | 480 | 402 |
| 5.0-5.5b | 34 | 16 | 21 | 9 | 19 | 239 | 69 | 258 | 277 | 473 | 399 |
| 5.5-6.0 | 40 | 22 | 19 | 11 | 22 | 273 | 31 | 242 | 293 | 506 | 410 |
| 6.0-6.5 | 17 | 10 | 11 | 6 | 11 | 151 | 26 | 148 | 149 | 490 | 398 |
| 6.5-7.0 | 29 | 17 | 17 | 9 | 20 | 239 | 58 | 258 | 270 | 420 | 350 |
| 7.0-7.5 | 28 | 20 | 18 | 10 | 21 | 250 | 43 | 242 | 282 | 479 | 397 |
| 7.5-8.0 | 32 | 18 | 17 | 9 | 19 | 203 | 43 | 203 | 205 | 363 | 300 |
| 8.0-8.5 | 39 | 23 | 25 | 13 | 22 | 267 | 73 | 268 | 277 | 461 | 391 |
| 8.5-9.0 | 37 | 18 | 26 | 10 | 24 | 272 | 58 | 266 | 289 | 467 | 389 |
| 9.0-9.5 | 47 | 24 | 25 | 14 | 28 | 323 | 75 | 319 | 393 | 536 | 454 |
| 9.5-10.0 | 34 | 19 | 25 | 10 | 20 | 257 | 70 | 260 | 268 | 483 | 404 |
| 10.0-10.5 | 38 | 19 | 23 | 10 | 21 | 254 | 55 | 255 | 263 | 460 | 382 |
| 10.5-11.0 | 14 | 17 | 22 | 12 | 21 | 272 | 78 | 299 | 288 | 455 | 382 |
| 11.0-11.5 | 50 | 27 | 33 | 14 | 28 | 344 | 74 | 371 | 357 | 531 | 440 |
| 11.5-12.0 | 33 | 17 | 19 | 9 | 18 | 207 | 48 | 226 | 223 | 396 | 327 |
| 12.0-13.0 | 54 | 24 | 26 | 11 | 25 | 282 | 53 | 265 | 270 | 478 | 378 |
| 13.0-14.0 | 33 | 17 | 20 | 9 | 19 | 234 | 42 | 222 | 243 | 420 | 338 |
| 14.0-15.0 | 37 | 17 | 18 | 9 | 17 | 201 | 35 | 187 | 192 | 381 | 298 |
| 15.0-16.0 | 23 | 11 | 5 | 7 | 16 | 174 | 34 | 164 | 168 | 333 | 268 |
| 16.0-17.0 | 17 | 9 | 16 | 7 | 17 | 194 | 33 | 166 | 190 | 391 | 292 |
| 17.0-18.0 | 28 | 10 | 11 | 6 | 13 | 137 | 28 | 116 | 124 | 253 | 188 |
| 18.0-19.0 | 13 | 4 | 4 | 2 | 5 | 52 | 13 | 47 | 49 | 110 | 82 |
| 18.0-19.0b | 11 | 3 | 4 | 2 | 6 | 58 | 14 | 51 | 47 | 118 | 87 |
| 19.0-20.0 | 0 | 1 | 1 | 1 | 3 | 5 | 1 | 26 | 24 | 49 | 37 |
| 20.0-21.0 | 4 | 2 | 1 | 1 | 2 | 21 | 5 | 20 | 19 | 41 | 30 |
| 21.0-22.0 | 3 | 2 | 1 | 1 | 2 | 19 | 5 | 19 | 17 | 35 | 26 |
| 22.0-23.0 | 1 | 1 | 1 | 1 | 2 | 21 | 6 | 23 | 23 | 36 | 0 |
| 23.0-24.0 | 4 | 4 | 0 | 0 | 0 | 23 | 7 | 29 | 29 | 47 | 38 |
| 24.0-24.5 | 0 | 0 | 138 | 0 | 0 | 5 | 2 | 25 | 49 | 113 | 97 |
| 24.5-25.5 | 10 | 5 | 5 | 2 | 6 | 65 | 19 | 61 | 63 | 121 | 94 |
| 25.5-26.5 | 4 | 2 | 2 | 0 | 2 | 24 | 6 | 26 | 23 | 40 | 31 |
| 26.5-27.5 | 2 | 2 | 0 | 0 | 0 | 7 | 2 | 9 | 11 | 10 | 8 |

[a]naph: naphthalene; naph-C1: naphthalene-C1; aceny: acenaphthylene; acen: acenaphthene; fluo: fluorene; phen: phenanthrene; anth: anthracene; phen-C1; phenanthrene-C1; phen-C2: phenanthrene-C2; fla: fluoranthene; pyr: pyrene; ret: retene; pyr/fla-C1: pyrene/fluoranthene-C1; pyr/fla-C2: pyrene/fluoranthene-C2; b[*a*]a + triph: benz[*a*]anthracene + triphenylene; chr: chrysene; b[*b*]f + b[*k*]f: benzo[*b*+*k*]fluoranthenes; b[*e*]p: benzo[*e*]pyrene; b[*a*]p: benzo[*a*]pyrene; pery: perylene; d[*a,h*]a: dibenz[*a,h*]anthracene; ind: indeno[1,2,3-*c,d*]pyrene.

**Table 1 (continuation).** Concentrations of PAHs in Inner Penobscot Bay (IPB) sediment samples.

| Depth Interval (cm) | concentration (ng/g)[a] ret | pyr/fla-C1 | pyr/fla-C2 | b[*a*]a+ triph | chr | b[*b*]f+ b[*k*]f | b[*e*]p | b[*a*]p | pery | d[*a,h*]a | ind | Tot PAH |
|---|---|---|---|---|---|---|---|---|---|---|---|---|
| 0-0.5 | 120 | 242 | 115 | 234 | 139 | 187 | 157 | 118 | 92 | 14 | 122 | 3084 |
| 0.5-1.0 | 87 | 233 | 111 | 196 | 121 | 188 | 155 | 67 | 48 | 10 | 105 | 2832 |
| 1.0-1.5 | 74 | 313 | 190 | 342 | 163 | 248 | 209 | 233 | 155 | 23 | 207 | 4129 |
| 1.5-2.0 | 87 | 276 | 140 | 216 | 150 | 214 | 176 | 16 | 35 | 13 | 111 | 3182 |
| 2.0-2.5 | 89 | 284 | 155 | 266 | 152 | 216 | 178 | 25 | 40 | 18 | 154 | 3359 |
| 2.0-2.5b | 68 | 316 | 172 | 319 | 152 | 227 | 181 | 193 | 104 | 14 | 167 | 3871 |
| 2.5-3.0 | 83 | 318 | 184 | 302 | 161 | 237 | 194 | 212 | 194 | 19 | 171 | 4032 |
| 3.0-3.5 | 69 | 247 | 164 | 222 | 117 | 195 | 156 | 129 | 107 | 10 | 103 | 3092 |
| 3.5-4.0 | 77 | 258 | 149 | 259 | 163 | 227 | 189 | 33 | 64 | 16 | 160 | 3399 |
| 4.0-4.5 | 107 | 245 | 137 | 201 | 144 | 175 | 147 | 8 | 18 | 10 | 127 | 2875 |
| 4.5-5.0 | 88 | 231 | 140 | 181 | 140 | 177 | 150 | 12 | 23 | 13 | 106 | 2738 |
| 5.0-5.5 | 75 | 320 | 218 | 287 | 146 | 205 | 169 | 143 | 91 | 15 | 122 | 3608 |
| 5.0-5.5b | 68 | 308 | 227 | 297 | 147 | 215 | 176 | 179 | 118 | 14 | 134 | 3696 |
| 5.5-6.0 | 80 | 294 | 211 | 227 | 129 | 216 | 178 | 16 | 34 | 11 | 120 | 3387 |
| 6.0-6.5 | 52 | 306 | 200 | 247 | 132 | 211 | 168 | 68 | 80 | 12 | 115 | 3009 |
| 6.5-7.0 | 107 | 281 | 182 | 268 | 129 | 214 | 165 | 175 | 162 | 14 | 113 | 3496 |
| 7.0-7.5 | 82 | 302 | 223 | 240 | 150 | 200 | 165 | 61 | 70 | 11 | 113 | 3406 |
| 7.5-8.0 | 82 | 240 | 155 | 228 | 107 | 170 | 135 | 144 | 116 | 10 | 102 | 2901 |
| 8.0-8.5 | 93 | 297 | 190 | 308 | 156 | 208 | 169 | 194 | 182 | 16 | 155 | 3825 |
| 8.5-9.0 | 80 | 296 | 216 | 305 | 147 | 204 | 168 | 155 | 108 | 17 | 152 | 3704 |
| 9.0-9.5 | 99 | 346 | 236 | 329 | 152 | 230 | 187 | 178 | 114 | 14 | 128 | 4249 |
| 9.5-10.0 | 74 | 323 | 217 | 322 | 154 | 224 | 181 | 193 | 125 | 16 | 149 | 3829 |
| 10.0-10.5 | 75 | 286 | 192 | 282 | 131 | 219 | 170 | 162 | 109 | 13 | 122 | 3540 |
| 10.5-11.0 | 105 | 296 | 182 | 285 | 150 | 210 | 173 | 169 | 162 | 16 | 137 | 3744 |
| 11.0-11.5 | 104 | 338 | 216 | 348 | 161 | 247 | 200 | 227 | 144 | 22 | 180 | 4456 |
| 11.5-12.0 | 97 | 252 | 133 | 256 | 138 | 186 | 150 | 150 | 120 | 14 | 132 | 3151 |
| 12.0-13.0 | 80 | 279 | 175 | 310 | 133 | 218 | 160 | 177 | 105 | 14 | 113 | 3632 |
| 13.0-14.0 | 75 | 249 | 156 | 267 | 113 | 200 | 144 | 148 | 91 | 10 | 97 | 3151 |
| 14.0-15.0 | 65 | 234 | 135 | 245 | 104 | 173 | 138 | 149 | 94 | 12 | 107 | 2848 |
| 15.0-16.0 | 60 | 194 | 156 | 208 | 96 | 146 | 118 | 129 | 85 | 12 | 98 | 2506 |
| 16.0-17.0 | 77 | 202 | 141 | 237 | 106 | 151 | 109 | 77 | 67 | 8 | 70 | 2578 |
| 17.0-18.0 | 56 | 134 | 102 | 170 | 69 | 115 | 79 | 83 | 83 | 6 | 58 | 1870 |
| 18.0-19.0 | 24 | 62 | 43 | 71 | 28 | 53 | 39 | 41 | 76 | 3 | 32 | 852 |
| 18.0-19.0b | 25 | 65 | 40 | 78 | 31 | 59 | 40 | 40 | 75 | 3 | 32 | 890 |
| 19.0-20.0 | 14 | 32 | 23 | 33 | 15 | 25 | 18 | 19 | 78 | 2 | 14 | 419 |
| 20.0-21.0 | 12 | 25 | 19 | 26 | 11 | 20 | 14 | 14 | 73 | 1 | 8 | 370 |
| 21.0-22.0 | 12 | 22 | 18 | 22 | 10 | 19 | 2 | 1 | 8 | 1 | 7 | 251 |
| 22.0-23.0 | 14 | 25 | 19 | 25 | 11 | 19 | 2 | 2 | 8 | 1 | 9 | 249 |
| 23.0-24.0 | 12 | 34 | 22 | 28 | 17 | 23 | 17 | 18 | 81 | 3 | 18 | 452 |
| 24.0-24.5 | 5 | 95 | 71 | 107 | 48 | 63 | 47 | 53 | 86 | 4 | 43 | 1052 |
| 24.5-25.5 | 45 | 74 | 52 | 78 | 39 | 55 | 44 | 50 | 83 | 5 | 40 | 1015 |
| 25.5-26.5 | 10 | 26 | 17 | 24 | 12 | 18 | 15 | 15 | 91 | 2 | 13 | 404 |
| 26.5-27.5 | 5 | 9 | 9 | 7 | 4 | 6 | 4 | 3 | 83 | 0 | 0 | 181 |

[a]naph: naphthalene; naph-C1: naphthalene-C1; aceny: acenaphthylene; acen: acenaphthene; fluo: fluorene; phen: phenanthrene; anth: anthracene; phen-C1; phenanthrene-C1; phen-C2: phenanthrene-C2; fla: fluoranthene; pyr: pyrene; ret: retene; pyr/fla-C1: pyrene/fluoranthene-C1; pyr/fla-C2: pyrene/fluoranthene-C2; b[*a*]a + triph: benz[*a*]anthracene + triphenylene; chr: chrysene; b[*b*]f + b[*k*]f: benzo[*b*+*k*]fluoranthenes; b[*e*]p: benzo[*e*]pyrene; b[*a*]p: benzo[*a*]pyrene; pery: perylene; d[*a,h*]a: dibenz[*a,h*]anthracene; ind: indeno[1,2,3-*c,d*]pyrene.

**Table 2**. Concentrations of PAHs in Jordan Basin (JB) sediment samples.

| Depth Interval (cm) | concentration (ng/g)[a] | | | | | | | | | | | |
|---|---|---|---|---|---|---|---|---|---|---|---|---|
| | naph | aceny | acen | fluo | phen | anth | phen-C1 | phen-C2 | fla | pyr | pyr/fla-C1 | b[*a*]a |
| 0.5-1.0 | 17 | 5 | 2 | 9 | 31 | 3 | 10 | 1 | 35 | 26 | 25 | 12 |
| 1.0-1.5 | 16 | 5 | 2 | 6 | 52 | 8 | 18 | 3 | 37 | 27 | 28 | 14 |
| 1.5-2.0 | 17 | 5 | 2 | 6 | 31 | 4 | 14 | 1 | 42 | 46 | 27 | 14 |
| 2.0-3.0 | 21 | 5 | 1 | 8 | 28 | 5 | 13 | 3 | 41 | 28 | 27 | 15 |
| 2.0-3.0 | 21 | 4 | 2 | 5 | 27 | 4 | 14 | 5 | 40 | 26 | 26 | 14 |
| 3.0-4.0 | 19 | 5 | 1 | 7 | 28 | 4 | 13 | 4 | 38 | 25 | 27 | 13 |
| 4.0-5.0 | 19 | 5 | 2 | 6 | 29 | 5 | 14 | 7 | 40 | 42 | 32 | 14 |
| 5.0-6.0 | 20 | 5 | 2 | 7 | 29 | 6 | 14 | 6 | 39 | 28 | 37 | 14 |
| 6.0-8.0 | 11 | 10 | 6 | 11 | 42 | 5 | 13 | 2 | 23 | 31 | 16 | 17 |
| 6.0-8.0 | 10 | 10 | 7 | 6 | 60 | 4 | 13 | 2 | 33 | 26 | 18 | 17 |
| 8.0-10.0 | 71 | 11 | 5 | 14 | 29 | 4 | 10 | 2 | 40 | 26 | 18 | 15 |
| 10.0-14.0 | 7 | 11 | 4 | 10 | 30 | 3 | 9 | 4 | 37 | 25 | 19 | 18 |
| 14.0-18.0 | 150 | 7 | 4 | 11 | 52 | 25 | 13 | 8 | 36 | 38 | 22 | 15 |
| 18.0-22.0 | 455 | 36 | 7 | 0 | 38 | 0 | 11 | 0 | 25 | 19 | 19 | 11 |
| 22.0-30.0 | 731 | 32 | 8 | 6 | 62 | 6 | 16 | 0 | 35 | 40 | 21 | 15 |
| 30.0-38.0 | 48 | 18 | 0 | 13 | 16 | 4 | 7 | 0 | 57 | 25 | 22 | 20 |
| 38.0-46.0 | 135 | 46 | 3 | 0 | 26 | 5 | 9 | 0 | 42 | 25 | 21 | 15 |
| 46.0-54.0 | 157 | 36 | 7 | 0 | 38 | 0 | 11 | 0 | 25 | 19 | 19 | 11 |
| 54.0-56.0 | 45 | 0 | 0 | 0 | 35 | 4 | 9 | 0 | 18 | 11 | 0 | 9 |

[a]naph: naphthalene; aceny: acenaphthylene; acen: acenaphthene; fluo: fluorene; phen: phenanthrene; anth: anthracene; phen-C1; phenanthrene-C1; phen-C2: phenanthrene-C2; fla: fluoranthene; pyr: pyrene; pyr/fla-C1: pyrene/fluoranthene-C1; b[*a*]a: benz[*a*]anthracene; chr: chrysene; b[*b*]f: benzo[*b*]fluoranthene; b[*k*]f: benzo[*k*]fluoranthene; b[*e*]p: benzo[*e*]pyrene; b[*a*]p: benzo[*a*]pyrene; pery: perylene; d[*a,h*]a: dibenz[*a,h*]anthracene; b[g.h.i]p: benzo[g,h,i]perylene; ind: indeno[1,2,3-*c,d*]pyrene; cor: coronene.

**Table 2 (continuation).** Concentrations of PAHs in Jordan Basin (JB) sediment samples.

| Depth Interval (cm) | concentration (ng/g)[a] | | | | | | | | | | |
|---|---|---|---|---|---|---|---|---|---|---|---|
| | chr | b[*b*]f | b[*k*]f | b[*e*]p | b[*a*]p | pery | d[*a,h*]a | b[*g,h,i*]p | ind | cor | Tot PAH |
| 0.5-1.0 | 24 | 61 | 51 | - | - | 24 | 4 | 38 | 47 | 23 | 499 |
| 1.0-1.5 | 26 | 70 | 47 | 64 | 15 | 43 | 6 | 38 | 53 | 12 | 644 |
| 1.5-2.0 | 25 | 67 | 42 | 57 | 31 | 45 | 6 | 48 | 63 | 22 | 668 |
| 2.0-3.0 | 24 | 72 | 41 | 60 | 40 | 43 | 7 | 37 | 54 | 16 | 640 |
| 2.0-3.0 | 26 | 54 | 40 | 32 | 80 | 47 | 75 | 0 | 7 | 60 | 661 |
| 3.0-4.0 | 26 | 67 | 57 | 61 | 35 | 52 | 7 | 39 | 56 | 19 | 654 |
| 4.0-5.0 | 26 | 74 | 53 | 48 | 30 | 49 | 7 | 36 | 49 | 10 | 647 |
| 5.0-6.0 | 26 | 50 | 37 | 66 | 31 | 47 | 5 | 36 | 48 | 16 | 621 |
| 6.0-8.0 | 28 | 67 | 34 | 45 | 22 | 38 | 13 | 36 | 52 | 18 | 1,040 |
| 6.0-8.0 | 27 | 58 | 36 | 42 | 24 | 37 | 12 | 33 | 53 | 19 | 1,046 |
| 8.0-10.0 | 29 | 66 | 40 | 52 | 22 | 33 | 10 | 35 | 53 | 17 | 1,103 |
| 10.0-14.0 | 28 | 66 | 37 | 49 | 23 | 36 | 9 | 32 | 53 | 19 | 1,029 |
| 14.0-18.0 | 32 | 71 | 39 | 52 | 28 | 35 | 12 | 34 | 53 | 17 | 1,255 |
| 18.0-22.0 | 18 | 49 | 24 | 33 | 16 | 44 | 12 | 33 | 46 | 18 | 1,414 |
| 22.0-30.0 | 29 | 67 | 41 | 38 | 18 | 36 | 8 | 39 | 60 | 19 | 1,830 |
| 30.0-38.0 | 27 | 79 | 40 | 48 | 34 | 36 | 9 | 40 | 63 | 22 | 1,125 |
| 38.0-46.0 | 24 | 71 | 37 | 47 | 25 | 40 | 2 | 37 | 62 | 22 | 1,191 |
| 46.0-54.0 | 18 | 49 | 24 | 33 | 16 | 44 | 12 | 33 | 46 | 18 | 1,118 |
| 54.0-56.0 | 13 | 34 | 18 | 23 | 14 | 43 | 4 | 20 | 31 | 12 | 843 |

[a]naph: naphthalene; aceny: acenaphthylene; acen: acenaphthene; fluo: fluorene; phen: phenanthrene; anth: anthracene; phen-C1; phenanthrene-C1; phen-C2: phenanthrene-C2; fla: fluoranthene; pyr: pyrene; pyr/fla-C1: pyrene/fluoranthene-C1; b[*a*]a: benz[*a*]anthracene; chr: chrysene; b[*b*]f: benzo[*b*]fluoranthene; b[*k*]f: benzo[*k*]fluoranthene; b[*e*]p: benzo[*e*]pyrene; b[*a*]p: benzo[*a*]pyrene; pery: perylene; d[*a,h*]a: dibenz[*a,h*]anthracene; b[*g.h.i*]p: benzo[*g,h,i*]perylene; ind: indeno[1,2,3-*c,d*]pyrene; cor: coronene.